

Biofilm Dynamics in Drinking Water Biofiltration & Downstream Nanofiltration Biofouling

by

Paul Markin

A thesis

presented to the University of Waterloo

in fulfilment of the

thesis requirement for the degree of

Master of Applied Science

in

Civil Engineering (Water)

Waterloo, Ontario, Canada, 2018

© Paul Markin 2018

Author's Declaration

This thesis consists of material all of which I authored or co-authored: see Statement of Contributions included in the thesis. This is a true copy of the thesis, including any required final revisions, as accepted by my examiners.

I understand that my thesis may be made electronically available to the public.

Statement of Contributions

Funding was provided by the Ontario Research Fund (ORF), the Natural Sciences and Engineering Research Council of Canada (NSERC) as an Industrial Research Chair in Water Treatment at the University of Waterloo. Chair partners included Associated Engineering Group Ltd., the cities of Barrie, Brantford, Guelph, Hamilton and Ottawa, Conestoga-Rovers & Associates Limited, EPCOR Water Services, GE Water & Process Technologies Canada, Lake Huron and Elgin Area Water Supply Systems, the Ontario Clean Water Agency (OCWA), the Regions of Durham, Halton, Niagara and Waterloo, Toronto Water, and the Walkerton Clean Water Centre.

The pilot biofiltration and nanofiltration facility, located at the Region of Waterloo's Mannheim Drinking Water Treatment Plant, was refurbished and, where necessary, fabricated by former NSERC Chair students Ahmed Elhadidy and Brad Wilson. Operation of the plant during the course of the current work was shared with Chair MSc student Jangchuck Tashi. The Region of Waterloo kindly provided services to support the operation of the pilot plant. The Region of Waterloo also provided raw water quality data including measurements of ammonia, conductivity, dissolved organic carbon, hardness, ortho-phosphate, pH, nitrate and total iron, which was invaluable for the current work.

The current work was designed to build upon the PhD work by former Chair student Dr. Ahmed Elhadidy, and his contributions are described herein, as well as in the methods and results sections of this thesis where they are specifically identified and referenced. Dr. Elhadidy collected and archived biofilter feed water and media biofilm samples in an ultra-low freezer from October 2014 to February 2015, and these were provided along with the corresponding data on biomass, including total cell count and extracellular polymeric substances (EPS). As well, Dr. Elhadidy provided data over this time period on NOM removal by the biofilters, including dissolved organic carbon (DOC) and liquid chromatography – organic carbon detection (LC-OCD) removal data. In the current study, Dr. Elhadidy's contributions were used alongside biofilter media analyses and biofilter performance data that were collected from May 2015 to December 2015, which together provided monitoring data for a full year. In addition to biofilter samples, Dr. Elhadidy

provided archived nanofiltration membrane samples, as well as their corresponding biomass, EPS and feed channel pressure data, and these were used for the current study on nanofiltration biofouling community dynamics. The current methodology for extraction and separation of biofilm cell from EPS components using cation exchange resin was provided by Ahmed Elhadidy along with a MATLAB code for defining and integrating LC-OCD area peaks specifically for biofilm EPS samples.

Under the direction of Dr. Sigrid Peldszus, Dr. Monica Tudorancea performed LC-OCD analysis on water and EPS samples, and provided raw data files that were analysed in the current study. Chair MAsC student Victoria Chennette assisted with DOC measurements. During the course of the labwork, undergraduate research assistants helped with various tasks including Rachel Blowes and Sharon Chen.

Abstract

Natural organic matter (NOM) is a concern in many surface waters and must be removed by water treatment processes for cost-effective production of safe and aesthetically pleasing drinking water. Biological filtration is an appealing NOM removal method due to its simplicity and low maintenance requirements. Biofiltration is not traditionally used in water treatment headworks, however biofiltration without pretreatment (BF_{wp}) breaks with common practice to function as both particle and biodegradable NOM removal as a 1st stage process. BF_{wp} makes use of indigenous microbial populations embedded in a biofilm matrix to remove biodegradable organic matter (BOM) from raw source water. This configuration is a viable pretreatment strategy for both low and high pressure membrane filtration due to its ability to remove both particulate and soluble BOM, thereby mitigating biofouling on the membrane surface. Biofouling has been described as the “Achille’s heel” of membrane filtration (Flemming et al., 1997) due to its effects of increased operational cost and shortened membrane life-span. Therefore, a targeted effort is needed to understand how biofilter ecology affects performance both in the biofilter and downstream in membrane filtration units.

Two parallel pilot scale BF_{wp} units with dual-media were used in the current study for a seasonal characterisation of biofilter microbial dynamics and performance. Refurbishment of the biofilter pilot plant was performed by Dr. Ahmed Elhadidy and Brad Wilson, former students of the NSERC chair in water treatment. The current seasonal characterization spanned 14 months and made use of both new sample material as well as archived samples from Dr. Elhadidy. Biofilter media biomass was assessed using both adenosine tri-phosphate (ATP) and flow cytometric methods. Total protein, carbohydrate and free DNA of the media biofilm extracellular polymeric substances (EPS) were determined. Polymerase Chain Reaction – Denaturing Gradient Gel Electrophoresis (PCR-DGGE) was used to create microbial community fingerprint profiles of the biofilter feed and media. It was found that source water quality played a significant role in shaping BF_{wp} microbial communities. Multivariate analysis of the PCR-DGGE fingerprints showed a media biofilm community shift occurred in response to high ammonia, high low molecular

weight acids (LMW-acids) concentrations in the raw feed during January-February 2015. This low temperature, high ammonia and LMW-acids induced shift was accompanied by a rise in media biomass and EPS. Lower DOC and biopolymer removals were observed during the January-February 2015 community shift, however this was attributed largely to the effects which lower feed temperatures have on microbial biodegradation kinetics. No differences were found in community structures between media types, depths, or biofilter columns, however source water exhibited lower diversities and markedly different community structure than those of media biofilms. It was determined that media diversity and richness were high and did not exhibit seasonal fluctuations. As such these parameters could not be reliably related to biofilter DOC and biopolymer removal performance.

In his investigation of biofiltration as a pretreatment for nanofiltration (NF), Dr. Elhadidy archived samples for molecular analysis that were used in the current study. PCR-DGGE was performed on extracted DNA from source water, media, and fouled membrane samples for bacteria, archaea, and fungi. Archaea were present in all samples, however their abundance was roughly 1000 fold less than bacteria, which made it difficult to assess their significance in the biofiltration and NF processes. Fungi were only screened for in one media and one source water sample during method development; both samples were positive. Archaeal community organisation was similar to that of bacteria during the autumn BF-NF experiment, however no community organisation was discernible during the winter experiment. Bacterial community structures from the autumn experiment showed that fouled NF membranes fed raw water clustered together with biofilter media, indicating feed water rather than substrate material influences bacterial community organisation. Comparatively, NF membranes fed with biofilter effluent produced a cluster of drastically dissimilar bacterial communities, which corresponded with improved flux and reduced biofoulant biomass.

The microbial communities of biofiltration exhibited dynamic responses to feed water quality in both the seasonal and the nanofiltration studies. Biomass and EPS were highly correlated and their levels changed in response to community shifts, which in the seasonal and nanofiltration studies, were precipitated by changes in feed ammonia and BOM.

Acknowledgements

I would like to thank my supervisor Dr. Peter Huck and senior Chair Microbiologist Dr. Michele Van Dyke for their guidance and the opportunity to explore such an exciting interdisciplinary topic; I'd also like to thank them for sending me to Singapore to assist with collaborative research at the Nanyang Technological Institute; finally I am grateful to them for their support of my decision to finish my studies part time while working in Vancouver, BC.

I'd also like to express a big thank you to Dr. Ahmed Elhadidy and his former PhD supervisors for their contributions; Ahmed's PhD work served as a springboard for my research, and thereby expanded the range of possibilities for this thesis.

Thank you to Dr. Tony Fane, Dr. Stanislaus Raditya Suwarno and Hwee Sin Tan for welcoming me into their pilot scale research consortium in Singapore, and for sharing their insights and passion for the field of water technology.

Thank you to all the NSERC Chair personnel whose help and companionship took the edge off my time spent in Ontario (Dr. Monica Tudorancea, Ahmed Elhadidy, Jangchuck Tashi, Victoria Chenette, Brad Wilson, Fei Chen, Rachel Trower, and Rachel Blowes). Finally, this work would not have been possible without the NSERC Chair in Water Treatment at the University of Waterloo, and its industrial and municipal partners. The full list of Chair partners can be found at (www.civil.uwaterloo.ca/watertreatment).

Dedication

To my future wife, Katarina Axwik. Your love and support colours my world.

Table of Contents

Author’s Declaration	ii
Statement of Contributions	iii
Abstract	v
Acknowledgements	vii
Dedication	viii
Table of Contents	ix
List of Figures	xiii
List of Tables	xviii
List of Abbreviations	xx
Quote	xxii
Chapter 1 Introduction	1
1.1 Problem Statement	1
1.3 Research Objectives	3
1.4 Thesis structure	4
Chapter 2 Background	5
2.1 Biofiltration	5
2.1.1 Applications of Biofiltration	5
2.1.2 Mechanism of Biofiltration	6
2.1.3 Factors Affecting Performance of Biofiltration	7
2.1.4 Metrics for Evaluation of Biofiltration Performance	10
2.2 Nanofiltration Membranes in Drinking Water Treatment	12
2.2.1 Overview	12
2.2.2 Nanofiltration Membrane Fouling	13
2.2.3 Biofouling of Nanofiltration Membranes	13
2.2.4 Biofouling Control	14
2.3 Biofilms in Drinking Water Treatment	15
2.3.1 Introduction to Biofilms	15
2.3.2 Extracellular Polymeric Substances	16
2.3.3 Biofilm Development	16
2.3.4 Biofilter Biofilm Ecology	18
2.3.5 High Pressure Membrane Biofoulant Ecology	21
2.4 Biofiltration as Membrane Pretreatment	23

2.5 Effect of Seasonality on Biofiltration.....	23
2.6 Research Gaps.....	25
2.6.1 Relationship between microbial ecology, biofilm dynamics and BOM removal performance within BF_{wp}	25
2.6.2 Impact of seasonal water quality fluctuations on BF_{wp} biofilm dynamics and community structure	26
2.6.3 Unexplored microbial community dynamics of nanofiltration membrane biofoulant pre-treated by biofiltration.....	26
2.6.4 Limited information on the dynamics of archaea within biofiltration and high pressure membrane systems	27
2.7 Approach.....	27
Chapter 3 A seasonal-scale investigation of biofilm dynamics and process performance in dual-media drinking water biofiltration with no prior treatment	30
3.1 Summary	30
3.2 Introduction	31
3.3 Materials and Methods.....	35
3.3.1 Biofilters	35
3.3.3 Sampling Protocol.....	36
3.3.4 ATP Assay.....	37
3.3.5 Extraction of Cells and EPS from Biofilter Media Biofilm.....	38
3.3.6 Cell Enumeration by Flow Cytometry	38
3.3.7 Quantification of Total Carbohydrates, Total Protein, and Extracellular DNA	39
3.3.8 Liquid Chromatography – Organic Carbon Detection	40
3.3.9 Bacterial DNA Isolation	41
3.3.10 DGGE Analysis.....	42
3.3.11 Statistical Analyses	44
3.4 Results.....	47
3.4.1 Biofilter Feed Water Quality.....	47
3.4.2 Community Profiling of Feed Water and Biofilter Media Biofilms by DGGE Analysis	52
3.4.3 Biofilter Media Biofilm Biomass Characterization	66
3.4.8 Biofilter Performance.....	81
3.4.9 Association of Biofilter DGGE Groups with Biofilm Parameters and Process Performance.....	85
3.5 Discussion.....	93
3.5.1 Biofilter Feed Water Quality.....	93
3.5.2 DGGE Profiling of Biofilter Feed and Media Bacterial Communities	94

3.5.3 Seasonal Relationships Between Water Quality and Biofilter Community Structure.....	98
3.5.4 Biofilter Feed and Biofilm Bacterial Community Diversity	100
3.5.4 Biofilter Biofilm Dynamics.....	103
3.5.7 Relationship between biofilm dynamics and Biofilter Performance	110
3.5.10 Conclusions.....	115
Chapter 4 Fighting Biofilms with Biofilms: Characterisation of Bacterial and Archaeal Communities in Pilot-Scale Biofiltration-Nanofiltration Coupled Process.....	118
4.1 Summary	118
4.2 Introduction	119
4.3 Materials and Methods.....	122
4.3.1 Experimental Configuration.....	122
4.3.2 Samples, Storage and DNA Isolation	125
4.3.3 PCR Amplification of Extracted Nucleic Acids	125
4.3.4 DGGE Conditions	126
4.3.5 Statistical Analysis and Interpretation	127
4.4 Results.....	128
4.4.1 Detection of microorganisms in biofilter-NF samples by PCR amplification.....	128
4.4.2 Bacterial & Archaeal Community Profiling.....	129
4.4.3 Comparing Community Diversity with Membrane Fouling Data.....	143
4.5 Discussion.....	148
4.5.1 Hierarchical Clustering of Bacterial Community Data Based on DGGE Profiles	149
4.5.2 Diversity of Bacterial Groups	153
4.5.3 Hierarchical Clustering of Archaeal Communities Based on DGGE Profiles	154
4.5.4 Diversity of Archaeal Groups.....	155
4.5.5 Presence of Fungi Within Pilot Plant Setup.....	157
4.6 Conclusions	158
Chapter 5 Research Summary & Relevance	160
5.1 Summary of Research	160
5.2 Relevance to Drinking Water Industry	163
5.3 Future Research	164
References	165
Appendix A: Supplementary Information for Chapter 3.....	178
Appendix B: Supplementary Information for Chapter 4	187
Appendix C: Backwash Procedures	188

Appendix D: Glassware Cleaning Procedures for DOC, LCOCD and EPS Quantification 189

List of Figures

- Figure 3.1 Example LC-OCD chromatograms of biofilter feed water (a), and biofilm EPS extracted from sand media (b).....41
- Figure 3.2 Feed water quality including (a) temperature, turbidity and dates media was collected; squares show Elhadidy while triangles show Markin sample dates. (b) feed water NH₃, ortho-P and total iron concentrations; NH₃ values below the detection limit of 0.1 mg-N/L are shown as 0.05. (c) feed water DOC, nitrate and hardness. (d) LC-OCD fractions including biopolymers (BP), humic substances (HS), building blocks (BB), low molecular weight acids (LMW-A), and low molecular weight neutrals (LMW-N).....48
- Figure 3.3 DGGE electropherogram of biofilter media and feed water bacterial communities. Lanes labelled “M” are marker lanes, lanes 1-5 and 7-12 were from biofilter media samples, and lane F was a biofilter feed water sample.....52
- Figure 3.4 Mantel optimal number of clusters as determined by Pearson’s correlation between Bray-Curtis distances and Ward assembled dendrograms cut at different heights (representing number of groups). Optimal number of clusters (k) was 5 at a Pearson r of 0.76.....54
- Figure 3.5 Dendrogram of biofilter feed water and media samples from Oct 2014 to Nov 2015. Samples are identified by date (month/year), sample type [feed, BF(A), BF(B)], media type [sand (S) or anthracite (A)] and sample depth (10, 20 or 60 cm from media surface). Five clusters were identified and labelled A to E, with groups A and B composed of planktonic feed water communities and groups C to E composed of media biofilm.....56
- Figure 3.6 Boxplots displaying the ANOSIM dissimilarity between and within DGGE groups. Width of boxes represents number of entries within group, horizontal black bars show median, and lower and upper box edges represent 1st and 3rd quartiles. Error bars represent the upper and lower range of dissimilarity. Circles are outliers. ANOSIM statistic was determined to be $R = 0.923$ ($p = 0.001$, $\alpha = 0.05$).....58
- Figure 3.7 Detrended correspondence analysis for biofilter feed water and media bacterial communities and water quality parameters. DGGE community profiles for each sample are represented by small open circles, while the DGGE profile groups are represented by coloured ellipses, with the group letter positioned in ellipsoid centres. Post-hoc environmental gradients including temperature (Temp), turbidity (Turb), pH, ortho-phosphorous (Ortho.P), total iron (T.Iron), nitrate (NO₃) and ammonia

(NH ₃) are represented by blue arrow vectors and correspond to the correlation strength between the variable and the DCA ordination.....	60
Figure 3.8 Detrended correspondence analysis for biofilter feed water and media bacterial communities and natural organic matter fractions as measured by DOC and LC-OCD. DGGE community profiles for each sample are represented by small open circles, while the DGGE profile groups are represented by coloured ellipses, with the group letter positioned in ellipsoid centres. Post-hoc environmental NOM gradients are represented by blue arrow vectors and include dissolved organic carbon (DOC), biopolymers (BP), humic substances (HS), humic building blocks (BB), low molecular weight acids (LMWA), and low molecular weight neutrals (LMWN).....	61
Figure 3.9 Bacterial community diversity (Shannon Index) (a) and richness (b) in feed water and media biofilms. Media samples were obtained from the 20 cm depth in BF(A) and BF(B).....	63
Figure 3.10 Barplot showing Shannon diversity index (a) and richness (b) parameters as a function of biofilter media depth across seasonal conditions.....	65
Figure 3.11 Seasonal trends in biofilter media bulk ATP (a), cell count (b), and femtogram ATP/cell (c).....	68
Figure 3.12 Biofilter media bulk ATP (a), live cells (b), and femtogram ATP/cell (c) over media depth (10, 20 and 60 cm below the media surface).....	71
Figure 3.13 Seasonal trends in EPS from biofilter media including total carbohydrates (measured as D-glucose) (a), total proteins (measured as bovine serum albumin) (b), the CH:PN ratio of carbohydrates to proteins (c), and extracellular DNA (d). Samples were obtained from the 20 cm media depth.....	74
Figure 3.14 Biofilter media EPS as a function of media depth. total carbohydrates is represented as D-glucose equivalent (a), proteins as bovine serum albumin (b), and carbohydrate to protein (CH:PN) ratio (c) for the 11 sampling campaigns. Note that depth data for eDNA is restricted to Aug 2015.....	76
Figure 3.15 Amount of EPS per cell at 20 cm media depth for both biofilters and media types. Carbohydrates were measured in µg D-glucose equivalents (a) and proteins were measured in µg BSA equivalents (b).....	78
Figure 3.16 LC-OCD fractions for biofilm EPS including HMW-OC (a), IMW-OC (b), and LMW-OC (c). Note that this analysis was not performed in May 2015.....	80
Figure 3.17 Biofilter biofilm LC-OCD fractions per cubic centimetre of media. Several depths are considered across warm and cold conditions.....	81

Figure 3.18 Biofilter performance for BF(B) and BF(A) as measured by percent removal of DOC from Oct 2014 to Nov 2015. Vertical dash indicates change in operation from 100 L/h (3.08 m/h) to 50 L/h (1.54 m/h).....	82
Figure 3.19 Biofilter performance for BF(A) and BF(B) as measured by percent removal of biopolymers from Oct 2014 to Nov 2015. Vertical dash indicates change in operation from 100 L/h (3.08 m/h) to 50 L/h (1.54 m/h).....	84
Figure 3.20 Biofilter performance for BF A (a) and BF B (b) from Oct 2014 to Nov 2015 as measured by percent removal of the NOM fractions as measured by LC-OCD, including humic substances, humic building block (BB), low molecular weight acids/humics (LMWA) and low molecular weight neutral compounds (LMWN) . Vertical dash indicates change in operation from 100 L/h (3.08 m/h) to 50 L/h (1.54 m/h). Nov 2015 LMWA y-axis value was -61.5.....	84
Figure 3.21 Bar charts presenting BF(A) and BF(B) % removal of a) dissolved organic carbon (DOC), b) biopolymers (BP), c) humic substances (HS), d) building blocks (BB), e) low molecular weight acids (LMW-A), and f) low molecular weight neutrals (LMW-N) relating to DGGE profile media biofilm groups C and D/E as defined by DCA clustering.....	87
Figure 3.22 Bar charts presenting biofilm parameters associated with DGGE profile media biofilm groups C, D and E, for both sand and anthracite media. Biofilm parameters presented include a) Shannon diversity, b) richness, c) ng ATP/cm ³ , d) cell counts/cm ³ , e) fg ATP/cell, f) ug D-glucose/cm ³ , g) µg BSA/cm ³ , and h) CH:PN ratio.....	90
Figure 3.23 Sand biofilm femtogram ATP/cell as a function of a) BF(A) DOC % removal, b) BF(A) biopolymer % removal, c) BF(B) DOC % removal, and d) BF(B) % biopolymer removal. Outliers removed for clarity, which involved a fg ATP/cell value of 46 in figures a) and b). Blue points present cold condition data (≤ 10 °C), and red points present warm condition data (> 10 °C).....	92
Figure 3.24 Anthracite biofilm femtogram ATP/cell at 20 cm media depth, as a function of a) BF(A) DOC % removal, b) BF(A) biopolymer % removal, c) BF(B) DOC % removal, and d) BF(B) % biopolymer removal. Blue points present cold condition data (≤ 10 °C), and red points present warm condition data (> 10 °C).....	93

- Figure 4.1 Example bacterial 16S rDNA DGGE community fingerprint. Lanes 1, 6, 11 and 16 were loaded with a custom molecular marker and denoted by “M”. Lane 2 presents a fungal community profile while lanes 3– 5 were NF samples (NF-Fall-BF(B)-4-R2, NF-Fall-BF(B)-4-R1, NF-Fall-Raw-4). Lanes 7 – 10 were NF-Winter-Raw-4, NF-Winter-BF(B)-8, NF-Winter-BF(A)-8, and NF-Winter-Raw-8. Lanes 12 – 15 were Eff-Apr-BF(A), Eff-Apr-BF(B), Feed-Apr, and Eff-Mar-BF(A).....130
- Figure 4.2 Dendrogram plot showing hierarchical clustering of bacterial community DGGE profile data for biofilter feed and effluent, biofilter media and NF samples. All media samples shown were taken from 20 cm depth. Bray-Curtis Distances were used in conjunction with the Ward algorithm. Y axis represents dissimilarity height between samples, where increasing height between nodes indicates greater dissimilarity between sample communities. A total of seven groups were identified and given a group letter. A legend of each sample is in Table 4.2.....132
- Figure 4.3 Mantel optimal number of clusters (k) using Ward algorithm with bacterial DGGE profile data. The Pearson correlation suggests the validity of different numbers of groups. The optimal group number was highest for 5 and 7 ($r = 0.72$).....133
- Figure 4.4 Correspondence analysis of bacterial DGGE community profiles. Each data point represents the DGGE profile of a sample from the dendrogram groups (A to G) defined in Figure 4.3 The variance of the two axes is 19.2 and 10.6 % for CA1 and CA2 respectively.....136
- Figure 4.5 Hypothesis testing using analysis of similarity (ANOSIM) of bacterial DGGE profile data. ANOSIM significantly validated group membership ($p=0.001$, $R=0.979$). Dissimilarity is represented by the y-axis and group width shows the number of members within each group. Within each box, the horizontal bar shows the group median dissimilarity, while top and bottom of the box shows 1st and 3rd quartile, respectively. Whiskers denote minimum and maximum values. Group G possessed two outliers (autumn raw-NF samples).....137
- Figure 4.6 Example archaeal 16S rDNA DGGE community profile. Lanes 1, 6, 11 and 16 were loaded with a custom molecular marker and denoted by “M”. Lanes 2 – 5 present media biofilm community profiles. Lanes 7 – 10 present Feed and effluent profiles138
- Figure 4.7 Mantel optimal number of clusters using Ward algorithm with archaeal DGGE profile data. Bar height represents Pearson’s correlation between original distance matrix and various numbers of groups possible within a Ward assembled dendrogram. Optimal number of archaeal groups was 5, with a Pearson r correlation of 0.65.....139

Figure 4.8 Dendrogram plot showing hierarchical clustering of archaeal community DGGE profile data. Five groups were identified at a cut height of 0.90, and given a designated group letter. All NF membrane samples used in the archaeal analysis were 4 cm distant from the MFS feed inlet. A legend of each sample is in Table 4.3.....140

Figure 4.9 Correspondence analysis of archaeal DGGE community profiles. Each data point represents the DGGE profile of a sample from the dendrogram groups H to L defined in Figure 4.12. The variance of the two axes is 18% and 15% for CA1 and CA2 respectively.....142

Figure 4.10 Hypothesis testing using analysis of similarity (ANOSIM) on archaeal DGGE profile data. ANOSIM validated group membership and number ($p=0.001$, $R=0.865$). Dissimilarity is represented by the y-axis and the “between” as well as “within” group dissimilarities are illustrated by boxplot height, whose size varies according to number of members within each group.....143

Figure 4.11 Shannon diversity (a), species richness (b), and evenness (c) for bacterial community DGGE profile groups derived from biofilter feed, effluent and media, and NF biofoulant layers from fall 2014 and winter/spring 2015.....145

Figure 4.12 Shannon diversity (a), species richness (b), and evenness (c) for archaeal community DGGE profile groups derived from biofilter feed, effluent and media as well as MFS biofoulant layers from fall 2014 and winter/spring 2015.....147

List of Tables

Table 3.1 Biofilter feed water quality during warm and cold conditions.....	49
Table 3.2 t-test results (two tailed; $\alpha = 0.05$) comparing water quality parameters at cold (≤ 10 °C) and warm (> 10 °C) conditions. Significant differences are marked with an asterisk (*).....	51
Table 3.3 Paired t-test comparing diversity and richness of BF(A) vs BF(B). Sand and anthracite were compared separately, and were sampled from the 20 cm depth media intermixing zone. Values were obtained using PCR-DGGE bacterial community profiling.....	63
Table 3.4 Analysis of variance (ANOVA, $\alpha = 0.05$) comparing biofilter diversity and richness between seasonal groups at 20 cm depth. Seasonal groups were winter 2014/2015, summer 2015 and fall 2015. Additionally, feed water diversity and richness means were compared with sand and anthracite biofilm (ANOVA, $\alpha = 0.05$).....	64
Table 3.5 Shannon diversity and richness results for DGGE Groups as defined by hierarchical and DCA clustering analyses.....	66
Table 3.6 Paired t-test comparing volumetric ATP, cell counts and ATP/cell between BF(A) and BF(B) for sand and anthracite media collected at 20 cm depth. Significant results are indicated by asterisks (*).....	69
Table 3.7 Analysis of variance (ANOVA, $\alpha = 0.05$) comparing biofilter biomass in media samples collected at 20cm depth. Seasonal groups were winter 2014/2015, summer 2015 and fall 2015. Tukey honest significant difference analysis was performed on significant ANOVA results. Significant results are indicated by asterisks.....	70
Table 3.8 Analysis of variance (ANOVA) comparing biofilter media EPS carbohydrates, proteins and carbohydrate to protein ratio between seasonal groups at 20 cm depth, with alpha set to 0.05. Seasonal groups were winter 2014/2015, summer 2015 and fall 2015. Sand and anthracite were compared separately, and were sampled from the 20 cm depth of the media intermixing zone. Significant results are indicated by asterisks (*).....	75
Table 3.9 Paired t-test comparing biofilter media carbohydrates, proteins and carbohydrate to protein ratio (CH:PN) between BF(A) and BF(B). Sand and anthracite were compared separately, and were sampled from the 20 cm depth of the media intermixing zone. Significant results are indicated by asterisks (*) ($\alpha = 0.05$).....	75

Table 3.10 Results of paired t-test analysis comparing biofilter NOM removals between BF(A) and BF(B). Statistically significant differences are marked with asterisk (*)...	85
Table 3.11 ANOVA results comparing biofilter NOM removals between the seasonal groups of winter 2014/2015, summer 2015 and fall 2015. Statistically significant differences are marked with asterisk (*).....	85
Table 3.12 Compiled F-test and t-test values from comparisons of biofilter media biofilm parameters between DGGE groups C and D/E. Significantly different variances between Groups C and D/E (significant F-tests) for some parameters required the use of unequal variance t-tests for all data presented. Alpha = 0.05. Significant results are denoted by an asterisk (*).....	88
Table 4.1 Biomass parameters measured for biofilter and NF samples for the fall 2014 and winter 2015 MFS experiments.....	124
Table 4.2 Legend explaining x-axis labels in the dendrogram of Figure 4.2.....	134
Table 4.3 Legend explaining x-axis labels in the archaeal community dendrogram of Figure 4.12.....	141
Table 4.4 Shaprio-Wilke test for normality of bacterial and archaeal Shannon diversity and community richness data-sets. Asterisk (*) denotes non-normal distributions.....	145
Table 4.5 Bacterial diversity data compared between DGGE groups, and the results of Kruskal-Wallis and post-hoc Dunn's test. Asterisk denotes significant p values.....	146
Table 4.6 Table of p values from unpaired Mann-Whitney U comparison of total bacteria and archaea ecological parameter means. Asterisk denotes significant p values.....	146
Table 4.7 Archaeal MFS diversity data was compared between DGGE groups, and the results of a Kruskal-Wallis rank-sum test are presented for each parameter. Asterisk (*) denotes significant p values.....	148

List of Abbreviations

ANOVA.....	Analysis of Variance
AOC	Assimilable organic carbon
ATP	Adenosine triphosphate
BDOC	Biodegradable dissolved organic carbon
BEOP.....	Biofilm enhanced osmotic pressure
BF _{wp}	Biofiltration without pre-treatment
BOM.....	Biodegradable Organic Matter
BSA	Bovine serum albumin
C/N	Carbon to nitrogen ratio
DCA.....	Detrended Correspondence Analysis
CER	Cation exchange resins
CLPP	Community level physiological profiling
CLSM	Confocal laser scanning microscopy
Da.....	Dalton
DBP.....	Disinfection by-product
DCA.....	Detrended Correspondence Analysis
DGGE	Denaturing gradient gel electrophoresis
DO.....	Dissolved oxygen
DOC	Dissolved organic carbon
DOM	Dissolved organic matter
EBCT.....	Empty bed contact time
eDNA	Extracellular DNA
EDTA.....	Ethylenediaminetetraacetic acid
EPS.....	Extracellular polymeric substances
ESOC.....	Emerging Substance of Concern
GAC.....	Granular activated carbon
HMW EPS	High molecular weight EPS
HPC.....	Heterotrophic plate count
IMW EPS.....	Intermediate molecular weight EPS

LC-OCD	Liquid chromatography organic carbon detector
LMWA	Low molecular weight acids
LMWN	Low molecular weight neutrals
MFS	Membrane fouling simulator
MWCO.....	Molecular weight cut off
NF	Nanofiltration
NOM	Natural organic matter
NTU.....	Nephelometric Turbidity Units
PBS.....	Phosphate buffered saline solution
PCA.....	Principal component analysis
PCR.....	Polymerase Chain Reaction
PES.....	Polyethersulfone
PLFA.....	Phospholipid fatty acids
PP	Polypropylene
RO.....	Reverse osmosis
SDS.....	Sodium dodecyl sulfate
TEP.....	Transparent exopolymer particles
TFC.....	Thin film composite
TOC.....	Total organic carbon
UF.....	Ultrafiltration
UV.....	Ultraviolet

Quote

“It is usually not recognized that for every injurious or parasitic microbe there are dozens of beneficial ones. Without the latter, there would be no bread to eat nor wine to drink, no fertile soils and no potable waters, no clothing and no sanitation. One can visualize no form of higher life without the existence of the microbes. They are the universal scavengers. They keep in constant circulation the chemical elements which are so essential to the continuation of plant and animal life.”

-Selman A. Waksman

Winner of the 1952 Nobel Prize
in physiology and medicine

Chapter 1

Introduction

1.1 Problem Statement

The next generation of water treatment technology will have to confront new challenges associated with the demands of population growth coupled to the stressors of a changing climate. Seawater, wastewater and compromised groundwater will likely become more common as source waters for major utilities. Drinking water infrastructure and utilities will therefore have to innovate to meet the challenges and costs currently associated with treating these source waters. As awareness of the effects of different biodegradable organic matter (BOM) fractions within specific unit treatment processes grows, so too will the use of simple and low cost biologically active technologies such as biofiltration. Biofiltration reduces concentrations of particles, turbidity, BOM and some inorganic nutrients, which makes it ideal for biofouling control via reducing concentrations of nutrients in water treatment plants.

Any filter that is operated without a disinfectant in its influent will become biologically active. Biofiltration takes advantage of this phenomenon whereby influent BOM can be adsorbed by the media-biofilm matrix and, for some BOM components, undergo hydrolysis for either assimilation or degradation by the biomass. Although microbial growth and the associated formation of extracellular polymeric substances (EPS) are ubiquitous to biofiltration, currently available monitoring tools are limited in their ability to represent and interpret the complex microbial systems which are responsible for BOM removal performance. Biomass is often measured via adenosine triphosphate; while this is an important parameter, especially during media ripening and biofilm maturation, it fails to accurately capture or predict BOM removal performance (Pharand et al., 2014). Conversely, EPS monitoring is seldom reported in the literature (Lauderdale et al., 2012; Mauclaire et al., 2004) and the contribution of different EPS fractions to biofilter performance is not well

understood. The fluctuations of these fundamental biofilm parameters in response to microbial community shifts, as well as standard ecological metrics, can have important implications for biofilter performance and management. Therefore a closer look at biofilter ecology across seasonal time frames will add a depth of process understanding which simple biomass monitoring cannot approximate on its own. Several studies examining the bacterial communities of biofiltration exist (e.g. Kaarela et al., 2015; Liao et al., 2013; Pinto et al., 2012; Werner, 1982), however the majority of these efforts are hampered by excessive taxonomic information and do not relate ecological parameters such as diversity and structure directly to process performance.

Unlike biofiltration, a biologically active filter membrane is anathema, since the resultant biofilm either reduces flux or increases the pressure and energy required for operation; this is known as biofouling. Therefore membranes must follow a regular hydrodynamic and chemical cleaning schedule in order to remove and destroy the nuisance cells and slime matrix of associated biofilms. Nanofiltration membranes are used in the exclusion of soluble components of 100 - 1000 Da and as such are highly susceptible to biofouling (Hilal et al. 2004). Recently, biofiltration has been shown to significantly mitigate biofouling of ultrafiltration membranes (Halle et al., 2009). Although nutrient limitation for membrane biofouling control has received much speculation within the literature (Dreszer et al., 2013; Fonseca et al., 2007; Flemming et al., 1997; Naidu et al., 2013; Persson et al., 2006; Shon et al., 2013; Vrouwenvelder et al., 2009) the impact of biofiltration on downstream NF membranes has to-date received limited attention. Moreover, the effect of biofiltration on downstream biofoulant microbial community structure, and how these effects may be related to membrane performance, has received minimal attention within the literature (Jeong et al., 2016). In their review of the literature, Vanysacker and colleagues (2014) discussed the evidence supporting biofouling as an active process where complex microbial communities differentiate from those of the feed. Ivnitsky and colleagues (2007) investigated the biofoulant community structure and diversity of NF membranes polishing treated wastewater and found that although membrane colonization by multiple Proteobacteria subphyla was rapid, permeability was most effected by nuances in EPS. It has also been shown that the NF biofilms are highly adaptive to operational changes, being able to modify

ecological structure in response to chemical as well as physical stressors including fluid velocity (Al Ashab et al., 2014). Therefore, when biofiltration is applied as a membrane pretreatment, changes in downstream microbial ecology are likely given that biofiltration is particularly effective at nutrient and BOM attenuation.

Completion of the work to address the research objectives below would result in a deeper understanding of the biological systems within biofiltration and how these change over a utility's seasonal constraints, and this insight could direct operation and monitoring practices at full scale. Secondly, a detailed understanding of the biofilm characteristics between beneficial biofilter biofilms and nuisance biological fouling of membranes can aid in the optimisation and harmonisation of this innovative coupling of unit processes.

1.3 Research Objectives

1. Assess variations in biofilter media biofilm dynamics (bacterial community structure, diversity, biomass and EPS production) over a seasonal time-scale.
2. Compare biofilter media biofilm dynamics to environmental parameters such as nutrient concentrations, temperature, media type, and contact time.
3. Compare biofilter media biofilm dynamics to feed water NOM removal performance.
4. Screen for the presence of archaea and fungi in a biofiltration-nanofiltration coupled process, and evaluate whether these organisms contribute to the function of either process.
5. Determine the impact of biofiltration on downstream nanofiltration biofoulant community structure and diversity for both bacteria and archaea, and relate observations to system performance.

1.4 Thesis structure

Chapter 2 presents background material to provide information on the major research concepts within this thesis. Chapters 3 and 4 are formatted in the style of journal articles and as such contain separate introduction, materials & methods, results, discussion and conclusion sections. Chapter 3 presents a seasonal investigation into the biofilm dynamics of dual-media pilot scale drinking water biofilters without prior treatment. The study time period spans 14 months and includes analyses of bacterial community organization, as well as measurements of diversity, biomass, EPS, and water quality parameters to characterise feed-water composition and biofilter performance. Media type, depth and EBCT are also assessed for effect on bacterial community structure. Samples and data from October 2014 to February 2015 were provided by an NSERC Chair colleague (Elhadidy, 2015). Chapter 4 is a characterisation of bacterial and archaeal community structures on NF membrane samples originating from Ahmed Elhadidy's PhD investigation into the efficacy of biofiltration as a pretreatment to downstream nanofiltration membranes (Elhadidy, 2015). The effect of biofiltration on downstream nanofiltration membrane biofoulant community structure, and the relationship this has on membrane operation, is presented.

Chapter 2

Background

This chapter presents background information separated into 6 major parts which describe biofiltration, nanofiltration, biofilms and pertinent microbial ecology, biofiltration as a membrane pre-treatment, seasonal impacts on biofiltration and gaps in the research literature (Sections 2.1 to 2.6). Section 2.1 describes the applications of biofiltration, the mechanisms behind its function, factors affecting its performance as well as several methodologies used to assess process health and efficacy. Section 2.2 presents a discussion on membrane filtration with special attention given to nanofiltration. Biofouling development and proactive measures for its control are examined. Section 2.3 explores the biofilms in drinking water treatment and examines the biofilm matrix in detail, including such topics as biomass, EPS, biofilter media ecology, biofilm development and nanofiltration biofoulant microbial ecology. Section 2.4 presents a review of the application of biofiltration as a pretreatment to membrane systems and gives examples from use in both nanofiltration and reverse osmosis systems. Section 2.5 looks at how biofilm dynamics could vary across seasonal time scales while contributing to biofilter BOM removal. Section 2.6 identifies gaps in the current understanding of biofiltration as an engineered biological process. Lastly, Section 2.7 discusses the current work's experimental approach and contributions made from other research students.

2.1 Biofiltration

2.1.1 Applications of Biofiltration

There are several reasons why drinking water utilities employ biologically active filters, otherwise known as biofilters, with the most common being the removal of particles, inorganic nutrients and biodegradable organic matter (BOM) (Urfer et al., 1997). Particle reduction decreases turbidity which facilitates pathogen removal, while BOM removal is

necessary to reduce disinfection by-product (DBP) precursors, oxidant demand, taste and odour attenuation and to mitigate regrowth potential in distribution networks (Juhna & Melin, 2006; Servais et al., 1991). Furthermore, biofiltration can potentially remove emerging substances of concern (ESOCs) such as ibuprofen and naproxen (Halle et al. 2008).

Several configurations of biofiltration are employed by water utilities, both with and without various forms of pretreatment, and over the decades several operational terms for this process have emerged. First stage biofiltration usually refers to floc and particle removal, while second stage biofiltration usually refers to nutrient (organic and inorganic) removal (Niquette et al., 1998). Some processes, such as ozonation, have been responsible for increased adoption of biofiltration at full scale, with many European utilities using the ozonation-biofiltration process (Juhna & Melin, 2006). Ozonation is a common drinking water treatment process as it can provide effective disinfection without producing chlorine-containing disinfection by-products. Ozonation also transforms recalcitrant high molecular weight NOM to more biodegradable intermediates which are more amenable to removal (Basu et al., 2016); however since ozonation increases BOM in bulk water, further treatment is recommended to ensure distributed ozone-treated water is biostable, with biofiltration often used for this purpose (von Gunten, 2003). Biofiltration without pretreatment (BF_{wp}) was defined by Huck et al. (2015), and involves feeding biologically active filters with raw water and is sometimes referred to as direct biofiltration. This configuration is a very simple and robust unit process which has been shown to have potential as a pretreatment to reduce fouling of both low pressure (Halle et al., 2009; Huck et al., 2011; Rahman et al., 2014; Siembida-Lösch et al., 2015; Tashi, 2015; Wilson, 2015) and high pressure (Elhadidy, 2013; Elhadidy, 2015; Griebe & Flemming, 1998; Jeong et al., 2016) membranes.

2.1.2 Mechanism of Biofiltration

Biofiltration analogues have historically been used as ground infiltration, bank, and slow sand filtration, with modern rapid flow granular biofilters initially used following ozonation in the Mülheim process (Sontheimer et al., 1978). Within biologically active filters an active microbial biomass grows on support media which together participate in particle and BOM removal. Regular backwashing is used to remove excess particles and to some

extent biomass so that headloss through the filter bed is minimized. Conventional treatment processes (coagulation/flocculation/sedimentation and non-biological filtration) have difficulty in removing BOM and DBP precursors but biofiltration fills this void via biological attenuation (Basu et al., 2016). The active component of biofiltration is a heterogeneous biofilm composed of heterotrophic and sometimes lithotrophic bacterial cells embedded in a matrix of extracellular polymeric substances (EPS) (Cai et al., 2015; Kaarela et al., 2014) however archaea (Bai et al., 2013) and protists (Madoni et al., 2000) have also been observed. The biodegradable portion of NOM serves as the substrate for sessile biofilter communities, and thus a portion of the NOM is either mineralized or assimilated into new biomass as it passes through the filter. Given that biofilms are adept at adsorption of dissolved constituents such as humic substances (Flemming & Wingender, 2010), adsorption likely plays a role as a mechanism of nutrient and BOM removal as well. It is also important to note that biofilms produce new biodegradable material that may exit the filter (Huck et al., 2013).

2.1.3 Factors Affecting Performance of Biofiltration

The most important factors affecting performance in an acclimated biofilter are pretreatment with ozone, contact time, media type, influent temperature, influent composition, and backwashing procedure (Urfer et al., 1997). Empty bed contact time (EBCT) is one of the easiest factors for operators to control. While BOM removal increases with EBCT, this relationship is not proportional (Huck et al. 2013). EBCT is calculated as filter volume divided by water flow rate (Juhna & Melin, 2006). A good EBCT would allow for attachment of cells to media without excessive accumulation (Hozalski et al., 1995) while allowing sufficient contact time for biological degradation of influent BOM; therefore the optimal EBCT may change depending on temperature and influent water quality (Basu et al., 2016). It should be noted however that for relatively recalcitrant contaminants, longer EBCT values are needed (Gibert et al., 2013; Zearley & Summers, 2012).

Common media types are granular activated carbon (GAC), anthracite, or sand, with filters often using mixed media. GAC has adsorptive qualities, however these become exhausted upon full ripening of the media (Gibert et al., 2013). Although GAC is dominated

by micro and mesopores (1 – 100 nm) these are too small to accommodate a bacterial cell (Urfer et al., 1997), yet GAC's higher porosity, surface area, roughness, and different charge characteristics compared to sand and anthracite can support a denser microbial community (Dussert & Stone, 2000). Dual-media filters such as GAC/sand and anthracite/sand have been shown to remove BDOC at similar rates (Huck et al., 2013), however Emelko et al (2006) found that GAC had higher BOM removal at low (≤ 10 °C) temperatures than the sand and/or anthracite filters.

Backwashing is a cleaning step where accumulated particulate matter and excess biofilm is removed while maintaining the integrity of the biofilm itself (Juhna & Melin, 2006). Regular backwashing is important to maintain effluent quality and to minimize headloss, which increases with filter run time and excessive biological growth (Evans et al., 2013). The practice of backwashing has been shown to rejuvenate BOM removals impacted by accumulated material (Prevost et al., 1995; Liao et al., 2015), and therefore proper backwashing will not deleteriously affect BOM removal (Huck et al., 2013). In order for BOM removal to be negatively affected by backwashing, biofilm removal would need to be in excess of 60% (Hozalski & Bouwer 2001a,b); similarly Liao and colleagues (2015) found that 50% of biomass (as phospholipid fatty acid) could be removed with no effect on performance, with a recovery of biomass to pre-backwash levels as quickly as 2 days later. Several factors have been investigated in backwashing procedures and they include chlorination, air scour, flow rate, and bed expansion (Urfer et al. 1997). Current BF_{wp} backwashing best practices for downstream membrane filtration would include the use of air scour with sub-fluidization velocities which create collapse pulse conditions (Amirtharajah, 1993), followed by 50% bed expansion (Wilson, 2015). Given that biomass adheres to filter media more strongly than inorganic particles, a high amount of shear stress is required for the removal of excess biomass so that effluent quality is maintained (Juhna & Melin, 2006). This underscores the need for tailored backwashing procedures for any given treatment facility.

Lower temperatures result in lower BOM removals, as microbiological enzyme kinetics, also known as biomass activity, become depressed (Juhna & Melin, 2006; Laurent et al., 1999; Urfer et al., 1997). Surprisingly however, no relationship has been found between

temperature and biomass (ATP) content in dual-media biofilters (Pharand et al., 2014; Rahman, 2013). This makes temperature an important factor controlling BOM removal, while its effect on biofilm dynamics is poorly understood. A detailed discussion on temperature is provided in Section 2.5.

Lastly, percentage biofilter removal of BOM is proportional to the influent concentration and therefore it is considered a first order process (Huck et al., 2013), where mass transfer is not limiting. Zhang and Huck (1996) demonstrated that mass transfer was not limiting for AOC removal under drinking water conditions. In addition, increases in hydraulic loading (velocity) for a fixed EBCT were unable to increase BOM removal rate (Urfer et al., 1997). Soluble BOM therefore is likely to possess good biofilm penetration abilities; when considered alongside the thin volume of a drinking water biofilter media biofilm, this observation seems sound. Although backwashing contributes to the removal of excess biomass, it is basically the lower nutrient levels in drinking water compared to a wastewater which result in a relatively thin biofilm. In addition to BOM, inorganic nutrients such as ammonia, nitrate, nitrite and ortho-P have been identified as important for bacterial growth and biofilter performance; in bench-scale research, nutrient additions are usually applied in a C:N:P ratio of 1:10:100 (Evans et al., 2013; LeChevallier et al., 1991). Biofilms in drinking water treatment are usually carbon limited, however in certain circumstances where a high BOM content is observed, P-limitation may exist (Yu et al., 2003). Lauderdale et al. (2012) claimed that addition of phosphoric acid and liquid ammonium sulphate to pilot scale biofilters showed a 15% decrease in terminal headloss (relative to control) with improvements in DOC removal, which they attributed to the >30% increase in biomass coupled to a >30% decrease in EPS. In contrast, Azzeh and colleagues (2015) found no improvement to biofilter headloss and performance (DOC and biopolymer removal) upon addition of phosphoric acid and ammonium chloride; in fact a decrease in performance was observed when nutrient addition was increased to 100:40:20. The authors attributed their results to possible BOM-limited conditions within the source water. Rahman et al. (2016) observed that biofilters fed a riverine source water designated as P-limited did not exhibit changes to biomass, activity or performance when dosed with K_2PO_4 . This indicates a need

for more sensitive measurements of BOM to be used to ensure biodegradable levels of C are accurately assessed.

2.1.4 Metrics for Evaluation of Biofiltration Performance

Aside from head loss build-up and filter run length time, biofilter performance can be separated into particle removal vs biological performance when particle and BOM removal are sought within a single stage system (Urfer et al., 1997). Conventional performance can be indirectly assessed by measuring turbidity as a surrogate for particle removal, while the assessment of BOM removal is decidedly more complex. Although DOC removal is often used as a metric for biological performance, more appropriate techniques exist for the measurement of biodegradable fractions in water and their removals via biofiltration.

Water contains natural organic matter (NOM) which is a heterogeneous mix of dissolved and particulate products from the chemical and biological decomposition of plant, animal and microbial biomass (Thurman, 1985). The specific chemical composition of NOM in water can be very complex and is usually unknown (Uhl, 2008). The majority of NOM is composed of recalcitrant humic substances which make up around 50% of DOC (Thurman, 1985), with the rest being composed of carbohydrates, proteins, amino acids, lipids and transphilic acids (Metsämuuronen et al., 2014). Although DOC removals can be used for measuring biofiltration performance, these removals are low as DOC contains recalcitrant as well as labile NOM. Given this complexity it wasn't until the 1980's that tests which could more closely assess BOM and the regrowth potential in raw water were created (Uhl, 2008). BOM is therefore typically measured as assimilable organic carbon (AOC) or biodegradable dissolved organic carbon (BDOC) (Uhl, 2008). BDOC is the fraction of NOM which can be mineralized by heterotrophic biomass, while AOC is the fraction of NOM that results in microbial growth (Huck, 1990). The BDOC method involves biofilms grown on a support media, which in addition to utilizing easily biodegradable compounds are also able to hydrolyse larger polymeric molecules via biofilm embedded exoenzymes; therefore in comparison with AOC, the BDOC method should be able to detect a greater range of organics than the easily metabolized fractions involved in AOC (Persson et al., 2006). The

classic AOC-P17/NOX method measures the regrowth of two pure culture inocula in a water sample, and targets easily biodegradable low molecular weight compounds. AOC is measured as $\mu\text{g/L}$ acetate-C equivalents and typically comprises between 0.1 - 9.0% of TOC (Escobar et al. 2001). The type of BOM metric used would depend on the application; for example AOC would be used for bacterial regrowth potential and BDOC would be used for chlorine demand or DBP formation potential (Huck 1990).

The latest AOC technique utilizes flow cytometry to rapidly count fluorescently stained autochthonous cells incubated in the test water; compared to the older plate-count method, this new AOC technique is much faster, less labour intensive and uses the test water's natural microbial consortium (Hammes & Egli, 2005). As well, these methods may be able to measure a broader range of BOM. Recent work by Elhadidy et al. (2016) used a natural inoculum AOC method that measured regrowth using flow cytometry. This study found that the method could measure the removal of both high molecular weight biopolymers and low molecular weight acids. In addition, (van der Kooij, 2015) proposed adding a third type of bacterial inoculum to the AOC-P17-NOX method that could measure removal of high molecular weight BOM. Though AOC and BDOC are "complimentary but not exclusive" (Frias et al 1995), Escobar et al. (2011) aptly depict BDOC as a "hydrolyzable pool of carbon available for AOC formation".

An innovative NOM analysis platform which has recently been introduced to the study of drinking water and biofiltration is LC-OCD (liquid chromatography - organic carbon detection) (Boon et al., 2011; Chen et al., 2016; Halle et al., 2009; Huber et al., 2011). In natural waters, fractionation of NOM by LC-OCD typically detects 5 groups with different susceptibilities to biodegradation (biopolymers, humic substances, humic building blocks, low molecular weight acids, and low molecular weight neutrals). Biofiltration is adept at removing the majority of the biopolymer fraction, which includes proteins and polysaccharides (Halle et al. 2009), while humic acids, which compose most of NOM, are fairly recalcitrant and typically exhibit lower removals (10 to 15%) by biofiltration (Chen et al., 2016). Humic building blocks and low molecular weight acids and neutrals are generally more biodegradable than humic substances, however mixed results are often encountered which could be due to changing compositions of these fractions (Chen et al., 2016; Elhadidy

et al., 2016). Huber and colleagues (2002) found that biopolymers and low molecular weight acids were significantly removed from surface water following biological sand treatment, while Elhadidy and colleagues (2016) found both biopolymers and low molecular weight acids to be readily biodegradable. Chen et al. (2016) found biopolymers were readily removed by biofiltration, while humic substances and low molecular weight neutrals were only partially removed, and finally observed no trends for building blocks and low molecular weight acids. Biopolymers are especially important for membranes as this fraction of NOM has been shown to be associated with biofouling of low (Halle et al., 2009) and high (Elhadidy, 2015) pressure membrane filtration. High pressure membranes are particularly susceptible to biological fouling, and given that low molecular weight compounds can, depending on feed water, be highly biodegradable, their removal by biofiltration is also important. The LC-OCD method is not as sensitive to low molecular weight fractions as AOC methods, and therefore a combination of approaches could be valuable for accurate measurement of NOM removal.

2.2 Nanofiltration Membranes in Drinking Water Treatment

2.2.1 Overview

Membrane filtration uses thin, semi-permeable membranes to separate fluids, gases, particles or solutes. Water is purified as it passes across the membrane when solutes are rejected, primarily by size exclusion or electrostatic repulsion (Hilal et al., 2004) as a minimum transmembrane pressure (TMP) facilitates transport of water across the membrane thickness. Generally, the smaller the pore size (specified as the molecular weight cut-off), the more pressure required to produce permeate (Thorsen & Flogstad, 2006). Therefore nanofiltration (NF) and reverse osmosis (RO) membranes require higher pressure when compared to micro and ultrafiltration. NF membranes possess rejection characteristics in between those of ultrafiltration (UF) and RO. NF is used to remove hardness (multivalent salts) and organics (DBP precursors, pesticides, colour and emerging contaminants) and have a molecular weight cut-off as low as 200 - 400 da (Fonseca et al., 2007; Hilal et al., 2004). Due to its lower operation pressure and higher flux, nanofiltration has frequently been used

as a pretreatment for reverse osmosis membranes (Hilal et al., 2004). Nanofiltration membranes are constructed from synthetic organic polymers, usually 0.2 mm thick, held by a thicker support medium on the permeate side. The most popular membrane materials are thin film composite, polyamides, regenerated cellulose and cellulose acetate deposited on a mechanical support such as polysulphone or polyethersulphone (Shon et al., 2013; Thorsen & Flogstad, 2006).

2.2.2 Nanofiltration Membrane Fouling

Decline in membrane functionality is due to fouling of the membrane surface and in some cases pores, which either reduces flux or increases transmembrane pressure (TMP). This process can include particulate (deposition of particles and colloids), inorganic (scaling of SiO_2 , $\text{Fe}(\text{OH})_3$, CaCO_3), organic (NOM deposition) and biological fouling, the latter of which is the proliferation of a microbial biofilm on the membrane surface, being described as the “Achilles heel” of membranes (Flemming et al., 1997; Vanysacker et al., 2014). Fouling of NF membranes is dependent on the type of foulant molecule, its charge, the charge of the membrane, pH and ionic strength of solution, as well as membrane surface roughness (Hilal et al., 2004). In strict terms, reversible fouling is defined as that which can be resolved with backwashing and or chemical treatment while irreversible fouling cannot be remedied; however, irreversible fouling can also be defined as material that can only be removed by chemical cleaning (Vanysacker et al., 2014).

2.2.3 Biofouling of Nanofiltration Membranes

Biofouling is especially difficult to remedy; it is operationally defined as an increase of transmembrane resistance due to biofilms and can impact permeate quality and increase operation and maintenance costs (Dreszer et al., 2013; Hu et al., 2005). The formation of the biofoulant layer has been shown to be a distinct process and is not due to the bulk compaction of feed material, but is caused by growth of bacterial communities which are quite different from those of the bulk liquid (Vanysacker et al., 2014). Besides increasing TMP, additional effects of biofouling are degradation of membrane glue lines, particulate deposition into EPS and scale precipitation (Dreszer et al., 2013). The increase of high

pressure membrane TMP from biofilms is due mostly to increases in concentration polarization which the biofoulant promotes (Dreszer et al., 2013). Nanofiltration membranes incur concentration polarisation, where increases in nutrients on the feed side of the membrane lead to increased biofilm growth which in turn increases concentration polarization; this positive feedback loop is known as the biofilm enhanced osmotic pressure (BEOP) effect (Chong et al., 2008; Herzberg & Elimelech, 2008). The BEOP effect has been shown to contribute 70% of TMP increase in RO membranes under laboratory conditions; furthermore higher flux levels (and their associated increases in concentration polarisation) lead to faster biofilm development (Chong et al., 2008).

Factors affecting biofouling are membrane material, configuration (dead end vs cross-flow), hydrodynamics, temperature, pH and feed BOM concentration (Hu et al., 2005; Vanysacker et al., 2014). The charge or zeta potential of the membrane surface can participate in solute rejection (Shim et al., 2002), and also inhibit biofouling via electrostatic repulsion. Hydrophobic membranes exhibit greater colonization (Pasmore et al., 2001), while membranes with negative zeta potentials are more resilient to biofouling (Fonseca et al., 2007). This phenomenon is likely due to the formation of a larger hydration layer on the membrane surface which acts like a barrier to adhesion, however it has proved extremely difficult to develop materials that are outright immune to bacterial cell attachment (Simões et al., 2010). However, once biofouling is advanced, original surface materials may be masked (Flemming et al., 1997). Flux is also an important operational consideration in biofouling. Increases in flux from 20 to 100 L m⁻¹h⁻¹ resulted in increased membrane resistance but decreased biofilm thickness (Dreszer et al., 2013). The most important factors in biofouling however have been identified as nutrient concentrations and shear forces (Flemming et al., 1997).

2.2.4 Biofouling Control

In the 1990's, the two most prevalent strategies to prevent biofouling were the physical removal of bacteria via pretreatment or the inactivation of bacteria via biocides, oxidants and irradiation. However, more recent approaches include nutrient limitation and membrane material modification (Vrouwenvelder et al., 2009). Common approaches to

mitigate biofouling include the application of a tangential shear force, backwashing, and cleaning via biocidal agents (Zhang et al. 2006). The destruction of bacterial cells via biocides is limited in its efficacy as the cell debris and EPS are still present on the membrane after chemical treatment; these remnants contribute substantially more to flux decline and act as BOM for rapid regrowth (Dreszer et al., 2013; Flemming et al., 1997). A promising mitigation strategy in biofouling reduction is nutrient (C, P or N) starvation, as total inhibition of biofouling is not likely. This can be achieved via biofiltration (Dreszer et al., 2013; Fonseca et al., 2007; Hu et al., 2005).

2.3 Biofilms in Drinking Water Treatment

2.3.1 Introduction to Biofilms

Biofilms can be defined as communities of bacteria attached to a surface, or more technically as aggregates of bacteria and their extracellular polymeric substances (EPS), which grow at phasic interfaces (Flemming & Wingender, 2010). Biofilms confer distinct advantages compared with planktonic (free living) strategies; these benefits include increased resistance to a multitude of stressors including nutrient, pH, redox, and moisture fluctuations, antibiotics and predation (Costerton, 1995; O'Toole et al., 2000). The architecture of mixed species biofilms contains pores, channels and voids which allow for penetration of nutrients and removal of wastes in an advective and diffusive manner, which ultimately results in convection currents within the biofilm that further facilitate mass transport (Costerton et al. 1995). The majority of biofilm mass (90%) is not attributed to the bacterial cells, but rather the EPS (Flemming & Wingender, 2010). This massive investment in EPS production by the bacteria ensures that the cells will remain immobilized, providing a three dimensional structure within which cell-cell chemical communication (quorum activity) can occur (Flemming & Wingender, 2010). This quorum sensing allows within the community a cooperative response to environmental changes, leading some authors to call this activity a “primitive homeostasis” resemblant of more advanced eukaryotic tissues (Costerton, 1995).

2.3.2 Extracellular Polymeric Substances

EPS has many functions within a biofilm and at their core is composed of the four biological macromolecules: polysaccharides, nucleic acids, proteins and lipids; an exception to these would be humic substances, which are not endogenously produced and can be adsorbed into the biofilm EPS matrix from the bulk liquid (Flemming & Wingender, 2010). Several macromolecular types are encountered in an aqueous environmental biofilm, performing a given function via synergy; for example structural integrity is often a result of the interactions of a base polysaccharide-DNA matrix linked together by lectins and other proteins (Flemming & Wingender, 2010). Most exopolysaccharides in a biofilm are heteropolymers (both neutral and charged), and are frequently polyanionic; this negative character enables many exopolysaccharides to engage in adhesion to negatively charged surfaces by way of divalent cation bridging (Flemming & Wingender, 2010). EPS also serves in trapping nutrients from the bulk fluid, allowing exoenzymes to hydrolyse large or recalcitrant organics into a soluble form more favourable for transport across bacterial membranes. These embedded enzymes can also ameliorate oxidative stressors (reduction of O₂ via cytochromes) and acquire nutrients (corrosion of steel via hydrogenase) by way of redox reactions at the periphery of the matrix (Beech & Sunner, 2004). In short, the best way to interpret the vast array of exoenzymes within the biofilm matrix is to regard them as an “external digestive system” (Flemming & Wingender, 2010).

2.3.3 Biofilm Development

In general, the ability of a surface to grow biofilms is determined by roughness, hydrophobicity, and surface conditioning. Given the genetic diversity inherent in bacterial communities, practically any surface can be colonized under the right conditions (Simões et al., 2010). A multitude of different environmental signals can cause a cell to convert from a planktonic phenotype to an adhering sessile one. Depending on the given species, these signals can be amino acids, oxygen levels, temperature, osmolarity, pH, Fe, etc. (O’Toole et al. 2000). A prediction of a cell’s ability to attach to a given surface cannot reliably be made by judging the cell’s overall charge or zeta potential, as bacterial cell surfaces contain a variety of surface components with different charges, and these can change in response to

the environment. Furthermore depending on the surface and bulk fluid characteristics, a single species can produce different biofilm types by way of different signal pathways: for example *V. cholera* possesses at least three different pathways for biofilm formation, depending on whether it is within a human versus shellfish host or simply in an aquatic environment (Toole et al., 2000). Tariq et al. (2012) however found that *E. faecalis* cultures expressing a heterogeneous zeta potential were more successful at biofilm formation than homogeneous serotypes.

The first step in biofilm development is the conditioning of the surface to be colonized, and typically involves adherence of organic molecules such as glycoproteins and proteins (sometimes referred to as the pellicle) to the surface (Toole et al., 2000). These conditioning molecules can effectively change the chemistry of the surface regardless of the material underneath (Vanysacker et al., 2014). Following some level of conditioning, a cell must engage in surface recognition and attachment. Several different cell-surface structures can be used in this process, including lipopolysaccharides, pili and even flagella (O'Toole et al., 2000; Palmer & White, 1997; Reisner et al., 2003). Attached cells then divide to produce a monolayer upon the surface while initiating EPS production, eventually producing microcolonies (Palmer & White, 1997; Toole et al., 2000). Depending on genetic potential, these microcolonies will further expand to produce a multispecies consortium with superstructure voids, channels, pillars and mushroom-like shapes (O'Toole et al., 2000; Reisner et al., 2003). This stage is known as "maturation" (Palmer & White, 1997). Lastly, mature biofilms detach aggregates which may participate in seeding downstream surfaces (Vanysacker et al., 2014). Cell/aggregate detachment and dissemination is achieved by shear forces, but also endogenously by EPS-cleaving enzymes (such as alginate lyase in the case of *P. aeruginosa*) and the reversion of sessile phenotypes to the planktonic form; the triggering signal associated with this stage is assumed to be depletion of local nutrients (Toole et al., 2000). It should be noted that none of these processes are regarded as stochastic, and have been shown to be highly regulated and involving multiple gene loci (Toole et al., 2000). Such processes commonly involve quorum sensing mechanisms, and in fact the commercialization of quorum molecules has already begun, with companies such as BioSol

(Cheltenham, Australia) claiming to stimulate reversion of sewer biofilms to detached planktonic phenotypes.

2.3.4 Biofilter Biofilm Ecology

2.3.4.1 Ecology Overview

Biofilm communities are typically highly heterogeneous and can include an array of metabolisms, including both lithotrophic and heterotrophic organisms. In the environment it is rare to find a single species biofilm. The cells in a biofilm are phenotypically distinct from their planktonic counterparts; this “phenotypic plasticity” is a drastic shift in gene expression and is in part what makes biofilms so successful as the preferred mode of growth for bacteria in aqueous environments (Costerton, 1995; Palmer & White, 1997; Toole et al., 2000). Furthermore a single species is capable of differentiating into several different phenotypes, each with a specific task (sporulation, acquisition of nitrogen, chemotaxis) in order to increase the overall fitness of the population (Claessen et al., 2014). Interspecies co-metabolism has also been observed (Toole et al., 2000). Thus biofilms can be highly cooperative, exhibiting division of labour and recycling of waste and cell debris. In fact primitive junctions allowing direct molecular exchange (called septosomes or crosswalls) have been observed between certain pure culture aggregates; however due to their nature biofilms are also a highly competitive environment where exploitation and biocidal exclusion can also take place (Claessen et al., 2014). Biofilm bacterial communities, whether in membrane filtration systems or in dental plaque, regularly undergo succession where the community composition changes as communities mature and the matrix volume increases (Bereschenko et al., 2010; Palmer & White, 1997).

2.3.4.2 Biofilm Biomass Abundance

Biofilter biomass concentrations have been reported to be between 1×10^{10} and 5×10^{11} cells/cm³ in the top few centimetres of sand/anthracite biofilters as measured by total direct cell counts (TDCC) (Hallé et al., 2009) and back-calculation using ATP data (Lautenschlager et al., 2014), while 5×10^{10} to 1×10^{13} cells/cm³ were reported for GAC biofilters using confocal laser scanning microscopy (CLSM) (Gibert et al., 2013). There is disagreement within the literature as to if and how much biomass decreases along depth of

the biofilter (Pharand et al., 2014), with some authors reporting no decrease (Halle, 2009; Lautenschlager et al., 2014) and others reporting more pronounced reductions in biomass associated with depth (Gibert et al., 2013; Liao et al., 2013a; Rahman, 2013; Urfer & Huck, 2001). These data could be affected by BOM levels and biodegradability, as well as temperature, backwashing type and frequency, maturity of the biofilter, media type, upstream treatment processes and the method of biomass quantification used (Gibert et al., 2013; Lautenschlager et al., 2014; Pharand et al., 2014). Biomass has been shown to increase with higher influent temperature, higher DOC, longer EBCT and upstream ozonation (Lautenschlager et al., 2014; Pharand et al., 2014), although Liao et al. (2013a) presented evidence that increased EBCT lead to decreased biomass. Cell density usually stabilizes near 100 days of operation and is aided by the practice of backwashing (Gibert et al., 2013). One study of a GAC biofilter found significant differences in biomass stratification initially, but after 200 days of operation this stratification disappeared as media colonization extended into the depth of the biofilter (Gibert et al., 2013). Although biomass levels can vary with depth and acclimation, the amount of biomass within a biofilter does not predict the removal of DOC (Pharand et al., 2014; Urfer et al., 1997).

2.3.4.3 Biofilm Community Dynamics

A variety of methods are available to assess process microbial community dynamics, with most modern methods relying on nucleic acids (RNA & DNA) extracted from feed, media and effluent samples. Many DNA based methods are built on the amplification of template DNA using polymerase chain reaction (PCR), where molecular probes known as primers are used to target and amplify conserved regions of DNA to glean taxonomic or functional information from individual populations or the entire community. PCR based methods are fast, relatively cheap, and highly discriminatory (Hagedorn et al., 2011). A wealth of taxonomic information regarding biofiltration bacterial communities has been gained through the use of genetic fingerprinting and sequencing techniques; among these methods, denaturing gradient gel electrophoresis (DGGE) and next generation sequencing (NGS) have become the most popular. NGS platforms such as Roche 454 and Illumina have made vast improvements to the taxonomic understanding of biofilter microbial communities and provided insights to the major phyla present. High diversity and an absence of a core

biofiltration consortium appear to be a common finding across the literature (Kaarela et al., 2014; Lautenschlager et al., 2014; Liao et al., 2013a; White et al., 2012); in other words, identification of a core microbiome between all or most biofilters is unlikely. Meanwhile, fingerprinting techniques such as PCR-DGGE have provided important insights into the dynamics of microbial community structure and diversity during start-up and across operational conditions (Boon et al., 2011; Fonseca et al., 2001; Yang et al., 2011).

Studies on biofiltration community analysis have reported significant differences between a given biofilter's media and effluent communities using pyrosequencing, with the latter exhibiting higher species richness and a taxonomy dominated by Proteobacteria (Lautenschlager et al., 2014). Boon et al. (2011) found that biofilter community dynamics and species richness were low in the upper reaches of a pre-ozonated biofilter media bed and increased with media depth; the authors concluded that greater process function could be attributed to higher community richness and evenness (high evenness in this context being lack of a dominant species). Another study using a GAC biofilter fed ozonated and chemically filtered water reported that although biomass stability had been achieved after six months of operation, the community was still undergoing large shifts at the genus level, which began to stabilize at the 12 month mark when the study ended (Liao et al., 2013a). Several studies have investigated the taxonomic identities of biofilter bacterial communities, and no evidence of pathogenic contamination of filter media has been reported (Gibert et al., 2013; Lautenschlager et al., 2014; White et al., 2012).

Since there exists a growing body of work presenting taxonomic observations within biofiltration and this work is indirectly related to the current work, a brief review of the major and important taxonomies of biofiltration is provided below. The most dominant phyla observed across two separate studies of pre-ozonated biofilters were Proteobacteria, Acidobacteria, Planctomycetes and Bacteroidetes. The most abundant of these was Proteobacteria, with α -Proteobacteria the most common; the *Sphingomonas* and *Bradyrhizobium* genera were the most abundant of this class (Lautenschlager et al., 2014; Liao et al., 2013a); other studies (which include BF_{wp}) have also shown Proteobacteria to be the dominant biofilter phylum (Liao et al., 2013b; Zeng et al., 2013). The α -Proteobacteria are a slow growing oligotrophic class of bacteria capable of degrading recalcitrant humic

substances (Newton et al., 2011), and could be a fulcrum group for DOC degradation in biofilters (Liao et al., 2013a). The *Sphingomonas* and *Bradyrhizobium* genera have been shown to be adept at degrading several different types of toxic organics (Liao et al., 2013a), and *Sphingomonas* in particular has been implicated as a pioneer colonizer of RO (Bereschenko et al., 2010; Gutman et al., 2014). Interestingly Actinobacteria, a dominant phylum in the freshwater systems of source water, was not observed in secondary GAC biofilters (Lautenschlager et al., 2014), however in direct biofiltration (with no pre-ozonation), hyphae-like Actinobacteria were observed via confocal laser scanning microscopy (CLSM) (Gibert et al., 2013). This shows that upstream processes shift biofilter communities at the phylum level. In fact, Moll and colleagues (1998) found that the use of pretreatment with ozone shifted the bacterial community structures in pilot scale biofiltration units.

Changing nutrient concentrations can also affect biofilter ecology by shifting the community structure (Lautenschlager et al., 2014; Liao et al., 2013a). Liao and colleagues (2013b) proposed that a high variability in α , β , and γ -Proteobacteria between biofilters fed different influent water was due to differences in ammonia, with the ammonia oxidizing phylum Nitrospirae becoming more abundant with increases of influent ammonia to 1.11 mg/L.

2.3.5 High Pressure Membrane Biofoulant Ecology

Membrane biofoulant bacterial communities are dynamic and persistent; their community structures have the ability to rapidly adapt to physical and chemical changes in their environment so that key components of the community may survive. Any biofoulant control strategy, whether its functional properties arise from chemical oxidation, hydrodynamic scouring, or nutrient limitation from pre-biofiltration, will stress the microbial communities in the receiving biofilm. How these communities adapt to such environmental perturbances is of interest because such knowledge can aid in developing better biofoulant control strategies. Furthermore, ecological comparisons of biofilter and high pressure membrane filter bacterial communities can provide insights for better management of diversity, biomass and EPS within each system.

Biofoulant communities have a lot in common with biofilter consortia in that they are very dissimilar to the planktonic communities of the feed. For example within wastewater membrane bioreactors, biofilm communities were dominated by *proteobacteria* (Lim et al., 2012; Zhang et al., 2006), and were significantly different from planktonic communities. Like biofiltration biofilms, the bacterial communities of NF biofouling are dominated by the subphylums α -*proteobacteria* (Ivnitsky et al., 2007; Bereschenko et al., 2010) and sometimes β -*proteobacteria*. In addition to nutrient contents in the feed, biofilm age (maturity) as well as the amount of hydrodynamic shear can affect which subphylum is dominant, thereby resulting in biofoulant community shifts (Al Ashhab et al., 2014) which raises the possibility that backwashing can exert an effect on biofilter media communities. Indeed, one study observed hydrodynamic shear from backwashing resulted in a shift in bacterial community structure, which reverted to pre-backwash structure over the course of 2 to 5 days (Liao et al., 2015). Bereschenko and colleagues (2011) report bacterial community shifts on RO membranes as early as 5 days into a non-cleaned cycle compared to day 1; furthermore, they observed bacterial cells from a variety of subphyla still present the day after control membranes received chemical cleaning, albeit with collapsed biofilm structures and no visible EPS surrounding the individual cells as determined by CLSM and scanning electron microscopy (SEM). Similarly, Calderon and colleagues (2011) found that after cleaning an anaerobic membrane bioreactor with NaClO, a basal community of *Methanosaeta* archaea and *Sphingomonas* were not removed. This shows that biofilms, whether present as a foulant layer on nanofiltration membranes or on biofiltration media, are highly sensitive to both physical and chemical changes in their environment and frequently shift community structures in response. This sensitivity is not a sign of weakness, but a protean capacity to bring forth the consortium's under-utilized metabolic potentials during periods of stress in order for the microbiome to persist; such a potential likely increases with diversity (Read et al., 2011). Therefore the high diversity of most environmental biofilms acts as a reservoir of metabolic redundancy that can be called upon during times of stress. This can help explain the persistence of biofilms and their difficulty to remove within industrial processes. Therefore it is clear that the strategy of intermittent doses of biocide can never be perfected in that community regrowth and succession begins almost immediately after dissipation of biocide residual. This is why, from the perspective of microbial ecology, chronic nutrient

limitation would be the preferred agent of fouling mitigation as the system will simply not possess sufficient electron donors to support a robust biofoulant community.

2.4 Biofiltration as Membrane Pretreatment

Biofiltration without preceding coagulation or ozonation has been investigated as a pretreatment for both low and high pressure membranes treating a variety of source waters. Lower fouling rates are observed when biofiltration is used as a pretreatment for ultrafiltration, primarily due to the removal of biopolymers (Azzeh et al., 2015; Halle et al., 2009; Rahman et al., 2014; Siembida-Lösch et al., 2015). Over the years, biofiltration has also been recommended by the wider scientific community as a pre-treatment to reduce membrane biofouling given that the process efficiently removes BOM (Fonseca et al., 2007; Flemming et al., 1997; Naidu et al., 2013; Persson et al., 2006; Shon et al., 2013; Vrouwenvelder et al., 2009). Griebe and Flemming (1998) successfully demonstrated that biofiltration can reduce biofouling of high pressure membranes and does not serve as a source of bacterial contamination providing proper backwashing is performed. Similar encouraging conclusions have been reached by others using biofiltration as a membrane pretreatment for a variety of applications including treating groundwater for RO (Weng et al., 2015), synthetic humic-laden water for NF (Mosqueda-Jimenez & Huck, 2009), and UF filtered surface water for RO (Brouwer et al., 2006).

2.5 Effect of Seasonality on Biofiltration

Seasonality can be described by several means, and for the purposes of biofiltration the discussion should involve seasonal fluctuations in water quality parameters, temperature and their effects on biofilter performance and ecology. Using the above definition, investigations regarding the effect of seasonality on biofiltration performance, biomass and microbial communities remain scarce. In temperate climates, feed water temperature varies by more than 20 C° over the course of a year, and this can have profound

effects on biofiltration performance. Laurent and colleagues (1999) used a radio-labelled glucose respiration method to measure biofilter biomass activity at different temperatures. Activity was found to decrease by 60 to 77% when feed temperature was lowered from 25 °C to <10 °C. This information was used in model calibration which predicted decreases of BDOC removal by about half over the same temperature range. Conversely, Pharand (2015), using fluorescein diacetate (FDA), found activity remained stable over high and low (< 10 °C) temperatures using. Nonetheless it is well established that temperature is a key factor in determining biofilter performance at a given EBCT (Basu et al., 2016; Evans et al., 2013; Huck et al., 2013; Urfer et al., 1997). Persson et al. (2006) noted that while temperature affected biofilter activity and BDOC removal, feed BDOC concentration was more closely related to removals, citing first order kinetics to explain this observation.

Temperature plays little if any role in determining biofilter biomass as measured by ATP (Pharand et al., 2015; Rahman, 2013), however others have reported lower bacterial growth rates (Velten et al., 2011) and biomass levels (Moll & Summers, 1999) at temperatures below 15 °C. Similarly, bacterial community diversity and evenness have been reported as quite stable and independent of feed temperature variations (Kim et al., 2014; LaPara et al., 2015). For example, Kim et al. (2014) noted that large temperature decreases from September to December did little to affect community composition within the time period observed, but that a temperature increase from May to August did in fact result in changes to the composition; the authors concluded that while temperature could partially explain changes to community composition, it could not explain the observed changes to abundances or diversity. It is possible that temperature can alter biofilter communities insofar as it induces seasonal changes to water quality, wherein the community structure exhibits a delayed or lag response to due to the slower metabolic rates under these conditions coupled to gradual changes in the water quality.

Therefore in lieu of temperature, water quality parameters may be more likely to affect biofilter biomass and bacterial community structure, especially if seasonal fluctuations in surface water nutrient compositions are taken into account. Certain nutrients, like AOC, ortho-P and ammonia-N would be expected to affect biofilter media bacterial community structures due to their importance in bacterial metabolism (LeChevallier et al., 1991).

Furthermore, seasonal variation in surface water DOC composition is known to occur (Paul et al., 2012), which could subsequently select for different community compositions. For example Liao et al. (2015) noted changes in bacterial diversity and community composition were related to feed DOC and ammonia-N concentrations. Yang and colleagues (2011) observed higher $\text{NH}_3\text{-N}$ and AOC concentrations during wet seasons in an agriculturally impacted watershed due to higher river flows, but found that pre-ozonation and not raw feed ammonia concentration was the primary driver of biofilter microbial community structure. The authors also noted that a longer EBCT resulted in community differentiation deeper in the filter, however this was likely due to the attenuation of residual ozone in addition to consumption of labile BOM in the upper reaches of the filter, which in turn would provide the lower reaches with greater amounts of soluble microbial products. This elucidates a problem within the biofiltration literature, where many studies investigating biofiltration microbial dynamics utilize prior treatment such as ozone, which substantially alters feed water chemistry as well as downstream ecology. Indeed, seasonal fluctuations in surface runoff, algae growth, dissolved oxygen, nitrogen cycling etc. can all affect freshwater nutrient compositions and the microbial communities which rely on those inputs. Tatari and colleagues (2016) found that ammonia oxidizing bacteria (AOB) populations (as measured by qPCR) increased two orders of magnitude from cell densities of 10^{10} to 10^{12} cells/ m^3 media when ammonia loading was increased from 16 to 275 g $\text{NH}_4\text{-N}/\text{m}^3$, with AOB density decreasing with biofilter depth. Unfortunately, comparisons of increased nutrient (N and P) loading against both community composition and media biomass are scarce.

2.6 Research Gaps

2.6.1 Relationship between microbial ecology, biofilm dynamics and BOM removal performance within BF_{wp}

Most studies thus far have focused on characterising the taxonomy of biofiltration (Kaarela et al., 2015; Lautenschlager et al., 2014; Liao et al., 2013a; White et al., 2012) and have not proceeded to relate ecological characteristics such as diversity and community structure with BOM removal performance. Furthermore these efforts used pre-treated

influent (ozonation and/or chemically assisted settling), which can (individually) alter feed water chemistry and biofilm ecology (Moll et al., 1998). The measurement of media EPS is rare within biofiltration literature (Azzeh et al., 2015; Elhadidy, 2015; Mauclair et al., 2004) and an evaluation of the relationships between EPS, biomass and diversity has yet to be presented. Given its substantial presence in biofilter media and its effect on filter hydraulics, the relationship between EPS, biomass and community structure would be valuable in predicting process behaviour during process upsets and community shifts.

2.6.2 Impact of seasonal water quality fluctuations on BF_{wp} biofilm dynamics and community structure

Temperature (Evans et al., 2013; Laurent et al., 1999; Pharand et al., 2015) and nutrient concentration (Lauderdale et al., 2012; LeChevallier et al., 1991; Yu et al., 2003) can affect BOM removal performance of biofiltration. Given the significant variation of these parameters within the Grand River during the course of a year (GRCA, 2013) it is possible that they can affect biofilter community structure and diversity as well. The response of biofilter community ecology to seasonal water quality fluctuations has yet to be fully explored, with few investigations thus far (Kim et al., 2014; LaPara et al., 2015; Yang et al., 2011). More information is needed to assess changes in the community structure and diversity of BF_{wp} over seasonal time scales and which water quality parameters are most important for biofilter ecology.

2.6.3 Unexplored microbial community dynamics of nanofiltration membrane biofoulant pre-treated by biofiltration

Despite widespread use, high pressure membrane filtration has long suffered from problems of biofouling (Flemming et al., 1997). Yet there have been limited investigations into the microbial dynamics of the biofoulant (Gutman et al., 2014; Ivnitsky et al., 2007; Vanyacker et al., 2014). Biofiltration can be a viable pre-treatment method for high pressure membrane filtration (Griebe & Flemming, 1998) due to its reduction of feed nutrient concentrations. Yet if biofouling reduction through biofiltration is to be optimized, a thorough understanding of the microbial communities across these two processes is needed.

To date an investigation of this type (namely exploring the ecology of high pressure membrane biofouling and its relationship with the biofilms of upstream biofiltration) has not been performed.

2.6.4 Limited information on the dynamics of archaea within biofiltration and high pressure membrane systems

Limited investigations into the presence and role of archaea within drinking water biofiltration systems have been performed (Bai et al., 2013; Moll et al., 1998). Given the ubiquitous distribution of archaea in soil, marine and freshwater habitats, archaea are likely also present in BF_{wp} media. Information regarding their abundance, distribution and niche affiliation within BF_{wp} and nanofiltration membrane biofouling would expand the breadth of biodiversity observed within these processes and would complement bacterial investigations to better conceptualize and manage drinking water systems ecology.

2.7 Approach

Considerable effort has been given to optimizing biofiltration monitoring and operation, however the majority of this work has focused on the physicochemical aspects of the process, with investigations into biological mechanisms focussing mostly on biomass. Currently there is substantial evidence to suggest that biomass is not quantitatively related to performance after proper acclimation of the media (Boon et al., 2011; Emelko et al., 2006; Pharand et al., 2014) and that a substantial amount of biomass can be removed from the media during backwashing without negatively affecting BOM removal (Liao et al., 2015). Therefore a more nuanced approach is needed which can investigate the biological basis behind biofilter BOM removal performance. To this end, community profiling has been applied (Boon et al., 2011; Kaarela et al., 2015; Lautenschlager et al., 2014; Liao et al., 2015). These investigations have produced important insights into the richness, diversity and major subphyla involved, however they stop short of characterising biofilter community dynamics across annual variations in feed, and how these perturbations may impact both the communities involved and the performance of the process. Furthermore, a seasonal

dataset of biofilm EPS abundance and composition, and how this relates to biofilter communities and process performance, is lacking within the literature. The study of EPS, biomass, diversity and community structure has seldom been applied to the development of membrane biofouling (Bereschenko et al., 2010; Fonseca et al., 2007; Ivnitsky et al., 2007; Vanysacker et al., 2014) and a review of the literature has not identified an investigation which concomitantly examined all of these parameters; moreover the relationships between these parameters across two complimentary processes such as biofiltration without pretreatment and nanofiltration has yet to be established.

The current work addressed these shortcomings using a pilot scale biofiltration and nanofiltration plant at the Region of Waterloo's Mannheim Drinking Water Treatment Plant. The biofiltration pilot plant received significant upgrades by former NSERC Chair in Water Treatment students Ahmed Elhadidy and Brad Wilson (Elhadidy, 2015; Wilson, 2015). The PhD work of Dr. Elhadidy involved a characterisation of the biomass and EPS associated with biofilter media as well as novel EPS and biomass extraction techniques and evaluation methodologies. His work also assessed seasonal biofilter performance fluctuation and the associated response of media biofilm biomass, EPS, and physiological activity. Finally, Dr. Elhadidy investigated biofiltration as a pretreatment to bench scale nanofiltration membranes, and the effects which this had on biofoulant biomass and EPS. The current work builds on Dr. Elhadidy's efforts by providing molecular fingerprinting of microbial community structures for biofilter media across seasonal time scales and investigating how water quality variation impacts both the ecology and performance of biofiltration. Secondly, the current work describes the effects which biofiltration has on downstream nanofiltration biofoulant microbial community structures when used as a pretreatment, and how these ecological considerations reflect on membrane fouling and performance.

Dr. Elhadidy contributed archived samples of biofilter feed-water and effluent, cells extracted from biofilter media, and archived nanofiltration membranes from the months of October 2014 to February 2015. These samples were archived from his PhD research specifically for molecular community analysis at a later date, and provided the first 4 months of samples for analysis in the current work. In addition, the current work continued sampling biofilter feed water and media from May 2015 to November 2015, and to build

upon the archived samples by creating a time-series seasonal sample set to provide valuable information on biofilter community dynamics. Molecular analyses of community structure was performed by the polymerase chain reaction - denaturing gradient gel electrophoresis (PCR-DGGE) method, which is a method that is frequently used for molecular analysis of large sample sets. The method requires upstream genomic DNA extractions, followed by PCR amplification of a 16S rDNA gene target region. Biomass and extracellular polymeric substances (EPS) of the associated biofilm communities also examined, as well as biofilter removals of feed water DOC and NOM fractions. This study utilized molecular techniques for the examination of cellular and extra-cellular constituents of the biofilm matrix and related these uncommon process parameters to more conventional ones to identify improved operation and monitoring practices.

Chapter 3

A seasonal-scale investigation of biofilm dynamics and process performance in dual-media drinking water biofiltration with no prior treatment

3.1 Summary

Two dual media pilot scale drinking water biofiltration units with no prior treatment (BF_{wp}) were used to study bacterial community structure and its relationship with biofilter media biofilm dynamics and BOM removal performance over the course of 14 months. Polymerase chain reaction (PCR) was used with denaturing gradient gel electrophoresis (DGGE) to generate bacterial community profiles. Biofilter performance at several empty bed contact times was assessed by measuring the removal of dissolved organic carbon (DOC) and discrete fractions of natural organic matter (NOM) as determined by liquid chromatography – organic carbon detection (LC-OCD).

The feed water bacterioplankton were very dissimilar to the media biofilm community structure and possessed lower Shannon diversity and richness in comparison. The biofilm community structure of BF_{wp} underwent a shift in response to seasonal changes in water quality, which was accompanied by increased media biomass and EPS content and lower DOC and biopolymer percent removal during the winter of 2014/2015. Ammonia and the LC-OCD defined low molecular weight acids were shown by detrended correspondence analysis (DCA) to be the water quality parameters most responsible for the dynamic biofilm response. In addition to media biofilm community shift, decreasing feed temperatures and potential compositional changes in BOM served to impede biofilm biodegradation performance. Shannon diversity and community richness were shown to be stable irrespective of changing biofilm community structure.

Media biomass and EPS showed strong positive correlations with one another, and negative correlations with BOM removal performance; such parameters (ATP, cell count, EPS carbohydrates, EPS proteins and extracellular DNA) decreased with depth from 20 to 60 cm, while community structure, diversity and richness did not. Shannon diversity and richness of the biofilm were not associated with BOM removal performance. Within the media biofilm matrix, a protein to carbohydrate to eDNA ratio of roughly 6:3:1 was observed; however, during the water quality mediated biofilm community shift, a lower relative protein content was observed, which indicates that although temperature is the dominant factor controlling biofilter BOM removal performance, shifts in community structure and associated EPS composition may also affect the media's biodegradation abilities.

3.2 Introduction

With respect to nuisance natural organic matter (NOM), the purpose of biofiltration is to transform the biodegradable fraction of NOM to CO₂, biomass, and extracellular polymeric substances (EPS). In the absence of disinfectants, indigenous microorganisms suspended in the bulk flow of the feed water colonize biofilter media, and through cell-cell signalling produce dynamic biofilms (Lautenschlager et al., 2014; Simões et al., 2010). Several configurations exist for the use of biofiltration in drinking water treatment trains, with some of the more common designs involving biofiltration after initial treatment steps such as particle removal (coagulation, flocculation, sedimentation, filtration) and ozonation (Evans et al., 2013; Urfer et al., 1997). Biofiltration without pretreatment (BF_{wp} as defined by Huck et al. (2015) is intended to achieve particle and BOM removal from untreated water in the same stage. Many benefits are associated with biofiltration, chief among them are the production of treated water with lower biological regrowth and disinfection by-product (DBP) formation (Huck & Sozański, 2011). BF_{wp} also shows promise as an inexpensive pretreatment to reduce fouling of membranes such as ultrafiltration (Peldszus et al., 2012), nanofiltration (Elhadidy 2015a), and reverse osmosis membranes (Hu et al., 2005).

Assessing biofilter microbial ecology is an important endeavour as information regarding composition, community structure, richness, diversity and taxonomic sequences could offer insights into potential novel operation and management practices (Kaarela et al., 2015). Biofilter ATP is currently the most common method for measuring biofilter biomass, but other methods include total direct cell counts (Magic-Knezev & van der Kooij, 2004), heterotrophic plate counts (Hammes & Egli, 2010), and cell membrane phospholipid concentration (Emelko et al., 2006). Some studies report biofiltration biomass levels decreasing with depth (Gibert et al., 2013; Pharand et al., 2014; Urfer & Huck, 2001; Velten et al., 2011; Elhadidy 2015a), whereas others report no change with depth (Fonseca et al., 2001; Lautenschlager et al., 2014). Where biomass decreases occur, it is reasonable to consider that biodegradation in the upper parts of the filter has led to measurable decreases in substrate concentration as a function of depth. In addition, the substrate components of lower biodegradability would form a greater percentage of the overall substrate concentration lower in the filter. Several other factors have been shown to influence filter biomass levels including upstream oxidation (Moll et al., 1998; Fonseca et al., 2001), backwashing (Fonseca et al. 2001, Emelko et al. 2006), temperature (Velten et al., 2011) and biofilter maturity (Gibert et al., 2013). Some of these observations are controversial as Pharand and colleagues (2014), in a review of published ATP data, as well as full-scale investigations (Pharand et al., 2015), showed that temperature, EBCT and backwashing did not affect biomass levels as measured by ATP, using feed temperature ranging from 3 to 28 °C, EBCT ranging from 26 to 51 min, and a backwashing regime that included 5.5 minutes of air scour, 3 minutes of 400 L/s low wash and 7 minutes of 800 L/s high wash using non-chlorinated water. These findings illustrate the need for better biological monitoring methods beyond bulk biomass values; as such, improved biological monitoring may show potential to infer and predict NOM removal so that process operation and management can be tailored to identify and achieve the upper limits of system performance.

Biofilter biofilm community structure investigation via electrophoretic profiling can elucidate population shifts due to seasonal, diel or other perturbations (Muyzer & Smalla, 1998). Biofilter community diversity and richness are generally considered to be quite stable whether ozonation is used or not (Liao et al., 2013; White et al., 2012); however the effects of

seasonal fluctuations in water quality and temperature on biofilter diversity are unclear. Microbial community profiling techniques such as denaturing gradient gel electrophoresis (DGGE) excel at assessing the diversity and temporal variation of microbial consortia when large numbers of samples are required yet are limited in that identification of populations requires laborious post-hoc procedures (Samarajeewa et al., 2015; Vaz-Moreira, Egas, Nunes, & Manaia, 2013). Small ribosomal subunit tag sequencing can identify the major groups of bacteria present, their community diversity statistics, as well as their organization, but at the expense of more sophisticated and costly equipment than electrophoretic profiling. Given that the motivation for this work was the relationships between biofiltration performance and microbial community dynamics (and not taxonomic identification), sequencing was not pursued. Boon and colleagues (2011) used DGGE to show that, within non-backwashed pilot scale GAC biofilters receiving ozonated water, there was an increase in community richness and evenness (measured as phylotype abundance and phylotype relative dominance, respectively) at increasing media depth, presumably due to the absence of residual oxidant which they hypothesized led to higher metabolic efficiency at greater depths. This led the authors to conclude that richness and community structure, not biomass as ATP, were the most important parameters determining DOC removal. Fonseca and colleagues (2001) found that community structure based on DGGE did not change with depth, however the addition of ozone caused significant community differentiation compared to a non-ozonated control. The high diversity typically encountered within biofiltration acts as a reservoir of functional redundancy in the face of process upsets (Boon et al., 2011; Fonseca et al., 2001; Lautenschlager et al., 2014; Liao et al., 2013a). However direct comparisons between biofilter performance and ecological parameters like diversity, community structure and EPS remain scarce. Therefore, a greater understanding in how biofilter ecology affects process performance is required.

Bacterial community fingerprinting requires that bacterial cells be extracted or concentrated from the environmental matrix in which they are found. Bulk DNA is then isolated from the sample and genes encoding a conserved sequence of the 16S ribosomal subunit are used as a molecular marker "tag". These marker tags are amplified several million times using polymerase chain reaction (PCR) which, when the copy number

becomes high enough, can be detected and used in downstream analyses. These 16S rDNA tags contain genetic information which can be used to separate genera, species and subspecies; however taxonomic information is not obtained using DGGE, different bacterial populations are referred to as phylotypes instead of species. After amplification of the target gene sequences using PCR, the amplicons are loaded into a poly-acrylamide gel which contains an increasing gradient of DNA denaturing chemicals. An electric current is applied, and as the amplicons migrate through the gel matrix, their double stranded DNA begins to denature and unwind, thereby retarding the amplicon's migration. An oligonucleotide clamp prohibits complete denaturation to single strands and the amplicon migration is finally halted. The location in the gel where a phylotype gene sequence stops migration is based on the melting point of the DNA fragment. The DNA bands are then visualized by staining with a fluorescent dye. Taken over the entire gradient, several populations of phylotypes can be discriminated and thus the community profile obtained. The presence, location and intensity of these phylotype bands are then used in downstream statistical analyses to compare communities over space and time (Muyzer et al., 1993).

The factors which affect biofilter NOM removal are generally regarded to be temperature, empty-bed contact time, backwashing, media type and size, and feed water quality (Basu et al., 2016; Urfer et al., 1997; Zhang et al., 1996). However the extent to which these factors may influence biofiltration performance depends on other factors such as biomass maturity (Boon et al., 2011; Velten et al., 2011), source water characteristics (Basu et al., 2016) and the presence and type of pretreatment (Fonseca et al., 2001). In addition, the relationship between biofilm biomass (including cells and EPS) and biofilter performance is also unclear. It has been postulated that excess biofilm, which includes EPS, can affect biofilter performance. Lauderdale (2012) found that strategies to control the formation of EPS in biofilters (through nutrient and peroxide dosing) improved hydraulic performance of the biofilters and maintained or increased microbial activity and DOC removal. Azzeh and colleagues (2015) similarly found peroxide led to decreased headloss when 0.5 mg/L H₂O₂ was applied, but decreased NOM removal at 1 mg/L. This improved functionality was attributed to peroxide oxidation of EPS (measured as proteins and polysaccharides), since lower EPS levels were observed in peroxide treated biofilters compared to control. The

authors further noted that peroxide addition below demand levels would add to the pool of biodegradable carbon via the oxidation of NOM and EPS, which could aid biofilm growth.

Seasonal effects such as temperature are known to affect biofilter NOM removals (Emelko et al., 2006; Laurent et al., 1999; Persson et al., 2006; Pharand et al., 2015), but this change is not reflected by biomass ATP (Pharand et al., 2015) or phospholipid (Emelko et al., 2006) levels. It is unknown if seasonal-related changes in NOM removal are exclusively the result of temperature-dependent enzyme kinetics as Laurent et al., (1999) suggest, or if changes in NOM properties and altered microbial community compositions also play a role. Therefore, the purpose of this study was to better understand the seasonal relationships between BF_{wp} process performance and media biofilm parameters such as bacterial community ecology, and biomass levels including EPS abundance and composition.

3.3 Materials and Methods

3.3.1 Biofilters

Pilot-scale sand-anthracite dual media filters were refurbished by Brad Wilson and Ahmed Elhadidy of the NSERC Chair in Water Treatment and commissioned in April 2014, with the media having undergone a prior 6 months of low flow pre-acclimation in a separate vessel operated in up-flow mode. This pre-acclimation used the same surface water and was initiated in the summer months of 2013 to take advantage of warmer feed temperatures to enhance biofilm growth. A schematic of the pre-acclimator can be found in the thesis by Wilson (2015). Two biofilter columns were used in the current study, each consisting of a 25.4 cm inner diameter clear PVC column. Biofilter A (BF(A)) contained 20 cm anthracite over 20 cm sand, while Biofilter B (BF(B)) contained 20 cm anthracite over 60 cm sand; a 5 cm layer of gravel occupied the bottom of both biofilters. The sand and anthracite media ratios were determined by the needs of previous pilot plant investigations. The filters were located at the Mannheim DWTP and fed using the same Grand River water as the full-scale plant's intake, which is affected by the activity of upstream dammed reservoirs, multiple wastewater treatment utilities, and various agricultural activities. The Mannheim DWTP extracts and holds river water in storage lagoons prior to use. At the pilot plant, the raw

water from the lagoons first passed through a roughing filter composed of 10 cm crushed gravel for reduction of turbidity spikes. The feed water was then pumped from the roughing filter to the biofilters using a centrifugal pump and passed through the filters by gravity. Flow rates were maintained with an electronic flow controller at 100 L/h (3.08 m/h) in the winter and summer (October 2014 – August 2015), and 50 L/h (1.54 m/h) in the autumn (September 2015 – November 2015). This meant BF(A) and BF(B) had empty bed contact times of 8 and 16 minutes in the winter and summer, which increased to 16 and 32 minutes in the autumn. The change in biofilter operation was required to accommodate the needs of another investigation. A detailed description of pilot plant flow controller and instrumentation setup can be found in the thesis by B. Wilson (2015), which includes the setup for continuous monitoring of pilot plant influent temperature and turbidity. Backwashing consisted of 3 min collapse-pulse air scour to remove particles and slough excess biofilm, followed by 10 min at 50% bed fluidization to expel backwash water. Backwashing was performed 3 times per week in the winter and summer period of the study, and twice per week in the autumn. A detailed backwash procedure can be found in **Appendix C**. The Region of Waterloo graciously provided plant influent water quality data from its full-scale DWTP operations at Mannheim, which includes dissolved organic carbon (DOC), pH, electric conductivity (EC), ortho-P, ammonia (NH₃), hardness (as calcium carbonate CaCO₃), and nitrate (NO₃⁻).

3.3.3 Sampling Protocol

Between October 2014 and November 2015, 11 sampling campaigns were completed over 14 months which yielded a total of 53 media and 11 feed water samples from the biofilter pilot plant. Sampling events from October 2014 to February 2015, were performed by A. Elhadidy. All sampling events from May to November 2015 were performed by P. Markin. No sampling was performed in November 2014, nor March and April 2015. Sampling took place 24 h after backwashing for all months except in July and August, where biofilters were in operation for 40 h before sampling because of issues relating to site access. In a study of full-scale biofilters that were also fed using the Grand River, biofilter biomass and activity levels were shown to remain unchanged throughout the filter cycle, therefore

time since backwashing would not be expected to alter the biofilm (Pharand et al., 2015). Furthermore Basu et al. (2016) presented several studies where proper non-chlorinated backwashing did not affect biofilter performance, however this may not be the case for all systems as Liao et al. (2015) noted changes to biofilter biomass levels (as nmol-P) for 5 days following backwashing. Feed water was sampled downstream of the roughing filter before it entered the biofilter columns in 1 L DOC clean glass bottles, for which the bottle cleansing protocol can be found in **Appendix D**. Biofilter effluent was also sampled from each column using the same protocol as feed water. Water samples were kept cold and analysed within 24 hours. To collect biofilter media, the biofilter column was drained, and media sampled via purpose-built ports using autoclaved sampling straws and placed in 50 mL polypropylene centrifuge tubes, which were kept cold and processed within 4 hours. Ports 1 and 2 in both biofilters corresponded to a depth from the media surface of 10 and 20 cm, respectively. The majority of media sampled was at port 2 which aligned with the anthracite-sand interface. Port 3 was exclusive to BF(B) at 60 cm depth and located in the sand layer. For each sample, sand was separated from anthracite using a sieve. Separated media was placed in a 50 mL falcon tube and gently inverted for rinsing 3x using respective biofilter effluent followed by final rinsing with phosphate buffered saline (PBS) to remove loosely attached biofilm. Rinsed separated media was subjected to two workflows: immediate bulk ATP analysis or further processing with cation exchange resin to separate cells from EPS. Both workflows are described below.

3.3.4 ATP Assay

ATP analysis was performed on media following the separation of sand from anthracite, using the method described by Elhadidy et al (2017). One gram wet weight media was placed in a 15 mL centrifuge tube along with 5 mL of lysis buffer (UltraLyse 7, LuminUltra). Media and buffer was then vortexed for 20 s and left to incubate at room temperature for 10 min. Following incubation 20 μ L of supernatant from each sample was added to a 96 well plate which was then placed in a microplate luminometer (GloMax, Promega, USA). The luminometer aliquoted 100 μ L of luciferase enzyme (ENLITEN ATP Kit, Promega, USA) into a well and recorded the response over 10 s. A 5-point standard

curve was created using ATP concentrations from 10^{-5} to 10^{-1} μM ATP, with dilutions prepared in UltraLyse 7 buffer.

3.3.5 Extraction of Cells and EPS from Biofilter Media Biofilm

A cation exchange resin (CER) methodology was used on separated sand and anthracite media to extract cells and EPS from media grains and had been optimized by Ahmed El Hadidy et al (2017). For all analyses using cells counts (flow cytometry), EPS quantification and DNA based investigations (DGGE and biodiversity), the CER method for cell and EPS extraction was required. In summary, Dowex Marathon C cation exchange resin (Sigma Aldrich, USA) was rinsed with 100 bed volumes of Milli-Q water to remove residues from manufacturing. Three (3) g wet weight of rinsed media was added along with an equal wet weight of resin to a 50 mL centrifuge tube. After addition of 20 mL 6 mM PBS, tubes were shaken at 350 rpm at 15 °C for 1 h. The PBS had been sterilized by filtration through a 0.2 μm polyethersulphone (PES) syringe filter (VWR, Canada). After shaking, the resin was removed by settling, and then the liquid was withdrawn and centrifuged at 5000 x g for 20 min to pellet cells. The supernatant was withdrawn and filtered through 0.2 μm PES syringe filters (VWR, Canada) and stored at 4 °C for downstream EPS analysis. Cell pellets were re-suspended in 10 mL sterile 6 mM PBS for downstream flow cytometry, and aliquots were also frozen at -80 °C for PCR-DGGE community profiling.

3.3.6 Cell Enumeration by Flow Cytometry

Flow cytometry was performed as described by Elhadidy et al (2017). CellTrics 10 μm filters (Partec, USA) were used to remove large particles from resuspended cells before analysis by flow cytometry (Sysmex-Partec Cube6, Germany). One part suspended cells was diluted in 9 parts PBS before staining with SYBR Green I (Invitrogen, USA) to a 1x stain concentration. Incubation of stained cells was for 15 min at 35 °C. Stained samples were then further diluted 1:10 in PBS and, immediately before analysis, diluted 1:5 in 0.2 μm filter sterilized ultrapure (Milli-Q) water. The flow cytometer flow rate was 4 $\mu\text{L/s}$ and cell counts were measured using the electrode count mode and plotted using a combination of FL-1 (536 \pm 20 nm) green and FL-3 (> 615 nm) red channels, which allowed for the distinction of

living cells vs dead cells and debris. Gating and final counts were performed in FCS Express 4 (De Novembero Software, USA).

3.3.7 Quantification of Total Carbohydrates, Total Protein, and Extracellular DNA

Total protein was quantified in the EPS extracted samples using a Pierce BCA Protein Assay Kit (ThermoFisher Scientific), which is a bicinchoninic acid based colourimetric test. Bovine serum albumin (BSA) was used to create triplicate standards at 0, 1, 2.5, 5, 7.5, 10, 20, and 40 $\mu\text{g}/\text{mL}$ concentrations. 1.8 mL of sample was vortexed with 1.8 mL bicinchoninic acid working solution and incubated at 60 °C for 1 h in borosilicate glass test tubes. Samples were then measured at 562 nm on a Cary 100 UV/VIS spectrophotometer (Agilent Technologies, USA) using a 1 cm glass cuvette.

Total carbohydrates were measured using the phenol-sulfuric acid method (DuBois et al., 1956). Triplicate D-glucose standards were used in 0, 1, 2.5, 5, 7.5, 10, 20, and 40 $\mu\text{g}/\text{mL}$ concentrations. Pipette tips were rinsed 4x with Milli-Q water to remove any organic contamination. Each 9 mL borosilicate glass test tube received 0.5 mL sample, 0.5 mL phenol and 2.5 mL H_2SO_4 (98-99%; Sigma Aldrich, USA) and was subsequently incubated at 30 °C for 15 min. Phenol solution was prepared by dissolving solid crystal (Sigma Aldrich, USA) at 5% w/v in Milli-Q water. Measurements were performed at 490 nm using a Cary 100 UV/VIS spectrophotometer (Agilent Technologies, USA) with a 1 cm glass cuvette. Glass vials for both protein and carbohydrate assays were cleaned using a special procedure involving HCl which can be found in **Appendix D**.

Extracellular DNA was quantified using the Invitrogen QuBit 2.0 platform (ThermoFisher, USA) where 10 μL filtered EPS was fluorescently stained using the dsDNA BR Assay Kit (ThermoFisher Scientific, USA). Samples were incubated in thin clear wall 0.2 mL PCR tubes (VWR, Canada) in the dark for 2 min at room temperature. Kit standards consist of 0 and 100 ng/ μL DNA and were used for calibration curves.

3.3.8 Liquid Chromatography – Organic Carbon Detection

A variant of size exclusion chromatography based on the Gräntzel thin-film UV reactor for detection of ppb ($\mu\text{g/L}$) levels of organic carbon was used to characterize major fractions of natural organic matter (NOM); this technology, otherwise known as liquid chromatography – organic carbon detection (LCOCD) (Huber et al., 2011), was used on biofilter feed, effluent and EPS extractions from media. A sample chromatogram of LC-OCD data from July 2015 feed water can be found in **Figure 3.1-a**. Operation and maintenance of the equipment was performed by Monica Tudorancea under the direction of Sigrid Peldszus of the NSERC Chair team. In water samples, the five major fractions (as defined by Huber et al. (2011) and their approximate elution times are biopolymers (10 kDa or greater; 25-35 min), humic acids (40 min), building blocks such as the breakdown products humic substances (52 min), low molecular weight acids (55 min) and low molecular weight neutrals such as ketones, aldehydes and simple alcohols, sugars and amino acids (60 min or greater) (Huber et al., 2011). The method detection limits for biopolymers, humics, humic building blocks, LMW-acids and LMW-neutrals were 0.009, 0.009, 0.026, and 0.044 mg/L C, respectively, and the reproducibility was 5, 2, 12, and 9% standard deviation, respectively. Feed and effluent samples were pre-filtered using 0.45 μm polyethersulphone (PES) filter (VWR, Canada), and resulting data were integrated using ChromeCalc and ChromeRes software (DOC-Labor, Germany). Low molecular weight humics co-elute with low molecular weight acids, and the DOC-Labor software accounts for this by default. This mechanism was turned off for the current study, meaning the LMW-acids fraction included both LMW-acids and LMW-humics. Biofilm EPS samples were filtered via 0.2 μm PES syringe filters (VWR, Canada) to sterilize and filter particulates. Biofilm EPS chromatograms presented different response from that of surface water and as such were interpreted via a custom MATLAB (MathWorks, USA) algorithm as described by Elhadidy et al. (2016) where the areas observed under the 3 peaks were integrated and the ppb amount quantified. The first EPS peak is denoted high molecular weight (HMW) and corresponds to sizes larger than 13 kDa, eluting at 25 to 35 minutes. Elhadidy et al (2016) found that the HMW peak was primarily composed of protein-like substances with a secondary contribution of other compounds such as polysaccharides. The EPS intermediate molecular weight (IMW) peak

represents compound sizes between 2 and 13 kDa and elutes at 35 to 45 min, which is similar in size to the humic and fulvic acids fraction in feed water LC-OCD chromatograms. However, Elhadidy et al (2016) found that the IMW EPS fraction was complex and contained proteins, carbohydrates and humic-like substances. Finally, the low molecular weight (LMW) EPS peak eluted in excess of 45 min and therefore relates to sizes smaller than 2 kDa; and is likely composed of low molecular weight compounds such as peptides, amino acids, monosaccharides etc. The HMW, IMW and LMW EPS peaks are illustrated in **Figure 3.1-b**.

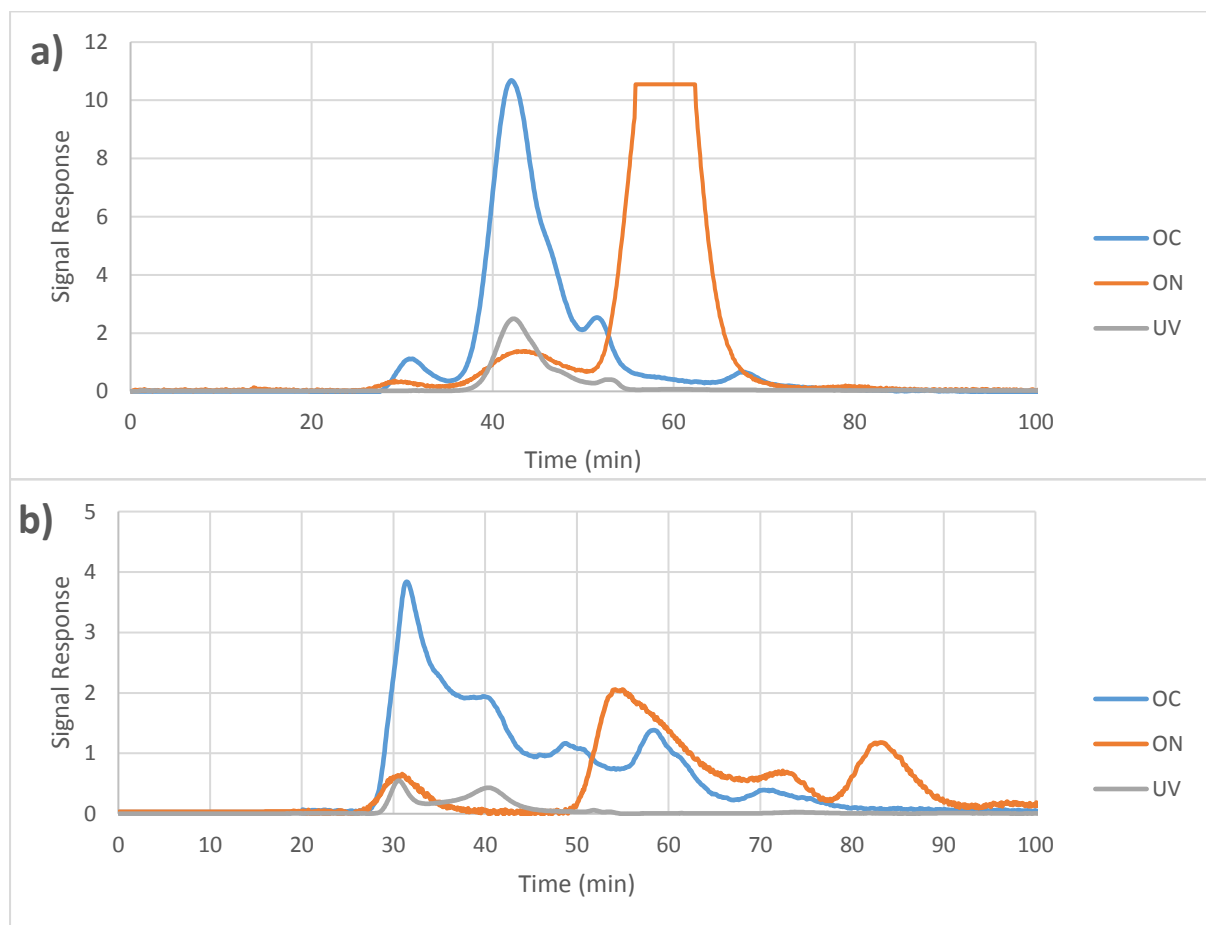


Figure 3.1: Example LC-OCD chromatograms of biofilter feed water (a), and biofilm EPS extracted from sand media (b).

3.3.9 Bacterial DNA Isolation

For each liquid sample, one litre of feed water was filtered using two stages of polyethersulfone (PES) filters. The first round of filtration used 0.8 μm 47 mm diameter Supor® membrane filters while the second round used 0.2 μm 47 mm Supor® filters (Pall corporation, USA). This two stage approach ensured timely filtration of feed water with

high cell retention for downstream nucleic acid analysis. DNA was isolated from feed water filtrate and media biofilm cellular extracts. Samples archived previously by A. Elhadidy were used in the current study in conjunction with those gathered and archived by P. Markin. Archived water samples were stored as retentate on filter paper in 5 mL centrifuge tubes (VWR, USA). Media extracted samples were stored as cell suspensions in 15 and 50 mL polypropylene falcon tubes (VWR, USA; as per the methodology in Section 3.3.5). All samples were stored at -80 °C until molecular work with PCR and DGGE could begin in October 2015.

Sand and anthracite associated DNA was isolated from archived cell extracts using the PowerLyser PowerSoil kit (MoBio, USA). DNA isolation was performed on 300 µL of thawed and vortexed cell suspensions without the centrifugation for cell concentration, since this would result in the loss of freeze-thaw lysed cell DNA within the supernatant. The protocol resulted in sufficient DNA concentrations for downstream molecular analyses.

Isolated DNA was assessed for quantity and quality via fluorometric quantitation and agarose gel electrophoresis, respectively. A QuBit 2.0 fluorometer with dsDNA BR Assay Kit (ThermoFisher Scientific) was used with 0.5 mL thin walled PCR tubes (ThermoFisher Scientific) to determine isolation yield of double stranded nucleic acids. One percent (w/v) agarose gels were prepared in 1× Tris-acetate EDTA (TAE) buffer along with 10 µL of GelRed agarose visualization dye (Biotium, USA). A 100 bp ladder (Amresco, USA) and 2 µL of isolated DNA were each mixed with 4 µL 1× TAE and separated by electrophoresis at 100 V for 60 min and visualized using the GelDoc platform (BioRad, USA) and QuantityOne 1-D Analysis Software (BioRad, USA).

3.3.10 DGGE Analysis

Bacterial 16S rRNA genes were amplified using a F968 forward primer with a 40 base pair (bp) GC clamp, and a 1401.1b reverse primer which together targeted the V6-V8 16S region (Heuer et al., 1997). These primers have been successfully used in other electrophoresis based microbial community profiling studies (Brons & Van Elsas, 2008; Gomes et al., 2001; Pereira e Silva et al., 2012). Primers were purchased from Sigma Aldrich.

The method described by Brons & Van Elsas (2008) required modification in order to remove non-specific bands. The MgCl₂ concentration was optimized, and the best results (least amplicon smearing in agarose at the 500 bp region) were achieved when DMSO and BSA were used. The difficulty associated with achieving a single defined amplicon band could be due to a combination of primer design and the use of a GC clamp, which if not optimized, could result in heteroduplex formation and mispriming which leads to non-target by-products in the final PCR product, visible as fuzzy or smeared amplicon bands in agarose (Lorenz, 2012).

Final PCR conditions were as follows, and used a Bio-Rad C1000 thermocycler. Each 50 µL reaction volume contained 20 mM Tris-HCl (pH 8.4), 50 mM KCl, 3.75 mM Mg²⁺, 5% v/v DMSO (supplier), 2% w/v BSA, 0.2 mM dNTPs (Bio-Rad), 0.2 mM forward and reverse primers, and 5 ng DNA template. Tubes were incubated at 94°C for 5 min, and then 2.5 U/reaction of iTaq polymerase (Bio-Rad) was added, to further minimize non-specific amplification. The touchdown amplification protocol included: 1 min at 94 °C, 1 min at 60 °C, and 2 min at 72 °C; followed by a decrease in annealing temperature of 0.5 °C per cycle until 55 °C was reached. Following this the program consisted of 20 cycles of 94 °C for 1 min, 55 °C for 1 min, and 72 °C for 2 min with a final extension of 72 °C for 10 min. Bacterial PCR amplicons were checked for yield and target size using fluorometry and agarose gel electrophoresis in the same way as bulk environmental DNA, as outlined above. Bacterial DGGE conditions were optimized and performed using the DCode universal mutation detection system (Bio-Rad). A 6% polyacrylamide gel was used, and the denaturing gradient was 45-60%, where 100% consisted of 40 mL formamide and 42 g urea per 100 mL solution. Gel polymerization was catalysed with 13.2 µL of 20% TEMED-APS (N,N,N'N', - tetramethylethylenediamine – ammonia persulfate; AMRESCO) per mL gel solution. Approximately 450 ng of amplification product was loaded into profile lanes along with a custom made DGGE marker. The DGGE marker was prepared by combining PCR products from several different bacterial pure culture isolate, as described by Van Dyke & McCarthy, (2002). DGGE markers are used to align profile bands between lanes to overcome distortions in denaturing gradients and aid in lane comparisons. As well, an inter-gel marker composed of the amplification product from an August 2015 biofilter feed water sample was included

in each gel, in order to accurately compare profiles between gels. Electrophoresis was performed in 0.5× TAE buffer for 18 h at 60 °C and 50 V. Gels were stained for 90 min using 1× PAGE GelRed (Biotium) in 0.5× TAE buffer and subsequent visualization was performed on GelDoc XR (Bio-Rad) using QuantityOne software (Bio-Rad). In addition to intra-gel markers, quality control was ensured via inter-gel marker comparisons.

3.3.11 Statistical Analyses

Intensity matrices were created from electropherograms using BioNumerics v7.0 (Applied Maths) and analysed using several packages in the open-source Project R software (R Core Team, 2013). Detailed information on settings used in BioNumerics can be found in the analogous section of Chapter 4. Statistical analysis of the DGGE profiles was accomplished by analysing the presence and intensity of the banding patterns they provide. Each lane within the profile is loaded with the extracted and PCR amplified DNA from a single sample type which, after electrophoresis and staining, produces the observed patterns of phylotype bands when exposed to UV. The location of a lane's bands were measured and used to generate a presence/absence matrix. If band intensities are used, such as in the current study, relative abundances are measured and the matrix is said to be quantitative. The banding patterns and intensities of individual samples within the matrix can then be compared against each other using multivariate statistical techniques such as principal component analysis (PCA), correspondence analysis (CA) or hierarchical clustering; in this way DGGE analysis of microbial communities is in effect no different from other types of fingerprinting, such as chemical or metabolite profiling. In this study, cluster analysis was performed using agglomerative hierarchical clustering and detrended correspondence analysis (DCA). Agglomerative hierarchical clustering approaches start with individual samples and then progressively join together similar samples into clusters. In this case a distance coefficient matrix is created with the resultant distances assembled into a dendrogram. Hierarchical clustering was performed using Bray-Curtis distances assembled via the Ward algorithm. Bray-Curtis distances (dissimilarity) allow for rare species to affect the distances (Legendre & Legendre, 1998), while the Ward algorithm was selected because it is a reliable agglomerative methodology and because of its ability to arrange data

according to cluster centroids (Legendre & Legendre, 1998). DCA is a multivariate technique which clusters phylotype data in reduced space while adjusting for “arch-effect” problems inherent to ecological datasets due to their unimodal distributions (Borcard et al., 2011); vectors representing environmental gradients are added and their strength of correlation with the phylotype data is presented by means of vector length. In order to produce a usable ammonia vector for inclusion in DCA analysis, values below the method detection level (DL) of 0.1 mg-N/L were substituted with (DL/2) as described by Farnham et al. (2002). A Mantel optimal number of clusters test (Borcard et al., 2011) was used to statistically determine the optimal number of clusters within the dataset by comparing Pearson correlation values between the original Bray-Curtis distances against the Ward assembled dendrogram after the latter was cut at different heights, representing different number of clusters. In addition, analysis of similarity (ANOSIM) was performed using the Vegan package (Oksanen et al., 2016). ANOSIM provides hypothesis testing on the similarity within and between groups and therefore is able to impart whether a group is cohesive at a defined significance level.

Biodiversity statistics (Shannon diversity index and richness) were obtained using BioDiversityR (Kindt & Coe, 2005). The approaches used in multivariate investigations of the DGGE matrices were informed by Borcard et al. (2011), Legendre & Legendre (1988), and Whitlock & Shluter (2009). Several methods are often used to assess the complexity of DGGE profiles, among them are band number or richness (Boon et al., 2011; Lyautey et al., 2005), which are used to infer how many species are present in a sample, and Shannon diversity (Duarte et al., 2012; Moura et al., 2009; Vaz-Moreira et al., 2013). Shannon diversity (H') describes the number of species in a given habitat and their relative abundance. Shannon diversity is calculated from community richness (the number of species or phylotypes in a community). Diversity is an important measure for assessing a community’s complexity, resilience and maturity, and was calculated using **Equation 3.1**,

$$H' = \sum_{i=1}^s p_i \ln p_i$$

Eq. 3.1

where H' is diversity, S is the number of species in the community (also known as the community richness), and p_i is the proportion of the i^{th} species. This means that a community with one species will have an H' of 0, whereas this value will increase with increasing richness (Molles & Cahill, 1998). Furthermore, depending on the relative abundance of individual phylotypes, it is possible for two communities to exhibit different Shannon indices while possessing the same number of species (richness). For the current research, the Shannon-Weiner diversity index was selected due to ubiquity within the literature, which makes comparisons with other data possible.

Water quality means for warm ($> 10\text{ }^{\circ}\text{C}$) and cold ($\leq 10\text{ }^{\circ}\text{C}$) conditions were compared using t-tests. Water quality was also compared between DGGE profile groups, which included feed water communities as well as media biofilm communities using t-tests. Given that 50% of feed ammonia data were below detection limit (DL) of 0.1 mg/L and considered non-detects, t-test means comparisons using ammonia data were subjected to maximum likelihood estimation (MLE) using the NADA package (Lee, 2017) in R; use of this technique produces estimated mean and standard deviation (not replacement data) and allows non-detects to be used in means comparisons; this type of technique is therefore the preferred methodology over substitution and non-parametric approaches for dealing with means comparisons of non-detect data-sets (USEPA, 2000). Note that in contrast, DL/2 substitutions were made for ammonia data pertaining to the DCA plot, as the DCA plot required replacement data and therefore could not use the descriptive statistics produced by the MLE approach.

For comparisons of mean biomass, EPS, NOM removal and community diversity between BF(A) and BF(B), a paired Student's t-test was used. Seasonal NOM removals were also compared using ANOVA analysis. Finally, Pearson r multiple correlations were performed on water quality, biomass, EPS, biodiversity and NOM removal values.

3.4 Results

3.4.1 Biofilter Feed Water Quality

Several water quality parameters were measured in the raw river water used to feed the biofilters and are presented in **Figure 3.2**. Standard metrics included temperature and turbidity (which were continuously measured by on-line equipment at the pilot plant; **Figure 3.2-a**), as well as parameters measured by the Region of Waterloo on a weekly (NH_3 , NO_3^-) or monthly (ortho-P, total iron, conductivity, hardness and pH) schedule (**Figure 3.2-b**). Water quality data is also presented as the range of values obtained during cold and warm conditions (**Table 3.1**).

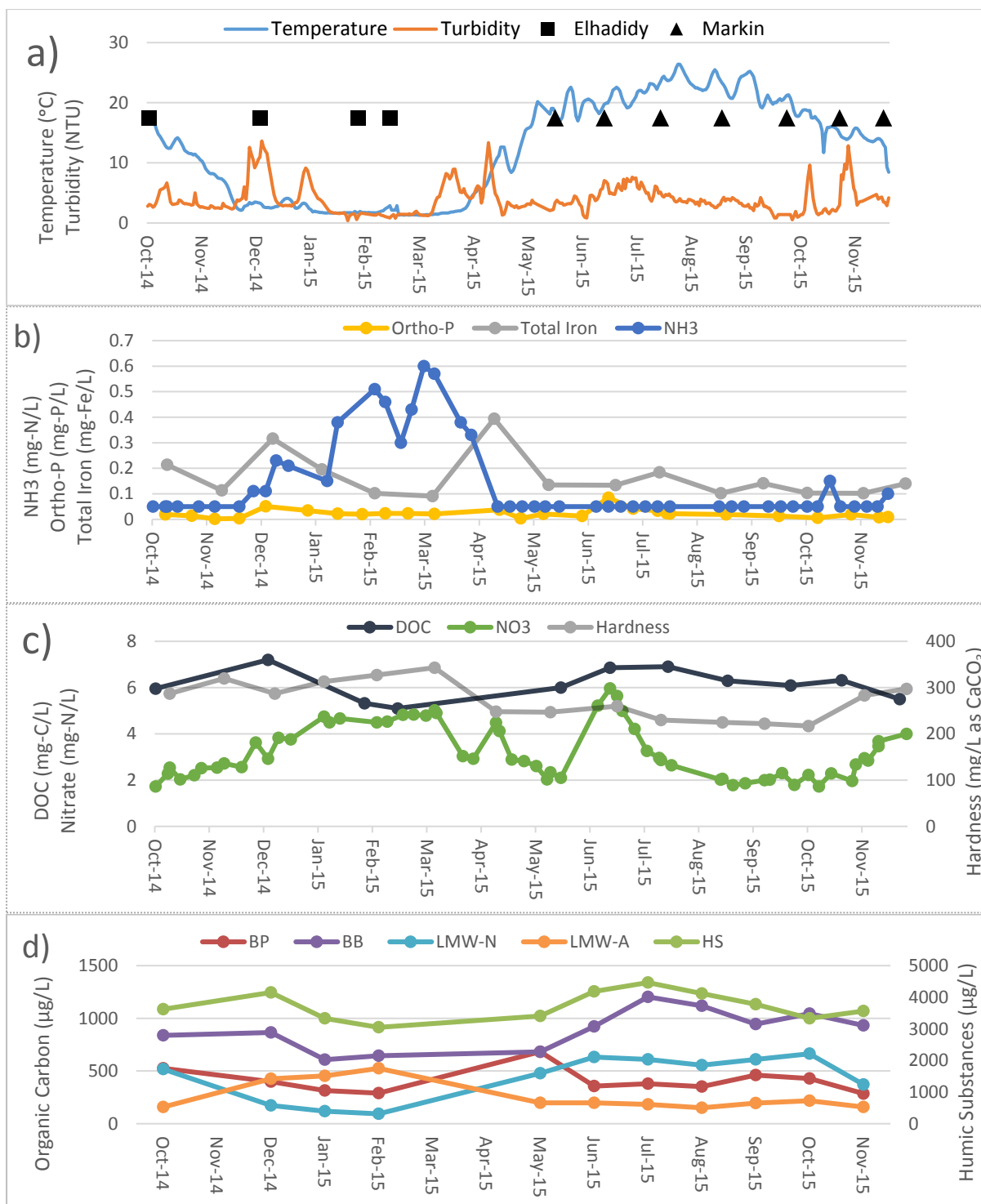


Figure 3.2: Feed water quality including (a) temperature, turbidity and dates media was collected; squares show Elhadidy while triangles show Markin sample dates. (b) feed water NH₃, ortho-P and total iron concentrations; NH₃ values below the detection limit of 0.1 mg-N/L are shown as 0.05. (c) feed water DOC, nitrate and hardness. (d) LC-OCD fractions including biopolymers (BP), humic substances (HS), building blocks (BB), low molecular weight acids (LMW-A), and low molecular weight neutrals (LMW-N).

Table 3.1: Biofilter feed water quality during warm and cold conditions.

Parameter	Unit	Warm Feed Water (>10°C)			Cold Feed Water (≤10°C)		
		MIN	MAX	n	MIN	MAX	n
Temperature ^a	°C	10.50	26.40	NA	1.29	9.93	NA
Turbidity ^a	NTU	0.55	12.84	NA	0.39	13.63	NA
DOC	mg C/L	5.5	6.9	8	5.1	7.2	3
Biopolymers OC	µg C/L	286	683	8	289	398	3
Humics OC	µg C/L	3330	4465	8	3048	4148	3
BB OC	µg C/L	683	1203	8	608	866	3
LMW-Acids OC	µg C/L	151	218	8	427	525	3
LMW-Neutrals	µg C/L	479	664	8	94	173	3
Ortho - Phosphate ^b	mg P/L	0.006	0.085	13	0.002	0.05	9
Ammonia / Ammonium ^b	mg N/L	0.10	0.15	24	0.10	0.60	15
Nitrate ^b	mg N/L	1.73	5.96	31	2.54	5.02	18
Total Iron ^b	mg/L	0.102	0.184	8	0.09	0.32	5
pH ^b	mg/L	8.09	8.23	8	7.99	8.24	5
Conductivity (at 25 °C) ^b	µmhos/cm	575	685	8	647	1080	5
Hardness (as CaCO ₃) ^b	mg/L	217	297	8	287	343	5

a and *NA* denote continuous on-line monitoring at biofilter pilot plant; *b* denotes data from by Region of Waterloo

Cold condition sampling events were those where the temperature of the feed water entering the biofilters was at or below 10 °C (December 2014, January & February 2015). Warm sampling events were those where the feed temperature was above 10 °C (October 2014 as well as May to November 2015). The 10 °C temperature point has been used as a demarcation between warm and cold water conditions in other biofiltration work (e.g. Pharand et al., 2015), as temperature conditions below this point are associated with slower biofilter microbial activity and lower NOM removals (Laurent et al., 1999).

Line charts of seasonal water temperature and turbidity for the 14 month total span of the current study (**Figure 3.2-a**) shows that monthly mean temperature was highest in August 2015 (23.1 °C) and lowest in March 2015 (1.6 °C). **Figure 3.2-a** also shows turbidity levels during the study period, which ranged from a high monthly mean of 7.08 NTU in December 2014 and a low monthly mean of 1.33 NTU in February 2015. For the majority of the year, turbidity was low, averaging below 5 NTU.

Figure 3.2-b presents ammonia, ortho-phosphate and total iron during the 14 month time span of the current study. Note that ammonia levels were below detection limit (0.1 mg-N/L) during many of the warmer months and were higher during cold conditions. Biofilter samples collected in February 2015 were taken during this period of high ammonia concentration, where the monthly concentration averaged 0.43 mg-N/L. As much of the ammonia data were below the detection level, the data set was adjusted to make parametric means comparisons possible; the data adjustment method was maximum likelihood estimation (MLE), which estimates descriptive statistics, yet does not generate replacement values. For means comparisons, the MLE approach is widely favoured over substitution techniques, which can bias the data (Helsel, 2005; Huston et al., 2009; USEPA, 2000). However, the proportion of non-detect data (67%) was higher than the method guideline of $\leq 50\%$ (USEPA, 2000), and therefore caution was required in assessing differences in mean ammonia concentrations between warm and cold conditions. Ammonia concentrations were shown as significantly higher in cold ($\leq 10\text{ }^{\circ}\text{C}$) conditions (**Table 3.2**; t-test using maximum likelihood estimation, $p < 0.001$, $\alpha = 0.05$). In addition to means comparisons, ammonia data were also used in detrended correspondence analysis (DCA) in section 3.4.2.; however, the use of MLE type approaches were incompatible with DCA as the latter required raw data and not generated descriptive statistics (which MLE provides); therefore substitution of ammonia data (half the detection limit) was used in the DCA method. Ortho-phosphate and total iron concentrations did not show a significant difference between temperature categories (**Table 3.2**). Turbidity also did not show significant differences between warm and cold conditions (**Table 3.2**; t-test, $p = 0.787$, $\alpha = 0.05$)

Figure 3.2-c presents DOC, nitrate and hardness levels during the study period. DOC concentrations ranged from a high of 7.2 mg/L in December 2014 to a low of 5.1 mg/L in February 2015, but there was no significant change in DOC with water temperature (t-test, $p = 0.333$; $\alpha = 0.05$; **Table 3.2**). Nitrate concentrations spiked twice during the study: once in winter where concentrations ranged from 4.5 to 4.9 mg-N/L during a period spanning January to March 2015, and again in June where concentrations peaked at 5.96 mg-N/L. Low nitrate concentrations were observed in October 2014 (1.73 mg-N/L), May 2015 (2.03 mg-N/L) and a period spanning August to October 2015 (~ 2 mg-N/L). Therefore nitrate

concentrations were not significantly different between warm and cold conditions (t-test, $p = 0.056$; $\alpha = 0.05$; **Table 3.2**). Both hardness and conductivity showed significant increases in cold conditions (t-test, $p = 0.003$ & 0.011 , respectively; $\alpha = 0.05$; **Table 3.2**).

DOC and NOM size fractions (as determined by LC-OCD) of the biofilter feed water were also measured during sampling events, as illustrated on **Figure 3.2-a**. Black squares indicate sampling events performed by Elhadidy while triangles show sampling performed by Markin. No sampling events occurred during November 2014, March 2015 or April 2015. **Figure 3.2-d** shows LC-OCD defined organic carbon fractions of the influent over the sample period. As is typical for river water, humic substances presented the highest levels out of the NOM fractions, at 65% of total C. Biopolymers on average composed only 7% of the feed total C. Building blocks, low molecular weight neutrals and acids composed 15, 8 and 5% of total C, respectively. The NOM fractions which demonstrated significant differences between warm and cold conditions were building blocks, low molecular weight acids and low molecular weight neutrals (t-test, $p = 0.041$, < 0.001 & < 0.0001 , respectively; $\alpha = 0.05$; **Table 3.2**). However, interpretation of the cold vs warm LC-OCD means comparison results should be met with caution due to the low number of samples in these cold condition data since $n = 3$ (**Table 3.1**).

Table 3.2: t-test results (two tailed; $\alpha = 0.05$) comparing water quality parameters at cold (≤ 10 °C) and warm (> 10 °C) conditions. Ammonia means comparison utilized maximum likelihood estimation technique (MLE) to account for censored data. Significant differences are marked with an asterisk ().*

Parameter	Warm vs Cold P value
Turbidity	0.787
DOC	0.333
Biopolymers	0.223
Humics	0.352
Building Blocks	0.041*
LMW-Acids	<0.001*
LMW-Neutrals	<0.001*
Ortho - Phosphate	0.855
Ammonia	<0.001*
Nitrate	0.056
Total Iron	0.275
pH	0.482
Conductivity (at 25 °C)	0.011*
Hardness (as CaCO ₃)	0.003*

3.4.2 Community Profiling of Feed Water and Biofilter Media Biofilms by DGGE Analysis

3.4.2.1 DGGE Profile Clustering

DGGE analysis was performed on 11 water samples and 53 biofilter media samples collected from October 2014 to November 2015. All sample amplicons were positive with a single band in agarose at the expected size of 473 bp, as well as no band in the negative reaction blanks. The amplicon yield was typically 2×10^4 ng / μ L. DGGE analysis was able to separate bacterial PCR amplification products into a large number of bands (phlotypes) as shown in **Figure 3.3**. Biofilter media sample communities showed visually different banding patterns compared to the feed water community (presented in Lane F) and media biofilms consistently displayed higher phlotype band number. Overall, the cumulative number of unique DGGE ribotypes from all samples was 84.

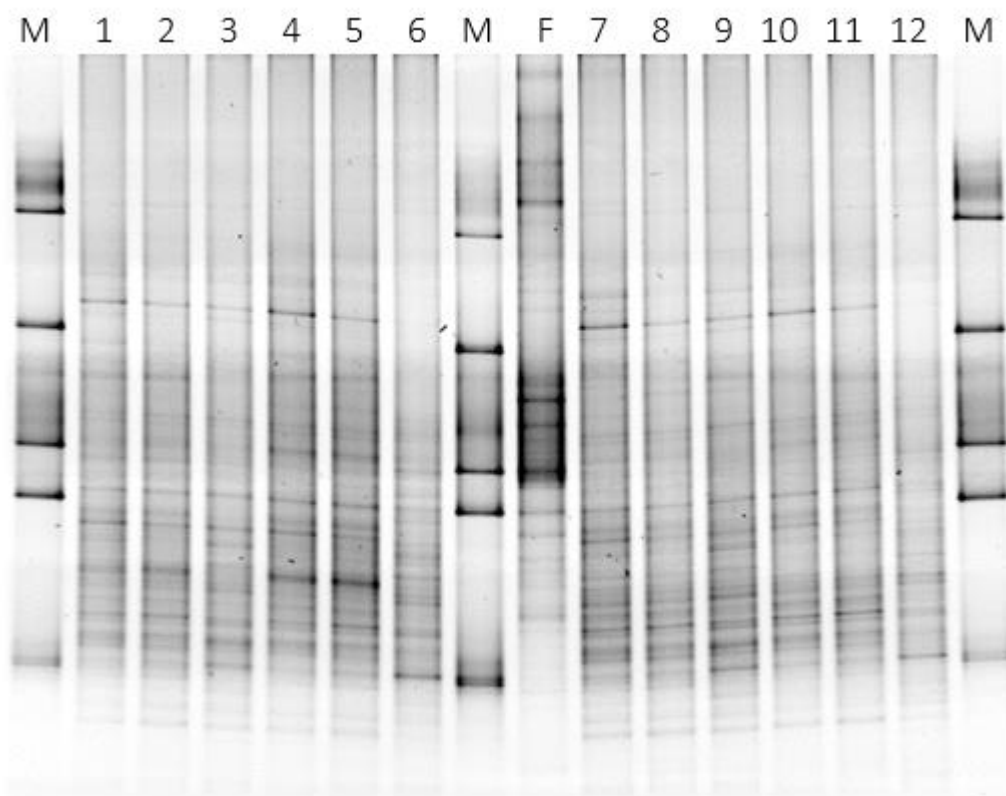


Figure 3.3: DGGE electropherogram of biofilter media and feed water bacterial communities. Lanes labelled "M" are marker lanes, lanes 1-5 and 7-12 were from biofilter media samples, and lane F was a biofilter feed water sample.

Information on the statistical analysis of DGGE results can be found in Section 3.3.11. In analysing the banding patterns of biofilter media and feed water samples, the x-axis of

Figure 3.4 shows the optimal number of clusters or groups (k) was 5, with a Pearson correlation of 0.76 between the distance matrix and the Ward-assembled dendrogram. The indicated 5 groups relate to a dendrogram height of 0.80 as shown in Figure 3.5. Hierarchically clustered distances show the relationships between sample communities and their immediate similarity to the nearest neighbour, which is quantifiable using the “height” scale located at the top of the figure. This height scale represents sample (dis)similarity, where a value of 0 represents no dissimilarity and a value greater than 0 represents increasing dissimilarity. The greater the height of the vertical bar connecting two clusters, the greater the dissimilarity between those clusters. This method of cluster representation clearly has advantages over ordinal (reduced dimensional space) clustering as the information is presented in a format where a sample’s location within the entire dataset can readily be assessed.

Reliability of DGGE profiles was evaluated using gel markers. Each DGGE gel included intra-gel markers for lane straightening and alignment, as well as a single inter-gel marker for comparisons between individual gels. In order to assess DGGE method reliability between individual gel profiles, the inter-gel patterns were assembled into a dendrogram using Bray-Curtis distances and the Ward algorithm (**Appendix A as Figure S1**). The greatest node height (dissimilarity) between gel profiles was 0.50, which is lower than the node height of 0.80 used to discriminate between the optimal number of sample clusters. This means that there was good reliability of DGGE gel profiles between gels.

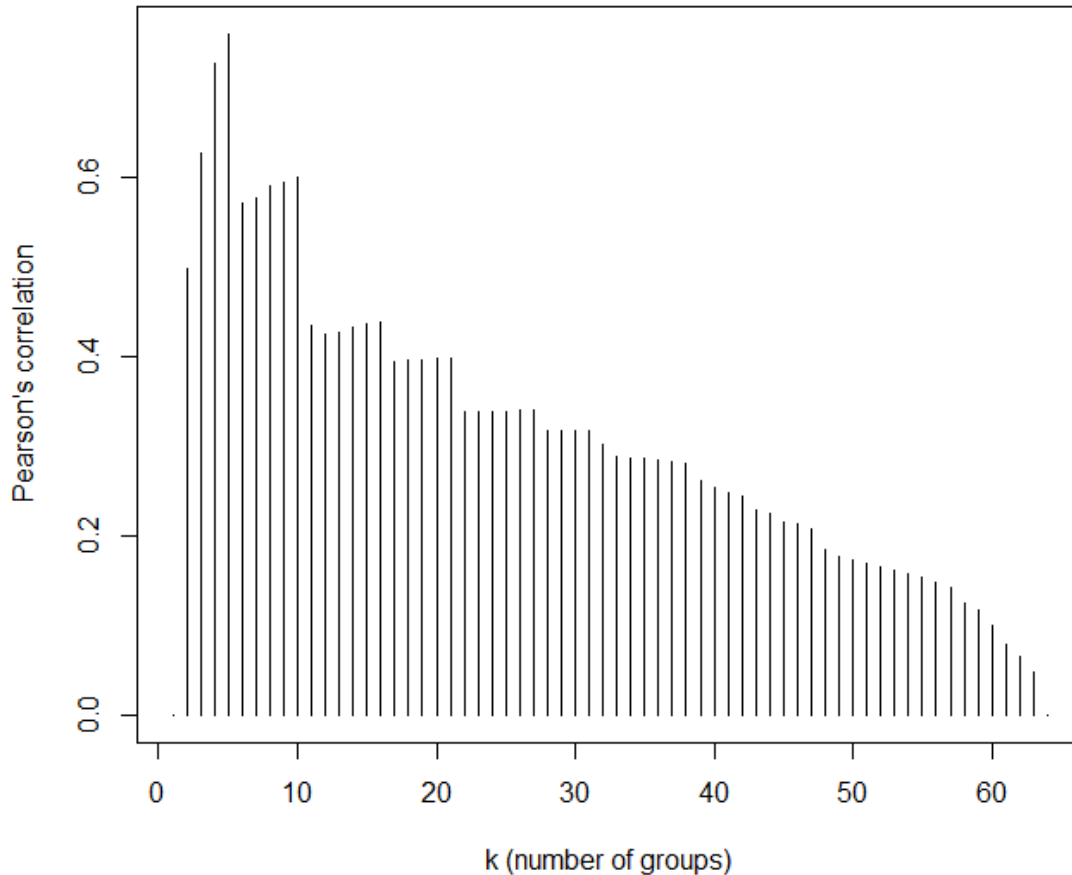


Figure 3.4: Mantel optimal number of clusters as determined by Pearson's correlation between Bray-Curtis distances and Ward assembled dendrograms cut at different heights (representing number of groups). Optimal number of clusters (k) was 5 at a Pearson r of 0.76

Figure 3.5 shows that a superstructure is easily observed in the DGGE profile dendrogram, where feed water (planktonic) bacterial communities exhibit a marked dissimilarity from bacterial biofilm communities. Within the two major planktonic and biofilm branches, each of the created clusters were assigned an alphabetical group name, with the feed water samples divided into two main clusters (A,B) and the media samples into three main clusters (C, D, E). Group A contain feed water samples from predominantly warm ($>10^{\circ}\text{C}$) conditions, with the exception of the December 2014 sample. Group B contains feed water samples collected during both warm and cold temperatures. Group C is the first of three media groups encountered. Group C contains all January and February 2015 media samples; these are cold condition ($\leq 10^{\circ}\text{C}$) media biofilm communities. However, December 2014, which is also a cold condition media biofilm community, is found in group E. Group D is composed solely of October 2014 media samples. The last media group is

Group E, which contains the all the warm condition 2015 media samples as well as the cold condition December 2014 media communities. Groups C and E present several sub-clusters organized by month, which are not organized in a chronological fashion. Community structures in **Figure 3.5** did not cluster according to media type, depth or biofilters A and B.

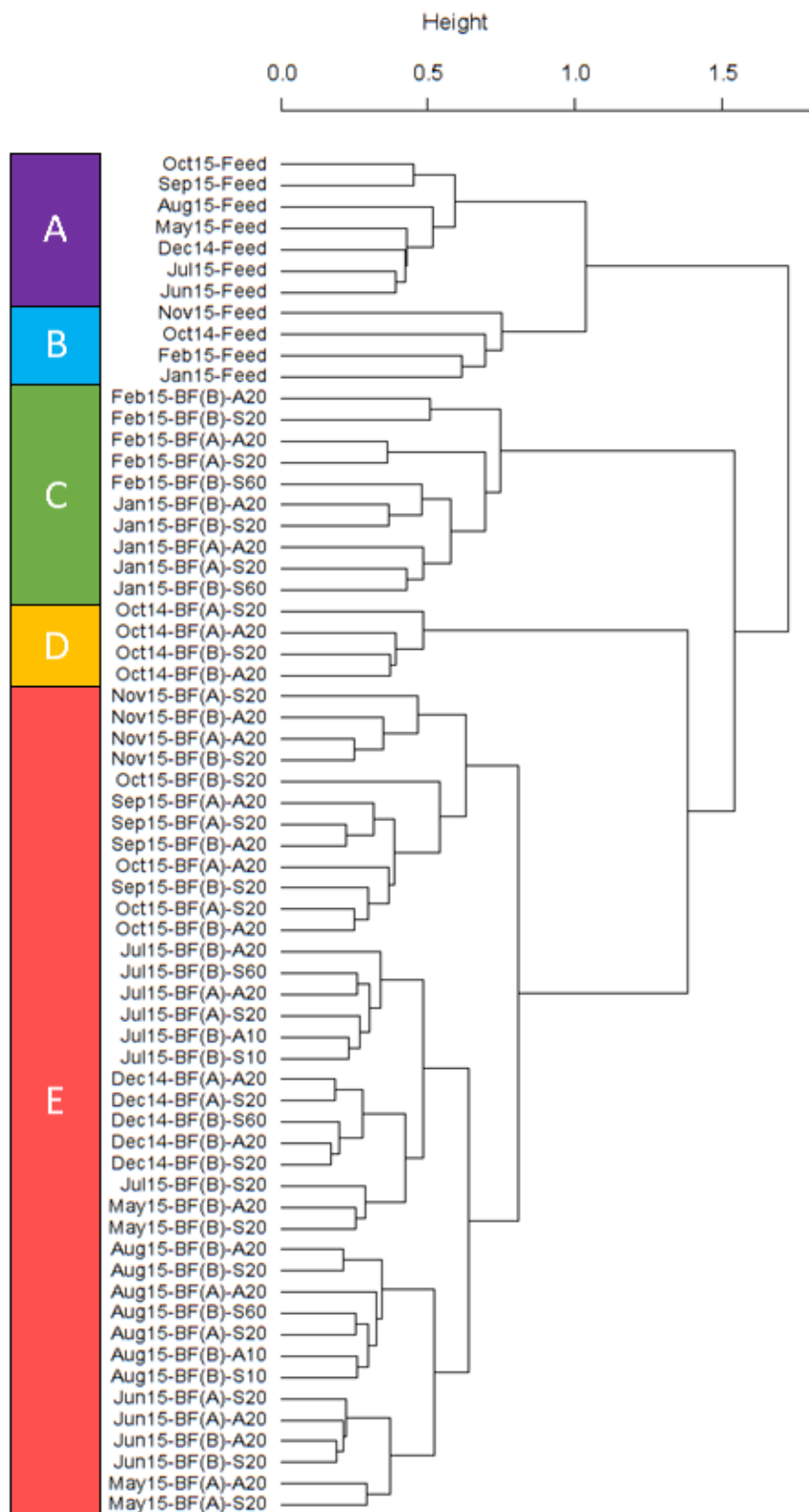


Figure 3.5: Dendrogram of biofilter feed water and media samples from Oct 2014 to Nov 2015. Samples are identified by date (month/year), sample type [feed, BF(A), BF(B)], media type [sand (S) or anthracite (A)] and sample depth (10, 20 or 60 cm from media surface). Five clusters were identified and labelled A to E, with groups A and B composed of planktonic feed water communities and groups C to E composed of media biofilm.

The dendrogram group cohesion of **Figure 3.5** could be evaluated using hypothesis testing. Boxplots were created to show results of analysis of similarity (ANOSIM; **Figure 3.6**), which evaluates the mean ranked Bray-Curtis distances (otherwise referred to as dissimilarities) between and within groups to allow for nonparametric hypothesis testing of multivariate data (Clarke, 1993). The ANOSIM statistic (R value) is a comparison of the ranked dissimilarity mean between groups to the mean within groups, where an R value close to 1 indicates high dissimilarity between groups. The ANOSIM statistic was determined to be $R = 0.92$ ($p = 0.001$, $\alpha = 0.05$), validating that the groups created using the clustering analyses yielded significant differences. Results also show that the “between” group dissimilarity was higher than the value within groups for all except the planktonic feed Group B. Group B contains feed water communities from sampling dates which span more than 12 months (October 2014, January, February and November 2015), and this could contribute to the greater dissimilarity observed within this group. Therefore, the high dissimilarity within Group B indicates that feed water Groups A and B could be considered a single cluster. In addition, Group E, the largest of the media biofilm clusters, contains 7 outliers all from the August 2015 media sub-cluster as shown in **Figure 3.6**

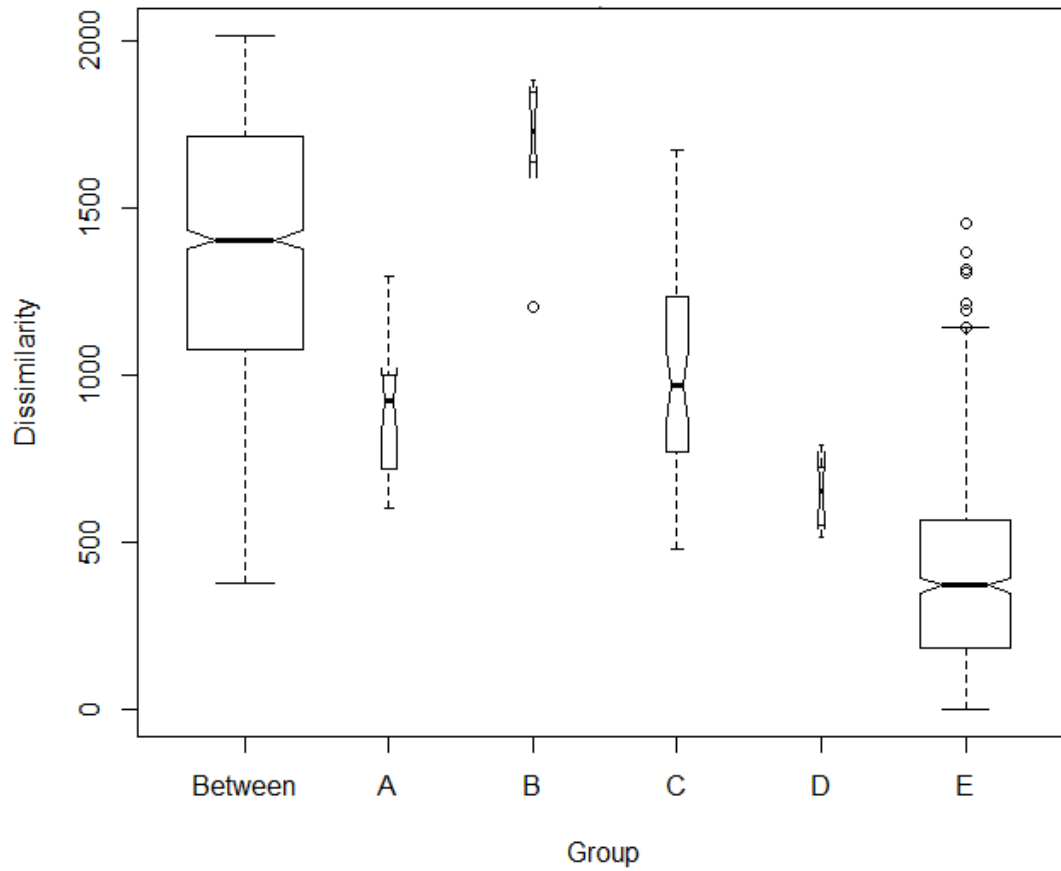


Figure 3.6: Boxplots displaying the ANOSIM dissimilarity between and within DGGE groups. Width of boxes represents number of entries within group, horizontal black bars show median, and lower and upper box edges represent 1st and 3rd quartiles. Error bars represent the upper and lower range of dissimilarity. Circles are outliers. ANOSIM statistic was determined to be $R = 0.923$ ($p = 0.001$, $\alpha = 0.05$).

In order to investigate relationships between feed water quality and DGGE profile community clustering, an ordination type analysis was used. CCA ordination was attempted, however an arched or “horseshoe” pattern was observed, which indicates a poor quality of analysis (Borcard et al., 2011; Legendre & Legendre, 1998). Therefore detrended correspondence analysis (DCA) was used (**Figures 3.7 and 3.8**), as it is more suited to the data set and is commonly favoured in ecological multivariate analyses (Legendre & Legendre, 1998). Bacterial communities (as determined by PCR-DGGE profiles) are represented by small open diamonds while group clusters are indicated by coloured ellipses. Blue arrows are water quality gradients (vectors) showing direction and strength of analyte correlation with species data. A DCA plot evaluating the influence of water quality parameters (DOC, nitrogenous compounds, phosphorus, iron, temperature, turbidity) is shown in **Figure 3.7**. The percent of variance

explained by the DCA plot axes in **Figure 3.7** is 19% and 10% for axes 1 and 2, respectively; this permits reasonable observations to be drawn from the figure, and is similar to the variances explained by DGGE mediated DCA and RDA analyses elsewhere (Wang et al., 2015). A second DCA plot was constructed to evaluate the relationship between the DGGE profile groups and feed water NOM fractions as determined by LC-OCD (**Figure 3.8**).

The DCA plots showed good agreement with hierarchical cluster arrangements for Groups A, B, C and E (**Figure 3.5**); these similarities served to support the previous dendrogram results. Group D of the DCA plot however is located within the larger Group E, and serves as the only major difference between the dendrogram and ordination multivariate methods. Therefore Groups D and E were combined into Group D/E for further statistical means testing. In comparing the DGGE profile data with the feed water quality data, the NH₃ vector within **Figure 3.7** was larger relative to other vectors, and indicates a proportional relationship with DGGE group C. As well, **Figure 3.8** shows that the low molecular weight acids vector is also oriented towards Group C (January-February 2015 biofilm) at high correlative strength. Group D/E (summer/fall biofilms) were associated with elevated temperature and DOC (**Figure 3.7**), and also the other NOM fractions (including biopolymers, humic substances and building block, and low molecular weight neutrals) (**Figure 3.8**) as indicated by vector arrow direction and length; the length and direction of these last NOM vectors is also important when interpreting Group C, as their direction (pointing away from Group C) indicates negative correlative with Group C.

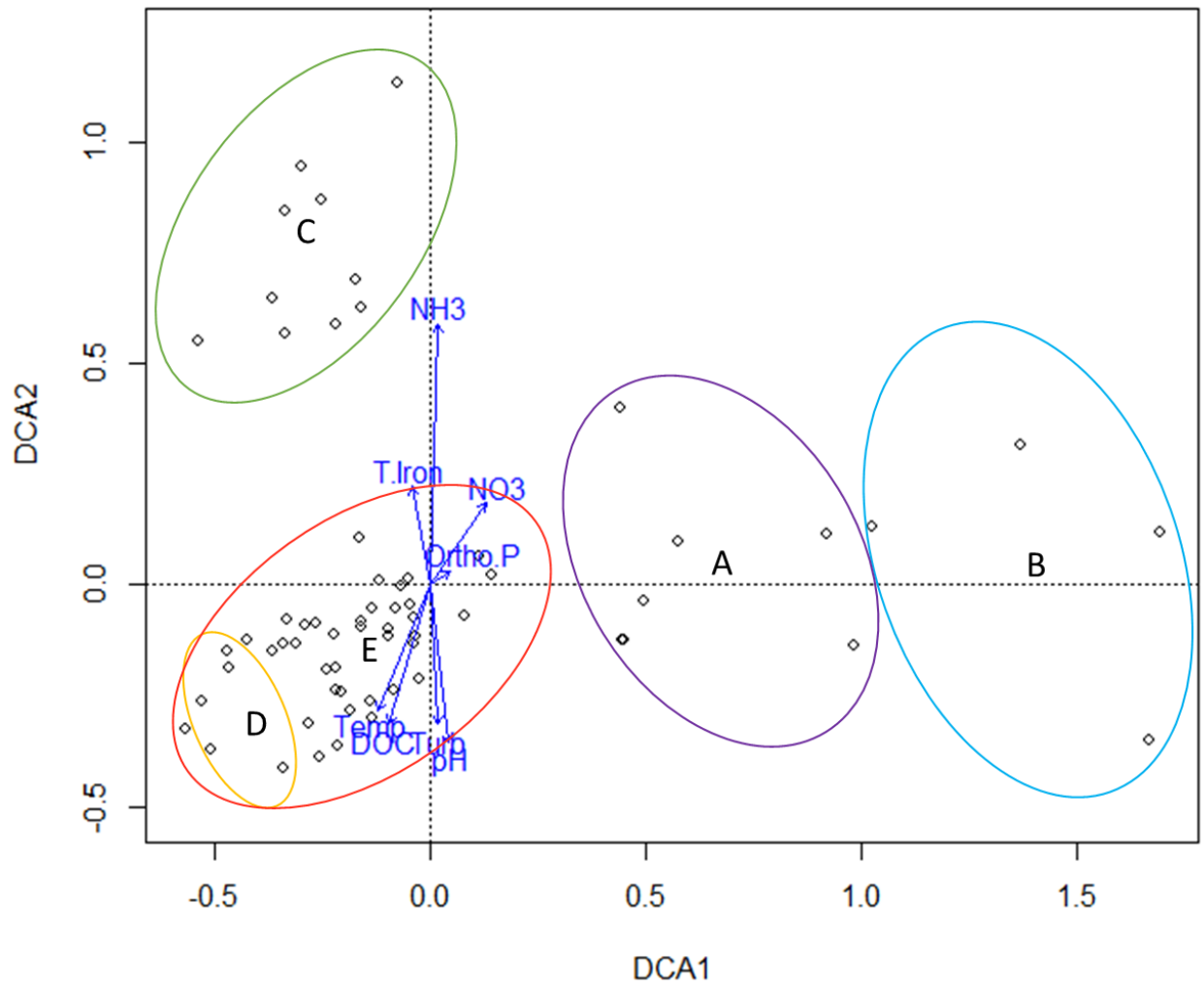


Figure 3.7: Detrended correspondence analysis for biofilter feed water and media bacterial communities and water quality parameters. DGGE community profiles for each sample are represented by small open circles, while the DGGE profile groups are represented by coloured ellipses, with the group letter positioned in ellipsoid centres. Post-hoc environmental gradients including temperature (Temp), turbidity (Turb), pH, ortho-phosphorous (Ortho.P), total iron (T.Iron), nitrate (NO₃) and ammonia (NH₃) are represented by blue arrow vectors and correspond to the correlation strength between the variable and the DCA ordination.

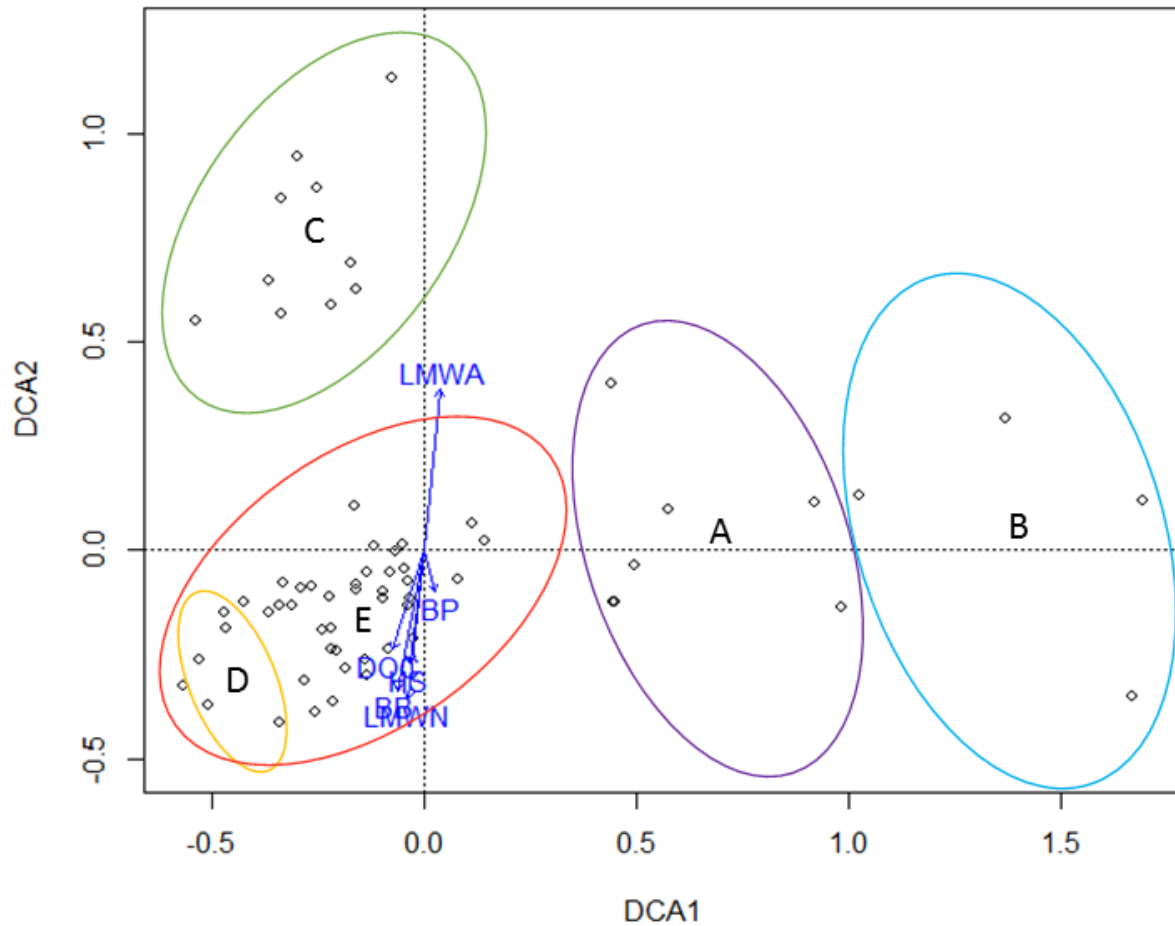


Figure 3.8: Detrended correspondence analysis for biofilter feed water and media bacterial communities and natural organic matter fractions as measured by DOC and LC-OCD. DGGE community profiles for each sample are represented by small open circles, while the DGGE profile groups are represented by coloured ellipses, with the group letter positioned in ellipsoid centres. Post-hoc environmental NOM gradients are represented by blue arrow vectors and include dissolved organic carbon (DOC), biopolymers (BP), humic substances (HS), humic building blocks (BB), low molecular weight acids (LMWA), and low molecular weight neutrals (LMWN).

3.4.2.2 DGGE Profile Diversity

Diversity in the biofilter feed water and media biofilm samples was measured using DGGE community profiles. **Figure 3.9** shows media Shannon-Weiner diversity (a) and richness (b) for samples collected from biofilter A and B at 20 cm depth, which is the interface between sand and anthracite. Sand and anthracite were separated and values for each parameter are presented separately. **Figure 3.9** also presents feed water diversity and richness for planktonic

communities. The biofilter loading rate was 3.08 m/h, and this was decreased to 1.54 m/h starting in September 2015. Paired t-tests showed that no differences were found between BF(A) vs BF(B) sand Shannon diversity (paired t-test, $p = 0.985$, $\alpha = 0.05$, **Table 3.3**) as well as richness (paired t-test, $p = 0.869$, $\alpha = 0.05$, **Table 3.3**). Anthracite however showed a significant difference between Shannon index means of BF(A) vs BF(B) (paired t-test, $p = 0.046$, $\alpha = 0.05$, **Table 3.3**), while no difference between columns was observed in the anthracite richness mean (paired t-test, $p = 0.126$, $\alpha = 0.05$, **Table 3.3**). The Shannon diversity index (H') values are shown over the 14 month experimental period for samples collected from both feed water and biofilter media collected from BFA and BFB at 20 cm depth (**Figure 3.9**). Overall, the feed water planktonic diversity and richness measurements were significantly lower than media biofilm sand and anthracite values (ANOVA, $p < 0.001$ & $p = 0.002$ for diversity and richness, respectively, $\alpha = 0.05$).

Results for the biofilter media samples (collected at 20 cm depth) show that the diversity of bacteria communities on biofilter media was low on the first sample date (October 2014), but increased by December. 2014 and remained relatively stable over the remaining study period (between 3.0 and 4.26), with average values of 3.80 ± 0.40 for sand and 3.74 ± 0.41 for anthracite communities at 20 cm depth. **Figure 3.9-a** shows that overall media diversity values were high and quite stable over the seasonal dataset. Community richness values in **Figure 3.9-b** were 67 ± 16 phylotypes in sand and 66 ± 14 phylotypes in anthracite, and were therefore less stable than H' values. This stability was despite the fact that feedwater values were generally lower on the first four sampling dates than on subsequent dates.

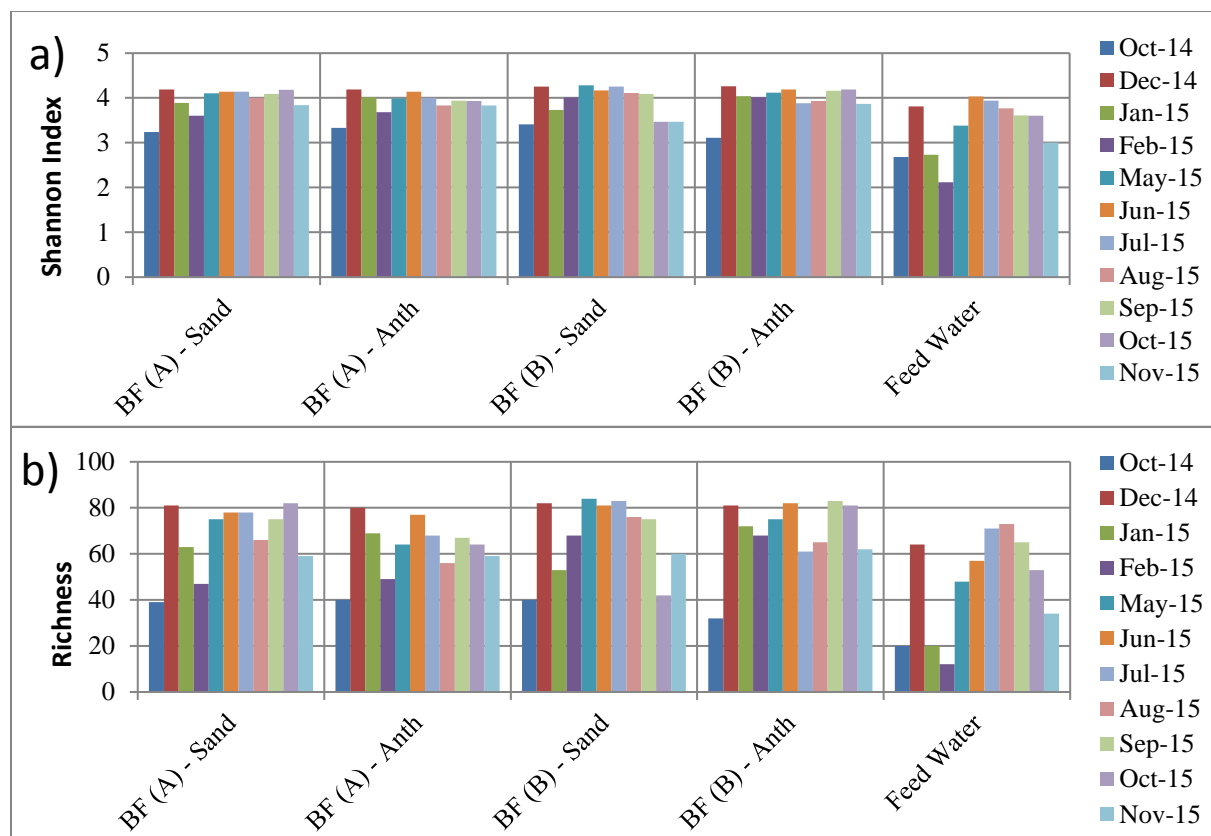


Figure 3.9: Bacterial community diversity (Shannon Index) (a) and richness (b) in feed water and media biofilms. Media samples were obtained from the 20 cm depth in BF(A) and BF(B).

Table 3.3: Paired t-test comparing diversity and richness of BF(A) vs BF(B). Sand and anthracite were compared separately, and were sampled from the 20 cm depth media intermixing zone. Values were obtained using PCR-DGGE bacterial community profiling. Significant results are indicated by asterisks (*).

Media	Parameter	p value
Sand	Shannon Diversity	0.985
	Richness	0.869
Anthracite	Shannon Diversity	0.046*
	Richness	0.126

Differences in biofilm means between 3 seasonal groups were tested using ANOVA (**Table 3.4**). The winter group consisted of those samples below 10 °C (December 2014, January & February 2015) during 100 L/h (3.08 m/h) operation, the summer group consisted of 100 L/h operation above 10 °C (May to August 2015), and the autumn group contained samples from September to November 2015 during 50 L/h (1.54 m/h) operation. **Table 3.4** presents the p-values of this analysis, with neither anthracite nor sand showing seasonal differences in richness or Shannon diversity means ($\alpha = 0.05$).

Table 3.4: Analysis of variance (ANOVA, $\alpha = 0.05$) comparing biofilter diversity and richness between seasonal groups at 20 cm depth. Seasonal groups were winter 2014/2015, summer 2015 and fall 2015. Additionally, feed water diversity and richness means were compared with sand and anthracite biofilm (ANOVA, $\alpha = 0.05$).

		ANOVA (p values)
Media	Parameter	Between Seasons Biofilm
Sand	Shannon Diversity	0.750
	Richness	0.807
Anthracite	Shannon Diversity	0.407
	Richness	0.437

Figure 3.10 presents Shannon diversity and richness data for samples collected throughout the depth of the biofilter, including those from the top 10 cm of anthracite media, the 20 cm mixing zone of sand/anthracite, and the 60 cm sand depth from BF(B). For media biofilm bacterial richness and diversity, no change was observed along increasing depths within the filter.

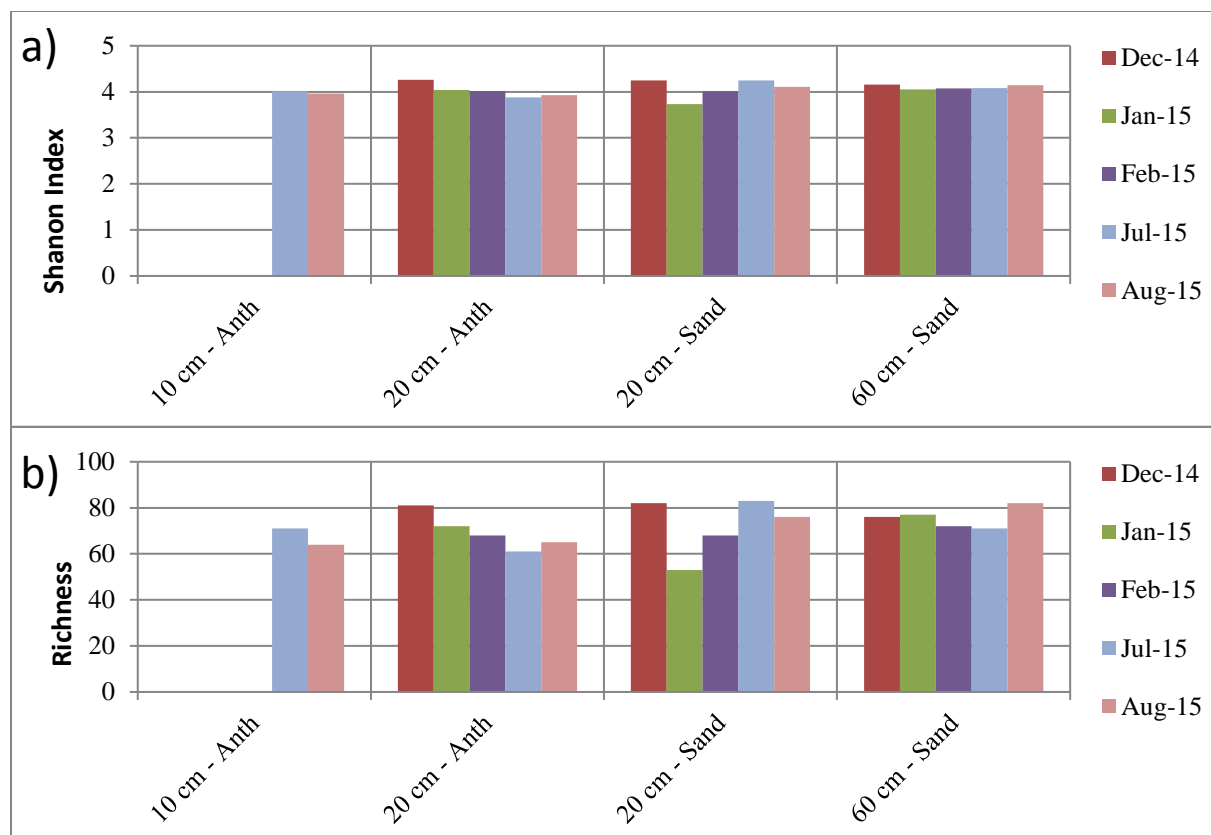


Figure 3.10: Barplot showing Shannon-Weiner diversity index (a) and richness (b) parameters as a function of biofilter media depth across seasonal conditions.

Pearson correlations between diversity metrics and water quality were performed (Tables S2 to S5 in App. A.) and results showed that there was no significant correlation between Shannon diversity, richness and water quality parameters, including DOC, NH₃ and Ortho-P, and values were all below 0.66 and above -0.71. As well, DGGE group (as defined by hierarchical clustering and later refined by DCA clustering) diversity parameters are presented in Table 3.5. Given that DCA analysis showed Groups D and E to be within the same cluster, they were combined into the group labelled as Group D/E (October & December 2014 as well as May to November 2015 samples) for further analysis; this Group D/E presented the highest diversity at 3.97 ± 0.33 and 3.94 ± 0.30 for sand and anthracite, respectively. Group C was composed of biofilter media biofilm communities from January and February 2015, and also had high diversity index values of 3.81 ± 0.18 and 3.94 ± 0.17 . Within the feed water samples, Group A had Shannon diversity of 3.73 ± 0.22 , while Group B had a Shannon diversity which was much lower, at 2.63 ± 0.37 . Table 3.5 also presents richness data for each DGGE group.

Richness for Group D/E richness was highest at 70 ± 15 and 70 ± 14 for sand and anthracite respectively. Group C richness was lower at 58 ± 10 and 65 ± 10 for sand and anthracite, respectively. Feed water community richness for Group A was 62 ± 9 while Group B was again much lower at 22 ± 9 .

Table 3.5: Shannon diversity and richness results for DGGE Groups as defined by hierarchical and DCA clustering analyses.

Type	Group	n	H' mean	H' st. dev.	Richness mean	Richness st. dev.
Water	A	7	3.73	0.22	62	9
Water	B	4	2.63	0.37	22	9
Sand	C	4	3.81	0.18	58	10
Anth	C	4	3.94	0.17	65	10
Sand	D	2	3.33	0.12	40	1
Anth	D	2	3.22	0.16	36	6
Sand	E	16	4.05	0.25	74	11
Anth	E	16	4.03	0.15	70	9
Sand	D/E	18	3.97	0.33	70	15
Anth	D/E	18	3.94	0.30	70	14

3.4.3 Biofilter Media Biofilm Biomass Characterization

3.4.3.1. Biofilm Cell Concentrations

Biomass levels on the biofilter media were measured using bulk media ATP values (ng ATP/cm³). As well, cell concentration (cells/cm³) of the biofilm extracted from the media was measured by flow cytometry. References to biomass will hereafter refer to ATP and cell count data. Data in **Figure 3.11** show media ATP (a), cell counts (b) and ATP/cell values (c) for samples collected from biofilter A and B at 20 cm depth, which corresponded with the sand/anthracite interface. Sand and anthracite were separated and values for each parameter are presented separately. The loading rate was 3.08 m/h, and this was reduced in December to 1.54 m/h starting in September 2015. As described earlier, the data shown from October 2014 to February 2015 were provided by Elhadidy (2016); while the data from May to November 2015

were measured in the current work using the same biomass characterization methods (Elhadidy et al., 2017).

Since biofilters A and B were fed using the same water and loading rates, no differences were expected between filters at the same sample depth. Indeed, no differences were found between BF(A) and BF(B) for either biomass parameter at 20 cm depth (paired t-tests, $\alpha = 0.05$, **Table 3.6**). **Figure 3.11-a** shows that, based on ATP, sand had more biomass per cm^3 than anthracite. This confirms the findings by Elhadidy (2016) by providing additional data over an extended sampling period. The ATP values of both biofilters were averaged for the 11 sampling campaigns spanning 14 months and were 2016 ± 705 ng ATP/ cm^3 for sand and 891 ± 453 ng ATP/ cm^3 for anthracite. The cell counts in **Figure 3.11-b** use a log scale wherein the trend of sand exhibiting more biomass than anthracite is less striking. Average cell counts were $4.86 \times 10^8 \pm 3.72 \times 10^8$ cells/ cm^3 for sand and $3.06 \times 10^8 \pm 2.56 \times 10^8$ cells/ cm^3 for anthracite.

For the results discussed just above, and for further results in this chapter where parameter values on anthracite and sand are compared, it is important to keep media size in mind. The 20 cm depth in both filters corresponded to the interface between anthracite and sand. Thus, the largest anthracite particles would be intermixed with the smallest sand particles, although media size measurements were not made. Since results are expressed per unit volume of media (cm^3), media diameter will play a role because when it is smaller there is a greater surface area for biofilm growth per unit filter volume. It would thus be expected that, other things being equal, results would be higher for sand than for anthracite. Although other factors may have affected observed differences between anthracite and sand were those occurred, it is important to keep media size in mind as a probable contributing factor.

Figure 3.11-a shows ATP values were generally highest in January and February 2015 (3443 ng ATP/ cm^3) and lowest in the summer months starting in July. Cell counts in **Figure 3.11-b** were similar to ATP, with the highest values in February 2015 and lowest in July 2015. **Tables S2 to S5 in App. A** show the correlations between ATP and cell counts were high for each biofilter and media type; Pearson r values ranged from 0.75 to 0.91 (**Tables S2 to S5**). Biomass shared a negative correlation with feed temperature (ranging from an r of -0.81 to -0.91 for ATP

and -0.68 to -0.76 for cell counts), yet a positive correlation with feed ammonium concentrations (ranging from an r of 0.78 to 0.95 for ATP and 0.73 to 0.78 for cell counts) in **Tables S2 to S5**. It is also important to note that ammonia levels were also highly correlated with temperature (-0.85), and that ammonia levels rose above detection limit exclusively during cold winter conditions (**Figure 3.2b**).

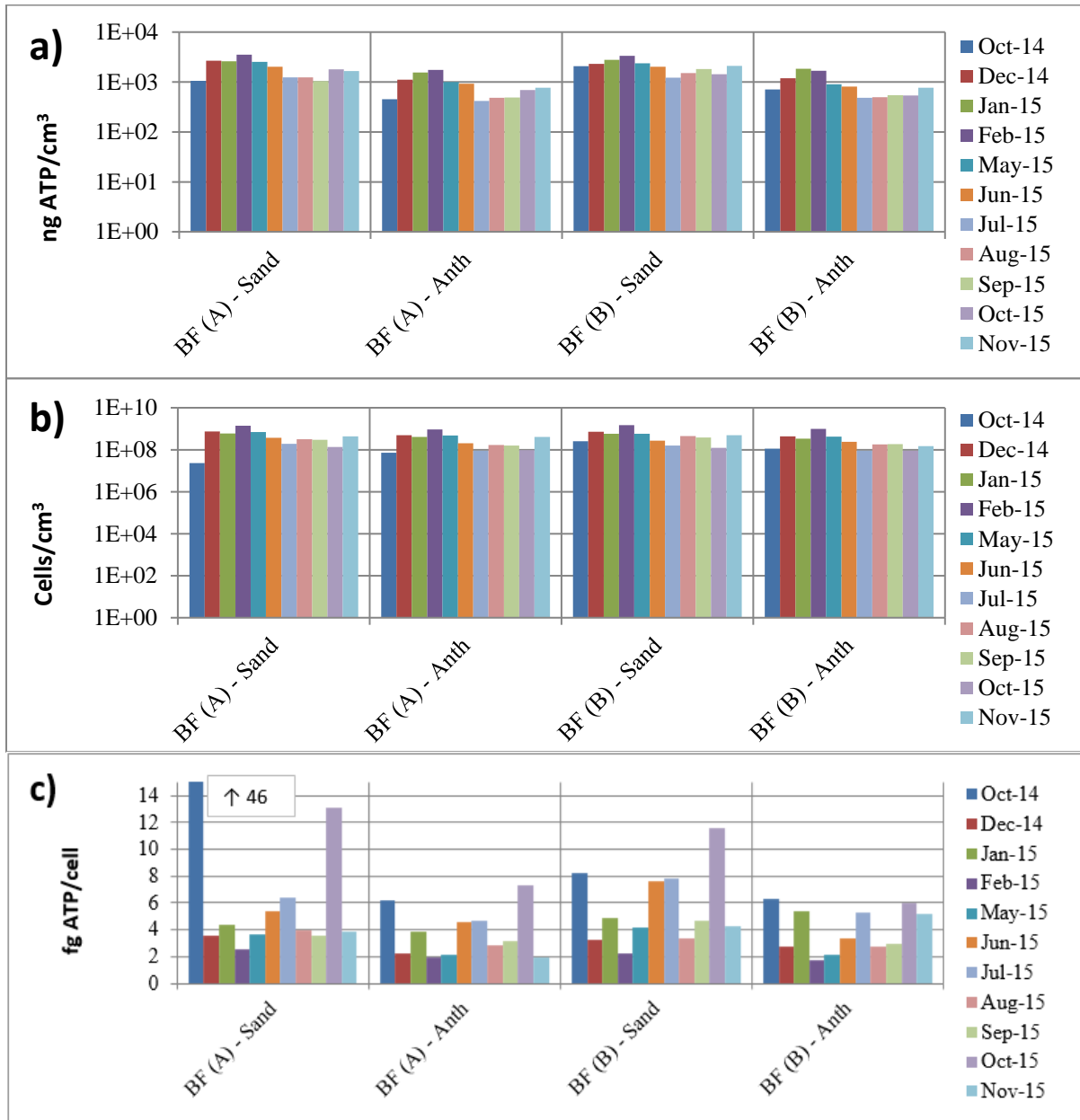


Figure 3.11: Seasonal trends in biofilter media bulk ATP (a), cell count (b), and femtogram ATP/cell (c).

Table 3.6: Paired t-test comparing volumetric ATP, cell counts and ATP/cell between BF(A) and BF(B) for sand and anthracite media collected at 20 cm depth. Significant results are indicated by asterisks (none in this table).

Media	Parameter	p value
Sand	ng ATP/cm ³	0.3860
	Cells/cm ³	0.7172
	ng ATP/cell	0.4550
Anthracite	ng ATP/cm ³	0.9772
	Cells/cm ³	0.1948
	ng ATP/cell	0.3936

In a seasonal comparison of biomass values using ANOVA, the winter ATP and cell count data were significantly higher than summer or fall 2015 values, for both sand and anthracite (ANOVA with post-hoc Tukey Honest Significant Difference (HSD), alpha = 0.05). A list of p values for the seasonal means comparison can be found in **Table 3.7**. **Figure 3.11-c** shows fg ATP/cell data for each biofilter and media type at 20 cm depth across the 14 month time span of the current study. Average values between both biofilters were 6.17±9.40 fg ATP/cell for sand and 3.84±1.51 fg ATP/cell for anthracite. ANOVA with post-hoc Tukey HSD (**Table 3.7**) showed that there was a significant difference between summer-fall and summer-winter sand ATP/cell values for sand media (p = 0.013 and 0.033 respectively, alpha = 0.05), but there was no significant difference in seasonal values for anthracite media.

Table 3.7: Analysis of variance (ANOVA, $\alpha = 0.05$) comparing biofilter biomass in media samples collected at 20cm depth. Seasonal groups were winter 2014/2015, summer 2015 and fall 2015. Tukey honest significant difference analysis was performed on significant ANOVA results. Significant results are indicated by asterisks.

Media	Parameter	ANOVA (p values)	Tukey Honest Significant Difference (p values)		
		Between Group	Summer- Fall	Winter- Fall	Winter- Summer
Sand	ng ATP/cm ³	0.0004*	0.9024	0.0033*	0.0006*
	Cells/cm ³	0.0002*	0.2496	0.0116*	0.0002*
	ng ATP/cell	0.0007*	0.0125*	0.6991	0.0326*
Anthracite	ng ATP/cm ³	0.0000*	0.9181	0.0003*	0.0000*
	Cells/cm ³	0.0005*	0.7465	0.0053*	0.0005*
	ng ATP/cell	0.7515	-	-	-

Figure 3.12-a to 3.12-c presents ATP, cell count and ATP/cell data for 10, 20, and 60 cm depths from BF(A) and BF(B) pertaining to both media types. For both ATP and cell counts, biomass generally decreased from 20 to 60 cm. However, samples collected at 10 cm depth on 2 occasions showed that anthracite biomass at the top of the biofilter was similar to that at 20 cm depth.

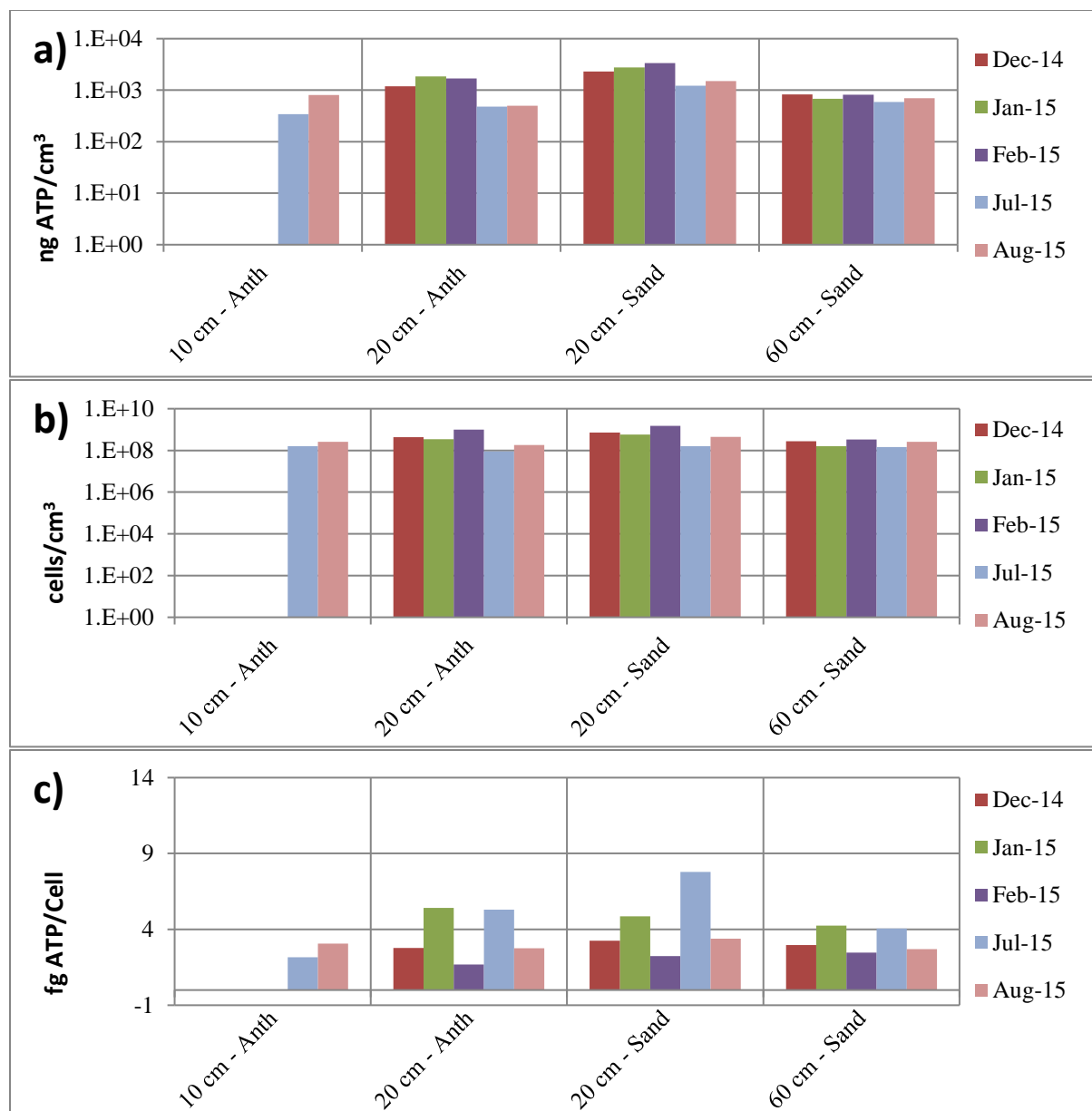


Figure 3.12: Biofilter media bulk ATP (a), live cells (b), and femtogram ATP/cell (c) over media depth (10, 20 and 60 cm below the media surface).

3.4.3.2 Biofilm EPS

Results in **Figures 3.13-a** and **3.13-b** show that sand had a higher concentration of proteins and carbohydrates than anthracite. Total carbohydrate averages were $56 \pm 39 \mu\text{g D-gluc/cm}^3$ for sand and $32 \pm 24 \mu\text{g D-gluc/cm}^3$ for anthracite. **Figure 3.13** shows for both types of media, EPS including both carbohydrates and proteins were highest in the winter months

(December, January, February) and were lower in the spring/summer months starting in May and continuing until the fall (November). In a seasonal comparison of EPS values using ANOVA, the winter carbohydrate and protein data were significantly higher than summer or fall 2015 values, for both sand and anthracite (ANOVA with post-hoc Tukey Honest Significant Difference (HSD), $\alpha = 0.05$). A list of p values for the seasonal comparisons of EPS means can be found in **Table 3.8**.

Figure 3.13-c shows carbohydrate: protein ratio (CH/PN) data for each biofilter and media type at 20 cm depth across the 14 month time span of the current study. Average CH:PN values at 20 cm depth were 0.50 ± 0.12 for sand and 0.46 ± 0.14 for anthracite. Significant differences in seasonal means for CH:PN were, as **Table 3.8** shows, present between sand summer-winter ($p < 0.001$) and fall-winter ($p = 0.005$) as well as anthracite summer-winter ($p < 0.001$) and fall-winter ($p = 0.001$) seasons. Means comparisons were performed using the ANOVA test with post-hoc Tukey HSD between winter, summer and fall values with alpha set to 0.05. These results show that EPS contains relatively more carbohydrates compared with proteins in the colder winter months, but in the summer months there is an opposite trend with EPS containing a higher proportion of proteins. Summer-fall means comparison showed no difference in the ratio of carbohydrates to proteins for either media (**Table 3.8**).

A more limited data set was evaluated to measure the concentration of extracellular DNA (eDNA) in EPS samples. **Figure 3.13-d** shows eDNA data for each biofilter and media type at 20 cm depth across a 4 month time span (from August to November 2015). Average $\mu\text{g eDNA}/\text{cm}^3$ values were 22 ± 4.4 for sand and 11 ± 1.4 for anthracite. Similar to the other EPS parameters, sand contained higher volumetric eDNA content than anthracite; as mentioned previously, sorting of media sizes at the interface may have contributed to this difference. The average EPS protein, carbohydrate and eDNA ratio was 5:3:1 for sand media and 6:3:1 for anthracite. EPS levels in the biofilms extracted from the biofilter media were also measured using bulk media total carbohydrate values ($\mu\text{g D-glc}/\text{cm}^3$) and total protein ($\mu\text{g BSA}/\text{cm}^3$) as measured by colourimetric methods. Similar to ATP and cell concentrations, no differences

were found between BF(A) and BF(B) for either EPS parameter at 20 cm depth for either media type (paired t-tests, $\alpha = 0.05$, **Table 3.9**).

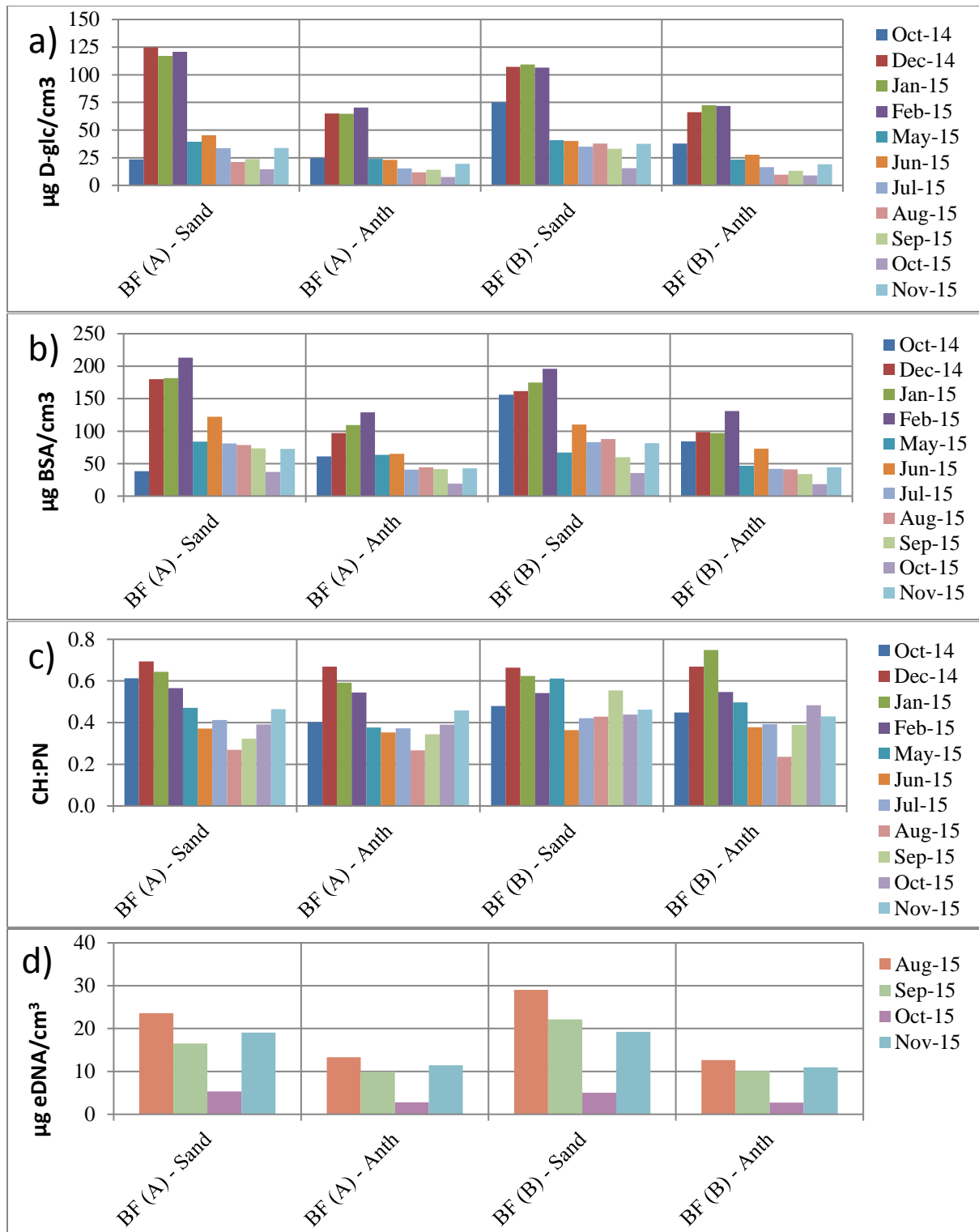


Figure 3.13: Seasonal trends in EPS from biofilter media including total carbohydrates (measured as D-glucose) (a), total proteins (measured as bovine serum albumin) (b), the CH:PN ratio of carbohydrates to proteins (c), and extracellular DNA (d). Samples were obtained from the 20 cm media depth.

Table 3.8: Analysis of variance (ANOVA) comparing biofilter media EPS carbohydrates, proteins and carbohydrate to protein ratio between seasonal groups at 20 cm depth, with alpha set to 0.05. Seasonal groups were winter 2014/2015, summer 2015 and fall 2015. Sand and anthracite were compared separately, and were sampled from the 20 cm depth of the media intermixing zone. Significant results are indicated by asterisks.

Media	Parameter	ANOVA (p values)	Tukey Honest Significant Difference (p values)		
		Between Group	Summer- Fall	Winter- Fall	Winter- Summer
Sand	µg D-glc/cm ³	0.0000*	0.9983	0.0000*	0.0000*
	µg BSA/cm ³	0.0000*	0.5186	0.0000*	0.0000*
	CH:PN	0.0001*	0.2130	0.0048*	0.0000*
Anthracite	µg D-glc/cm ³	0.0000*	0.0014*	0.0001*	0.0000*
	µg BSA/cm ³	0.0000*	0.2163	0.0000*	0.0001*
	CH:PN	0.0000*	0.3367	0.0008*	0.0000*

Table 3.9: Paired t-test comparing biofilter media carbohydrates, proteins and carbohydrate to protein ratio (CH:PN) between BF(A) and BF(B). Sand and anthracite were compared separately, and were sampled from the 20 cm depth of the media intermixing zone. Significant results are indicated by asterisks (alpha = 0.05).

Media	Parameter	p value
Sand	µg D-glc/cm ³	0.5289
	µg BSA/cm ³	0.6992
	CH:PN	0.3035
Anthracite	µg D-glc/cm ³	0.1085
	µg BSA/cm ³	0.9342
	CH:PN	0.0478*

Figure 3.14-a to 3.14-d presents volumetric media biofilm carbohydrate, protein, CH:PN and eDNA data for 10, 20, and 60 cm depths from BF(A) and BF(B) as well as from both media types. EPS exhibited a similar relationship with depth as biomass. Carbohydrates, proteins and eDNA all decreased from 20 to 60 cm. Similar to biomass, the total carbohydrate, protein and CH:PN values at 10 cm anthracite were similar to the 20 cm depth. The eDNA concentration at 10 cm were however slightly higher than at 20 cm.

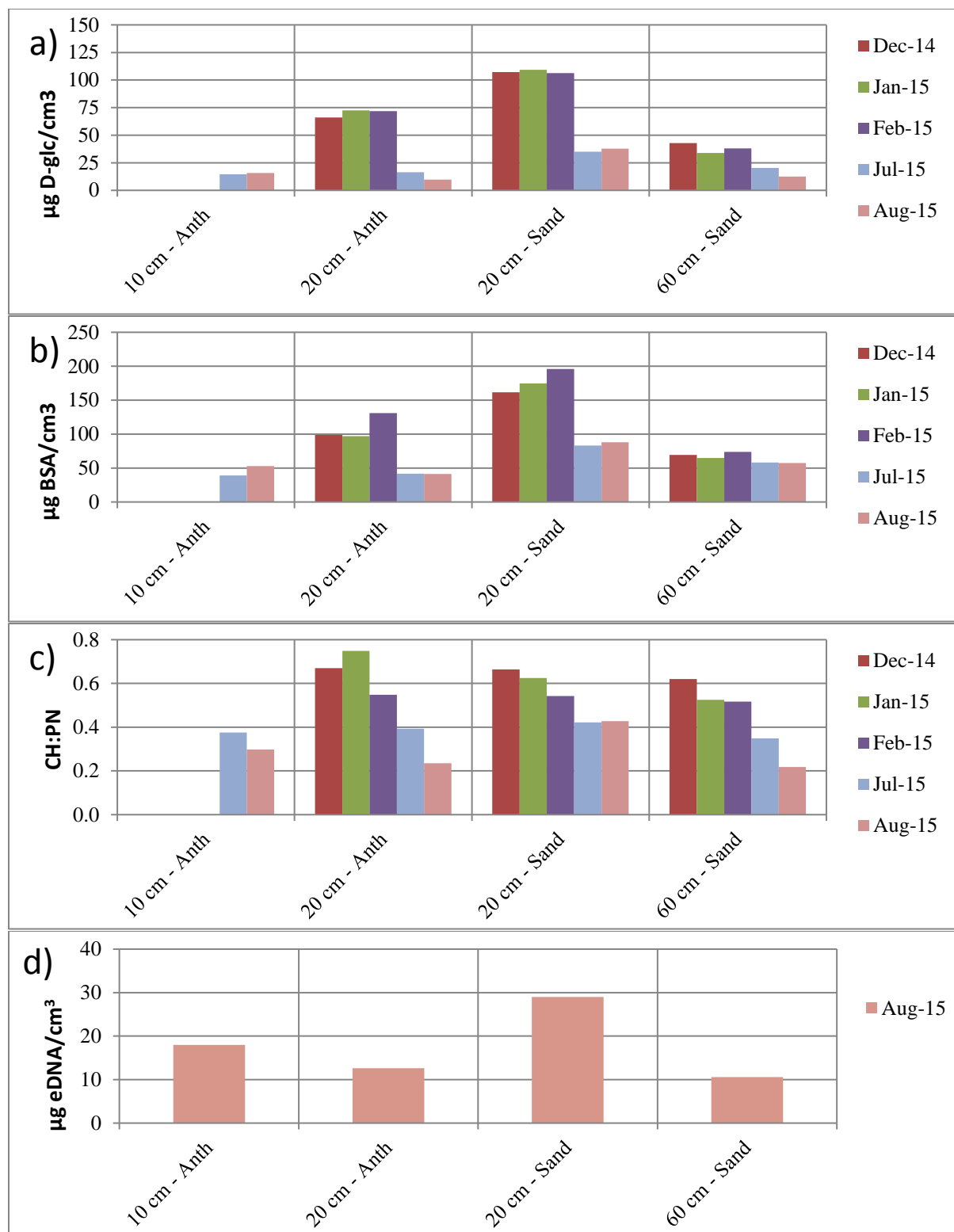


Figure 3.14: Biofilter media EPS as a function of media depth. Total carbohydrates is represented as D-glucose equivalent (a), proteins as bovine serum albumin (b), and carbohydrate to protein (CH:PN) ratio (c) for the 11 sampling campaigns. Note that depth data for eDNA is restricted to Aug 2015.

Tables S2 to S5 in App. A present Pearson correlations between total carbohydrates, proteins, ATP, cell count and pertinent water quality data. The correlations between EPS carbohydrates and proteins were high for each biofilter and media type (Pearson r values ranged from 0.92 to 0.96). EPS shared a negative correlation with feed temperature (ranging from an r of -0.88 to -0.94 for carbs and -0.70 to -0.85 for proteins), yet a positive correlation with feed ammonium concentrations (ranging from an r of 0.79 to 0.87 for carbs and 0.66 to 0.84 for proteins). This was quite similar to biomass, and in fact EPS and biomass values shared strong positive correlations in **Tables S2 to S5 in App. A**. For example BF(A) sand volumetric ATP and carbohydrate values correlated at a Pearson r of 0.83. For correlations between EPS and water quality data, see **Tables S2 to S5 in App. A**.

Figure 3.15-a and **3.15-b** presents EPS carbohydrates/cell and proteins /cell, respectively, for BF(A) and BF(B) as well as for both media types. Samples presented were from a 20 cm bed depth. Average sand EPS carbohydrate/cell and anthracite EPS carbohydrate/cell values were similar to one another, with sand values determined to be $1.72 \times 10^{-7} \pm 2.11 \times 10^{-7}$ $\mu\text{g D-glc/cell}$, and anthracite values as $1.36 \times 10^{-7} \pm 8.47 \times 10^{-8}$ $\mu\text{g D-glc/cell}$. Average sand EPS protein/cell and anthracite EPS protein/cell values per cell were also similar to one another, with sand values determined to be $3.38 \times 10^{-7} \pm 3.43 \times 10^{-7}$ $\mu\text{g BSA/cell}$, and anthracite values as $3.06 \times 10^{-7} \pm 1.91 \times 10^{-7}$ $\mu\text{g BSA/cell}$. Overall there were no seasonal trends in the EPS/cell values, and no differences between media type or loading rate, as evident by the similar values during the fall 2015 lower loading rate of 1.54 m/h.

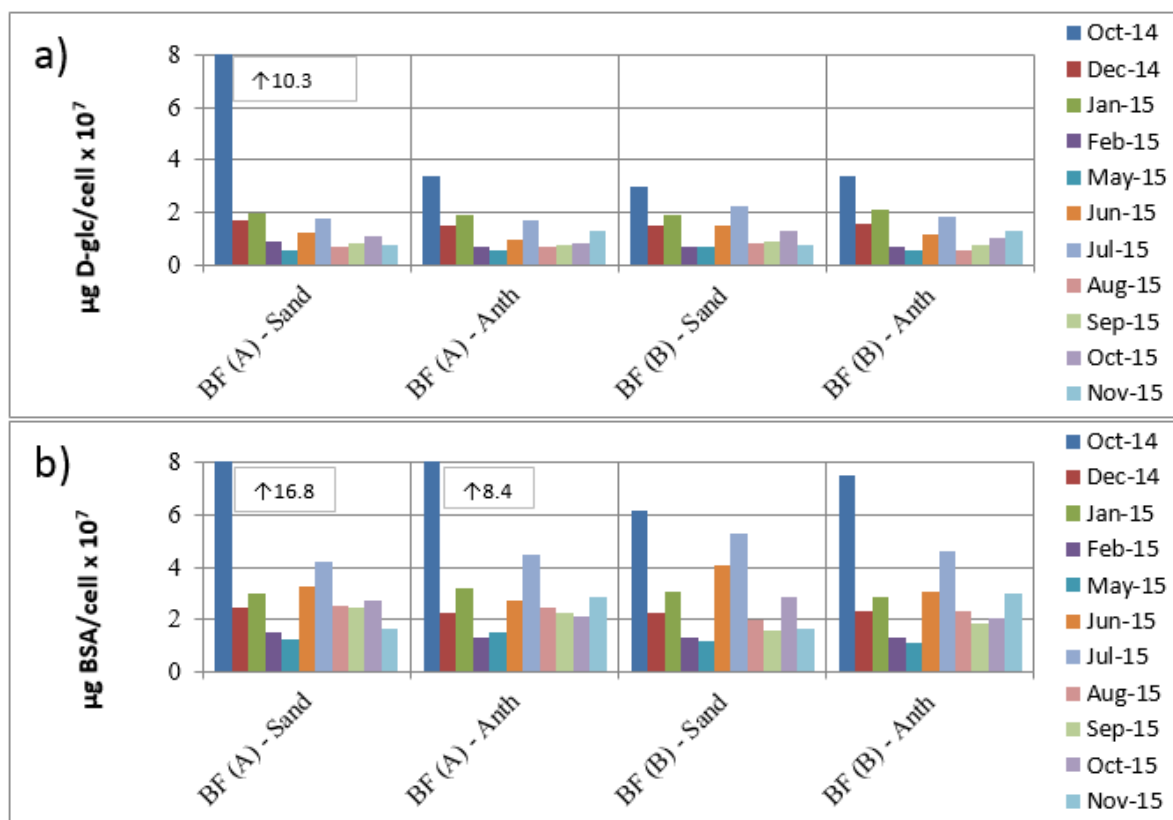


Figure 3.15: Amount of EPS per cell at 20 cm media depth for both biofilters and media types. Carbohydrates were measured in $\mu\text{g D-glucose equivalents}$ (a) and proteins were measured in $\mu\text{g BSA equivalents}$ (b).

LC-OCD defined NOM fractions were also quantified from the same biofilm EPS extractions used to assess total carbohydrates, proteins and eDNA, using the approach described by Elhadidy et al. (2017). The 3 fractions were defined as high molecular weight organic carbon (HMW-OC), intermediate molecular weight organic carbon (IMW-OC), and low molecular weight organic carbon (LMW-OC). Data in **Figure 3.16** show media biofilm HMW-OC (a), IMW-OC (b) and LMW-OC values (c) for samples collected from biofilter A and B at 20 cm depth. Due to delays with method start-up, EPS NOM fractions were not measured for May 2015 media samples. As with biomass and EPS measurements, sand had higher concentrations of LC-OCD defined EPS fractions than anthracite which again could have been due to media sorting effects at the sand/anthracite interface. The HMW-OC sand average was $34 \pm 13 \mu\text{g}/\text{cm}^3$ and for anthracite was $17 \pm 5 \mu\text{g}/\text{cm}^3$. **Figure 3.16-a** shows that BF(B) and BF(A) sand and anthracite HMW-OC levels were relatively stable over the course of the study period, and were poorly correlated with other biomass and EPS parameters (**Tables S2 to S5 in App. A**). IMW-OC $\mu\text{g}/\text{cm}^3$ were also averaged for both biofilters and were $39 \pm 14 \mu\text{g}/\text{cm}^3$ for sand and 24 ± 8

$\mu\text{g}/\text{cm}^3$ for anthracite. Averaged values for LMW-OC $\mu\text{g}/\text{cm}^3$ were $86 \pm 35 \mu\text{g}/\text{cm}^3$ for sand and $52 \pm 18 \mu\text{g}/\text{cm}^3$ for anthracite. **Figures 3.17-b** and **3.17-c** show similar seasonal variability for IMW-OC and LMW-OC, with higher values occurring in the winter. These two LC-OCD defined biofilm parameters shared strong Pearson r correlations with one another, ranging from 0.86 to 0.95. Furthermore, Pearson correlation r values between both IMW-OC and LMW-OC, and the biofilm carbohydrate, protein, ATP and cell count data were positive and ranged from low ($r < 0.70$) to strong ($r \geq 0.90$; **Tables S2 to S5 in App. A**), which indicates these two LC-OCD defined biofilm fractions followed similar seasonal and biomass-related patterns as the total proteins and carbohydrates values. Specifically, IMW-OC and LMW-OC correlations with ATP and cell count ranged from 0.59 to 0.88, while IMW-OC and LMW-OC correlations with proteins and carbohydrates were stronger and ranged from 0.83 to 0.96. The high correlation strengths between both IMW and LMW-OC parameters and traditionally defined EPS shows that seasonal means comparisons for IMW and LMW-OC can be inferred from prior EPS investigation.

Figure 3.17 presents media biofilm HMW, IMW and LMW-OC data for 10, 20, and 60 cm depths from BF(A) and BF(B) as well as from both media types. Biofilm LC-OCD fractions exhibited a similar relationship with depth as biomass, decreasing from 20 to 60 cm and (for the HMW fraction only) exhibiting a slight increase from 10 to 20 cm depth.

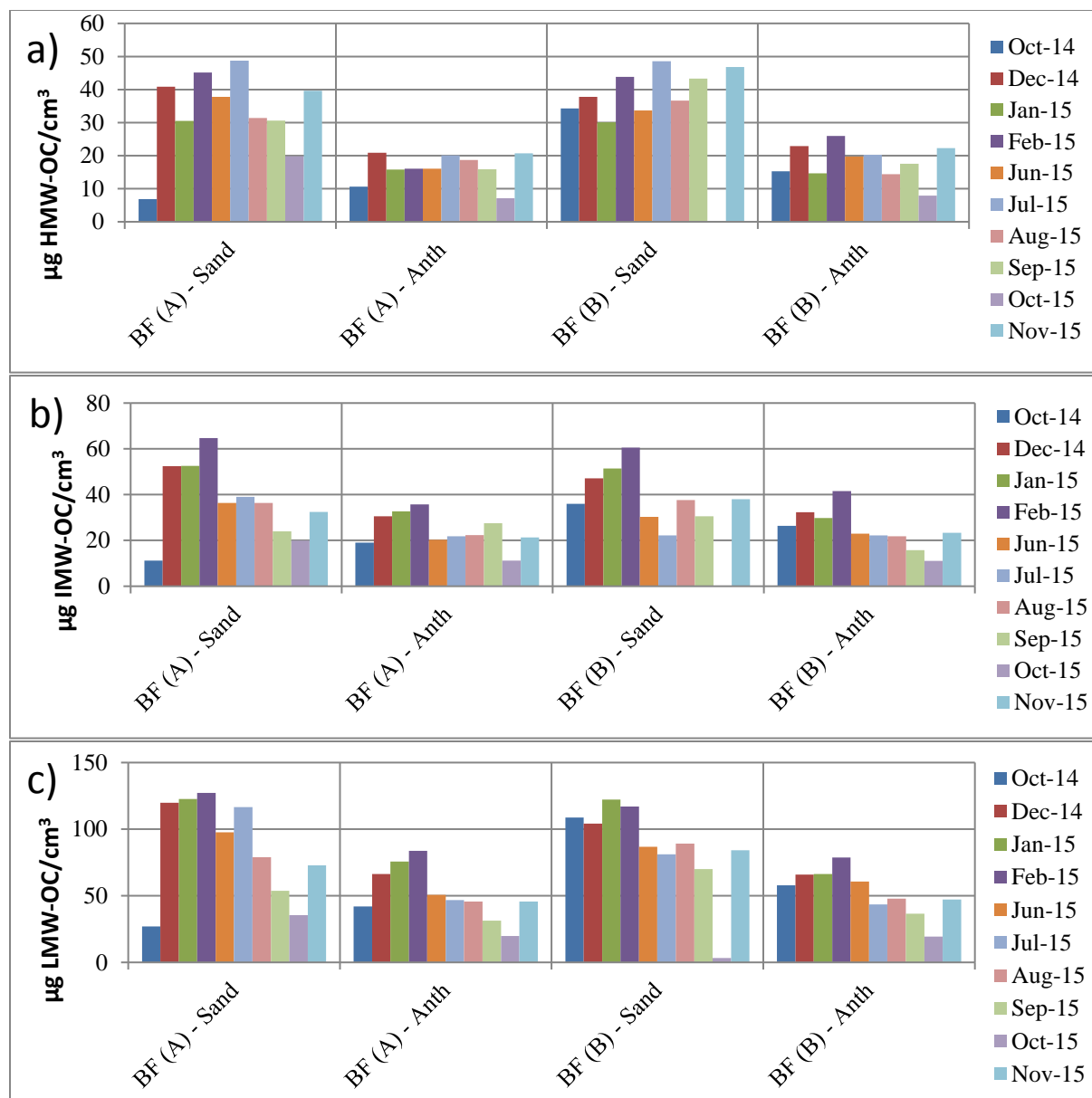


Figure 3.16: LC-OCD fractions for biofilm EPS including HMW-OC (a), IMW-OC (b), and LMW-OC (c). Note that this analysis was not performed in May 2015.

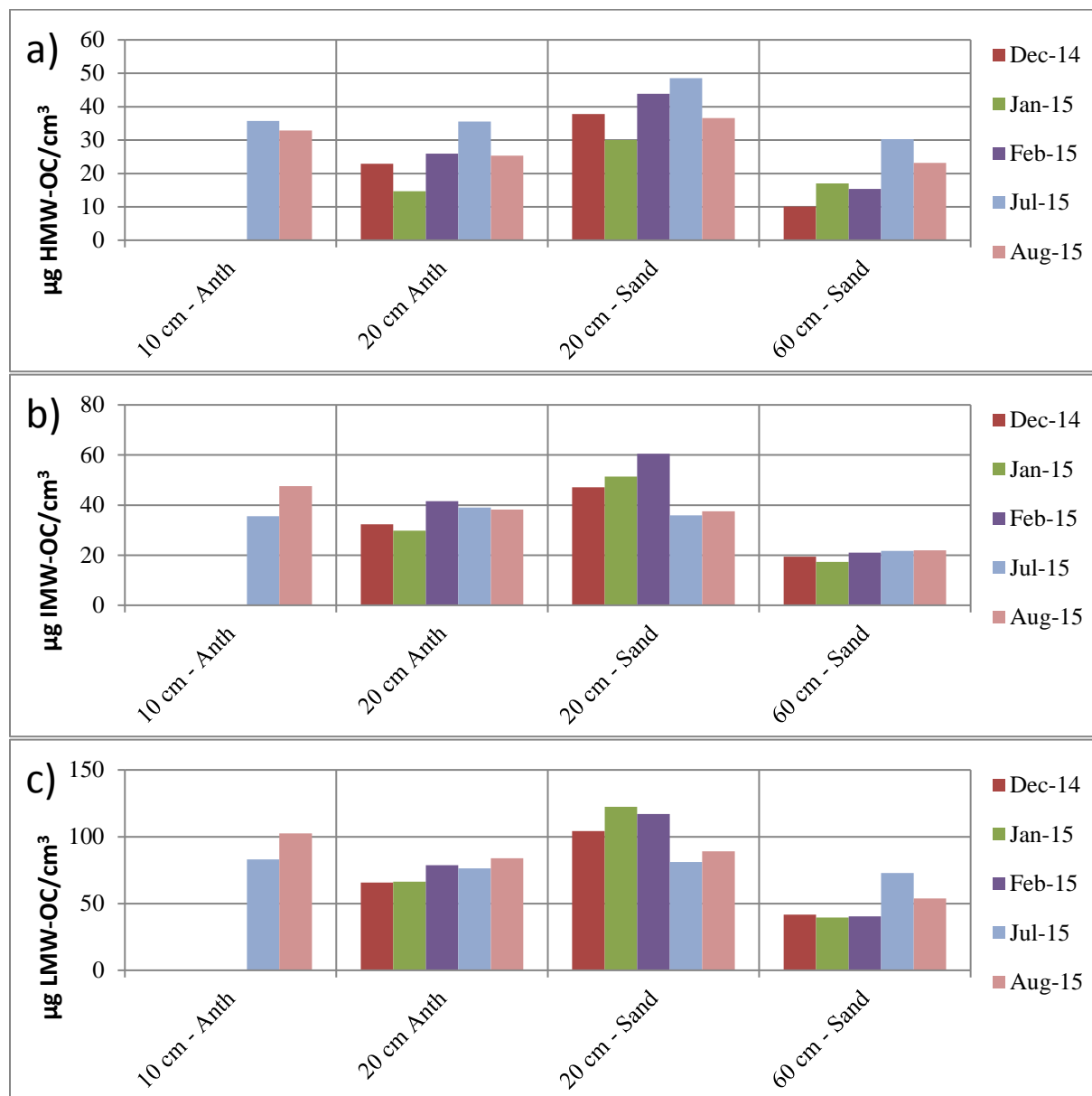


Figure 3.17: Biofilter biofilm LC-OCD fractions per cubic centimetre of media. Several depths are considered across warm and cold conditions.

3.4.8 Biofilter Performance

Performance of the 8 min EBCT biofilter A and 16 min EBCT biofilter B was measured by determining the percent removals of DOC and NOM fractions, of which the biopolymers had the largest molecular weight. **Figure 3.18** shows percent removal of DOC between October 2014 and November 2015 for both biofilters. The vertical dashed line indicates a decrease in

loading rate from 3.08 m/h to 1.54 m/h starting in September 2015. Average DOC removal for BF(A) was $10.0 \pm 3\%$. Winter operation had a loading rate of 3.08 m/h and temperatures below $10\text{ }^{\circ}\text{C}$ (sample dates of December 2015, January 2015 and February 2015; refer to **Figure 3.2**); during this period BF(A) had lower DOC removals ($5.8 \pm 0.3\%$), which increased in summer 2015 to $10.9 \pm 1.5\%$, and to $12.9 \pm 1.4\%$ during autumn (September, October and November 2015) at which time the loading rate was decreased to 1.54 m/h. DOC removal by the longer EBCT of BF(B) followed the same trends as BF(A) but removals were higher. The average DOC removal for the study period for BF(B) was $14.3 \pm 6.1\%$. Winter operation resulted in a low DOC percent removal by BF(B) of $6.7 \pm 0.4\%$, which increased to $17.3 \pm 2.5\%$ during summer 2015. BF(B) DOC removals then increased marginally in fall 2015 during the decreased loading rate period, but then decreased rapidly to 8.8% in November 2015.

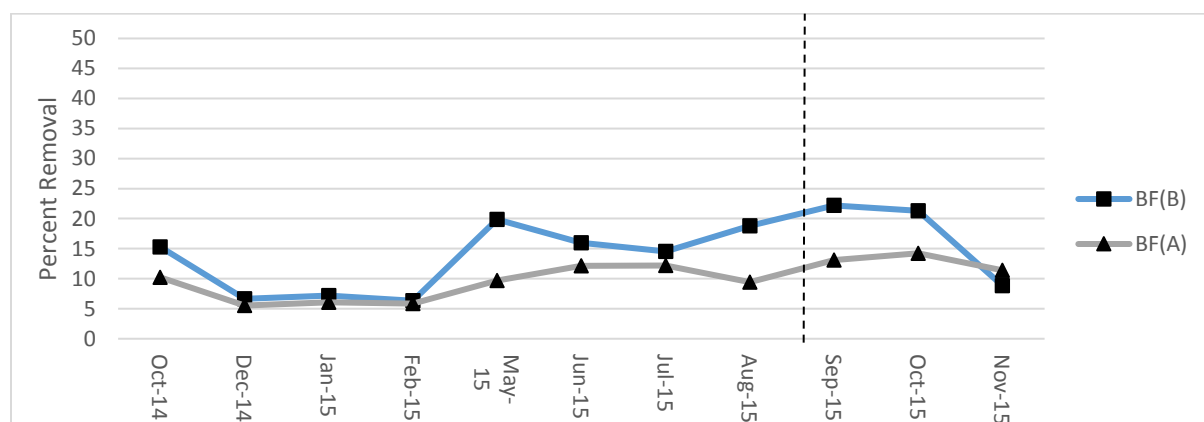


Figure 3.18: Biopfilter performance for BF(B) and BF(A) as measured by percent removal of DOC from Oct 2014 to Nov 2015. Vertical dash indicates change in operation from 100 L/h (3.08 m/h) to 50 L/h (1.54 m/h).

Biopolymer percent removal is depicted in the line chart of **Figure 3.19** while percent removals of the other 4 NOM fractions (humic substances, building blocks, low molecular weight acids/humics and low molecular weight neutrals) are presented in **Figure 3.20**. Average biopolymer removal for BF(A) was $47.6 \pm 19.4\%$. Winter operation resulted in a lower average biopolymer removal ($24.5 \pm 6\%$), which increased in summer 2015 (to $56.3 \pm 17.6\%$). The average biopolymer removal for the longer EBCT of BF(B) followed the same trends as BF(A) but, similar to DOC, removals were higher in BF(B). Average biopolymer removals for the study period by BF(B) were $63.4 \pm 26.1\%$. Winter operation resulted in a low biopolymer percent

removal by BF(B) at $28.0 \pm 11.6\%$, which increased to $80.3 \pm 16.6\%$ during summer 2015. Unlike DOC removal, biopolymer removal showed either no change (BFA) or a decrease (BFB) after the flow rate was decreased in September 2015. This could perhaps be related to coincidental changes in biopolymer character (and therefore potentially biodegradability) during this time.

Removal of the humics, BB and LMW fractions were lower (less than 25%) compared with the biopolymers fraction, and removal was variable with no temperature trends. Negative removal values that sometimes occurred in the BB and LMW fractions was likely due to their low concentrations and potential endogenous production within the filter bed. The observed higher % removals by BF(B) compared with BF(A) were tested using a paired student's t-test (**Table 3.10**). Of the 5 LC-OCD defined NOM fractions, only biopolymers exhibited significantly higher removal by the longer EBCT of BF(B) when compared against BF(A) ($p < 0.001$, $\alpha = 0.05$). DOC removal by BF(B) was also found to be significantly higher than BF(A) ($p = 0.007$, $\alpha = 0.05$).

The seasonal trends in biopolymer and DOC removal for both biofilters were tested using ANOVA between the 3 seasonal groups of winter (December 2014, January and February 2015), summer (May to August 2015) and fall (September to November 2015). Note that the fall seasonal period pertained to modified biofilter operation, when loading rates were decreased from 3.08 m/h to 1.54 m/h. **Table 3.11** shows that there were significantly different removals for both BF(A) and BF(B) between seasonal groups regarding DOC ($p = 0.0002$ and 0.0172 for BF(A) and BF(B), respectively; $\alpha = 0.05$) and biopolymers ($p = 0.0180$ and 0.0032 for BF(A) and BF(B), respectively; $\alpha = 0.005$). Additionally, BF(B) showed significantly different removals in the LMW-acids fraction ($p = 0.0231$, $\alpha = 0.05$). These seasonal trends are further supported by the multiple correlation data that compared NOM removal and water temperature as shown in **Tables S2 to S5 in App. A**. DOC removal had a positive correlation with temperature with a Pearson r value of 0.78 and 0.87 for BF(A) and BF(B), respectively. Biopolymer removal also had a positive correlation with temperature with a Pearson r value of 0.85 and 0.91 for BF(A) and BF(B), respectively.

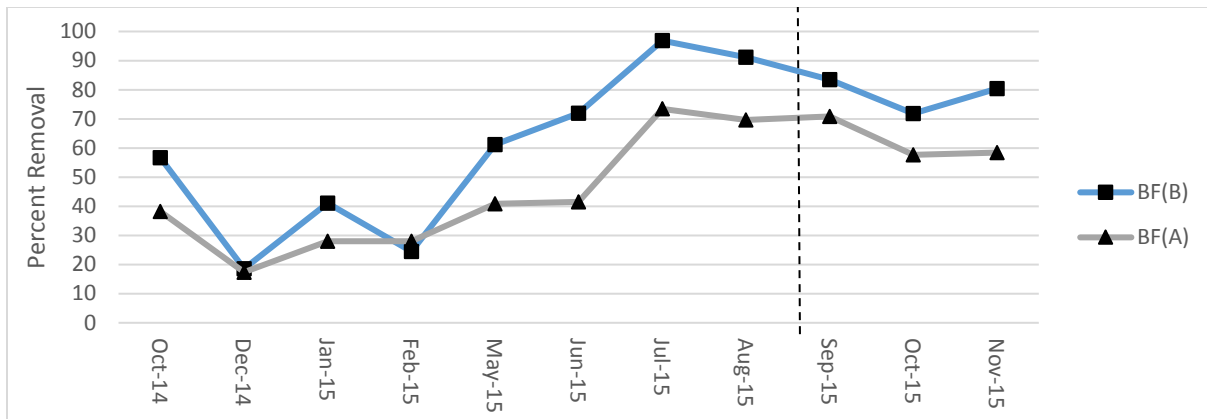


Figure 3.19: Biofilter performance for BF(A) and BF(B) as measured by percent removal of biopolymers from Oct 2014 to Nov 2015. Vertical dash indicates change in operation from 100 L/h (3.08 m/h) to 50 L/h (1.54 m/h).

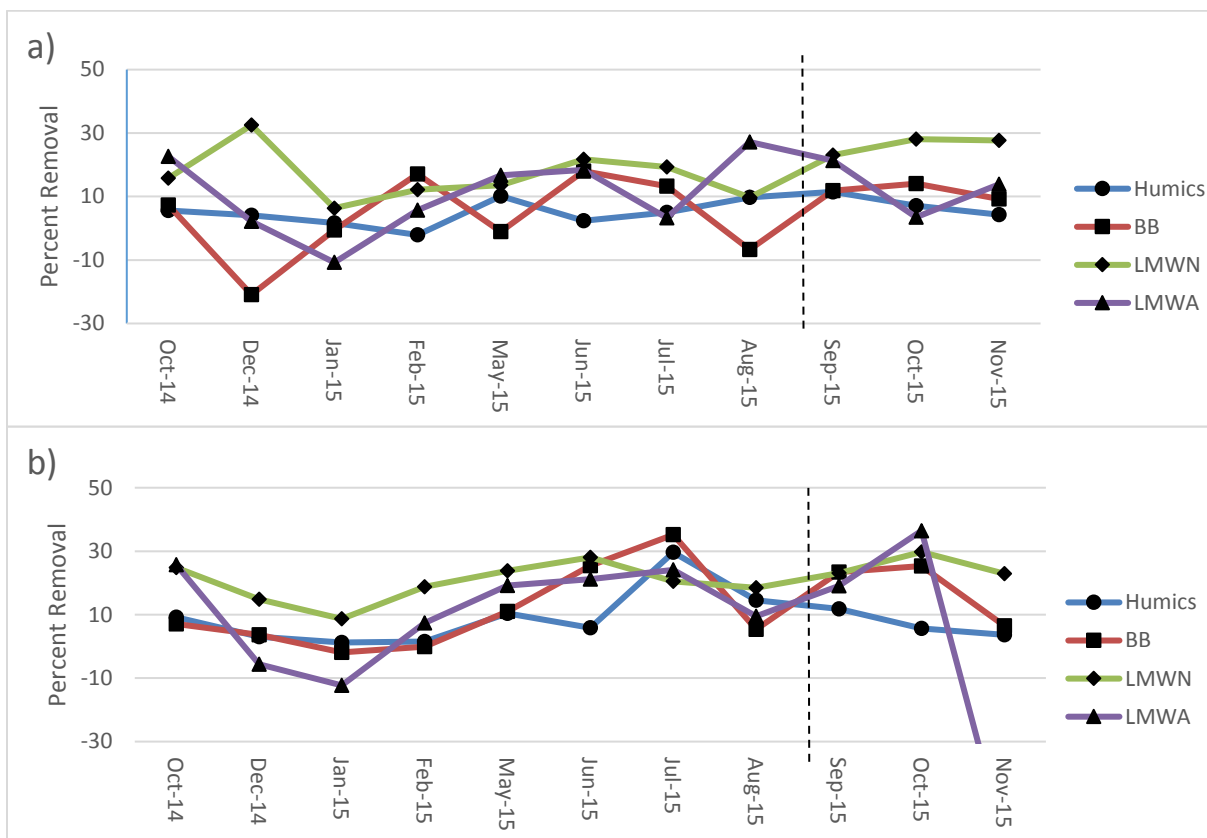


Figure 3.20: Biofilter performance for BF A (a) and BF B (b) from Oct 2014 to Nov 2015 as measured by percent removal of the NOM fractions as measured by LC-OCD, including humic substances, humic building block (BB), low molecular weight acids/ humics (LMWA) and low molecular weight neutral compounds (LMWN). Vertical dash indicates change in flow operation from 100 L/h (3.08 m/h) to 50 L/h (1.54 m/h). Nov 2015 LMWA y-axis value was -61.5.

Table 3.10: Results of paired t-test analysis comparing biofilter NOM removals between BF(A) and BF(B). Statistically significant differences are marked with asterisk (*).

Parameter	p value
DOC	0.0071*
Biopolymers	0.0004*
Humics	0.1603
Building Blocks	0.0729
LMW-Acids/humics	0.5058
LMW-Neutrals	0.7103

Table 3.11: ANOVA results comparing biofilter NOM removals between the seasonal groups of winter 2014/2015, summer 2015 and fall 2015. Statistically significant differences are marked with asterisk (*).

Media	Parameter	p value
BF(A)	DOC	0.0002*
	Biopolymers	0.018*
	Humics	0.0893
	Building Blocks	0.4380
	LMW-Acids	0.3045
	LMW-Neutrals	0.0678
BF(B)	DOC	0.0172*
	Biopolymers	0.0032*
	Humics	0.1104
	Building Blocks	0.1233
	LMW-Acids	0.0231*
	LMW-Neutrals	0.5078

3.4.9 Association of Biofilter DGGE Groups with Biofilm Parameters and Process Performance

The DGGE biofilm groups D/E & C were compared with their associated performance data (DOC and NOM LC-OCD fraction % removal) for both BF(A) and BF(B) as presented in **Figure 3.21**. Of the two DGGE profile media clusters, Group C had the lower average DOC percent removals (6.0 and 6.8% for BF(A) and BF(B), respectively), while Group D/E exhibited

higher DOC removal at 10.9 and 15.9% for BF(A) and BF(B), respectively. Group C biopolymer removal was lower (25.1 and 32.8% for BF(A) and BF(B), respectively), as were Group C LWM-acids removals, which were actually negative. Group D/E biopolymer percent removals were therefore higher at 53.7 and 72.0% for BF(A) and BF(B), respectively; LMW-acids removals were also higher at 9.8 and 14.3% for BF(A) and BF(B), respectively. Removals of other NOM fractions by the DGGE biofilm groups can be seen in **Figure 3.21**. Formal mean removal comparisons between DGGE groups were not possible given the small sample size available for Group C, given that biofilters A and B had to be treated separately and only two months of removal data were associated with this group.

Pearson r correlations showed strong relationships between DOC as well as biopolymer removal and temperature, with r values ranging from 0.93 and 0.85. It is not surprising that higher feed ammonia concentrations were associated with lower DOC removals, as higher feed ammonia occurred during the cold condition period. Pearson r values for ammonia and DOC removals ranged from -0.71 to -0.75 for BF(A) and BF(B), respectively. Feed nitrate concentrations were also negatively correlated with DOC and biopolymer percent removals but this relationship was not as strong (**Tables S2 to S5, Appendix A**). Percent removals for all LC-OCD defined NOM fractions were higher in Group D/E. As expected, DOC and biopolymer percent removal were well correlated (Pearson r values of 0.74 and 0.72 for BF(A) and BF(B), respectively, **Tables S2 to S5, Appendix A**).

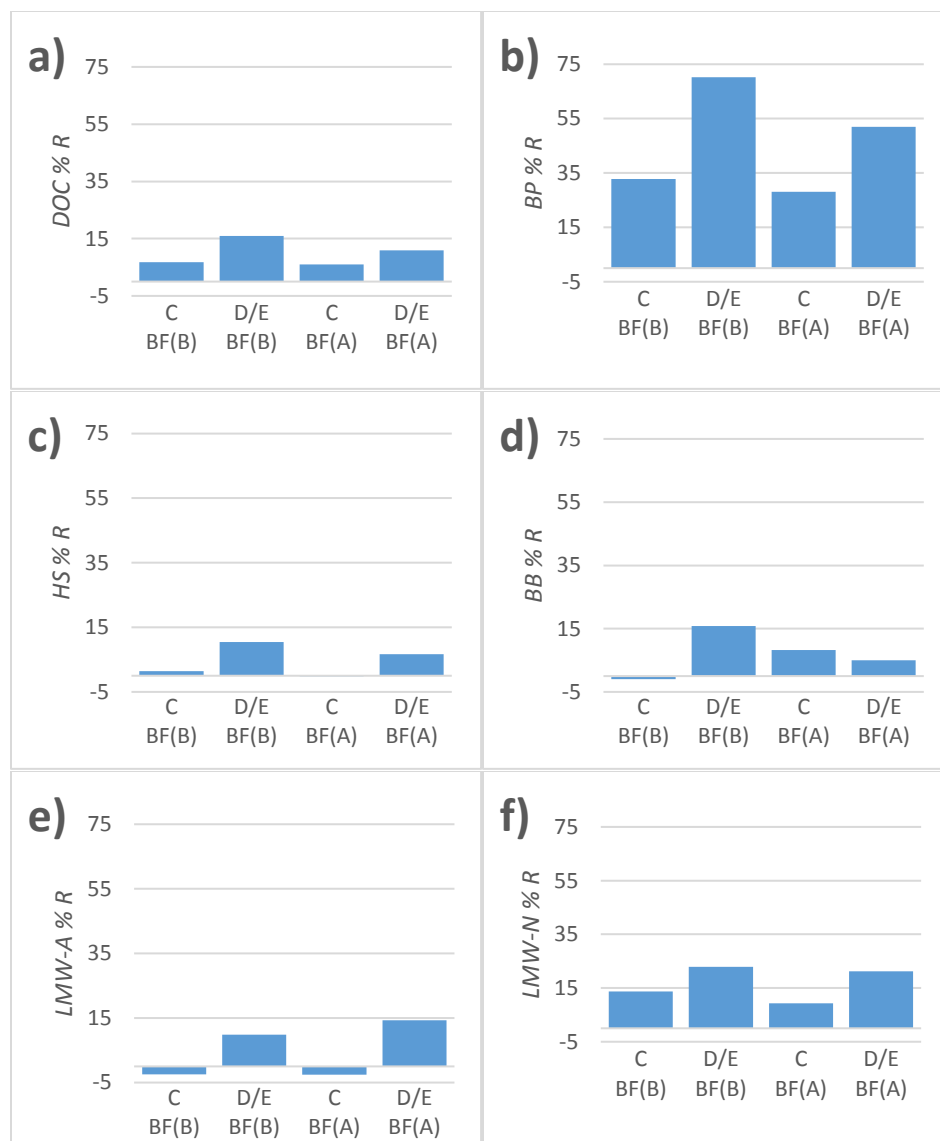


Figure 3.21: Bar charts presenting BF(A) and BF(B) % removal of a) dissolved organic carbon (DOC), b) biopolymers (BP), c) humic substances (HS), d) building blocks (BB), e) low molecular weight acids (LMW-A), and f) low molecular weight neutrals (LMW-N) relating to DGGE profile media biofilm groups C and D/E as defined by DCA clustering.

Biofilm characteristics including Shannon diversity, community richness, biomass and EPS were also compared between biofilter media DGGE community groups and arranged visually in **Figure 3.22**. Difference between group variances were tested using F tests (**Table 3.12**); given that several data sets showed unequal variance, means comparisons between DGGE group biofilm parameters were executed using t-tests for unequal variance. Diversity of media biofilm groups (**Figure 3.22**) were not significantly different between Groups D/E and C (t-test for unequal variance, $\alpha = 0.05$, $p = 0.108$ and 0.494 for sand and anthracite respectively,

Table 3.12); the same was observed for richness between DGGE groups (t-test for unequal variance, alpha = 0.05, p = 0.084 and 0.341 for both sand and anthracite respectively, **Table 3.12**)

Table 3.12: Compiled F-test and t-test values from comparisons of biofilter media biofilm parameters between DGGE groups C and D/E. Significantly different variances between Groups C and D/E (significant F-tests) for some parameters required the use of unequal variance t-tests for all data presented. Alpha = 0.05. Significant results are denoted by an asterisk ().*

Media	Test	p values							
		Shannon H'	Richness	ng ATP/cm ³	Cells/cm ³	fg ATP/cell	ug D-glc/cm ³	ug BSA/cm ³	CH:PN
Sand	F Test	0.170	0.233	0.467	0.008*	0.003*	0.015*	0.082	0.085
	t-Test	0.108	0.084	0.002*	0.042*	0.039*	< 0.001*	< 0.001*	0.002*
Anth	F test	0.203	0.341	0.136	0.009*	0.398	0.012	0.306	0.457
	t-Test	0.494	0.379	< 0.001*	0.042*	0.232	< 0.001*	< 0.001*	0.009*

Bulk ATP measurements are arranged by DGGE cluster group, and Group D/E presented ng ATP/cm³ media at 1782 and 709 for sand and anthracite, respectively. Recall that sorted media diameters at the sand-anthracite interface (largest anthracite grains against smallest sand grains) would have impacted the observed differences in biomass levels for each media type. Group C showed significantly higher ng ATP/cm³ at 3065 and 1710 for sand and anthracite, respectively (t-test for unequal variance, alpha = 0.05, p = 0.002 and p < 0.001 for sand and anthracite respectively, **Table 3.12**). In addition, flow cytometry cell counts were evaluated for each DGGE group as presented in **Figure 3.22**. Group D/E had a cells/cm³ media of 3.68x10⁸ and 2.26x10⁸ for sand and anthracite, respectively; Group C presented significantly higher cells/cm³ media at 10.18x10⁸ and 6.70x10⁸ for sand and anthracite, respectively (t-test for unequal variance, alpha = 0.05, p = 0.042 for both sand and anthracite respectively, **Table 3.12**). Group D/E presented higher fg ATP/cell media at 8.01 and 3.98 for sand and anthracite, respectively; Group C presented lower fg ATP/cell at 3.49 and 3.20 for sand and anthracite, respectively. The higher observed ATP/cell in Group D/E was only significant for sand media (t-test for unequal variance, alpha = 0.05, p = 0.003, **Table 3.12**).

For EPS parameters, carbohydrate EPS measurements are also arranged by group in the bar plot of **Figure 3.22**. Group D/E presented µg D-glc/cm³ values of 43.5 and 23.7 for sand and

anthracite, respectively; Group C presented significantly higher $\mu\text{g D-glc /cm}^3$ values at 113.3 and 69.8 for sand and anthracite, respectively (t-test for unequal variance, $\alpha = 0.05$, $p < 0.001$ for both sand and anthracite respectively, **Table 3.12**). Group D/E also presented lower $\mu\text{g BSA/cm}^3$ media at 89.4 and 50.8 for sand and anthracite, respectively; Group C again presented significantly higher $\mu\text{g BSA/cm}^3$ at 191.4 and 116.6 for sand and anthracite, respectively (t-test for unequal variance, $\alpha = 0.05$, $p < 0.001$ for both sand and anthracite respectively, **Table 3.12**). For the EPS total carbohydrates to proteins ratio (CH:PN), Group D/E presented lower values at 0.47 and 0.42 for sand and anthracite respectively, while Group C EPS CH:PN was again significantly higher at 0.59 and 0.61 for sand and anthracite, respectively, which indicates higher significantly higher carbohydrate EPS content in Group C biofilms (t-test for unequal variance, $\alpha = 0.05$, $p = 0.002$ and 0.009 for sand and anthracite respectively, **Table 3.12**).

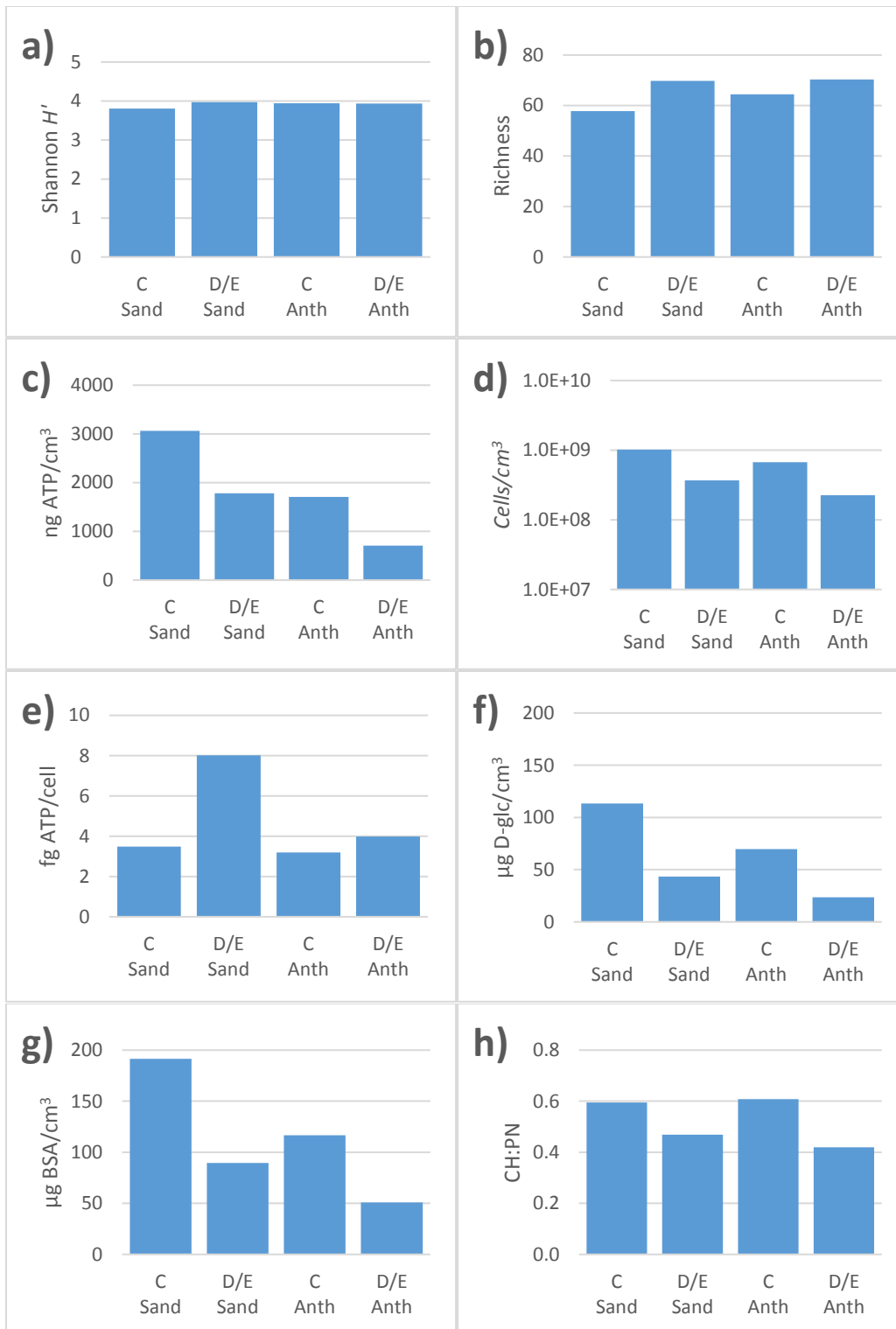


Figure 3.22: Bar charts presenting biofilm parameters associated with DGGE profile media biofilm groups C, D and E, for both sand and anthracite media. Biofilm parameters presented include a) Shannon diversity, b) richness, c) ng ATP/cm³, d) cell counts/cm³, e) fg ATP/cell, f) $\mu\text{g D-glucose/cm}^3$, g) $\mu\text{g BSA/cm}^3$, and h) CH:PN ratio.

Biofilm diversity, biomass and EPS data was also compared with performance data. Pearson r correlations showed Shannon diversity and community richness was not correlated with DOC and biopolymer percent removals (**Tables S2 to S5 in Appendix A**). ATP was negatively correlated with DOC removals (-0.67 to -0.80), and showed slightly stronger values associated with biopolymer removal (-0.82 to 0.86). This indicates that the increased biomass during the cold condition period was either not contributing to biofilter organic carbon removal performance, or if it was, the temperature dependent reductions in enzyme kinetics precluded detection. Not all biomass is heterotrophic, and some of the increased biomass may have been sustained via the lithotrophic ammonia oxidation pathway since ammonia levels increased during this period. Flow cytometric cell counts also showed negative correlations with biofilter performance, however at slightly reduced correlative strengths ranging from -0.63 to -0.73. Meanwhile ATP/cell exhibited weak positive Pearson r correlations with biofilter performance (DOC and biopolymer removal); **Figure 3.23** and **Figure 3.24** illustrates this relationship for sand and anthracite, respectively, where the scatterplots show cold condition (≤ 10 °C) samples exhibited similar ATP/cell to warm (> 10 °C) samples, and furthermore that increases in ATP per cell do not associate strongly with increased biofilter performance.

Biofilm EPS shared similar relationships to biofilter performance as biomass. Total carbohydrates showed strong negative correlations with performance ranging from -0.82 to -0.91, with similar values ascribed to both DOC and biopolymer removal (**Tables S2 to S5 in Appendix A**). Total proteins showed slightly less strength in the negative correlations with performance, and had Pearson r values ranging from -0.70 to -0.90. CH:PN ratios were also negatively correlated with biofilter performance, showing no preference to DOC or biopolymer removal, and ranged from -0.40 to -0.80. A full list of biofilm and performance values pertaining to each DGGE group is presented in **Table S1 in Appendix A**.

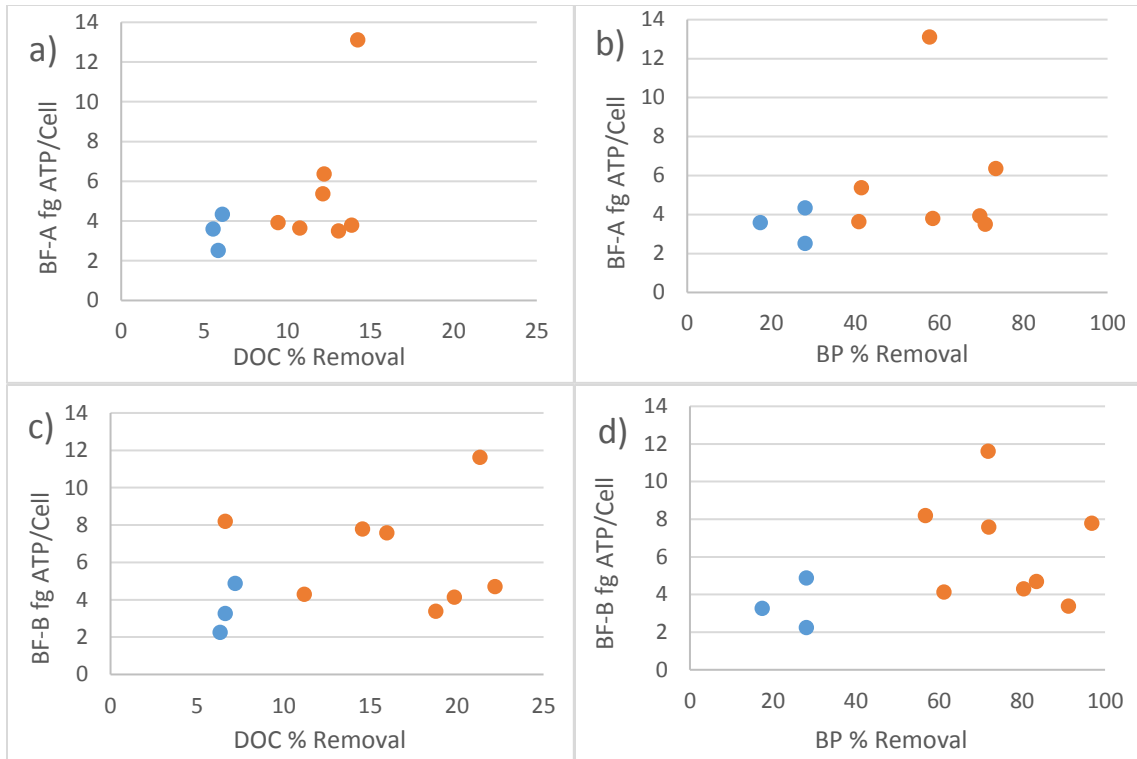


Figure 3.23: Sand biofilm femtogram ATP/cell as a function of a) BF(A) DOC % removal, b) BF(A) biopolymer % removal, c) BF(B) DOC % removal, and d) BF(B) % biopolymer removal. Outliers removed for clarity, which involved a fg ATP/cell value of 46 in figures a) and b). Blue points present cold condition data (≤ 10 °C), and red points present warm condition data (> 10 °C).

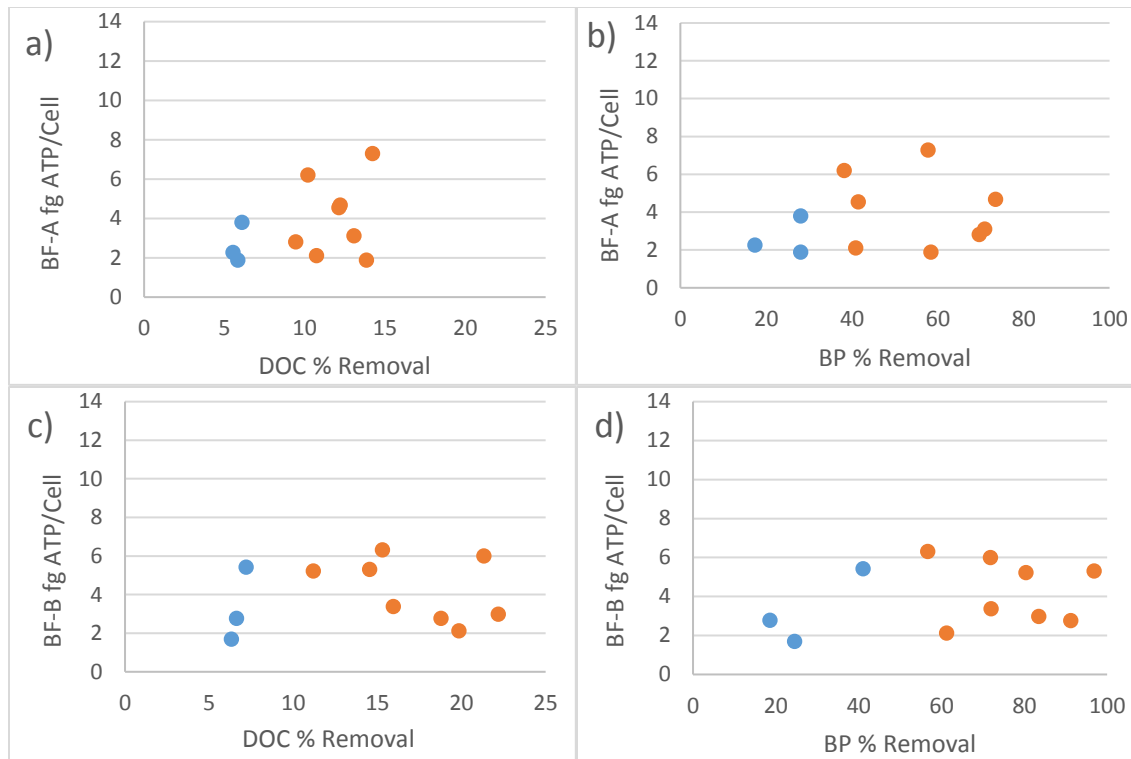


Figure 3.24: Anthracite biofilm femtogram ATP/cell at 20 cm media depth, as a function of a) BF(A) DOC % removal, b) BF(A) biopolymer % removal, c) BF(B) DOC % removal, and d) BF(B) % biopolymer removal. Blue points present cold condition data ($\leq 10\text{ }^{\circ}\text{C}$), and red points present warm condition data ($> 10\text{ }^{\circ}\text{C}$).

3.5 Discussion

3.5.1 Biofilter Feed Water Quality

Feed water quality data was gathered for the 14 month time span of the current study and was necessary to describe nutrient profile changes which could impact biofilter bacterial ecology and in turn, the performance of the process as a whole. Biofilter feed water quality (Figure 3.2-a and 3.2-d) displayed several significant differences within the seasonal dataset. During cold conditions ($T \leq 10\text{ }^{\circ}\text{C}$), ammonia, conductivity, hardness and the LMW-acid fraction concentrations increased compared to warm conditions, while the LMW-neutrals fraction decreased. Winter conditions within the Grand River are characterized by low surface runoff, which increases the proportion of groundwater in the river (GRCA, 2013); higher proportions of groundwater were likely responsible for the observed increase in hardness and conductivity. Although colder temperatures will increase the solubility of several analytes, ice

cover decreases the potential for volatilization and oxygenation; this latter phenomenon leads to decreased nitrification of ammonia in the winter due to reduced oxygen availability (GRCA, 2013). Furthermore the cold temperatures also lead to lower biological activity in the Grand River. These pertinent mechanisms result in the annual winter increase in ammonia (GRCA, 2013). Summer conditions result in much higher biological activity (including nitrogen cycling), which effectively removes ammonia from the surface water. **Table 3.2** shows that turbidity, DOC, biopolymers, humic substances, nitrate, ortho-phosphate, and total iron did not present significantly different concentrations in warm vs cold conditions; while building blocks ($p = 0.041$), LMW-acids ($p < 0.001$), LMW-neutrals ($p < 0.001$), ammonia ($p < 0.001$), conductivity ($p = 0.011$) and hardness ($p = 0.003$) concentrations were significantly different between cold and warm conditions (t-test, $\alpha = 0.05$, **Table 3.2**). These observations point towards a dynamic water quality in the Grand River which is largely temperature dependent.

3.5.2 DGGE Profiling of Biofilter Feed and Media Bacterial Communities

Cluster analysis showed that a superstructure existed in the DGGE profile data, where feed water (planktonic) communities possessed dramatic differences in the dominant phylotypes than media biofilm communities, and is a trend that has been previously shown in the literature (Lautenschlager et al., 2014; Pinto et al., 2012; Vanysacker et al., 2014; Wu et al., 2014). The cause of this difference in profile data likely stems from the difference in lifestyle habit between planktonic and sessile communities, which arises due to the biofilm's local physicochemical gradients (ORP, pH, nutrients and quorum molecules) increased cell density and heightened diversity (Flemming et al., 2016). When bacteria initiate or join a biofilm community, phenotypic changes rapidly take place, and gene expression changes in order to accommodate the demands of the new environment (Flemming et al., 2016). However there comes a point at which this biogenic habitat modification exceeds a phylotype's ability to adapt, and phenotypic plasticity is no longer sufficient.

In its upper reaches and at the surface of the biofilm, fast growing aerobes dominate and given their proximity to the bulk fluid, they have excellent access to electron donors and

acceptors. As the biofilm becomes thicker, these organisms deplete the most thermodynamically favourable electron donors and acceptors and this leads to a selection pressure on the bacteria below. This can result in a decrease in ORP, which would select for those bacteria which can utilize alternative electron acceptors including nitrate, sulphate, organic molecules or bicarbonate (Apgar & Witherspoon, 2008). Note that these ORP regions frequently overlap and can quickly change with modifications to flow rate and water quality (WEF, 2011) and likely also to backwashing frequency and intensity. The thin biofilms present on well managed biofiltration media likely do not contain a substantial ORP gradient due to the scouring effects of regular backwashing and low biodegradable carbon availability. To the author's knowledge no investigations have been made in the existence of anoxic microniches within drinking water biofiltration media. Free living feed water communities on the other hand are not subject to the same nutrient gradients and likewise are not protected by layers of EPS, which should account for much of the difference between the community structures of these two sample types.

Each of the DGGE hierarchically assembled clusters were assigned an alphabetical group name, and with the exception of Group B, were validated as statistically separate groups using ANOSIM (**Figure 3.6**). Group A contained predominantly warm condition feed water sample communities, with the exception of the December 2014 sample. Group B contained two cold water feed communities (January and February 2015) as well as the warm October 2014 and November 2015 communities. Group C is the first of three media groups encountered. Group C contains all January and February 2015 media samples; and included all cold condition media biofilm communities except for December 2014 samples which clustered with group E. Group D is composed solely of October 2014 media samples. This group is interesting because the hierarchical clustering sets it apart from the larger Group E, which contains all the other warm condition biofilm communities plus those from December 2014. One explanation for the separation of Group D in the hierarchical clustering is that this sample was taken before the bacterial communities in the biofilters had fully stabilized or acclimated. It is difficult to obtain an average time for BF_{wp} acclimation due to the lack of long-term community investigation research which also encompasses filter commissioning, and acclimation time will also be a

function of temperature. The Mannheim biofilter had been operating for 6 months by October 2014, and at this point the Mannheim biofilter biomass was still increasing (Elhadidy et al., 2016), indicating that biofilter acclimation, at least from a simple biomass standpoint, was ongoing. This compares with Servais et al (1995), who reported stabilization of pilot biofilter biomass after roughly 200 days of pilot filter operation. As well, (Xiang et al., 2013) found that although start-up of a pilot GAC biofilter showed steady-state dehydrogenase activity after only 40 days, community analysis using BioLog Ecoplate methods showed community structure changes were on-going. The last media group is Group E, which contains the majority of media samples and with the exception of December 2014 samples, were all collected during warm water conditions ($> 10\text{ }^{\circ}\text{C}$). Groups C and E present several sub-clusters organized by month, yet they are not organized in a chronological fashion. Therefore it seems that beyond the January-February 2015 shift of Group C, and the separation of a potentially immature October 2014 Group D, little reorganization of biofilm communities occurred across the seasonal timeline. DCA ordination analysis (**Figure 3.7**) shows agreement to cluster arrangements for Groups A, B, C and E; these similarities support the previous hierarchical clustering results. Group D of the DCA plot however is located within the larger Group E, and serves as the only major difference between the dendrogram and ordination multivariate methods. For means comparisons between biofilm DGGE groups, the DCA clustering results were used, which combined these two groups into Group D/E.

In the ANOSIM boxplots of **Figure 3.6**, the feed community represented by Group B had a high “within group” dissimilarity value, which begs that caution be exercised when considering this as a separate feed water group from the other feed water cluster (Group A). Group B contains feed water communities from sampling dates which span more than 12 months (October 2014, January, February and November 2015), and this could contribute to the greater dissimilarity observed within this group. For Group E, there were 7 outliers to the boxplots of **Figure 3.6**, despite having the lowest median of all group boxplots. These outliers originate from the August 2015 media sub-cluster in the dendrogram of **Figure 3.5**, where changing water quality parameters such as falling nitrate concentrations (from average values

of 5.5 and 3.2 mg/L in June and July, respectively, to 2.0 in August) may have influenced the biofilm community.

There was no difference in bacterial communities on media collected from biofilter columns A and B, as demonstrated by the hierarchical clustering dendrogram of **Figure 3.5**. As well, the clustering of **Figure 3.5** did not organize samples based on media type nor depth, showing that microbial communities within BF_{wp} are not affected by these factors. This is interesting, since the current study showed that biomass changed with depth (**Figure 3.12**), which is similar to other findings (Gibert et al., 2013; Liao et al., 2013a; Ishita Rahman, 2013; Urfer & Huck, 2001). Yet there is still disagreement in the literature whether depth affects biofilter community structure. Using DGGE fingerprinting, Fonseca et al. (2001) found no obvious differences in community structures of pre-ozonated biofilter communities with increasing depth. AP-PCR fingerprinting performed by (Moll et al., 1998) showed that community structure in biofilters without prior pretreatment also did not change with depth; however they did observe shifts in depth within biofilters fed with ozonated water. The work of Liao et al. (2013a) also showed community shifts with depth for biofilter fed with ozonated water, while Boon et al. (2011) reported drastically different richness (DGGE band numbers) as a function of depth within a pre-ozonated biofilter. However, Lautenschlager and colleagues (2014) found that a full scale GAC biofilter receiving ozonated water exhibited no change in DGGE community profiles with depth. It would appear that for the most part, depth only plays a role in biofilter community organization when upstream ozonation is involved, as it can affect biomass by increasing labile carbon content of the feed, or potentially by inhibition by residual ozone, or both. A lack of community change with depth within BF_{wp} may be due to high recalcitrance of the feed water (65% of DOC in the current study was from humic substances, with biopolymers and lower molecular weight more biodegradable components as a much smaller percentage of the DOC) coupled to the frequent biofilter backwashing. Although the filter bed generally goes back to the same configuration (media size as a function of depth) following backwashing, backwashing does provide at least some periodic mixing and de-stratification of the media communities.

3.5.3 Seasonal Relationships Between Water Quality and Biofilter Community Structure

The DCA plots of **Figure 3.7** and **Figure 3.8** separated the two feed clusters (A and B). Based on the DCA plot alone it is difficult to speculate what caused the observed planktonic community shifts. Although the ortho-phosphate vector in the DCA plot points along the axis differentiating the two feed communities, its length is small indicating little to no effect. Crump & Hobbie (2005) also found that over a 2.5 year period in Maine, river bacterioplankton communities differentiated into winter vs summer clusters as a result of temperature associated changes to water quality (such as dissolved organic nitrogen and nitrate) as well as bacterial production (labelled amino acid assimilation). Wang and colleagues (2015) observed that bacterioplankton communities in a subtropical river in China differed during wet and dry seasons, and used DGGE fingerprinting and redundancy analysis (RDA) to show that temperature, ammonia, orthophosphate and chlorophyll a were strongly correlated with bacterioplankton community structures. Primary production by phototrophic microalgae was noted as providing a ready carbon source for riverine bacteria. Organic carbon therefore may also influence the planktonic community structures. DOC is a blanket term for a cocktail of differing organic compounds which can change seasonally in response to many environmental conditions, thereby influencing the planktonic bacterial communities. For example, one study showed that changes in DOC abundance and composition varied with UV exposure, and selected for significantly different freshwater bacterioplankton communities; this shift consisted of changes in the α -proteobacteria populations, namely a decrease in *Sphingomonadaceae* which are responsible for recalcitrant NOM degradation and an increase in *Burkholderiaceae*, which are adapted for simple carbon substrates and UV impacted environments (Paul et al., 2012). Therefore seasonality such as solar intensity and exposure, along with other variables like storm surges and runoff, would affect DOC composition of the Mannheim DWTP feed water.

The increase in ammonia from < 0.1 in December 2014 to an average of 0.37 mg/L during the Group C sampling period of January and February 2015 corresponds with the biofilm community shift observed during the same period, and this is what the DCA ordination

plot of **Figure 3.7** clearly illustrates; the NH_3 vector extends in the direction of the Group C community shift, indicating a strong correlation between environmental gradients and community structure. Feed temperature was similar ($< 5\text{ }^\circ\text{C}$) for December 2014, January 2015 and February 2015; if the community shift of Group C was the result of temperature drop, the December 2014 media communities would have clustered with Group C, which they did not. Therefore this suggests that temperature itself was not the primary driver of BF_{wp} biofilm community organization, but instead may be due to temperature induced changes in feed water nutrients/composition. This indirect effect of temperature means that the biofilter biofilm community shift is delayed and the change may be a response to the change in surface water chemistry and not a direct response to temperature. Halle et al. (2009a) observed a seasonal lag effect on biofilter micro-contaminant removal performance, and noted that caution must also be used when relating temperature to biofilter performance. The current results, which depict delays in biofilter community shifts due to temperature-mediated changes in feed water quality, may provide insight into the mechanisms behind Halle's observations. In addition to the ammonia data of **Figure 3.7**, **Figure 3.8** shows that low molecular weight acids also strongly correlated with the Group C fingerprint data, meaning this NOM fraction may also play a role in the differentiation of Group C from Groups D & E. **Figure 3.2** shows that low molecular weight acids began rising in November 2014 and peaked in January 2015 at $525\text{ }\mu\text{g/L}$. During this time, low molecular weight neutrals and building blocks dropped to their lowest observed points during the study, at 94 and $643\text{ }\mu\text{g/L}$, respectively.

Ammonia and low molecular weight acids are commonly produced in municipal and animal waste, and as such it is possible that the concentrations of these compounds may be due to the network of 11 wastewater treatment plants and numerous agricultural operations found upstream of the Mannheim WWTP. The high ammonia and LMW-acids can persist longer than usual due to reduced river biological activity and ice cover which also prevents volatilization. Sonthiphand et al. (2013) noted local WWTPs to be significant sources of ammonia within the Grand River. Another study found higher river ammonia content associated with urban rivers receiving wastewater (Drury et al., 2013). Li et al. (2015) noted agriculture to be large non-point

sources of river ammonia concentrations. Similarly, bacterial community structure in an urban European river was shown to shift during winter in response to decreased autochthonous activity, changing inorganic nitrogen concentrations, and greater persistence of WWTP bacteria (García-Armisen et al., 2014). These results show that observed seasonal ammonia fluctuations can have effects on the BF_{wp} community ecology given that the process is fed with raw river water.

One study using PLFA analysis showed that temperature influenced the community structure of pilot scale biofilters fed with ozonated water (Fonseca et al., 2001), however these biofilters were in operation for less than one year. Kim and colleagues (2014) found that a decreasing feed temperature (similar to that of the current study) resulted in no effect to mature full-scale biofilter community composition. Therefore temperature mediated changes in nutrient compositions may influence community structures more than temperature alone. In a seasonal study using full scale BAC filters across 12 months, LaPara and colleagues (2015) observed that the dominant population in all samples was *Nitrospira* sp., which accounted for 13 to 21% of community OTUs; surprisingly the ammonia levels in that study were at or below the detection limit of 1 mg/L. This indicates nitrifier abundance may play a role in biofilter biomass fluctuations. Though the current study encountered ammonia levels up to four times higher than those reported in the findings of LaPara et al., nitrifier abundance was not assessed.

3.5.4 Biofilter Feed and Biofilm Bacterial Community Diversity

Time-series data for ecological parameters such as diversity and richness are important not only to describe a community's complexity and dynamics, but to also describe its maturity and robustness. Ecological parameters are useful as a monitoring tool in describing the biofilter microbiome health and adaptability. For example, dominance by a small number of species within a system leaves a community vulnerable to functional collapse in the face of perturbations (Wittebolle et al., 2009). It is therefore advantageous for a utility if there is a microbiome which exhibits robust measures of diversity, so that good functionality can be maintained (Boon et al., 2011). In practice, however, the steps that a utility can take to cultivate a

process microbiome are quite limited, since it is predominantly constrained by the incoming microbiome and water quality.

Figure 3.9-a shows that bacterial Shannon diversity (H') in the media biofilm was stable during the seasonal study period. Diversity values did not change according to media type, depth, or with the autumn change in flow rate. Relatively stable Shannon diversities were also observed by Kim and colleagues (2014), who examined conventional BAC bacterial communities over 12 months. Of the media biofilm DGGE profile groups, Group D (October 2014) demonstrated the lowest mean H' at 3.33 ± 0.12 and 3.22 ± 0.16 for sand and anthracite, respectively, compared the groups C ($H' = 3.81 \pm 0.18$ and 3.94 ± 0.17 for sand and anthracite, respectively) and E ($H' = 4.05 \pm 0.25$ and 4.03 ± 0.15 for sand and anthracite, respectively). The low diversity for group D may be because the biofilter was still acclimating and had not yet reached a stable biofilm community. The highest diversity values of the DGGE profile groups belonged to Group E, which consisted of the 2nd summer of operation for the biofiltration pilot plant. This demonstrates that over the course of the year, changes in the community structure were taking place and this is in turn reflected in the diversity indices of those communities. Media H' values in the current study were higher than those of a bench-scale GAC biofilter ($H' = 2.55$) fed with river water for one month as measured by LH-PCR (Wu et al., 2014). Using PLFA methodology, much lower Shannon diversity values were also encountered in a pilot scale biofilter receiving full scale GAC effluent amended with either glucose or acetate, which produced upper H' values of 0.97 and 1.25 for each amendment after several months of operation (Yu et al., 2009). However other studies have reported similar biofilter diversity values, including LaPara and colleagues (2015) who observed Shannon diversity levels between 4.6 and 4.8, and Feng et al., (2013) who observed Shannon diversity values between 2.3 and 3.6. Liao and colleagues (2015), working with GAC biofilter communities treating lake water in China, reported Shannon diversity levels on GAC biofilter media as high as 5.0 - 6.0; however diversity was determined using next generation sequencing, which can detect rare species which DGGE, TRFLP and clone library sequencing cannot (Liao et al., 2015). The present BF_{wp} media diversities therefore fall within the expected range for a biologically active DWTP

process. The high diversity observed represents good functional redundancy within the community (McCann, 2000) which implies that many populations exist which are ready to fill functional voids created by potential process upsets (Wittebolle et al., 2009).

Figure 3.9-b shows that media bacterial community richness exhibited more variation than the Shannon diversity index, with values ranging between 32 and 83 phylotypes in the biofilm samples. The Group D richness of October 2014 biofilm communities was markedly low (ranging from 32 to 40) and was roughly half of the study average. This increased rapidly for the next sampling event 2 months later in December 2014 to roughly 80 phylotypes. Group C (January & February 2015) richness were 58 ± 10 and 65 ± 10 phylotypes for sand and anthracite respectively. Group E (December 2014 and May to November 2015) however exhibited higher average richness at 74 ± 11 and 70 ± 9 phylotypes for sand and anthracite. In a comparison of different biofilter types including GAC, rapid sand filters and slow sand filter *schmutzdecke* fed with ozonated water, Lautenschlager and colleagues (2014) reported lower DGGE richness values of 24, 38, and 43, respectively. Similarly, a bioreactor fed with raw water from the South Saskatchewan river for 40 days exhibited DGGE fingerprint richnesses up to a value of 30 (Lawrence et al., 2004), while a full scale GAC biofilter in Zurich, which was fed pre-ozonated lake water, exhibited DGGE richness values from < 10 to almost 50 depending on the depth of the filter (Boon et al., 2011).

To determine if water quality factors related to diversity and richness within the biofilter media, Pearson r correlations were evaluated for each biofilter as well as media type (**Tables S2 to S5 in App. A**). Results showed that there were no significant correlations between biofilter ecological metrics and water quality. Notably ammonia and temperature did not correlate with biofilter media diversity. In an analysis of temperature effects on full scale biofilter bacterial communities receiving settled and ozonated river water, Kim and colleagues (2014) also found that temperature did not significantly affect community Shannon diversity or richness.

Bacterial feed water diversity was not as high nor as stable as media biofilm communities, and exhibited a strong seasonal response where values dropped during colder months. This indicates the selective advantage of the biofilm lifestyle habit, as the biofilter

diversity levels were much more stable. The average diversities for feed water Groups A and B was different at 3.73 ± 0.22 and 2.63 ± 0.37 , respectively, which could help resolve the underlying mechanisms of the bacterioplankton community shifts observed. The decreased diversity of Group B (October 2014, January, February & November 2015 feed water) was associated with lower temperatures (**Figure 3.2**). Bacterioplankton H' values (as determined by next generation sequencing) from the Yellow River were similar to the current results, and varied from 3.39 to 4.40 (Xia et al., 2014). On the other hand, Mannheim bacterioplankton diversity metrics were higher than those of another Chinese riverine DGGE fingerprinting study which reported H' values between 1.11 and 1.31 (Sekiguchi et al., 2002). The high dissimilarity of planktonic community structures relative to biofilm are also associated with significantly lower planktonic diversity and richness (ANOVA, $p < 0.001$ and $p = 0.002$ for diversity and richness, respectively, **Table 3.4**), which describes a less complex and more volatile bacterial assemblage in the biofilter feed water.

Planktonic richness values were 62 ± 9 and 22 ± 9 for Groups A and B respectively. This large difference between the planktonic DGGE groups is interesting, however little statistical support exists for the separation of Groups A and B (**Figure 3.6**). The bacterioplankton richness of the BF_{wp} feed water is similar to other DGGE fingerprinting values from river water, as Wang et al. (2015) observed a total study richness of 57 across multiple seasons, with an average sample richness of 22. Richness showed a more dramatic response to seasonality than diversity, with February demonstrating the lowest richness of the study period at only 12 phylotypes, which rose to a maximum of 73 phylotypes in July.

3.5.4 Biofilter Biofilm Dynamics

Biomass is a useful monitoring tool for biofiltration as it gives an indication of the biodegradation ability within the process; however a suitable biomass parameter that can predict NOM removal performance requires more research (Pharand et al., 2014). EPS monitoring is a complementary measurement to biomass, since biofilms can be upwards of 90% EPS by (dry) mass (Flemming & Wingender, 2010), and in excess it can affect biofilter hydraulic

performance (Evans et al. 2013). Biofilter media biomass was measured as ATP and cell counts, while EPS was measured as total proteins, total carbohydrates, extracellular DNA, as well as biofilm LC-OCD fractions as defined in Elhadidy (2016). The current study incorporated data collected previously by Elhadidy (2016) from October 2014 to February 2015, and extended the evaluation to include media sampling as well as biofilm biomass and EPS measurements until November, 2015. The resulting biofilm dataset was obtained for ATP, flow cytometric cell count and EPS values for 11 of the 14 months of the study timespan.

The extended sampling period (May to November 2015) confirmed results of the earlier data by Elhadidy (2016) that biofilters A and B presented a good degree of replication at the same depth, as **Table 3.6** presents no significant difference in biomass (cell concentration) levels between the biofilters for either sand or anthracite at 20 cm depth (paired t-test, $\alpha = 0.05$). As with biomass, no difference was detected at the same 20 cm depth between biofilters A and B in terms of EPS total proteins, carbohydrates and carbohydrate to protein ratio (**Table 3.9**), with the exception of anthracite CH:PN (paired t-test, $p = 0.048$, $\alpha = 0.05$). Due likely to its higher surface area per unit volume, sand had a higher biomass and EPS content than anthracite.

As expected, ATP and cell counts were strongly correlated, with Pearson r values ranging from 0.91 to 0.75 (**Tables S2 to S5, App. A**). EPS total proteins and carbohydrates shared a strong correlation, as the Pearson r values ranged from 0.96 to 0.92 (**Tables S2 to S5, App. A**). As is evident from the bar charts of **Figures 3.11** and **Figure 3.13**, biomass & EPS dynamics were very similar, and results showed that there were positive Pearson r correlations among the ATP, cell count, total protein and total carbohydrate data which ranged from 0.66 to 0.89 (**Tables S2 to S5, App. A**). This indicates that EPS is determined by filter biomass levels, which is supported by the carbohydrates and proteins per cell results presented in **Figure 3.15**, which were stable at $< 2.5 \times 10^{-7}$ μg D-glucose/cell and $< 5 \times 10^{-7}$ μg BSA/cell (with the exception of October 2014 which presented much higher EPS/cell due to low cell counts). The fact that there was not a significant increase in EPS production by the cells is interesting, as this is a common prokaryotic stress response and survival strategy. This may also be important to biofilter

operations, as EPS levels have been shown to affect biofilter hydraulic performance (Evans et al. 2013). Vanysacker et al. (2014) reports that elevated EPS production can be triggered by a variety of conditions including high oxygen levels, N limitation, desiccation, low pH, and low temperature. Therefore the conditions within the biofilters A and B during the study period were amenable for bacterial growth and did not present significant challenges to their metabolism.

Elhadidy (2016) observed a linear increase in biomass and EPS from his first sampling in August 2014 until his last sampling in February 2015, however values decreased afterwards over the summer 2015 sampling period. Biomass comparisons between winter 2014/2015, summer 2015 and autumn 2015 group means using ANOVA revealed significant differences for ATP and cell count data, with post-hoc Tukey HSD showing that these differences were between winter-summer and winter-autumn seasonal groups (**Table 3.7**). Similarly, ANOVA with Tukey HSD mean EPS comparisons between seasons showed significant differences between the same winter-summer and winter-autumn groups (**Table 3.8**). These seasonal differences in biomass and EPS stem from the higher values detected during December 2014, January & February 2015, and their decrease during the warmer period of 2015. As mentioned earlier, a community shift was observed during January & February 2015, possibly due to increased ammonia and LMW-acids within the feed water, and thus the shift in process microbiome organization, along with changing water quality, may have been responsible for the observed patterns in seasonal biomass and EPS concentrations.

Ammonia was positively correlated with biomass and EPS, with r values ranging from 0.95 to 0.66. Meanwhile, temperature was negatively correlated with biomass and EPS, with r values ranging from -0.94 to -0.68. At full scale, Pharand et al. (2015) found that biofilter ATP levels did not change across similar seasonal temperature and ammonia variations using pre-treated Grand River feed water, however these full-scale biofilters received feed water that had undergone extensive pretreatment including sand-ballasted clarification and ozonation, and therefore the biofilters were fed with considerably different NOM/nutrient composition compared to the Mannheim pilot-scale biofilters.

Although some works have described that biomass decreases with lower temperatures (Huck et al., 2000; Seger and Rothman, 1996), others have shown that biomass remains stable with changing feed temperatures (Evans et al., 2013; Pharand et al., 2015; Rahman, 2013). So far, no evidence within the literature has been found for biofilter biomass increasing with lower temperatures. This supports the hypothesis that increases in biomass during the cold period of December 2014 to February 2015 were not due to temperature decreases, but to changes in feed water quality. The drop in biomass during summer conditions could therefore stem from a return of feed ammonia and LMW-acids to autumn 2014 levels and conversion to the DGGE defined Group D/E community structure.

Media biofilm ATP, cell concentration, eDNA, total proteins and carbohydrates showed no difference with depth from 10 to 20 cm in both cold and warm conditions (**Figure 3.12** and **Figure 3.14** for biomass and EPS, respectively). However, there were decreases in all parameters from 20 to 60 cm depth. This would posit that a lower nutrient content via extended EBCT results in the lower biofilm values encountered at 60 cm. This hypothesis runs into difficulty when the biofilm values of the extended EBCT of autumn 2015 are considered, as the doubled EBCT during this period did not result in decreased biomass. However the autumn 2015 extended EBCT did not compare EBCTs using the same feed water, and so the effect of a changing water quality on biomass cannot be ruled out.

As mentioned earlier, no difference in biomass or EPS was observed between depths of 10 and 20 cm. Conversely, observations of an increase in filter biomass at mid-depth have been reported by some (Hallé, 2009; Pharand et al., 2014; Velten et al., 2011). A plausible and perhaps under-estimated explanation for suppressed biomass in the top 10 cm of biofilter media is the establishment of protozoan bacteriovores within the upper reaches of the media. Indeed, Husmann and colleagues (1982) observed 100 protozoan cells/mL of media in the upper reaches of biofilter media, which decreased 50 fold at a depth of 600 cm. Protists are known to have stabilizing effects on biomass by reducing biofilm volume, increasing porosity, and elevating nutrient transport into the biofilm (Böhme et al., 2009). Therefore it is possible that the decrease in biomass during spring 2015 was, in addition to changing water quality, also related to

enhanced protist activity. Protists have been shown to play significant roles in moderating the biomass levels of several engineered systems such as slow sand filtration (Wotton 2004), waste air biotrickling filters (Huub and Deschusses, 1999) and have even been shown to maintain and stabilize flux through the biofoulant gel layers in gravity driven membrane filtration (Kohler et al., 2014). Servais and colleagues (1995) also note that the decrease and subsequent stabilization of biomass which they observed within the first year of operation was likely due to the establishment of protozoans which assisted in stabilizing not only bacterial cell numbers, but biovolume as well. Such a development would indicate an inter-domain ecosystem succession. Interestingly, Madoni and colleagues (2000) showed that abundance and diversity of protozoa were associated with increased percent removal of ammonia and manganese within full scale drinking water biofilters; this phenomenon was likely due to grazing of bacteria by ciliates, which removed the outer heterotrophic biofilm layer that, in turn, increased diffusion of ammonium and manganese to the lithoautotrophs beneath.

ATP/cell values did not demonstrate clear seasonal trends and were not correlated with any water quality parameter, nor were they correlated with diversity parameters (**App. A Tables S2 to S5**). Media cell counts had higher variation between sampling events for both warm and cold conditions when compared to ATP and thus the ATP/cell levels also showed high variability (ranged from 2.51 to 13.52 femtograms ATP/cell). During mid to late 2014, the observed ATP/cell within Mannheim biofilter media decreased with colder temperatures (Elhadidy, 2016). However, based on the extended sampling campaign presented herein, the additional ATP/cell values showed enough variability as to indicate temperature-related ATP/cell effects were no longer present. Therefore the aforementioned temperature effect may have been unique to the acclimation phase. Unfortunately the factors controlling ATP/cell content remain unclear. There is evidence to suggest that viable but not culturable (VBNC) cells experience an increase in cellular ATP as a result of decreased metabolism and downregulated ATP catabolism (Su et al., 2016; Zhao et al., 2016). This is concerning, as it would mean stressed biomass could increase media ATP content, giving the illusion of a healthy, growing biofilm, which underscores the need for alternative biomass monitoring techniques. Magic-Knezev and

van der Kooij (2004) reported 2.1×10^{-2} fg ATP/cell in GAC filters and 3.6×10^{-1} fg ATP/cell in rapid sand filters treating ozonated water, while Hammes and colleagues (2008) reported between 2.49×10^{-1} and 7.61×10^{-2} fg ATP/cell in their investigation of process water from a Swiss DWTP; the fact that these values are lower than those encountered in the current study could be due to operational and feed water differences among locations and between conventional biofiltration and BF_{wp} , as well as differences in ATP/cell measurement techniques.

Media EPS carbohydrate to protein (CH:PN) ratios (**Figure 3.13-c**) decreased from the average cold (December to February) condition value of 0.62 ± 0.06 and 0.63 ± 0.08 (for sand and anthracite respectively) to 0.44 ± 0.09 and 0.39 ± 0.07 (for sand and anthracite respectively) in the warm condition period. These values indicate an increase in EPS protein content during the summer and fall periods, which is probably an opportunistic response by the biofilm to take advantage of increased availabilities of substrates due to higher surface nutrient runoff and riverine primary production. In support of this hypothesis, humic building blocks and low molecular weight neutrals were significantly higher in warm conditions ($p = 0.041$ and $p < 0.001$ for building blocks and LMW-neutrals, respectively, $\alpha = 0.05$, **Table 3.2**), therefore these fractions may have played a role in the falling CH:PN ratio during this period. The CH:PN ratios of the current study are similar to the average ratio of 0.4 found in earlier samples by Elhadidy (2016), in his analysis from August 2014 to February 2015.

EPS protein, carbohydrate and eDNA ratios (PN:CH:eDNA) were found to be approximately 5:3:1 and 6:3:1 for sand and anthracite biofilm, respectively. Within the biofilm matrix, carbohydrates (including monosaccharides as well as polysaccharides), serve to bind the biofilm together; meanwhile EPS proteins make up the majority of the EPS and serve a variety of functions, including hydrolysis of substrates, biofilm detachment, sorption, and the structural linkage of polysaccharides (Flemming & Wingender, 2010). Extracellular nucleic acids are not exclusive to cell lysis, as they play active roles in biofilm aggregation (Flemming & Wingender, 2010) and can be actively secreted by cells in biofilms, which take advantage of the large polyanionic molecules to bind divalent cations in a bridging role for flocculation and biofilm

cohesion (Flemming & Wingender, 2010). Together with lipids, extracellular nucleic acids may adjust the rheological properties of the biofilm matrix (Simões et al., 2010).

Biofilter biofilm EPS fractions were also measured using LC-OCD according to the method of Elhadidy (2016). The resulting chromatogram peaks were categorized into 3 major fractions: a high molecular weight organic carbon (HMW-OC), intermediate molecular weight organic carbon (IMW-OC) and low molecular weight organic carbon (LMW-OC). The HMW-OC fraction (**Figure 3.16**) was stable across both warm 2014 and cold 2015 conditions. Given the >13 kDa size of the HMW fraction, this group should contain biopolymers; however as **Tables S2 to S5 in App. A** shows, this fraction did not correlate strongly with total carbohydrates, total proteins or biomass parameters. However, an increase in both IMW and LMW-OC was observed during cold conditions, indicating these fractions may be more closely related to the measured total proteins and carbohydrates. Indeed, stronger correlations between IMW and LMW-OC and both proteins and carbohydrates were observed (**Tables S2 to S5, App. A**), and ranged from 0.96 to 0.83. Neither IMW or LMW-OC appeared to be better correlated with either proteins or carbohydrates fraction of the EPS. Both IMW and LMW-OC were well correlated with biomass, ranging in Pearson r values from 0.59 to 0.88. The IMW and LMW-OC fractions therefore represent alternative EPS parameters, and followed the same trends with media bed depth as previously examined EPS and biomass (**Figure 3.17**).

Given that the size of IMW-OC is between 2 and 13 kDa, this fraction likely contains within it humic substances, which was previously confirmed using fluorescence excitation emission matrices (Elhadidy 2017). Biofilms can adsorb humic substances (Flemming & Wingender, 2010) and therefore they may accumulate within biofilter media during cold conditions due to reduced exoenzyme kinetics at low temperatures (Elhadidy 2015). Consisting of a molecular weight below 2 kDa, the LMW-OC fraction was the last peak to elute in the EPS extract chromatograms, and was found to be the most concentrated of the 3 biofilm fractions (**Figure 3.16**). Elhadidy (2015) observed that LMW-OC increased in cold conditions compared to warm 2014 conditions, a similar trend to IMW-OC during the same time period. The extended sampling herein showed these 2 fractions again decreased upon resumption of warmer

conditions, correlating with temperature with Pearson r values ranging from -0.79 to -0.54 (Tables S2 to S5, App. A). Similar to bacterial community organisation, biomass, and other EPS parameters, the LC-OCD defined biofilm IMW and LMW-OC fractions were also related to changes in feed ammonia concentration, which presented Pearson r correlations ranging from 0.82 to 0.58 (Tables S2 to S5, App. A).

Elhadidy et al. (2017) found strong Pearson correlations between HMW-OC and proteins as well as carbohydrates, with the latter correlation being slightly lower in strength. The current results showed these trends did not persist into the warm 2015 season, as during this time, lower molecular weight biofilm LC-OCD fractions were better correlated with total protein and carbohydrate EPS parameters, with neither IMW nor LMW presenting stronger associations with proteins or carbohydrates. Further investigation into the differences between these biofilm fractions is therefore needed to understand their relationships with alternately defined EPS parameters.

3.5.7 Relationship between biofilm dynamics and Biofilter Performance

Biofilter performance was measured by percent removals of DOC and the five different dissolved NOM fractions as determined by LC-OCD. Measuring DOC and NOM fraction removals is essential to biofilter performance research as it provides removal results for both labile and recalcitrant fractions which can better approximate BOM removal than the measurement of DOC alone. Data from October 2014 to February 2015 were obtained by Elhadidy (2016), while data from May 2015 to November 2015 was obtained in the current study. On average the total NOM was composed of 7, 65, 15, 5 and 8% biopolymers, humic substances, building blocks, low molecular weight acids and low molecular weight neutrals, respectively. These percentages were quite stable over the year with the exception of biopolymers, which spiked in May 2015 to 12% of NOM; a similar seasonal trend with higher biopolymer concentration in the Grand River at warm water conditions ($>10^{\circ}\text{C}$) was observed by Pharand and colleagues (2015). There was a significant difference in NOM removal through BFA (8 min EBCT) for DOC and biopolymers. For BF(B) with a longer EBCT of 16 min, there

was significant removal of DOC, biopolymer and LMW-acids fraction (Table 3.11). The higher EBCT of BF(B) resulted in significantly higher DOC ($p = 0.007$) and biopolymer removals ($p < 0.001$, $\alpha = 0.05$, **Table 3.10**) compared to BF(A), while no differences in removal were observed for the other NOM fractions. Although the increase in DOC or biopolymer removal was not directly proportional to the increase in EBCT, this was expected since increasing EBCT eventually leads to diminishing returns on BOM removal performance (Huck & Sozański, 2008). As well, the flow rates for both biofilters were Decreased during autumn 2015, where the 100 L/h flow of October 2014 to August 2015 was decreased to 50 L/h for the months of September, October and November 2015. This was done in order to accommodate a different experiment that was being done at the pilot plant. Thus in the following section the data is partitioned into three operational groups: winter (December 2014, January & February 2015; 100 L/h), summer (May to August 2015; 100 L/h) and fall (September to November 2015; 50 L/h). Note that October 2014 performance data was binned in the summer 100 L/h group as feed temperature was above 10 °C and the flow was similarly 100 L/h. The autumn 2015 decreased in hydraulic loading rate corresponds with an increase in EBCT from 8 to 16 min for BF(A) and from 16 to 32 min for BF(B), however this change did not appreciably increase DOC or NOM removals (**Figure 3.19** and **Figure 3.20**, respectively). Assessing the effect of EBCT on BOM removal is difficult if feed water conditions are not kept constant, and results were also affected by decreasing autumn feed water temperature (**Figure 3.2**). Therefore it is difficult to know how these factors affected microbial BOM removal kinetics at the decreased hydraulic loading rate.

The summer months from May to August 2015 saw BF(A) and BF(B) removing an average of 10.9 and 17.3% of feed DOC, respectively, which are similar to full scale values from full-scale biofilters at a DWTP located 50 km downstream of the pilot plant (Pharand et al., 2015). When the winter results are compared to summer, a 1.9 and 2.6-fold increase in DOC percent removal is observed for BF(A) and BF(B), respectively, during warm (>10 °C) conditions. Thus the DOC removal performance of both biofilters was heavily dependent on feed temperature with a Pearson r correlation of 0.78 and 0.87 for BF(A) and BF(B), respectively (**Tables S2 to S5, App. A**). It is also possible that seasonal changes in NOM composition also

had an impact on removals. Both biofilters A and B (8 and 16 min EBCT at 100 L/h; 16 and 32 min EBCT at 50 L/h, respectively) exhibited significantly different DOC removals across the three groups of winter, summer and fall (ANOVA, $p < 0.001$ & $p = 0.017$ for BF(A) and BF(B), respectively; **Table 3.11**). Biopolymer removal also increased during the warmer conditions. Biopolymer removal of BF(A) and BF(B) correlated with feed temperature, as Pearson r correlations were 0.85 and 0.91 for each filter respectively (**Tables S2 to S5, App. A**). As such, significant differences in biopolymer removals across seasons were observed (ANOVA, $p = 0.018$ & 0.003 for BF(A) and BF(B), respectively; $\alpha = 0.05$; **Table 3.11**). The only other NOM fraction that showed an increase in removal at warmer temperatures was LMW-acids removal by BF(B) (ANOVA, $p = 0.023$, $\alpha = 0.05$, **Table 3.11**).

When temperature and DOC removal decreased, feed ammonia, feed LMW-acids, and media biomass and EPS concentrations increased (**Figures 3.2 and 3.11**), resulting in negative correlations between DOC percent removals and ammonia, LMW-acids, biomass and EPS (**Tables S2 to S5, App. A**). Biopolymer percent removal shared the same correlation trends as DOC for biofilm components; biomass, EPS and feed ammonia were all negatively correlated to its removal (**Tables S2 to S5, App. A**), as these values increased during the winter months when BOM removal performance declined .

Removal of NOM fractions were compared with biofilm characteristics including bacterial community DGGE groups. The bar plots in **Figure 3.21** clearly show that DGGE Group C was associated with the least amount of DOC and NOM biopolymers removal from the feed water. This is likely due to a combination of temperature effects, community dynamics and biofilm response. Group C had a mean temperature of 1.8 °C, while Group D/E had a mean temperature of 19.0 °C; this higher mean temperature was related to higher microbial degradation kinetics for Group D/E which is what the performance bar plot of **Figure 3.21** shows. Therefore the effects of elevated feed water ammonia and LMW-acids were not wholly responsible for the observed decrease in biofilter performance observed for Group C. It is possible however that water quality induced changes to the community genotype and phenotype could still contribute somewhat to the observed change in performance; for example,

the community shift from Group D/E to Group C was accompanied by a higher CH:PN ratio, which indicates lower protein content in the EPS. This could result in diminished enzymatic ability of the biofilm matrix to hydrolyse incoming dissolved and particulate organic matter, which in turn would yield less readily assimilable carbon. In fact the Pearson *r* correlations between biopolymer percent removal and CH:PN ranged from -0.72 to -0.80 (**Tables S2 to S5, App. A**), whereas correlations between DOC and EPS CH:PN were not as strong; this supports the hydrolysis theory, as biopolymers are a large molecular weight (≥ 10 kDa) and therefore require modification to transport across the cell membrane. Good correlations between biopolymer and DOC removals were expected and observed, as biopolymers are a fraction of the total dissolved organic carbon, and their removal is presumed to be catalysed by the same metabolic pathways following hydrolysis. Unfortunately, limited sample sizes in the BOM removals of Group C precluded mean performance comparisons between DGGE groups.

Figure 3.22 presents bar plots for sand and anthracite data divided into respective DGGE groups for the following parameters: Shannon diversity, community richness, ATP, cell counts, ATP/cell, total carbohydrates, total proteins, and the EPS carbohydrate to protein ratio. Group C showed similar community diversity to Group D/E, with no significant difference between groups detected (t-test, $\alpha = 0.05$, **Table 3.5**). The same trend was observed in the richness data between DGGE groups. This shows that diversity levels were stable throughout the majority of the study, and indicates mature biomass, since acclimated biofilter media usually exhibits stable diversity characteristics (Kim et al., 2014). As **Tables S2 to S5 in App. A** show, diversity parameters correlated weakly with other data in the current study (biomass, EPS & performance) and therefore biodiversity is better suited to measure start-up community succession and not long term measurement of performance, as diversity and richness data were not well correlated with DOC and biopolymer percent removals.

Of the three DGGE profile groups, **Figure 3.21** shows the highest biomass and EPS was encountered in Group C. The conspicuously high biomass and EPS observed within Group C clearly indicates that the community shift of January and February 2015 was associated with higher cell survival. This could be due to the biofilm being exposed to higher ammonia and

LMW-acids concentrations. Also, as stated earlier, reduced predation at cold temperature could have led to higher biomass levels in the biofilters. The significant differences seen in biomass and EPS between DGGE Groups C and D/E (**Table 3.5, Figure 2.22**) show that biofilter biofilm respond to seasonal fluctuations in water quality, which precipitated a shift in the community structure. The higher biomass and EPS of the Group C biofilm could, if growth was thick enough, hamper the diffusion of oxygen and nutrients to basal populations, which could in turn select for different ribotypes. Niquette and colleagues (1998) noted that excessive flocs and particles in a biofilter could act as diffusion barriers to dissolved oxygen and nutrients. Therefore it is possible the additional biomass and EPS could have a similar effect. Indeed a thin biofilm was shown to be required for optimal biofiltration performance (Liao et al., 2015). This infers that the biomass and associated EPS should be minimized to retain maximal biological activity. As mentioned previously, the role which the Group C community shift played in the reduced biofilter performance may also be related to decreased EPS protein content. In addition, low temperatures reduce the oxygen diffusion rate into the biofilm matrix (Stewart, 2003), which could thereby reduce aerobic NOM degradation. Nonetheless, caution should be exercised when assessing the observed negative correlations between biomass, EPS and performance in this study, as low temperatures can also affect enzyme kinetics.

It appears that no significant trends exist between performance parameters and biofilter media ATP/cell for the stabilized mature biofilm sampled in 2015. Although earlier results from late 2014 and early 2015 (Elhadidy 2015) indicated that higher ATP/cell was associated with higher filter performance during warm conditions, the same trends were not observed during the extended sampling campaign of the current study. The summer 2014 ATP/cell values were elevated because, as the DGGE hierarchical clustering analysis shows, media biofilms were still undergoing community succession and the filter may have had a higher proportion of colonizing cells in the growth phase, where ATP content is higher (Hamilton & Holm-Hansen, 1967). Overall the ATP/cell values observed in the Mannheim pilot biofilters were higher than the 0.021 and 0.36 fg ATP/cell reported in full scale filters (GAC and rapid sand, respectively) (Magic-Knezev & van der Kooij, 2004). In a review of various published ATP/cell values for

biofiltration, Pharand et al. (2014) showed that values from published studies ranged from 10^{-14} to 10^{-19} g ATP/cell, however the majority of reported values were within the range of 10^{-16} g ATP/cell (or an order of magnitude less than the femtogram (10^{-15} g) ATP/cell values seen in the current study). The reason for the consistently high ATP/cell values seen herein could be due to the absence of pretreatment in the raw BF_{wp} feed, which would result in a higher diversity of carbon and nutrients available for biological growth.

3.5.10 Conclusions

This chapter characterized the relationships between BF_{wp} bacterial ecology (community organization, diversity and richness) and how they related to biofilm dynamics (biomass and EPS) and performance (DOC and LC-OCD defined NOM removal) across a 14 month time span (11 sampling campaigns). Although DOC removals stabilized after 4 months of operation (Elhadidy 2015), it took approximately 11 months of operation for biofilter biomass levels to stabilize; in other words biofilter biomass did not reach stable levels until the second summer of operation (summer 2015). DGGE profile analysis showed two planktonic feed communities and two major biofilm communities, with the largest community dissimilarities in the analysis relating to the planktonic vs biofilm supergroups. The cold condition change in biofilm community structure was most influenced by seasonally induced changes to raw feed water quality including increased NH₃-N and LMW-acids concentrations. These conditions also resulted in high media biomass and EPS concentrations yet, surprisingly, low DOC and biopolymer removals (Group C; January-February 2015). This study shows that by monitoring the concentrations of key nutrients in the raw BF_{wp} feed, operations and maintenance staff can anticipate changes to filter biofilm behaviour.

The lack of correlations between biomass and performance in the current study reaffirmed the tenet that biomass is not a perfect tool for the monitoring of removal performance in mature biofilters. EPS levels closely followed biomass as EPS/cell production remained similar over the course of the study period. EPS composition was dominated by proteins whose proportion in the biofilm decreased during cold conditions, likely impacting the biofilm's

biodegradation capacity. Community diversity, richness and structure however remained the same throughout the depth of the filter. Biofilter biofilm diversity was higher than that of planktonic communities and showed relatively small variation across the seasonal analysis, indicating the robust and redundant metabolic qualities of the biofilm; however diversity shared little relationship with performance. It is likely that the differences in biofilter performance between cold and warm conditions were due mostly to lowered enzyme kinetics as a function of temperature, and to a lesser extent, to a water quality mediated shift in EPS and community composition of the biofilm. A change in the biodegradability of the incoming NOM, while not quantified, may also have played a role.

The increase in EBCT between BF(A) and BF(B) resulted in higher percent removals of DOC and biopolymers, however the biomass, EPS, diversities and community structures obtained from each biofilter showed, as would be expected, no significant differences between the two biofilters when sampled at the same 20 cm depth. Due to higher specific surface area, sand media displayed much higher volumetric biomass and EPS values than anthracite.

BF_{wp} is a useful process for cost effective BOM removal as a membrane pre-treatment, however the unique position of this process at the head of the treatment train can expose the biofilm communities to widely fluctuating feed water quality which invariably affects biofilm ecology, performance and composition. Further investigations are needed in order to elucidate which bacterial populations are responsible for the high biofilm cell counts and EPS observed during the cold high ammonia/LMW-acid conditions. The amount of protozoan activity within different depths of the media bed is also of interest in BF_{wp}, as protozoa may affect biofilm dynamics over the long term via bacterial grazing. Future seasonal investigations should include the following: sensitive measures of ammonium below the 0.1 mg/L detection limit of the current study in order to detect low summer ammonia values; quantification of wastewater and agricultural indicator bacteria (i.e. total coliforms); enumeration of bacterivorous protists at different depths; sequence analysis to determine the genotypic identities of changing community members; and finally the ecological results of still-acclimating biofilter media

communities should be compared to those of full scale 'steady state' biofilters in order to increase understanding of the acclimation process.

Chapter 4

Fighting Biofilms with Biofilms: Characterisation of Bacterial and Archaeal Communities in Pilot-Scale Biofiltration-Nanofiltration Coupled Process

4.1 Summary

Biofilms are considered nuisance biological growth in the majority of water treatment processes, including high pressure membrane filtration where biofilm growth is operationally defined as biofouling. The use of BF_{wp} as a low-cost alternative for nanofiltration (NF) pretreatment to reduce membrane biofouling was investigated previously (Elhadidy 2015) and yielded promising results. In the current study, the bacterial and archaeal community structures of the BF-NF coupled process were investigated in order to determine the microbial community dynamics associated with the observed reductions of feed channel pressure increase within bench-scale NF test cells. Two parallel pilot scale biofilters fed with surface water from the Grand River, Ontario, were operated with empty bed contact times (EBCT) of 8 and 16 min (loading rate of 3.08 m/h). Biofilter effluents were compared against raw water as feed for NF test cells. In total 54 prokaryotic community profiles were analyzed across summer and winter conditions via polymerase chain reaction – denaturing gradient gel electrophoresis (PCR-DGGE), with nested PCR used for archaeal samples. Archaea were shown to be ubiquitous across all sample types however their abundances (based on number of bands) were roughly 1000 fold less than bacteria and displayed no community organization across sample types. Bacteria exhibited distinct clustering according to season and source water type. Under warm water conditions (>10 °C) there was a shift in biofoulant bacterial communities on NF membranes when BF_{wp} effluent was used in comparison with raw feed. Furthermore, the use of

BF_{wp} resulted in biofoulant communities with decreased Shannon diversity indices compared to raw water feed. These differences were not observed during winter conditions. These results compliment the encouraging findings of Elhadidy (2015) and show that the observed reduction of NF feed channel pressure increase by upstream biofiltration is due not only to reductions in organic loading but also to fundamental changes in the biofoulant ecology.

4.2 Introduction

Nanofiltration (NF) came into being in the 1970s when membranes with lower pressures, higher permeability, and lower dissolved component rejections than RO were developed to save on energy costs, and these RO type membranes were subsequently referred to as NF (Hilal et al., 2004). Still regarded as high pressure membranes, NF is used to remove natural organic matter (NOM) which includes disinfection by-product (DBP) precursors, as well as trace-level substances such as taste and odour compounds and even emerging contaminants of concern such as pesticides (Fonseca et al., 2007). Furthermore NF has proven particularly successful at removing multivalent ions which makes it ideal for treating groundwater (e.g. for softening) (Cornelissen et al., 2010; Weng et al., 2015). Generally NF is regarded as any membrane which provides a molecular weight cut-off above 200 – 300 Daltons (Vanysacker et al., 2014) and as such, this intensive restriction on particulate and dissolved contaminants inevitably results in membrane fouling, of which biofouling is arguably the most difficult to manage (Flemming et al., 1997).

Biofouling occurs when labile NOM and other nutrients are assimilated by microorganisms which grow into nuisance biofilm on the membrane surface and feed spacer. Biofilm formation eventually results in reduced permeability and contaminant rejection as well as an increased feed channel and transmembrane pressure (Dreszer et al., 2014; Wood et al., 2016). The inherent nature of separating contaminants from permeate via membranes results in ideal conditions for biofilm growth, as the facilitated transport of nutrients and cells towards the surface of the membrane through permeation assists bacterial cells in overcoming hydrodynamic layers while simultaneously concentrating nutrients for improved assimilation

(Eshed et al., 2008; Ivnitsky et al., 2007). This concentration of dissolved chemical species near the membrane surface is referred to as concentration polarization, which is enhanced by the presence of a biofilm and serves to increase the pressure required to overcome osmotic forces – a phenomenon referred to as biofilm enhanced osmotic pressure or BEOP (Herzberg, 2010; Wood et al., 2016). In fact for high pressure membranes it has been postulated that the hydraulic resistance of biofilms does not contribute to increases in transmembrane pressure (TMP) nearly as much as the concentration polarization effect which they facilitate (Dreszer et al., 2013).

Several factors determine a membrane's propensity to grow nuisance biofilms, including membrane properties such as surface zeta potential, hydrophilicity, roughness and pore size as well as system properties such as crossflow velocity, pH, ionic strength, organic loading, application of biocides and permeation rate (Hilal et al., 2004; Ivnitsky et al., 2007; Vanysacker et al., 2014). Once a biofilm forms on the membrane surface however, original surface characteristics are negated by the tortuous, ubiquitous and diverse EPS matrix which interspecies biofilms secrete (Flemming et al., 1997), often cooperating and capitalizing on the previous succession's effort in ways that are only just beginning to be understood (Culotti & Packman, 2015). It is for this reason that interdisciplinary research on the mechanisms, ecology and prevention of biofouling are needed. To-date special attention has been given to those organisms which act as pioneer species, EPS powerhouses, or both. Such problem bacterial species, or phylotypes as they are known in the molecular context, include *Pseudomonas aeruginosa* and members of the classes *Sphingomonadales* and *Rhizobiales* (Bereschenko et al., 2010; Culotti & Packman, 2015; Ivnitsky et al., 2007; Wood et al., 2016). On average archaea exhibit more specialized and fastidious metabolisms compared to bacteria, and therefore they rarely, if ever, dominate heterotrophic assemblages such as those found in aqueous oligotrophic mesothermal systems; therefore their presence in systems such as drinking water treatment and distribution has received mixed reporting (Fish et al., 2015; Moll et al., 1998). To the author's knowledge, the presence of archaea within freshwater membrane biofoulant layers has not been established.

Biofiltration is a promising option for the reduction of membrane biofouling (Fonseca et al., 2007) as it removes biodegradable NOM and inorganic nutrients which are used to form biomass (Bereschenko et al., 2010). The use of biofiltration as a pretreatment for high pressure membrane filtration has been demonstrated with success before (Elhadidy, 2013; Griebe & Flemming, 1998; Mosqueda-Jimenez & Huck, 2009; Weng et al., 2015). In this regard, the assimilable organic carbon (AOC) concentration of process water is often used as an indicator to measure the potential for biofilm growth (Dreszer et al., 2013). Biofiltration without pretreatment enriches the biofilter media with an aquatic oligotrophic consortium similar to that on freshwater sediment, and indeed these biofilms perform the same role of “environmental purification” as their natural counterparts, which is a mass transfer of dissolved and particulate contaminants out of the bulk fluid and into the biofilm matrix, where they are physically filtered, sorbed, chelated, hydrolyzed and/or assimilated into biomass (Flemming et al., 2016). The bacteria found in drinking water biofilter biofilms are mostly Gram-negative, non-fermentative strains (Mittelman & Jones, 2016) and belong to the class *Alphaproteobacteria* and to a lesser extent *Betaproteobacteria* and *Gammaproteobacteria* (Kaarela et al., 2014; White et al., 2012). Other phyla than *Proteobacteria* such as *Bacteroidetes*, *Chloroflexi*, and *Planctomycetes* are often present, though in lower abundance (Liao et al., 2013a; Pinto et al., 2012).

The strategy of “fighting biofilm with biofilm” by using biofiltration as a pretreatment is a sustainable option for biofouling control. Other options to control biofouling development such as biocides would have to be regularly applied in high concentrations. Membrane cleaning of biofilms has included the use of many different oxidants including hypochlorite, chlorine dioxide, chloramines, ozone, sodium hydroxide, hydrogen peroxide, iodine and peracetic acid (Nguyen et al., 2012; Zularisam et al., 2006). However many of these biocides can damage the membranes themselves (NaOH, NaOCl, Cl₂, peracetic acid), produce disinfection byproducts (NH₂Cl, O₃, Cl-based) fails to remove assimilable organic carbon (AOC) and can even increase AOC levels which could compound regrowth downstream (Nguyen et al., 2012). Furthermore, toxic wastewater generated as a result of biocide use must undergo treatment or isolation before

release into the environment (Griebe & Flemming, 1998). This short term destruction of biomass really only treats the symptom and not the cause of biological instability.

As Pinto and colleagues (2012) stated, biofiltration gives utilities the “opportunity to control [the] DWTP microbiome by manipulating filter microbial communities”. Indeed, work conducted previously by our group showed that the use of biofiltration without pretreatment was itself an effective pretreatment for NF membranes by conducting experiments using membrane fouling simulators (MFS) (Elhadidy, 2015). Although biomass, EPS, physiological profiles and feed channel pressure data were obtained by Elhadidy (2015), genotypic methods were not explored; for this purpose, genomic materials in the form of fouled NF membranes and biofilter media biofilms were archived for the purpose of the current research. Therefore, this study aims to compare how biofiltration conditions affect the microbial community structure and diversity of downstream nanofiltration membrane biofoulants. In this study, archived samples were evaluated using 16S rDNA biomarkers and microbial communities were compared using denaturing gradient gel electrophoresis (DGGE). This approach added to the knowledge of NF biofouling processes and advanced efforts towards its mitigation.

4.3 Materials and Methods

4.3.1 Experimental Configuration

Pilot-scale drinking water biofilters located at the Region of Waterloo’s Mannheim Drinking Water Treatment Plant, Kitchener, Ontario, were used in the present study; for a detailed description of the biofilter setup refer to Chapter 3. As with the previous chapter, this work builds upon previous PhD work by Ahmed Elhadidy (2015), who conducted two experiments (autumn 2014 and winter 2015) to evaluate biofiltration as a pretreatment to control NF membrane fouling. NF fouling was assessed by measuring increases in the feed channel pressure drop (FCP) using membrane fouling simulators (MFS). The autumn 2014 (September 18th to October 19th) experiment lasted 700 hours (30 days) and consisted of one MFS unit receiving untreated raw feed water (referred to as raw-NF), and two replicate MFS

units receiving the effluent of the 16 min EBCT biofilter (BF-B). Replicate nanofiltration MFS units during the autumn experiment are referred to as BF(B)-NF-R1 and BF(B)-NF-R2.

The winter 2015 (February 23 to April 15) experimental duration was 1000 hours (42 days) and consisted of one MFS unit receiving untreated raw feed water, the second MFS unit receiving the effluent of the 16 min EBCT biofilter (BF-B), and a third MFS unit receiving the effluent of a parallel 8 min EBCT biofilter BF(A). Each MFS unit contained a 20 x 4 cm nanofiltration membrane and feed spacer in order to emulate cross flow in full scale spiral-wound elements. MFS units were designed to study feed channel fouling and therefore did not accommodate permeation (Vrouwenvelder et al., 2007). Data from Elhadidy's autumn and winter biofouling experiments are tabulated in **Table 4.1**, along with diversity and richness values obtained from the current study.

Table 4.1: Biomass parameters measured for biofilter and NF samples for the fall 2014 and winter 2015 MFS experiments.

Type	FCP % increase	Shannon Index	Richness	ng ATP/cm ² (NF) or cm ³ (media)	cell count/cm ²	ng D-Glucose /cm ²	ng BSA/cm ²
Feed-Mar	-	2.06	11	-	-	-	-
Eff-Mar-BF(B)	-	1.91	9	-	-	-	-
Feed-Feb	-	2.24	14	-	-	-	-
Eff-Mar-BF(A)	-	1.61	7	-	-	-	-
Eff-Feb-BF(B)	-	1.69	11	-	-	-	-
Feed-Oct02	-	2.33	16	-	-	-	-
Feed-Oct18	-	2.68	20	-	-	-	-
Eff-Oct-BF(B)	-	2.92	24	-	-	-	-
Feed-Apr	-	2.71	18	-	-	-	-
Eff-Apr-BF(B)	-	2.51	16	-	-	-	-
Eff-Apr-BF(A)	-	2.54	15	-	-	-	-
NF-Fall-BF(B)-R1-8	24.2	2.38	17	6.4	1.55E+06	ND	2.3
NF-Fall-BF(B)-R2-8	21.3	2.25	15	7	1.58E+06	ND	2.3
NF-Fall-BF(B)-R1-4	24.2	2.12	15	7.3	1.85E+06	ND	2.1
NF-Fall-BF(B)-R2-4	21.3	2.14	16	8.6	2.98E+06	ND	2.7
Sand-Winter-BF(A)	-	3.08	28	15.9	8.41E+06	633.0	1166.5
Anth-Winter-BF(A)	-	3.07	25	84.4	3.36E+07	2903.4	5111.0
Sand-Winter-BF(B)	-	3.28	32	30.4	1.36E+07	958.5	1772.4
Anth-Winter-BF(B)	-	3.2	27	40.4	2.40E+07	1727.7	3143.4
NF-Winter-Raw-4	101.7	2.97	25	16.5	2.71E+06	2.1	2.4
NF-Winter-Raw-8	101.7	3.06	26	11.1	6.01E+06	1.8	3.3
NF-Winter-BF(A)-4	18.17	3.31	33	13	1.76E+06	ND	2.5
NF-Winter-BF(A)-8	18.17	3.18	28	11.7	1.05E+06	ND	2.7
NF-Winter-BF(B)-4	2.81	3.22	32	6.4	3.09E+05	ND	1.7
NF-Winter-BF(B)-8	2.81	3.27	35	6.3	9.41E+05	ND	2.1
Sand-Fall-BF(A)	-	3.24	39	9.5	2.07E+05	217.0	343.6
Anth-Fall-BF(A)	-	3.33	40	10.8	1.75E+06	599.9	1463.7
Sand-Fall-BF(B)	-	3.41	40	18.7	2.29E+06	678.2	1410.7
Anth-Fall-BF(B)	-	3.11	32	17.0	2.69E+06	911.8	2015.6
NF-Fall-Raw-4	126.44	3.45	25	38.5	4.11E+07	2.9	7.5
NF-Fall-Raw-8	126.44	3.5	36	44.1	5.07E+07	3.7	8.7

4.3.2 Samples, Storage and DNA Isolation

Archived samples of cellular biomass from biofilter feed, effluent, media and NF membrane samples were provided by Dr. Elhadidy. Archived biofilter feed, effluent and media samples were processed for DNA isolation as described in Chapter 3. Nanofilter membrane samples from the previous study (each totalling 4 cm²) were stored at -80 °C in sterile polypropylene centrifuge tubes in the absence of PBS buffer. DNA extraction from NF membrane samples was done using the same method as the filters used to concentrate microorganisms from feed and effluent water samples described in Ch. 3. Briefly, the 4 cm² nanofiltration membrane sample was placed in a 5 mL bead tubes (PowerWater DNA Isolation Kit (Mo Bio, USA), and DNA was extracted and described by the manufacturer's protocol.

As outlined in Ch. 3, isolated DNA from all samples was screened by agarose gel electrophoresis for size and quality while the yield of double stranded nucleic acids was quantitated using a Qubit 2.0 fluorometer and dsDNA BR Assay Kit (ThermoFisher Scientific) in 0.5 mL thin walled PCR tubes (ThermoFisher Scientific).

4.3.3 PCR Amplification of Extracted Nucleic Acids

Bacterial DNA was amplified by PCR in the V6-V8 16S region using a GC-clamped F968 forward primer and r1401.1b reverse primer as outlined in Ch. 3. PCR amplification of Archaea was done using a nested PCR (nPCR) protocol as described in Pereira e Silva and colleagues (2012). The outer primer set contained an archaea-specific forward primer Arch21F (DeLong, 1992) with a universal bacteria reverse primer U1460R (Heijs et al., 2008); this first primer pair amplified a larger 1439 bp region while the inner primer set, composed of ARC344 with 40 bp GC clamp and reverse universal bacterial primer 517r, amplified a 173 bp region contained within the A21F/U1460R amplicons (Bano et al., 2004). PCR mixtures were adapted from Pereira e Silva (2012) to include hot start polymerase addition as well as the use of bovine serum albumin (BSA) and dimethyl sulphoxide (DMSO) (Heijs, 2008). The PCR mixture for the outer primer set consisted of 20 mM Tris-HCl (pH 8.4), 50 mM KCl, 2.3 mM Mg²⁺, 10% wt/vol BSA (BioRad, USA), 2% v/v DMSO (Sigma Aldrich, USA), 0.2 µM dNTPs (BioRad, USA), 0.5 µM of

each primer, 5 ng template DNA and 0.4 U iTaq polymerase (BioRad, USA). The PCR program was modified from Pereira e Silva and colleagues (2012) and consisted of 95 °C for 5 min, followed by 30 cycles of 1 min at 94 °C, 30 s at 57.5 °C, and 4 min at 72 °C, and a final extension of 7 min at 72 °C. The nested PCR reaction was performed with the ARC344f/U517r set in 50 µL total reaction volume based on the method described by Bano et al. (2004). PCR mixtures for this reaction were composed of 50 mM KCl, 20 mM Tris-HCl (pH 8.4), 2.5 mM Mg²⁺, 0.2 µM dNTPs and 0.4 µM of each primer, 5 ng template DNA and 1 U iTaq polymerase. PCR program consisted of the following steps: 95 °C for 5 min; 1 cycle at 94 °C for 45 s at; touchdown program from 65 to 62 °C decreasing 0.5 °C per cycle; touchdown program from 62 to 55 °C decreasing by 1 °C per cycle; one cycle at 72 °C for 30 s of; 30 cycles at 94 °C for 45 s, 55 °C for 45 s, 72 °C for 30 s; and a final 72 °C extension for 5 min. Archaeal amplifications were performed with a template-negative control as well as an *E. coli* negative control.

The fungal primer set targeted the 18S rDNA internally transcribed spacer (ITS) region, and included the ITS1 forward primer with GC clamp and an ITS2 reverse primer (Pereira e Silva et al., 2012). Fungal PCR reaction mixtures consisted of 50 mM KCl, 20 mM Tris-HCl (pH 8.4), 2 mM MgCl₂, 0.5 µg BSA, 0.25 mM dNTPs, 0.4 µM each primer, and 2.5 U Taq polymerase. The thermocycling program involved 94 °C for 5 minutes, 34 cycles of 94 °C for 30 s, 55 °C for 30 s, 72 °C for 30 s, with a final extension step of 72 °C for 5 min. All fungal amplifications were performed with a template-negative control for contamination detection.

4.3.4 DGGE Conditions

The bacterial, archaeal and fungal DGGE conditions were identical to the protocol described for bacteria in Ch. 3, except that archaeal amplicons were loaded into polyacrylamide gels with a 40 - 60% denaturing gradient. Fungal DGGE conditions used the same conditions and gradient as bacteria. DGGE gels were visualized on the GelDoc platform (Bio Rad, USA) using Quantity One software v4.6 (Bio Rad, USA) and imported to Bionumerics v7.5 (Applied Maths, Belgium). Separate databases were constructed for bacteria and archaea after fingerprint background subtraction and alignment to reference lanes. BioNumerics v7.0 settings included

arithmetic average least square filtering (cut-off below 0.5%, power of 2.0) as well as Richardson-Lucy deconvolution (50 iterations, kernel size 2.0 pixels). These settings allowed for greater background noise reduction of electropherogram images. A rolling disk of size 13 was used on all densitometric curves, with automatic band searching set at 4% relative to maximum density value. Noise bands resulting from aberrant photograph grains were removed as required. The quantitative (intensity) $m \times n$ matrices of band data were exported for further statistical processing in the open software Project R (R Core Team, 2013).

4.3.5 Statistical Analysis and Interpretation

As described in Chapter 3, intensity matrices were analysed using several packages in the open-source Project R software (R Core Team, 2013). Ordination and cluster analysis was performed using the *Vegan* (Oksanen et al., 2016) and *FactoMineR* (Le et al., 2008) packages, with biodiversity statistics obtained using *BioDiversityR* (Kindt & Coe, 2005). The approaches used in multivariate investigations of the DGGE matrices were informed by Borcard et al. (2011), Legendre & Legendre (1988), and Whitlock & Shluter (2009).

The strategy for interpretation of DGGE community profile data was the same used in Chapter 3 and summarized as follows. First the band intensity data were used in a Mantel optimal number of clusters test, followed by hierarchical clustering, detrended correspondence analysis (DCA), and finally analysis of similarity (ANOSIM) to provide hypothesis testing on the selected number of clusters. Given that densitometric curves were extracted from DGGE profile data, phylotype presence (band occurrence) as well as abundance (band intensities) were used. According to Legendre & Legendre (1998), a distance coefficient which can be applied to raw quantitative data while allowing for rare species to affect the dissimilarities is the Bray-Curtis distance (otherwise known as the Koczyński) coefficient; therefore Bray-Curtis distances were used for all cluster analyses. Hierarchical clustering of the distance matrix was performed using the Ward algorithm. The Ward algorithm uses the agglomerative approach to cluster analysis, which is both better suited and less error-prone than divisive methods due to the procedural nature of agglomeration (Legendre & Legendre, 1998). The Ward linkage algorithm

was selected for cluster assembly because it minimizes the sums of the squared distances between cluster centroids. This leads to clustering in which variance is minimized and gives cluster centroids a leading role in the cluster topology (Legendre & Legendre, 1998).

Diversity of the DGGE profiles (Shannon index etc.) was done as described in Chapter 3. Normality of the diversity data was tested using the Shapiro-Wilke test for normality in the stats package (R Core team, 2016) in Project R. Because the diversity data of the biofilter feed, effluent, media and NF membranes were determined to have a non-normal distribution using Shapiro Wilke tests, two non-parametric tests were used to compare means of diversity data; the Kruskal-Wallis rank-sum test, which determines if a significant difference exists on between-group means exists, and the post-hoc Dunn multiple comparison test with Bonferroni correction, which was used to compare pairs of sample means.

4.4 Results

4.4.1 Detection of microorganisms in biofilter-NF samples by PCR amplification

A total of 31 samples collected from both the fall and winter experiments were used for bacterial analysis, including NF membrane samples collected at both the 4 and 8 cm distance from the MFS feed inlet, as well as biofilter media, and biofilter feed water and effluent samples from the 8 min EBCT biofilter BF(A) and the 16 min EBCT biofilter BF(B). DNA isolation from environmental samples yielded high molecular weight bands. The bacterial primer pair yielded positive 16S rDNA amplification bands of the expected size (473 bp) with no contamination of PCR blanks. Qubit fluorescence quantitation showed that PCR amplicon yield was high, with the bacterial 16S gene double stranded DNA concentration between 18 and 25 ng/ μ L.

Fewer samples (15) were included in the archaeal analysis due to labour limitations. Samples collected from the fall and winter experiments were used, including NF samples collected only at 4 cm from the MFS feed inlet, and biofilter media samples from only the 16 min EBCT biofilter BF(B). A single biofilter feed and effluent sample from each of the autumn

and winter experiments were included. For Archaea, the first round of PCR produced no visible bands on agarose gel due to low concentration of amplicons. This necessitated use of a nested PCR (nPCR), where amplicons of the 1st round are used as template for a separate, smaller region of amplification in the 2nd round of PCR. Following the nested (2nd) archaeal PCR, positive 16S rDNA amplification bands of the expected size (213 bp) were observed with no contamination or non-specific PCR products for archaeal amplicons. After nested PCR, amplicon yield was approximately 20 ng/μL for each sample.

Only two preliminary samples were amplified for presence of fungal DNA during method development (August 2015 biofilter feed and August 2015 biofilter sand at 20 cm depth). Due to labour constraints a full evaluation of fungal communities in the biofilter and membranes samples could not be performed, however results are included here to provide information for future studies. Positive 18S rDNA amplification bands were observed in both samples evaluated. The observed bands were of the expected 350 bp size (Orgiazzi et al., 2012). This proves that fungi were a part of both the river water and the biofilter media communities. Fungal amplicon yield was 6.0 and 6.2 ng/μL for the media and feed water samples, respectively, and were therefore of lower concentration compared to bacteria but higher than archaea; therefore it would be worthwhile to further investigate fungal communities in biofilters in the future.

4.4.2 Bacterial & Archaeal Community Profiling

An example DGGE bacterial community profile is presented in **Figure 4.1**, and exemplifies the phylotypic diversity of the biofilter media biofilm bacteria.

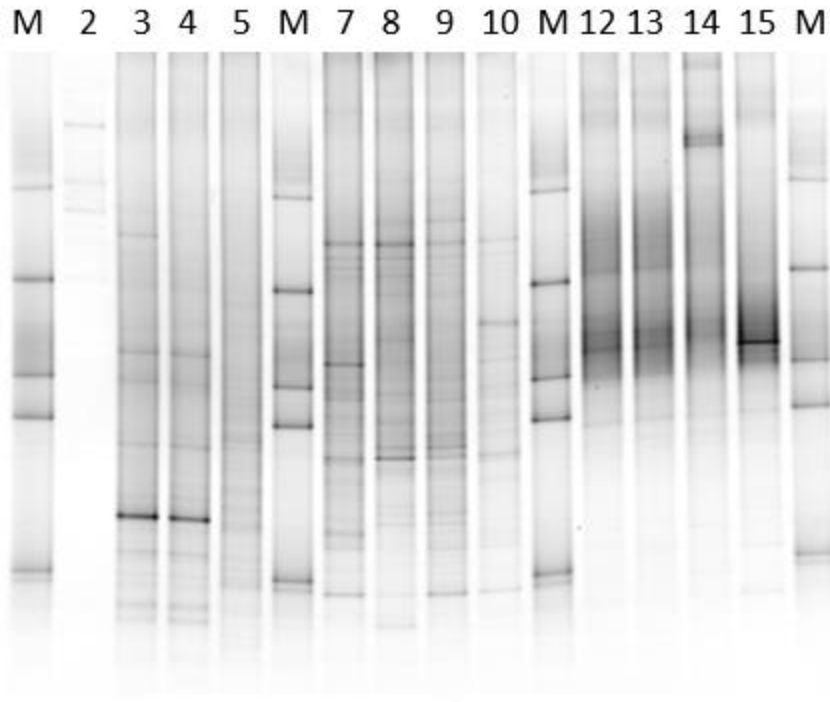


Figure 4.1: Example bacterial 16S rDNA DGGE community fingerprint. Lanes 1, 6, 11 and 16 were loaded with a custom molecular marker and denoted by “M”. Lane 2 presents a fungal community profile while lanes 3–5 were NF samples (NF-Fall-BF(B)-4-R2, NF-Fall-BF(B)-4-R1, NF-Fall-Raw-4). Lanes 7 – 10 were NF-Winter-Raw-4, NF-Winter-BF(B)-8, NF-Winter-BF(A)-8, and NF-Winter-Raw-8. Lanes 12 – 15 were Eff-Apr-BF(A), Eff-Apr-BF(B), Feed-Apr, and Eff-Mar-BF(A).

In order to determine the number of clusters (groups) present in the data, Mantel optimal number of cluster tests were used. The Mantel correlation is algebraically equivalent to the Pearson correlation and compares original distance matrix values against a constructed dendrogram cut at various heights, which represents groups (Borcard et al., 2011). The number of groups which best correlate to the original distances are depicted in **Figure 4.2**. For bacterial dendrogram construction, Bray-Curtis distance coefficients were assembled via the Ward algorithm and plotted within the dendrogram of **Figure 4.3**. A legend is presented in **Table 4.2** which describes the naming convention used for the community profiles in the dendrogram of **Figure 4.3**. For bacterial phylotypes across biofilter feed, media, effluent and NF membrane samples, the Mantel optimal number of clusters produced a tie between 5 and 7 clusters since each exhibits a Pearson’s correlation of 0.72 between the distance matrix and dendrograms cut for each group number. Therefore further analyses were necessary to determine the best way of partitioning the bacterial data.

The analysis presented in **Figure 4.2** provides insight as to whether the bacterial fingerprint data contains 5 or 7 groups. The number of groups was determined to be 7 since this better differentiated the NF, media and fall/winter groups at a cut height of 0.85. The 7 groups were labelled as A-G (**Figure 4.3**). Group A (purple) contains biofilter feed and effluent samples from cold water conditions (February and March 2015), Group B (light blue) contains raw feed communities from October 2014, Group C (dark blue) contains raw feed and biofilter effluent from April 2015 as well as biofilter effluent from October 18th 2014. Overall, results show that biofilter feed and effluent samples are confined to groups A, B and C, and these samples group separately from the media and membrane biofilm samples (groups D to G) at a dendrogram cut-off height of 2. The larger data set of biofilter feed water and media samples in Chapter 3 showed a similar grouping between sample types (planktonic and media biofilms). Group D (red) contains only NF biofoulant communities fed with biofilter effluent from the fall experiment, Group E (yellow) contains all winter biofilter media communities, Group F (green) contains all NF biofoulant communities from the winter experiment, and Group G (brown) contains all media biofilm communities from the fall experiment plus the NF biofoulant communities from the fall experiment that were fed using raw river water. All media communities presented in **Figure 4.3** were sampled from 20 cm depth at the interface between the upper anthracite and lower sand media.

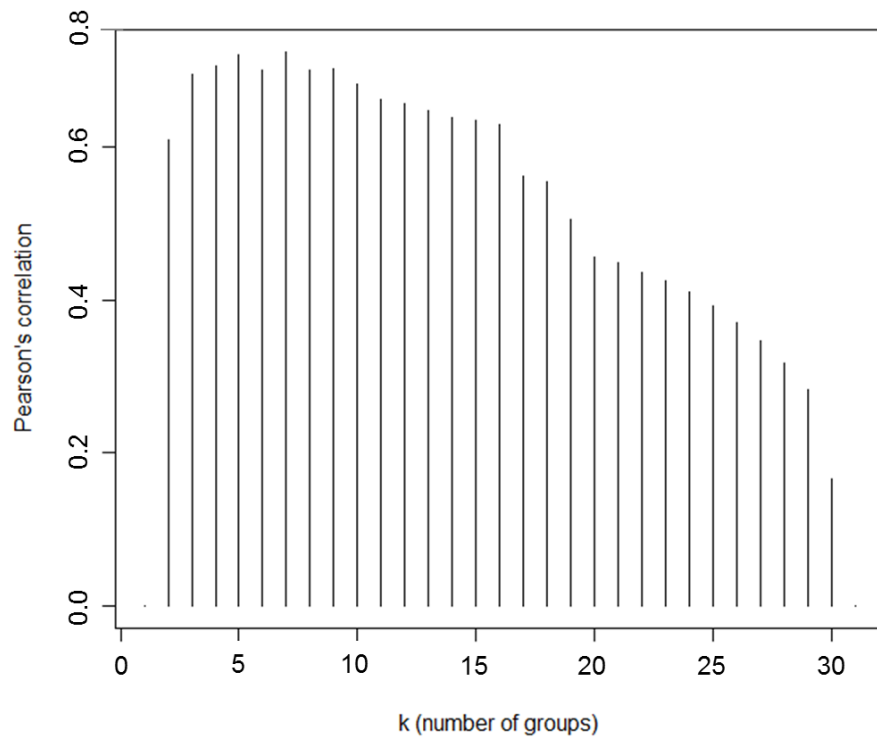


Figure 4.2: Mantel optimal number of clusters (k) using Ward algorithm with bacterial DGGE profile data. The Pearson correlation suggests the validity of different numbers of groups. The optimal group number was highest for 5 and 7 ($r = 0.72$).

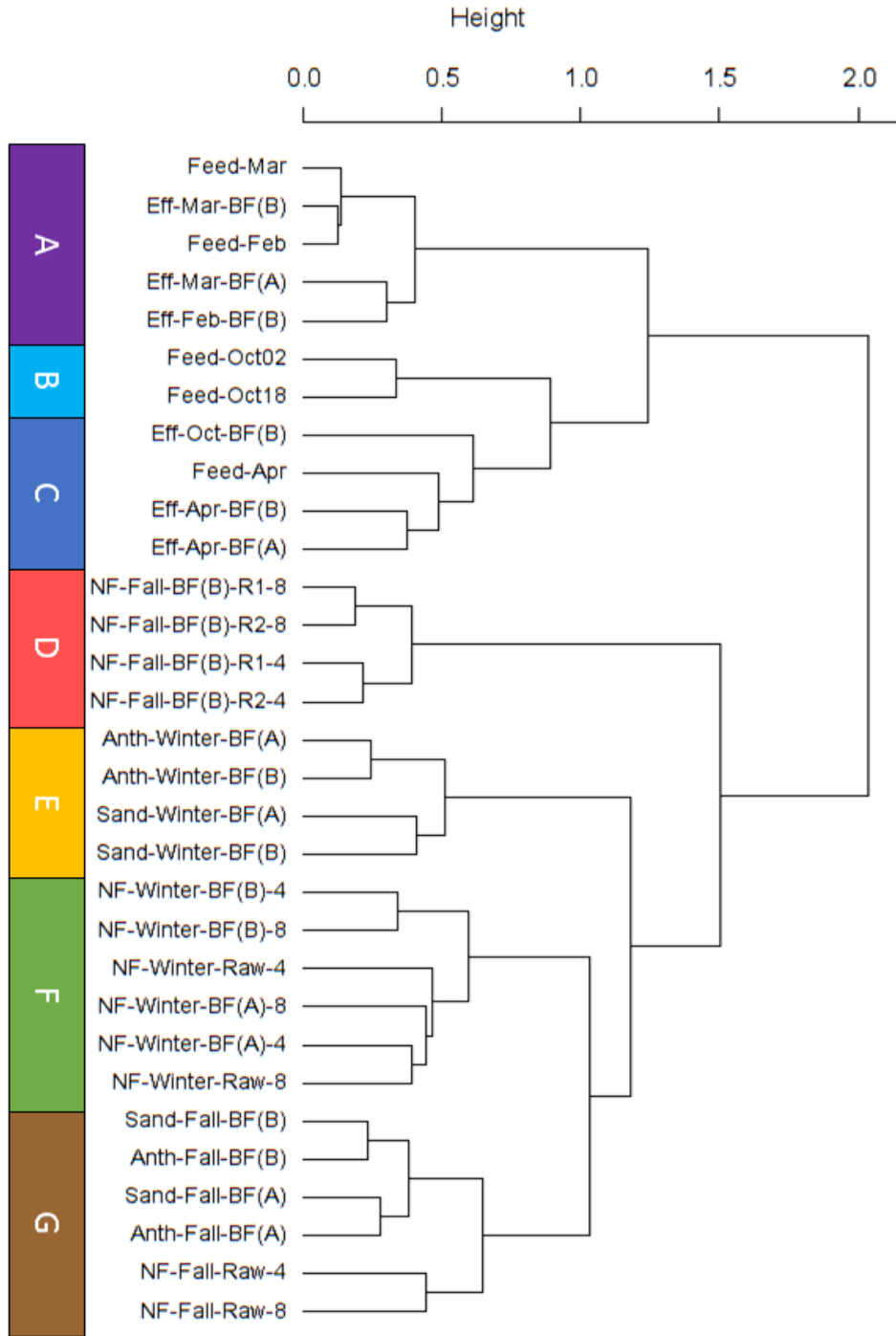


Figure 4.3: Dendrogram plot showing hierarchical clustering of bacterial community DGGE profile data for biofilter feed and effluent, biofilter media and NF samples. All media samples shown were taken from 20 cm depth. Bray-Curtis Distances were used in conjunction with the Ward algorithm. Y axis represents dissimilarity height between samples, where increasing height between nodes indicates greater dissimilarity between sample communities. A total of seven groups were identified and given a group letter. A legend of each sample is in Table 4.2.

Table 4.2: Legend explaining x-axis labels in the dendrogram of Figure 4.2.

Sample code (DGGE dendrogram)	Sample Type	Month	Experiment	Biofilter	Replicate	Distance from feed inlet (cm)
NF-Fall-BF(B)-R1-4	Membrane	Oct	Fall	BF(B)	1	4
NF-Fall-BF(B)-R2-4	Membrane	Oct	Fall	BF(B)	2	4
NF-Fall-BF(B)-R1-8	Membrane	Oct	Fall	BF(B)	1	8
NF-Fall-BF(B)-R2-8	Membrane	Oct	Fall	BF(B)	2	8
NF-Fall-Raw-4	Membrane	Oct	Fall	Raw	-	4
NF-Fall-Raw-8	Membrane	Oct	Fall	Raw	-	8
Sand-Fall-BF(A)	Sand	Oct	Fall	BF(A)	-	-
Anth-Fall-BF(A)	Anthracite	Oct	Fall	BF(A)	-	-
Sand-Fall-BF(B)	Sand	Oct	Fall	BF(B)	-	-
Anth-Fall-BF(B)	Anthracite	Oct	Fall	BF(B)	-	-
Feed-Oct02	Raw Water	Oct	Fall	-	-	-
Feed-Oct18	Raw Water	Oct	Fall	-	-	-
Eff-Oct-BF(B)	Effluent	Oct	Fall	BF(B)	-	-
NF-Winter-BF(A)-4	Membrane	Apr	Winter	BF(A)	-	4
NF-Winter-BF(A)-8	Membrane	Apr	Winter	BF(A)	-	8
NF-Winter-BF(B)-4	Membrane	Apr	Winter	BF(B)	-	4
NF-Winter-BF(B)-8	Membrane	Apr	Winter	BF(B)	-	8
NF-Winter-Raw-4	Membrane	Apr	Winter	Raw	-	4
NF-Winter-Raw-8	Membrane	Apr	Winter	Raw	-	8
Sand-Winter-BF(A)	Sand	Apr	Winter	BF(A)	-	-
Anth-Winter-BF(A)	Anthracite	Apr	Winter	BF(A)	-	-
Sand-Winter-BF(B)	Sand	Apr	Winter	BF(B)	-	-
Anth-Winter-BF(B)	Anthracite	Apr	Winter	BF(B)	-	-
Feed-Feb	Raw Water	Feb	Winter	-	-	-
Feed-Mar	Raw Water	Mar	Winter	-	-	-
Feed-Apr	Raw Water	Apr	Winter	-	-	-
Eff-Feb-BF(B)	Effluent	Feb	Winter	BF(B)	-	-
Eff-Mar-BF(A)	Effluent	Mar	Winter	BF(A)	-	-
Eff-Mar-BF(B)	Effluent	Mar	Winter	BF(B)	-	-
Eff-Apr-BF(A)	Effluent	Apr	Winter	BF(A)	-	-
Eff-Apr-BF(B)	Effluent	Apr	Winter	BF(B)	-	-

Samples from the dendrogram analysis labelled according to cluster group (A to G), were assessed using correspondence analysis (CA). CA is an ordination technique which conserves the chi-squared distances in lieu of using Euclidian distances (like principal

component analysis or PCA); the result is a clustering method which is better at handling species data. Species data is usually regarded as unimodal when plotted against environmental gradients, meaning that species concentration is highest around an optima with respect to an environmental variable (Borcard et al., 2011; Legendre & Legendre, 1998). This is also known as niche partitioning. CA is therefore a well respected multivariate analysis tool designed to handle unimodal data whereas PCA, which assumes a linear response curve to environmental variables, is commonly eschewed in such circumstances (Fromin et al., 2002). Moreover, the chi-squared distances in CA have been empirically tested and validated as ideal for the ordination of unimodal species data (Braak, 1985; Hill, 1974). Given that chi-squared distances are used, CA provides a measure of redundancy to the Bray-Curtis distances used in the dendrogram data as a way of validating the defined group memberships.

Results for the bacterial community profiles were ordinally clustered and plotted in the CA plot of **Figure 4.4**, with variance explained by the two axes of 19.2 and 10.6 for CA1 and CA2, respectfully. This technique presents the bacterial DGGE profile data in 2 dimensions where communities exhibiting high similarities to one another are presented closer together along the axes of CA1 and CA2. Results show that the feed water groups of A, B and C are located in close proximity to one another (except for one point in the B group), as are the media and NF membrane biofilm groups of E, F and G (which are even closer to each other). Thus a well defined differentiation exists between the biofilm and the planktonic communities, with only small dissimilarities observed among the respective biofilm and planktonic communities. However, the biofilter fed autumn NF membrane communities of Group D exhibited great dissimilarity from any other group in the plot. Therefore feed water and biofilter media communities present only small differences between autumn and winter conditions, while the BF-NF (biofilter fed NF communities) present dramatic differences between autumn and winter conditions. Group G shows tight clustering of the autumn media biofilm communities, with the two autumn raw-NF communities (NF-Fall-Raw-4 and NF-Fall-Raw-8) marking an exception since they appear to share greater similarity with Group E, winter media; this last observation was not apparent using hierarchical clustering.

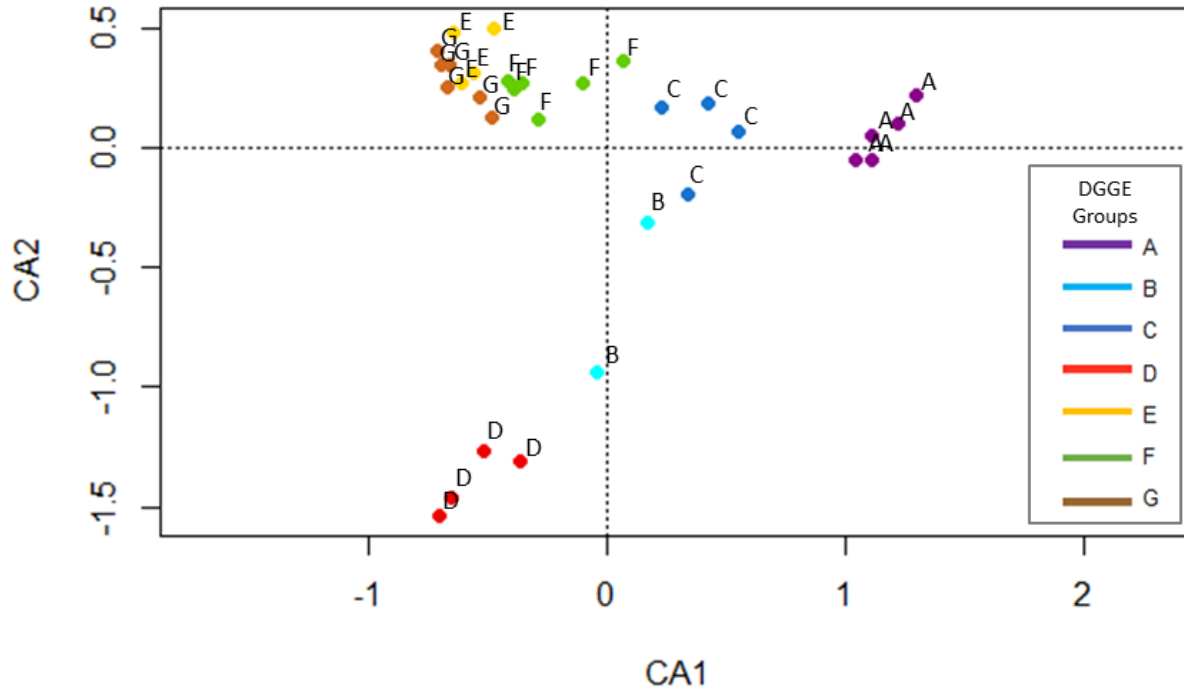


Figure 4.4: Correspondence analysis of bacterial DGGE community profiles. Each data point represents the DGGE profile of a sample from the dendrogram groups (A to G) defined in Figure 4.3. The variance of the two axes is 19.2 and 10.6 % for CA1 and CA2 respectively.

Examination of exploratory (clustering) analyses revealed a coherent k value of 7 for bacteria; therefore analysis of similarity (ANOSIM) was used on Bray-Curtis distances to provide hypothesis testing on the selected number of groups as well as to present the amount of within group dissimilarity; the results are illustrated in the box and whisker plot of **Figure 4.5**. The two outliers within Group G correspond to the two autumn raw-NF communities. The ANOSIM test uses the Bray-Curtis distance matrix rather than the raw DGGE profile intensity data, and therefore the y-axis of the boxplot figure represents the Bray-Curtis distance, or dissimilarity, between groups. Each group's dissimilarity is therefore shown by individual boxes, which are compared against the between group dissimilarity. Results (**Figure 4.5**) show that the null hypothesis is rejected for the bacterial profile ANOSIM test, as a p -value of 0.001 ($\alpha = 0.05$) and an R value of 0.98 is obtained. The ANOSIM statistic (R value) is a comparison of the ranked between group mean dissimilarity versus the mean within group dissimilarity, where an R value close to 1 indicates high dissimilarity between groups. The high R value and significant result provide a strong argument in favour of the selected k of 7.

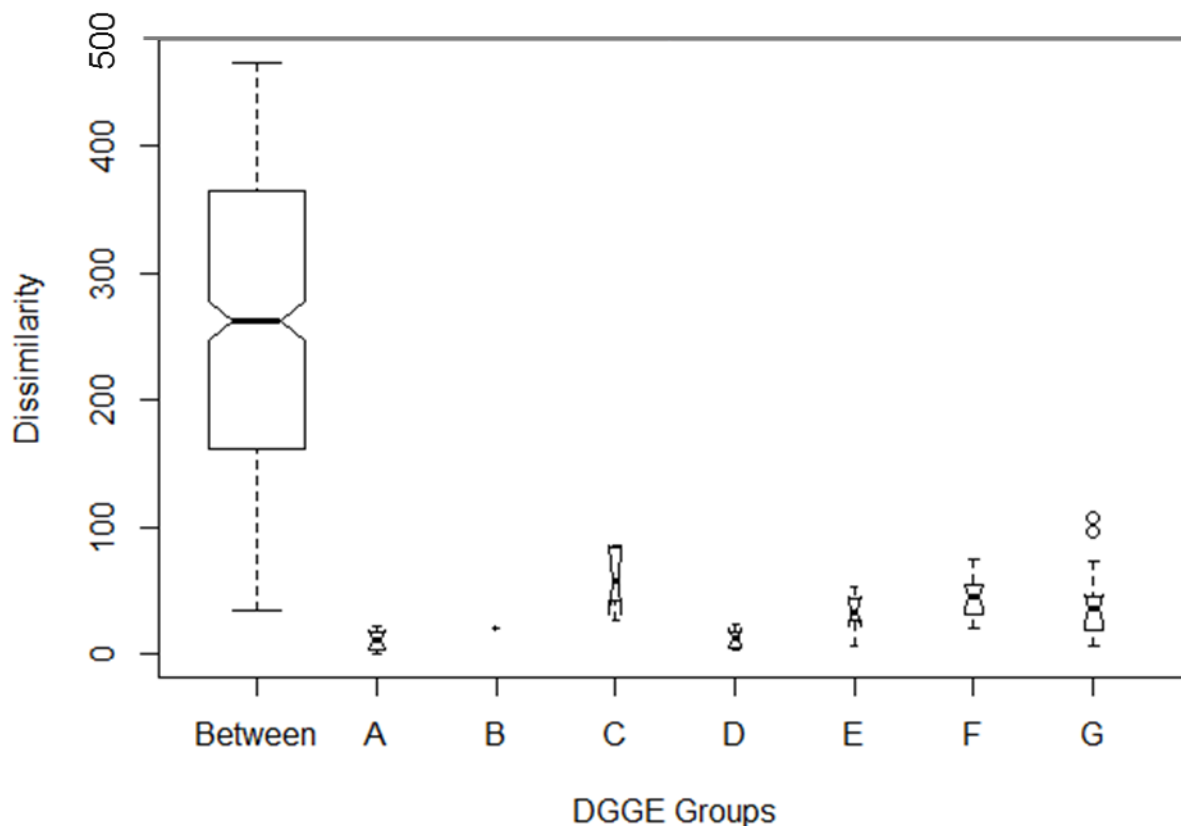


Figure 4.5: Hypothesis testing using analysis of similarity (ANOSIM) of bacterial DGGE profile data. ANOSIM significantly validated group membership ($p=0.001$, $R=0.979$). Dissimilarity is represented by the y-axis and group width shows the number of members within each group. Within each box, the horizontal bar shows the group median dissimilarity, while top and bottom of the box shows 1st and 3rd quartile, respectively. Whiskers denote minimum and maximum values. Group G possessed two outliers (autumn raw-NF samples).

In addition to assessing the community profiles of bacteria, the occurrence and diversity of archaeal communities was also assessed using PCR-DGGE, with an example profile presented in **Figure 4.6**. A Mantel optimal number of clusters analysis (**Figure 4.7**) was also performed on the archaeal profile dataset, and used the same distance coefficient and clustering algorithms as before; this analysis resulted in an optimal k of 5 at a Pearson's r of 0.65. This lower r value indicates less agreement between the archaeal distance matrix and any number of Ward assembled groups, relative to the bacterial analysis. Therefore in the dendrogram of **Figure 4.8**, 5 archaeal community clusters are present at a cut height of 0.85, with each group labelled alphabetically. Results show that the winter archaeal communities did not cluster according to sample type (planktonic feed water, media biofilm, membrane biofilm), and that the archaeal dataset as a whole presents a less well-defined structure compared to bacteria. Due

to time constraints, fewer samples were analyzed compared to bacteria. A legend for samples included in the archaeal data-set is found in **Table 4.3**.

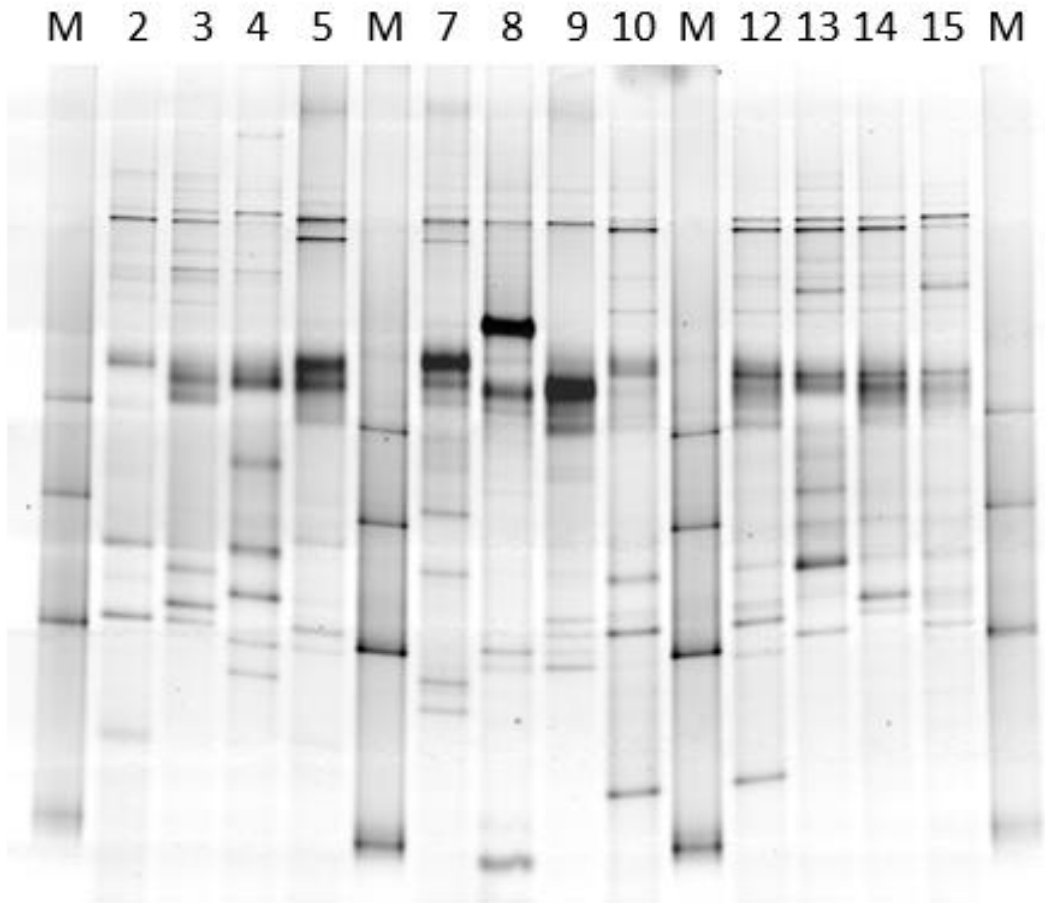


Figure 4.6: Example archaeal 16S rDNA DGGE community profile. Lanes 1, 6, 11 and 16 were loaded with a custom molecular marker and denoted by “M”. Lanes 2 – 5 present media biofilm community profiles. Lanes 7 – 10 present Feed and effluent profiles.

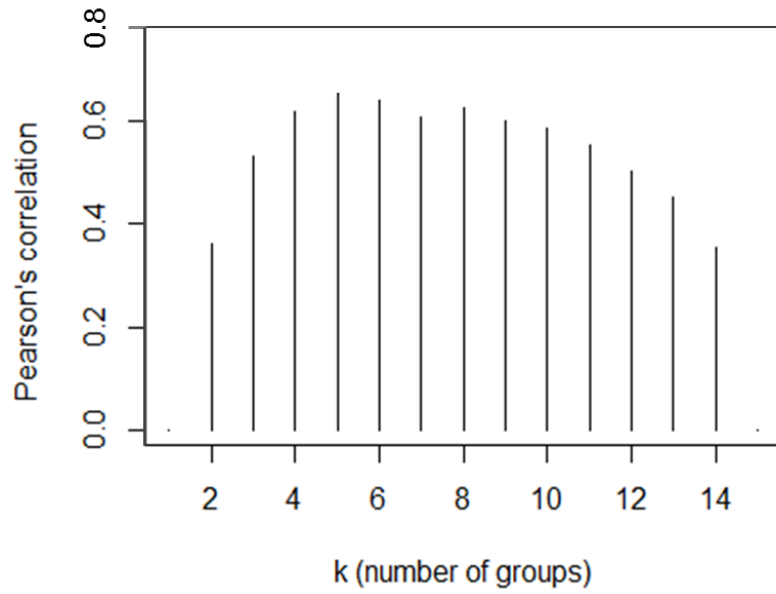


Figure 4.7: Mantel optimal number of clusters using Ward algorithm with archaeal DGGE profile data. Bar height represents Pearson's correlation between original distance matrix and various numbers of groups possible within a Ward assembled dendrogram. Optimal number of archaeal groups was 5, with a Pearson r correlation of 0.65.

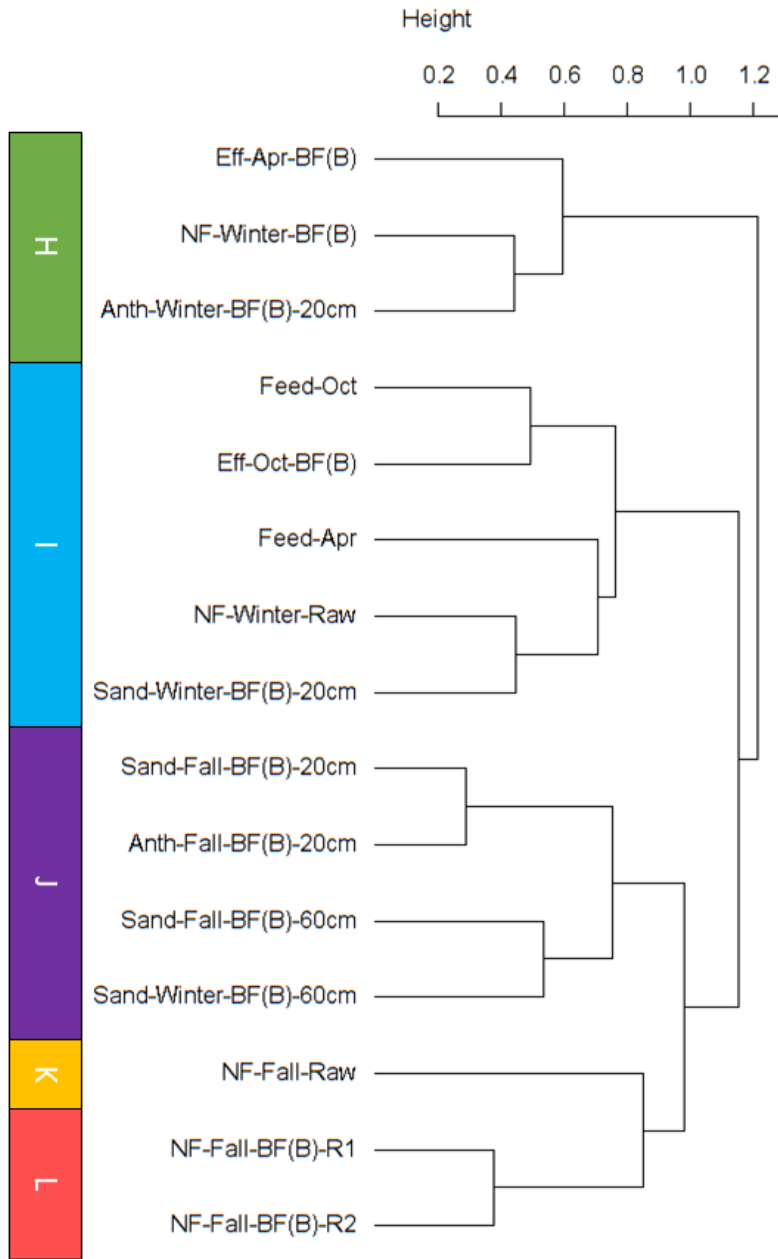


Figure 4.8: Dendrogram plot showing hierarchical clustering of archaeal community DGGE profile data. Five groups were identified at a cut height of 0.90, and given a designated group letter. All NF membrane samples used in the archaeal analysis were 4 cm distant from the MFS feed inlet. A legend of each sample is in Table 4.3.

Table 4.3: Legend explaining x-axis labels in the archaeal community dendrogram of Figure 4.12.

Sample code (DGGE dendrogram)	Type	Month	Experiment	Biofilter	Replicate	Depth (cm)
NF-Fall-BF(B)-R1	Membrane	Oct	Fall	BF(B)	1	-
NF-Fall-BF(B)-R2	Membrane	Oct	Fall	BF(B)	2	-
NF-Fall-Raw	Membrane	Oct	Fall	Raw	-	-
Sand-Fall-BF(B)-20cm	Sand	Oct	Fall	BF(B)	-	20
Anth-Fall-BF(B) -20cm	Anthracite	Oct	Fall	BF(B)	-	20
Sand-Fall-BF(B) -60cm	Sand	Oct	Fall	BF(B)	-	60
Feed-Oct	Raw Water	Oct	Fall	-	-	-
Eff-Oct-BF(B)	Effluent	Oct	Fall	BF(B)	-	-
NF-Winter-BF(B)	Membrane	Apr	Winter	BF(B)	-	-
NF-Winter-Raw-4	Membrane	Apr	Winter	Raw	-	-
Sand-Winter-BF(B)-20cm	Sand	Apr	Winter	BF(B)	-	20
Anth-Winter-BF(B) -20cm	Anthracite	Apr	Winter	BF(B)	-	20
Sand-Winter-BF(B) -60cm	Sand	Apr	Winter	BF(B)	-	60
Feed-Apr	Raw Water	Apr	Winter	-	-	-
Eff-Apr-BF(B)	Effluent	Apr	Winter	BF(B)	-	-

Correspondence analysis on archaeal results is plotted in **Figure 4.9**, with each sample labelled according to alphabetical DGGE group membership. The ordination of **Figure 4.9** shows a wide dispersal of data points; the percent of variance explained by the two axes are 16.4 and 14.1 for CA1 and CA2, respectively. The amount of variance explained by **Figure 4.9** is therefore similar to the bacterial CA plot (**Figure 4.4**), however it is clear that the archaeal data-set as a whole possesses less well defined group memberships, which is similar to the hierarchical analysis of **Figure 4.8**.

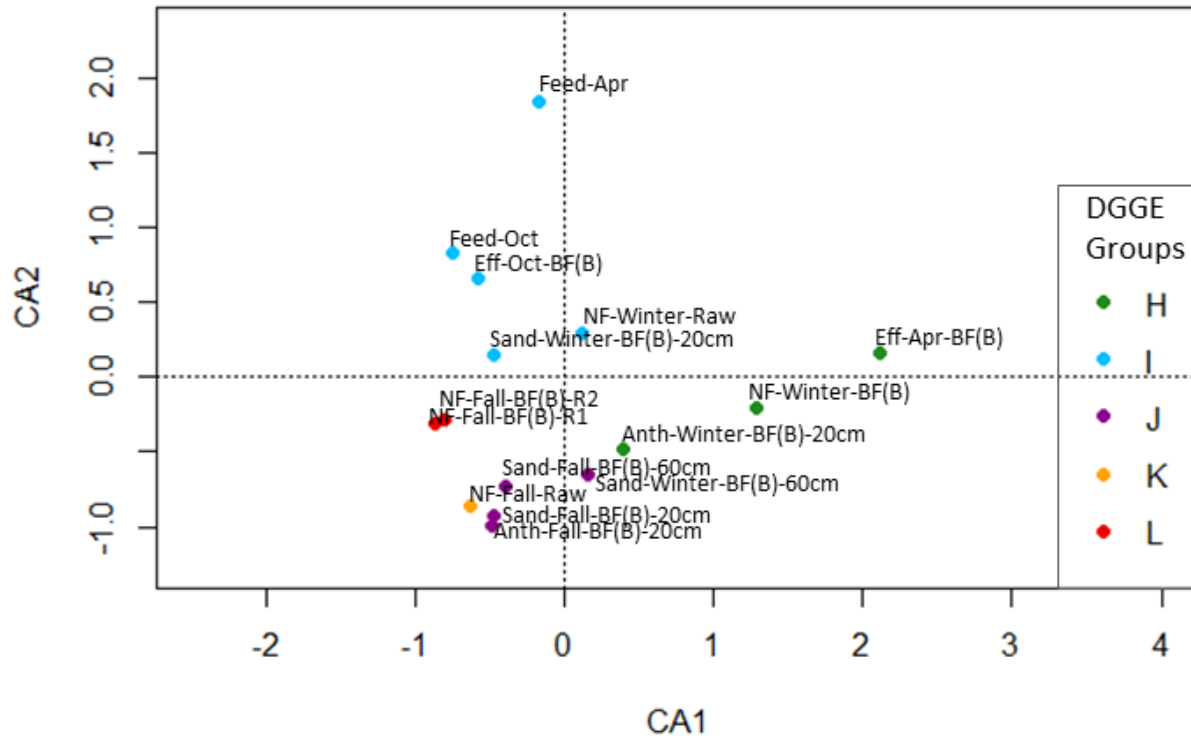


Figure 4.9: Correspondence analysis of archaeal DGGE community profiles. Each data point represents the DGGE profile of a sample from the dendrogram groups H to L defined in Figure 4.12. The variance of the two axes is 18% and 15% for CA1 and CA2 respectively

The exploratory analyses produced a k value of 5 for archaea and so an analysis of similarity (ANOSIM) was used on archaeal Bray-Curtis distances to evaluate the statistical significance of the chosen number of groups; the results are illustrated in the boxplots in **Figure 4.10** for archaea. Once again, the y axis in these figures represents the Bray-Curtis distances or dissimilarities within and between groups. Group K only had a single member entry and therefore it's within group dissimilarity could not be calculated, resulting in no box for that group. The width of each box is proportional to the number of entries within that group, and this is why Group L, with 2 group entries, possesses a small box within the plot. The null hypothesis is rejected for this test, with the resulting p-value being 0.001 (alpha = 0.05) and an R value of 0.87. However this R value is lower than in the bacterial ANOSIM and again indicates less well defined separation among groups.

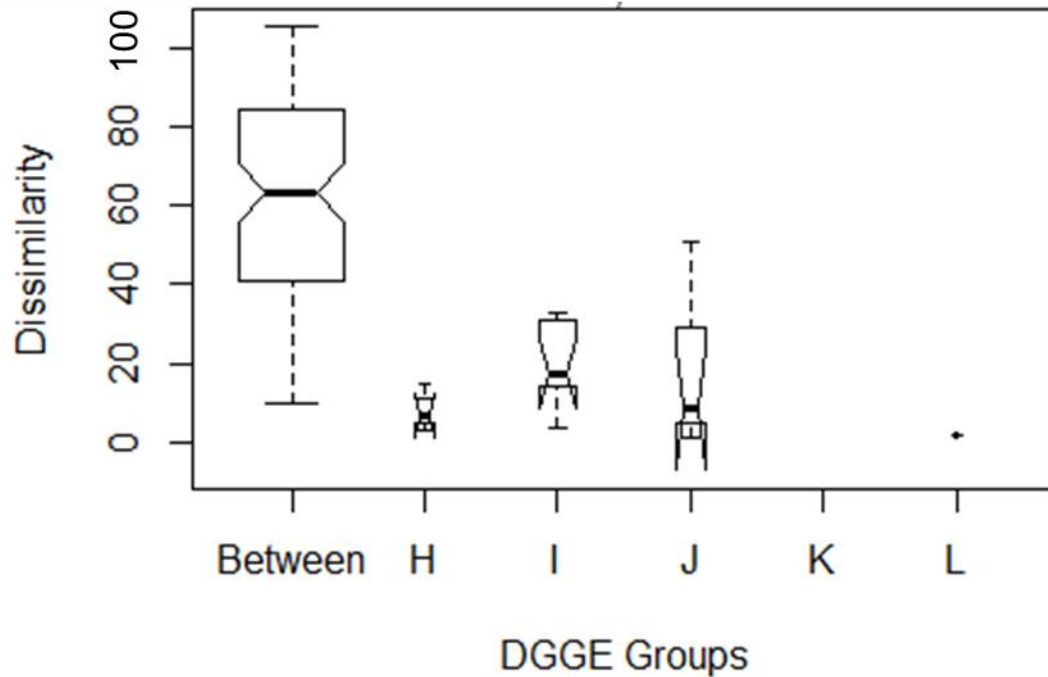


Figure 4.10: Hypothesis testing using analysis of similarity (ANOSIM) on archaeal DGGE profile data. ANOSIM validated group membership and number ($p=0.001$, $R=0.865$). Dissimilarity is represented by the y-axis and the “between” as well as “within” group dissimilarities are illustrated by boxplot height, whose size varies according to number of members within each group.

4.4.3 Comparing Community Diversity with Membrane Fouling Data

Shannon diversity (H') describes the number of species in a given habitat and their relative abundance; it is calculated from community richness (the number of species in a community) and community evenness (the relative abundance of species in a community) (Molles & Cahill, 1998). Richness is an important ecological parameter since it consists of the number of species observed which itself is inherently useful. Shannon diversity differs from richness in that it accounts for the proportions as well as the abundance of species within a community. Depending on the relative abundance of individual phylotypes, it is possible for a system to present different Shannon indices yet have the same richness, and therefore is an important measure for assessing a community’s complexity, resilience and maturity. Shannon diversity was calculated using **Equation 3.1** as seen in Ch. 3. The Shannon index was selected to measure community diversity due to its equal treatment of rare and dominant species (Morris et al., 2014). Furthermore, the ubiquity of H' within the literature makes comparisons to other biofiltration studies possible.

The bar plots in **Figure 4.11** show Shannon diversity and richness associated with different bacterial communities. Average bacterial Shannon diversity and richness values were 2.64 ± 0.49 and 19.26 ± 7.20 respectively. **Table 4.4** presents p-values for Shapiro-Wilke tests for normality within the distributions of the ecological parameters for both bacteria and archaea. The majority of ecological data-sets within the current study were not normally distributed and therefore require non-parametric tests. A Kruskal-Wallis rank-sum test on the bacterial Shannon diversity and richness data showed significant differences among bacterial DGGE groups for each of the three ecological data types ($p < 0.001$ for both, $\alpha = 0.05$, **Table 4.5**). **Figure 4.11-a** shows that Shannon diversity was lower for planktonic communities than most biofilm communities, with planktonic groups A, B and C exhibiting a Shannon diversities of 1.87 ± 0.18 , 2.31 ± 0.24 and 2.57 ± 0.10 , respectively. Dunn's multiple means comparison test (**Table 4.5**) showed that none of these group diversities were significantly different from one another ($p > 0.5$, $\alpha = 0.05$). If only the biofilm communities (media and NF samples) are considered, the autumn BF-NF Group D presented the lowest Shannon diversity at 2.17 ± 0.10 ; this was significantly lower than the autumn biofilter media Group G diversity which was observed to be 3.06 ± 0.11 (Dunn's test with Bonferroni correction, $p = 0.007$, $\alpha = 0.05$). Interestingly, the autumn media and raw-NF communities within Group G had very similar diversity values, which were also very close to that of Groups E and F (winter media and NF membranes), which presented Shannon diversity group means of 3.08 ± 0.18 and 3.03 ± 0.10 , respectively. **Table S1** in **App. B** presents the z scores from all Dunn comparisons performed.

Figure 4.11-b shows bacterial community richness levels for the different DGGE groups. Richness ranged from a high of 32 phylotypes in February 2015 BF(B) sand associated biofilm and a low of 8 phylotypes for March 2015 BF(B) effluent. As with Shannon diversity, similar trends are observed using the richness parameter, however it is evident that greater variance exists in the richness data. The average richness for Groups D and G were 14.25 ± 0.96 and 25.67 ± 2.16 , respectively. Dunn's test showed that the difference in group means was significant ($p = 0.025$, $\alpha = 0.05$, **Table 4.5**). Interestingly, though the winter experiment NF membranes and media were grouped into separate clusters (E and F), they presented similar diversity and

richness results and thus were not significantly different from each other in both cases (Table 4.5).

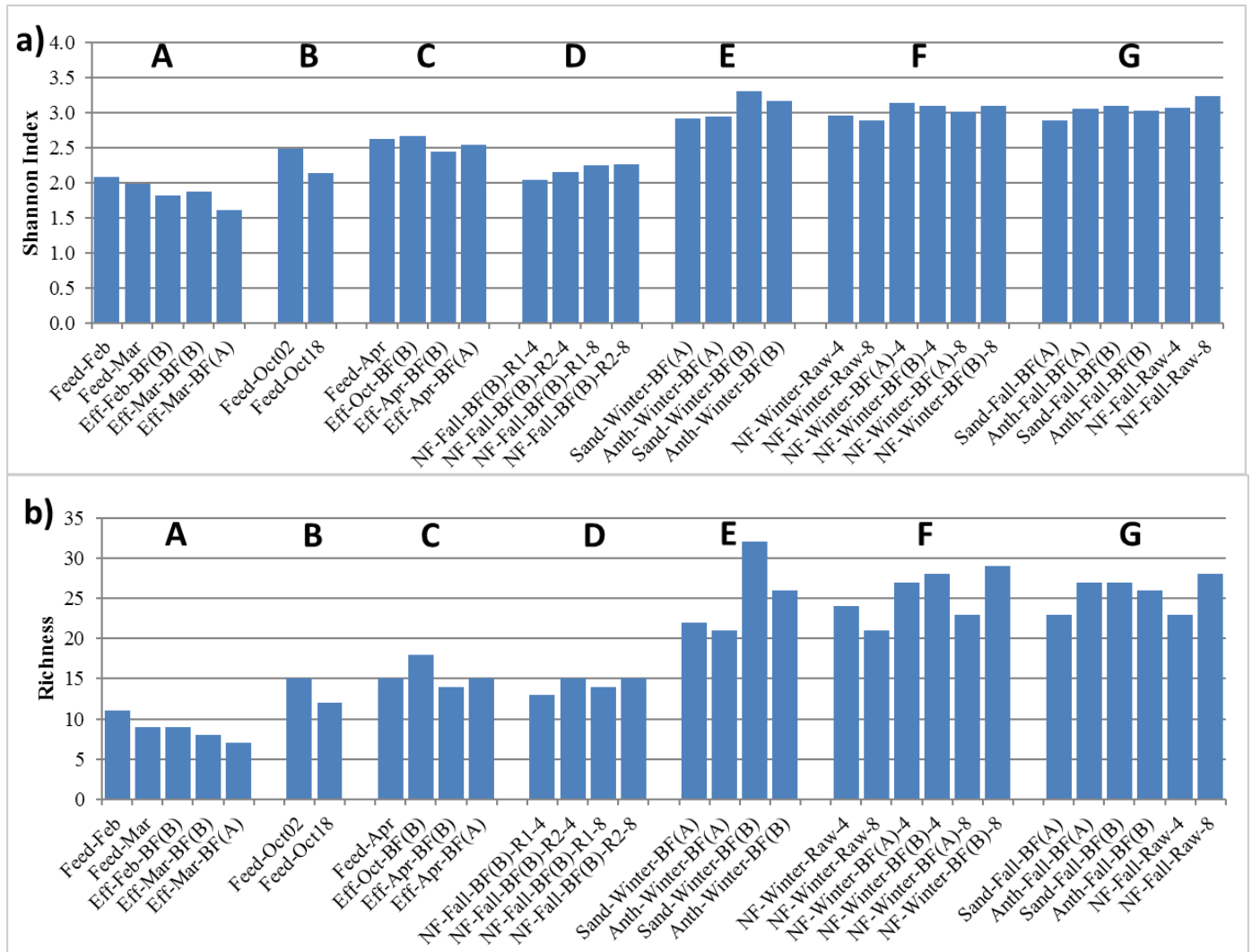


Figure 4.11: Shannon diversity (a) and species richness (b) for bacterial community DGGE profile groups derived from biofilter feed, effluent and media, and NF biofoulant layers from fall 2014 and winter/spring 2015.

Table 4.4: Shapiro-Wilke test for normality of bacterial and archaeal Shannon diversity and community richness data-sets. Asterisk (*) denotes non-normal distributions.

	Bacteria	Archaea
	p-value	p-value
Shannon	0.02*	0.4
richness	0.02*	0.4

Table 4.5: Bacterial diversity data compared between DGGE groups, and the results of Kruskal-Wallis and post-hoc Dunn's test. Asterisk denotes significant p values.

a)	Parameter	Kruskal - Wallis		p-values from Dunn's Test with Bonferroni Correction					
	Shannon Diversity	df	6		A	B	C	D	E
χ^2		27.27	B	1					
p		<0.001*	C	1	1				
			D	1	1	1			
			E	0.027*	1	1	0.324		
			F	0.013*	1	1	0.256	1	
			G	<0.001*	0.275*	0.141	0.007*	1	1

b)	Parameter	Kruskal - Wallis		p-values from Dunn's Test with Bonferroni Correction					
	Richness	df	6		A	B	C	D	E
χ^2		26.34	B	1					
p		<0.001*	C	1	1				
			D	1	1	1			
			E	0.025*	1	1	0.540		
			F	0.008*	1	0.841	0.345	1	
			G	<0.001*	0.476	0.082	0.025*	1	1

As presented in the methods section, **Table 4.1** provides a summary of MFS data for each sample as provided by ElHadidy (2015), including feed channel pressure increase, ATP ng/cm², cell count/cm², D-glucose ng/cm² and BSA ng/cm². Average archaeal Shannon diversity and richness values were 2.38 ± 1.08 and 15.44 ± 6.33 respectively. No significant difference was found between archaea and bacteria using Mann-Whitney U tests with Shannon diversity data ($p = 0.255$, $\alpha = 0.05$, **Table 4.6**), nor richness data ($p = 0.267$, $\alpha = 0.05$, **Table 4.6**).

Table 4.6: Table of p values from unpaired Mann-Whitney U comparison of total bacteria and archaea ecological parameter means. Asterisk denotes significant p values.

	p-value	w-value
Shannon	0.3	100
richness	0.3	200

Figure 4.12 shows that depth did not appear to affect archaeal diversity or richness between 20 and 60 cm within the sand media. The bar plots in **Figure 4.12** show archaeal

Shannon diversity and richness associated with the archaeal DGGE groups. A Kruskal-Wallis rank-sum test was performed on these groups and showed no significant differences between DGGE group means for Shannon diversity ($p = 0.41$, $\alpha = 0.05$) or richness ($p = 0.22$, $\alpha = 0.05$); the complete results of this analysis are presented in **Table 4.7**. Given that diversity was not shown to be significantly different between groups, post-hoc Dunn's tests were not performed.

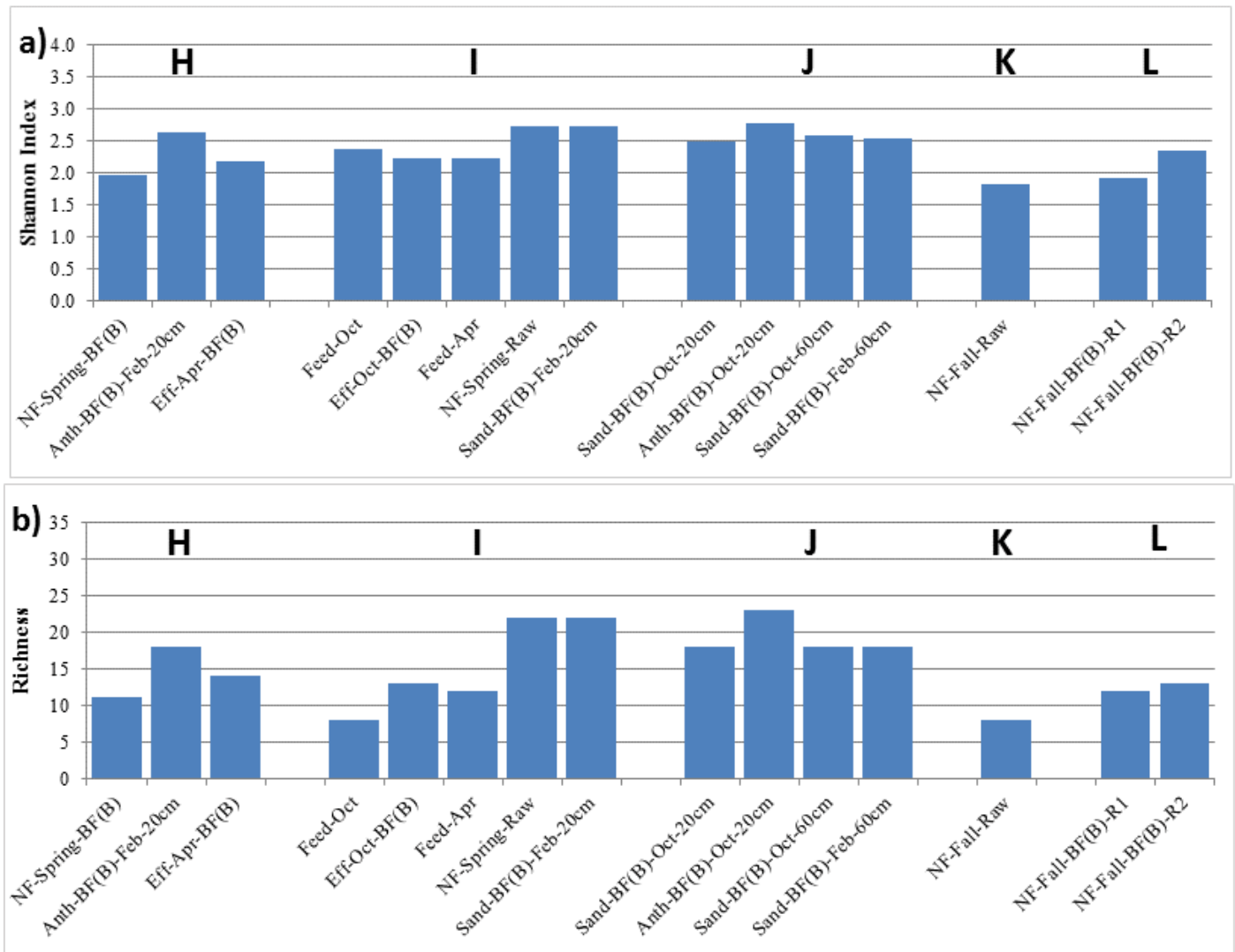


Figure 4.12: Shannon diversity (a) and ribotype richness (b) for archaeal community DGGE profile groups derived from biofilter feed, effluent and media as well as MFS biofoulant layers from fall 2014 and winter/spring 2015.

Table 4.7: Archaeal MFS diversity data was compared between DGGE groups, and the results of a Kruskal-Wallis rank-sum test are presented for each parameter. Asterisk denotes significant p values.

Parameter	Kruskal - Wallis	
Shannon Diversity	df	4
	χ^2	6.56
	p	0.16
Richness	df	4
	χ^2	6.96
	p	0.14

4.5 Discussion

Elhadidy (2016) observed that autumn MFS units which received raw water exhibited 3.6-fold faster feed channel pressure increase compared to units fed BF(B) effluent. Furthermore autumn raw water fed MFS units (raw-NF) had 5.7-fold higher biomass as ng ATP/cm², and notable differences in the protein:carbohydrate ratio of the biofoulant EPS. Total proteins (as μg BSA equivalent/cm²) for the autumn raw water MFS biofoulant were 4-fold greater than the BF(B)-NF biofoulant, whereas carbohydrates (as D-glucose equivalents) were present in raw water MFS biofoulant yet were below the limit of detection (1.5 ng/cm²) in the BF(B)-NF biofoulant. He also showed that the biofilters were able to remove readily biodegradable NOM, and this likely resulted in the decreased fouling of NF membranes. The winter MFS experiment exhibited similar trends to autumn, however biomass ATP, carbohydrates and proteins were similar or lower than the autumn experiment after a 40% longer run time. It was also noted that the rate of feed channel pressure increase were not as high during the winter experiment when compared to the autumn, and this can be related to the lower temperatures during cold ($\leq 10^\circ \text{C}$) conditions, which lowers biofilm activity (Laurent et al., 1999) and could result in slower biofilm/biofoulant development. Therefore the central question which the current research asked was if the differences in NF membrane biofoulant composition between treatments was the result of NOM removal by biofiltration alone, or if biofiltration treatment also induced a shift in the biofoulant microbiome that could in turn alter biofoulant composition. Samples were

selected for fingerprint analysis by DGGE so that comparisons could be made between planktonic and biofilm communities in warm and cold conditions, as well as between those biofilm communities present on the filter media and on the feed channel membrane surface.

4.5.1 Hierarchical Clustering of Bacterial Community Data Based on DGGE Profiles

Bacterial DGGE profile data were able to successfully partition the samples analyzed into significant groups or clusters, and inferences can be made from the structuring of the communities in **Figure 4.3**. Dendrogram results show that the sample banding patterns can be divided into two super groups composed of planktonic vs biofilm communities; this observation demonstrates the largest differences in bacterial community similarity within the DGGE data and is a common phenomenon within the literature (Lautenschlager et al., 2014; Pinto et al., 2012; Vanyacker et al., 2014; Wu et al., 2014). As discussed in Chapter 3, biofilms are established following attachment and growth of suspended bacteria indigenous to the source water and quickly adapt to the new micro-environment by differentiating phenotypically; eventually the developing biofilm creates micro-niches which select for a different set of dominant phylotypes than the feed water. These new sets of dominant phylotypes are successful in the new habitat as a result of different and more competitive metabolic capabilities (Flemming & Wingender, 2010) which results in the differences in DGGE profile superstructures between planktonic and biofilm samples. The fact that effluent communities clustered together with biofilter feed communities infers that sloughed biofilm bacteria were not dominant in the biofilter effluent, which illustrates the efficacy of the backwash regime in controlling biofilm growth and detachment cycles. Results showed that the planktonic communities divided into 3 partitions at a cut height of 0.85: Group A (February & March 2015 biofilter feed and effluent otherwise referred to as cold condition feed and effluent), Group B (October 2nd and 18th 2014 biofilter feed) and Group C (April 2015 biofilter feed and effluent, plus October 18th 2014 effluent). The fact that biofilter feed and effluent did not cluster separately is interesting, and indicates the biofilter units were not producing large amounts of detached or sloughed biofilm bacteria. It is difficult to assess if the differences in temperature or feed water quality caused the differentiation among the 3 planktonic communities; however,

the results of Ch. 3 in which a larger number of feed water samples was analyzed show that feed water ammonia and low molecular weight acids concentrations may play a role in determining both planktonic and biofilm bacterial community structures.

At a branch distance of 1.5 within **Figure 4.3**, Group D is formed and is composed of autumn BF(B)-NF membrane communities, whereas the autumn raw-NF samples clustered separately in group G. Bereschenko and colleagues (2010) noted that within RO simulator flow cells the majority of biofoulant biomass was located near feed inlets, a phenomenon also observed in the ATP levels along the axial length of the MFS units by Elhadidy (2015). In the current work, hierarchical clustering reveals that the distance from the MFS feed inlet may influence community similarity to a small degree, as the membrane communities located 4 cm from the feed inlet had higher similarity to each other than those from the 8 cm distance, which clustered with other 8 cm distant communities; however no difference in community diversity or richness could be attributed to distance from the MFS feed inlet (**Figure 4.11**).

Elhadidy (2015) showed that compared to the raw-NF membranes, the autumn BF(B)-NF samples had 83% less ng ATP/cm² and 75% less µg BSA/cm² protein, with no measurable carbohydrates. This means that the observed changes between the biofoulant layers of raw vs biofilter fed membranes must be due to differences in the respective feed. BF(B) effluent in fact presented on average 30% lower AOC concentrations compared to raw feed water. This difference is likely responsible for the changes in biofoulant composition across feed type. Since the BF-NF membrane communities presented no measurable carbohydrates and reduced proteins in the biofilm matrix, the possibility exists that the warm yet low nutrient conditions selected for unique populations which secrete different EPS and are unlike those seen on media and in raw-feed membrane units; indeed this is what the DGGE profiles show when they are plotted in the dendrogram of **Figure 4.3**. With few polysaccharides in the biofilm matrix, the biofoulant layer could be less cohesive as this fraction of EPS is a major contributor to biofilm structure (Ahimou et al., 2007). The fact that autumn raw-NF communities did not cluster with BF-NF communities and instead clustered with autumn media (Group G), supports the hypotheses that i.) feed water quality and not substrate material dictates biofilm community

structure and ii.) biofiltration without pretreatment is able to remove nutrients in a sufficient manner so as to cause downstream shifts in biofilm community structure. Of course these results are only present in the warm condition autumn experiment, indicating that the reduced biofoulant growth kinetics and the altered biofilter BOM removal performance during cold conditions impact not only the rate of biofilm development, but also the rate of community differentiation.

The dendrogram of **Figure 4.3** clearly shows the bacterial communities on the biofilter media in the winter months (labelled Group F) clustered separately from biofilter media in the autumn (Group G). A similar observation was made in Ch. 3, where winter media communities clustered separately from summer and autumn. Therefore the difference between the fall and winter experiments' media communities is likely due to changes in source water quality such as ammonia and low molecular weight acids concentrations.

Unlike the autumn data, winter NF membranes fed with biofilter effluent clustered in the same group as those fed with raw water (Group F). One factor which could contribute to this observation is temperature, in that a reduced biofilm activity could lead to slower biofilm development and differentiation. Slower biofilter bacterial enzyme activity and biofilm growth during cold conditions (Laurent et al., 1999) could result in winter bacterial biofilm formation being less mature than the faster growing autumn biofoulant, and thus had the experimental time period have been extended, the winter raw-NF communities may eventually clustered separately from the BF-NF as was observed during the autumn. Indeed if fine scale organization is considered, Group F shows that those membranes treated with longer 16 min EBCT BF(B) effluent had already begun to differentiate from the sub-cluster which contains both shorter 8 min EBCT BF(A)-NF as well as the raw-NF communities; this differentiation occurs at a height of 0.6 which is below the cut-off for partitioning performed earlier. In addition to a temperature-mediated differentiation of biofoulant growth rates between the experiments, feed biopolymers were lower in the winter and thus BF(B) BOM removal was lower in the winter experiment; therefore lowered or altered nutrient concentrations and removals at colder temperature may have also played a role in the lack of community

partitioning in NF biofilms of the winter experiment. In other words, lower nutrients in the feed during winter should not be underestimated. This would be corroborated by the findings of Ch. 3, which showed water quality to be a decisive factor in biofilm community organization and dynamics.

Overall, results show that nutrient limitation via biofiltration during mesophilic operation is sufficient to shift downstream membrane communities into very different clusters, reiterating the powerful effect biofiltration has on downstream microbial organization. Similar findings were observed in a work by Pinto and colleagues (2012), who found that sloughed bacterial phylotypes present in the effluent of dual media rapid sand filters overwhelmingly modified the distribution network microbial communities across multiple seasons. This led the authors to hypothesize that distribution network microbiomes can be controlled by managing upstream filter communities, which the results of the current study support.

The different clustering between autumn vs winter biofilm communities on biofilter media would seem to indicate that temperature has potential to drive biofilm as well as planktonic community structure; and yet, other authors have noted temperature has no effect on mature biofilter media biofilm biomass (Fonseca et al., 2001; Pharand et al., 2014) or community structure (Ivnitsky et al., 2007). Therefore, as was discussed in Chapter 3, the seasonal differences on the biofilter media can be attributed more to differences in water quality (for example, ammonia and low molecular weight acids concentrations, as well as changing compositions of all LC-OCD fractions although this is currently impossible to measure), while the development of biofilms on NF membranes would similarly be affected by water quality (i.e. upstream biofilter performance in addition to feed composition).

The same conclusions reached using hierarchical methods are readily drawn from the CA technique presented in **Figure 4.4**. Results show that the biofilter fed NF samples from the autumn experiment cluster separately from those in the winter experiment. Winter NF and winter media samples cluster close together, and although the autumn raw-NF membranes are associated with media samples, they are located closer to Group E (winter media) rather than Group G (fall media). This was also reflected by the ANOSIM boxplot results (**Figure 4.5**) which

shows the two raw-NF communities as outliers of Group G. The CA plot of **Figure 4.4** also shows Groups G and E (autumn and winter media, respectively) clustering close together relative to the other groups. This indicates that though community shifts did occur in the biofilter media between autumn and winter, these shifts were relatively small.

4.5.2 Diversity of Bacterial Groups

Measuring the diversity of biomass present in bioreactor technologies such as BF_{wp} is critical to describe observed differences in performance during acclimation and during system perturbances due to operational parameters or inhibitory compounds. As such, monitoring biofilm diversity across treatments is an important step in understanding how biological systems change under varying conditions, and can assist with the development of new process monitoring or management techniques.

With the exception of Group D (autumn BF-NF communities), all biofilm Shannon diversity levels were similar and fairly high, presenting index values around 3, which is common for bacteria of these sample types (Fish et al., 2015). Significantly lower mean Shannon diversity values were observed in Group D (autumn BF-NF) when compared against Group G (autumn media and raw-NF) as seen by the bar plot of **Figure 4.11-a** and the Dunn's test results in **Table 4.5** ($p = 0.007$, $\alpha = 0.05$). This shows that the community shift caused by upstream biofiltration also leads to a reduction in community diversity. A decrease in richness between Groups D and G was also observed in the richness data (Dunn's test, $p = 0.025$, $\alpha = 0.05$, **Table 4.5**). This means that the biofilter treated membrane biofoulant possesses less metabolic potential to deal with perturbances, which could include cleaning via hydrodynamic scouring and biocides. This observation could lead to new biofilm control strategies.

It is interesting to note that the ecological parameters for Group D (BF-NF) resembled those of the planktonic communities (Groups A – C). This raises the question as to whether there exists further similarities between planktonic communities and Group D. However the CA plot of **Figure 4.4** shows that the autumn BF-NF communities were separate from the planktonic groups within the reduced space of the ordination, meaning that although both the

planktonic groups and Group D share similar (low) diversity, their community organization is quite different.

Also of interest is the high diversity and richness values of the winter BF-NF communities of Group F. As previously mentioned, removal of certain BOM fractions by the biofilters (i.e. biopolymers, humics) was lower during the winter. Therefore it is possible that the high diversity observed in all winter NF biofilm samples, including BF-NF communities, was the result of decreased organic matter removal by the biofilters, or was affected by other changes in seasonal water quality, including the lower concentrations of biopolymers entering the biofilter during winter, as well as the increased feed ammonia concentrations (as discussed in Ch. 3).

4.5.3 Hierarchical Clustering of Archaeal Communities Based on DGGE Profiles

Though initially labelled “extremophiles” for their abundance in earth’s most hostile environments, the domain archaea are now known to be ubiquitous as they inhabit the microbiome of many freshwater (Ortiz-alvarez & Casamayor, 2016), marine, (Bano et al., 2004), soil (Maier et al., 2009) and engineered (Fish et al., 2015) environments. Archaeal contributions to many of these ecosystems remain to be fully understood, however two common functions within an environmental engineering context involve ammonia oxidation and methanogenesis (Maier et al., 2009). For example, ammonia-oxidizing archaea are capable of performing this key ecosystem function at low DO levels which would inhibit their bacterial counterparts (Liu et al., 2016).

Although archaeal amplicons were detected in every sample, the concentrations were much lower than for bacteria (> 1000 fold lower concentration) and a nested PCR protocol was required to produce sufficient amplicons for DGGE analysis. Archaeal abundance was so low that no bands were visible in agarose after the first round of PCR, yet appeared strong after the second round. Archaeal DGGE data was hierarchically clustered in the dendrogram of **Figure 4.8**, and results show that there was no differentiation between planktonic (biofilter feed and effluent) and biofilm association (media and NF) samples. Although the winter samples tended

to cluster in groups H and I, and the fall samples in groups J, K, L, not all samples followed these trends. Correspondence analysis of DGGE profile data (**Figure 4.9**) produced similar results. Additional sample data may be helpful to show trends between sample type and DGGE pattern, however the fact that planktonic, media and NF samples do not group separately, together with the low concentration of archaea compared with bacteria, suggests that in-depth analyses may not be warranted. Yet it is still instructive to note that in both the archaeal dendrogram (**Figure 4.8**) and CA plot (**Figure 4.9**), the autumn BF-NF archaeal communities appear to cluster separately from the rest of the data, which point to biofilter-mediated changes in water quality having an effect on archaeal biofoulant organization.

Given that the pilot plant used Grand River water, which notably has several wastewater treatment plants upstream of the Mannheim intake, ammonia-oxidizing archaea would likely be one of the dominant archaeal types. Sonthiphand et al. (2013) showed that within the Grand river, both ammonia-oxidizing archaea (AOA) and bacteria (AOB) were present, but as soon as total ammonia concentrations approached 0.05 mg/L and higher, AOA abundance in sediments and the water column plummeted as AOB dominated. The authors further concluded that AOB are likely the dominant ammonia-oxidizing prokaryotes in the non-headwater reaches of the Grand River. Given that ammonia levels increased dramatically during the winter MFS experiment, it would follow that archaeal abundance would similarly drop and this could help explain why seasonal patterns are one of the few trends that show promise based on the archaeal DGGE profiles, however the current dataset may not be large enough for a definitive conclusion therein.

4.5.4 Diversity of Archaeal Groups

The barplots in **Figure 4.12** show archaeal diversity and richness arranged by DGGE profile group. These diversity metrics were slightly lower for archaea than bacteria, since mean archaeal Shannon indices were 2.36 ± 0.30 whereas bacterial mean H' was 2.64 ± 0.49 ; this also indicates relatively higher variation within the archaeal dataset. A Mann-Whitney U test showed the differences in mean Shannon indices between archaea and bacteria were not

significant ($p = 0.3$, $\alpha = 0.05$, **Table 4.6**). Mean archaeal richness was 15.33 ± 4.91 which was not significantly different from the bacterial values of 19.26 ± 7.20 (Mann-Whitney U, $p = 0.3$, $\alpha = 0.05$, **Table 4.6**). Within a slow sand filter *Schmutzdecke*, Wakelin et al. (2011) recovered a total of 31 archaeal sequences via PhyloChip, which is double the observed phylotypes presented herein and could be related to the differences in filter operation; for example, several of the observed archaeal sequences were of methanogenic lineage which indicates anaerobic zones within that biofilm, while the biofilms of the current analysis are not expected to possess significant anaerobiosis. Wakelin (2011) further observed the majority of archaeal sequences to be of *Halobacteriales* origin, and concluded the primary function/metabolism of this group to be organoheterotrophic aerobes.

The similar Shannon diversity and community richness values of archaea and bacteria however requires some additional consideration, as archaeal abundances were much lower than bacterial. Findings from Neilson et al. (2014) showed multi-band DGGE profiles resulted from individual bacterial isolates, and that the same amplicon sequence could form more than one conformation in the DGGE gel matrix and thereby produce separate bands. This finding further complicates DGGE diversity analysis, as multiple rRNA operons commonly exist in bacterial genomes. Therefore the authors recommended caution be used when assessing diversity from DGGE plots, yet roundly maintained the DGGE method was highly reproducible and an excellent choice for high-throughput analysis of community structure.

A Kruskal-Wallis means comparison was performed on diversity data between archaeal DGGE groups, and no difference was detected ($p = 0.16$ and 0.14 for Shannon diversity and richness, respectively; $\alpha = 0.05$; **Table 4.7**). Shannon diversity results for archaea (2.62 ± 0.11) were slightly higher than reported by Pereira e Silva and colleagues (2012) in their analysis by DGGE of archaeal diversity of agricultural soils, which were in the range of 1.68 to 2.40. Similarly, Fish and colleagues (2015) reported lower archaeal diversity than the current study at 2.15 ± 0.67 within pilot drinking water distribution system biofilms; however their experiment lasted only 28 days which may have led to lower community diversity than the acclimated communities in the current work. However, Fish et al (2015) similarly found that that archaeal

diversity was lower than that of bacteria. It is not known if archaeal contribution to membrane biofouling is important, however the current results indicate that archaea, though ubiquitous, likely do not play major roles in drinking water membrane biofouling since their abundances are so low compared to bacteria. Likewise the low abundances in media samples indicates that the contribution of archaea to biofiltration performance is probably insignificant.

4.5.5 Presence of Fungi Within Pilot Plant Setup

Only two samples were investigated for fungi, including an August 2015 pilot plant feed water and BF(B) sand at 20 cm depth. Results show that fungi were present in both samples, proving that fungi were a part of both the summer feed and sand media communities. Little is known about the presence and function of fungal communities in the process biofilms of biofiltration and membrane filtration. Fungi are adept at degrading recalcitrant environmental compounds such as lignin (Maier et al., 2009), and therefore could be associated with humic substance degradation in biofiltration, or at least in playing a role in the co-degradation of NOM along with bacteria. Unfortunately the current work did not venture beyond this initial assessment.

Fungi were detected directly by PCR amplification without the requirement for a nested PCR procedure. The concentration of amplification product was 25 to 33% that of bacterial, which suggests that fungi may be present in river water and biofilter biofilms at high concentrations. However it is difficult to compare amplicon density across primer types and cycling programs. Only the fungal amplicons from the August 2015 feed water were analysed by DGGE, and showed multiple (9) bands confirming the presence of multiple fungal phylotypes. Fish and colleagues (2015) reported the presence of fungi in a model pilot scale drinking water distribution system; given that the pilot biofiltration units receive untreated feed water, the current finding that fungi are present within BF_{wp} is not surprising. Dominant fungi within the *Schmutzdecke* layer of a slow sand filter were determined to be *Ascomycota* and *Chytridiomycota*, which made up a total of 5 individual fungal sequences (Wakelin et al., 2011). In the current work, the DGGE results indicated gradient optimization outside of that used for

bacterial analysis (45-65%) was required for further investigation of fungal communities. Therefore further work is needed to assess drinking water biofilter and biofoulant fungal ecology in order to provide basic information regarding their presence, distribution, and potential contribution to process performance.

4.6 Conclusions

The microbial community composition of biofoulant material from polyamide thin-film composite nanofiltration membranes situated in membrane fouling simulator (MFS) units was evaluated and compared against BF_{wp} media biofilm. Bacteria and archaea were present in all sample types, however archaea abundances were roughly 3 orders of magnitude less than bacteria, and did not cluster according to sample type. Given their low abundances, archaea either do not contribute substantially to biofiltration or membrane biofouling, or if they do it was not possible to assess given the current methodology. Fungi were present in summer biofilter media biofilm as well as summer raw feed water, with an abundance of roughly a third to a quarter that of bacteria, and therefore the effects of fungi on biofilter performance merits further investigation. The current study made it clear that bacteria are the major component of biofilter and membrane foulants and that through habitat modification via biofilm formation they exert profound effects on pilot-scale water treatment processes.

Community profiling results showed that the driving factor shaping NF biofoulant community organization during warm (> 10 °C) conditions was BOM removal, rather than substrate type (sand, anthracite, polyamide membranes). For both the autumn and winter experiments, the NF biofoulant fed with biofilter effluent possessed less biomass and EPS, however only in the fall experiments was there a lower diversity and a shift in community structure between biofilter-treated membrane biofilm versus those fed raw water. The autumn bacterial NF biofilms fed with raw feed water resembled those of biofilter media, while those fed with biofilter-treated water were highly dissimilar to both biofilter media and bulk liquid communities. Therefore the improved operation of NF-MFS units pretreated by BF_{wp} compared to those fed raw source water is the result of using upstream managed biofilms to remove

biodegradable NOM for a biologically stabilized feed. This shows the use of biofilms to fight biofilms is a viable approach for enhanced management of biofouling on drinking water treatment membranes. Future efforts should include investigations into BF_{wp} as a pretreatment for RO membranes, the diversity and structure of biofilter and biofoulant fungal communities, as well as evaluate combination methods to biofouling mitigation, such as biofiltration coupled with regular chemical cleaning regimens.

Chapter 5

Research Summary & Relevance

5.1 Summary of Research

Biofiltration without pretreatment is capable of simultaneous particle, BOM and inorganic nutrient removal; when combined with other treatment options such as hybrid membrane processes, these qualities make it an ideal first stage process for drinking water treatment in both urban and remote communities. In order to improve BF_{wp} operation and monitoring within fluctuating temperature and water quality conditions, the biomass must be characterised in a way which reflects its responsive and dynamic nature. Research of this sort can provide insights for process design and can also be used to provide operational guidance information to better prepare operations staff for seasonal changes in biofilter behaviour and performance.

To this end, the first phase of this research set out to acquire a time-series dataset of physicochemical and ecological metrics relevant to biofiltration, so that a seasonal representation of biofilter microbial dynamics could be assembled. A sampling period spanning 4 seasons was designed and successfully completed on two parallel pilot scale biofilters with differing EBCT; the first four sampling campaigns (October & December 2014, January & February 2015) were obtained from archived cellular extracts and stored biomass, EPS and biofilter performance data, that was graciously provided by former Chair student Ahmed Elhadidy. The second phase of this research was to augment findings from the first phase with an investigation of downstream nanofiltration membrane biofoulant communities, fed with either biofiltered or raw water in both warm and cold (<10 °C) conditions.

The results of both phases are complimentary and provide a deeper understanding of biofilm response to both seasonal and engineered conditions; as such the conclusions of this research are as follows.

1. The BF_{wp} bacterial community structures as determined by PCR-DGGE on a seasonal sample set were highly dissimilar between feed and biofilm samples; as such the biofilm bacterial community dynamics cannot be inferred or approximated from those present in the feed.
2. Community structures were not affected by hydraulic loading rate, media type (sand versus anthracite), or bed depth within the biofilter, and therefore these factors were observed to have no effect on bacterial communities on biofilter media.
3. Within the seasonal dataset, multivariate analyses of DGGE patterns grouped samples into five major clusters, and this grouping was validated using ANOSIM ($R=0.93$, $p=0.001$). The feed water samples assembled into 2 clusters while the media biofilm assembled into 3 clusters. It is likely that changes in water chemistry including increased ammonia and LMW-acid concentrations in the feed during January-February 2015 were primarily responsible for the observed community shifts of each sample type.
4. Bacterial Shannon diversity values (H') within BF_{wp} were stable throughout the study period and were high compared to reported values. Average H' results at the intermixing zone were 3.80 ± 0.40 for sand and 3.74 ± 0.41 for anthracite media. The feed water Shannon diversity however was lower at $3.33 (\pm 0.61)$ and exhibited higher variability throughout the year. Biofilter media Shannon diversity and community richness however were not related to DOC or biopolymer removals.
5. Biomass (ATP and flow cytometric cell counts) increased linearly from commissioning in April 2014 until their peak in February 2015 at > 3000 ng ATP/cm³ for sand and > 1650 ng ATP/cm³ for anthracite. Biomass concentrations continued to increase well after steady-state DOC removals were observed in the early summer of 2014. This linear increase was likely due to ongoing maturation of the biofilter media. Changes in biomass concentrations in cold water conditions were correlated with changes in DGGE patterns.

6. Protein was shown to be the dominant fraction of EPS. Of the three EPS parameters examined (proteins, carbohydrates and eDNA), average values showed ratios of 5:3:1 and 6:3:1 existed for sand and anthracite media, respectively. EPS was highly correlated to biomass levels in both biofilters on both media types, and sand media consistently exhibited more biomass and EPS per unit filter volume than anthracite, at least in part as a result of its higher specific surface area.
7. As would be expected, DOC removal increased with EBCT, averaging $10.0 \pm 3\%$ for BF(A) and $14.3 \pm 6\%$ for BF(B), and was strongly correlated with feed temperature. Also as would be expected, the removal of the biopolymer fraction of NOM also increased with EBCT, averaging $47.6 \pm 19\%$ for BF(A) and $63.4 \pm 26\%$ for BF(B), and was strongly correlated with feed temperature.
8. EPS and biomass were negatively correlated with performance due to the high biomass recorded during cold conditions.
9. PCR-DGGE fingerprint analysis showed that NF membrane samples fed water pre-treated by BF_{wp} during warm ($> 10\text{ }^{\circ}\text{C}$) conditions possessed highly differentiated bacterial communities compared to those fed raw water, indicating the beneficial effects which BF_{wp} has on downstream nanofiltration membrane feed channel pressures are at least in part due to a drastically altered biofoulant ecology.
10. Warm condition membrane bacterial communities fed with raw water clustered in the same fingerprint group as biofilter media, which shows that in warm conditions feed type and not materials determine bacterial community organization.
11. Conversely, in cold ($<10\text{ }^{\circ}\text{C}$) conditions, all membrane biofoulant communities clustered together and were separate from both feed and media biofilm clusters. The winter membrane cluster contained membranes fed both BF_{wp} effluent and raw water, indicating that the effect which biofiltration had on downstream biofilm communities compared to raw water was minimal during these conditions.
12. Archaea were present in all sample types (feed, media, membrane) however they likely did not play a significant role in the examined processes as archaeal abundances were roughly 3 orders of magnitude less than bacteria. Archaeal community structures on NF

membranes responded similarly to bacterial communities during the warmer autumn experiment, giving rise to the hypothesis that feed water type and not substrate material affects archaeal community structure as well. No archaeal community shift was observed during the colder winter NF experiments.

5.2 Relevance to Drinking Water Industry

This research has produced several conclusions about the microbial communities of BF_{wp} systems and how their attributes relate to monitoring, performance and downstream communities.

1. BF_{wp} is a successful multifunctional unit process for the removal of particles, DOC and BOM (in terms of the biopolymers and other biodegradable components of the LC-OCD defined NOM fraction). Due in part to its stable and diverse microbiology, BF_{wp} is a strong contender for simple, robust and remote treatment systems.
2. Temperature decreases below 10 °C significantly impact biofilter DOC and biopolymer removal performance.
3. Seasonal changes in water quality precipitated a microbial community shift in the BF_{wp} media biofilm. Significant changes in microbial community structure were encountered during periods of elevated ammonia-N and LMW-acids; this water quality-mediated community shift was also associated with increased biomass and EPS production in the media biofilm. Therefore by monitoring key water quality nutrient parameters in the raw feed, operators can anticipate changes in BF_{wp} behaviour.
4. Shannon diversity and richness of biofilter media bacterial communities was stable year round and not related to process performance; however bacterial community structure was related to changes in biofilter biofilm behaviour (i.e. biomass and EPS concentration as well as ATP/cell and EPS protein content). Evidence suggests community structure may also be related to performance.
5. BF_{wp} successfully shaped the structure of downstream NF membrane communities during warm temperature, high BOM removal periods. This effect was not observed

during cold periods where lesser BOM removal occurred. This indicates that biofiltration can be used as a tool to shape and repress downstream biofilm in membranes and potentially in the distribution network when a threshold BOM is removed.

6. Archaea were ubiquitous and their biofoulant community structures were affected by biofiltration in a similar manner as the bacterial results. Due to their low abundance however they do not appear to be major contributors to the functioning of BF_{wp} using the current study's source water.

5.3 Future Research

The current work has shown it possible to control DWTP biofilms using the approach of biological BOM removal which could replace or augment more aggressive techniques such as biocide and detergent dosing as well as hydrodynamic shear. As a biological unit process, BF_{wp} is an open system since it receives raw source water inputs and with the exception of hydraulic loading rates and backwashing, is not a tightly controlled environment. This results in a highly diverse microbial community which is susceptible to seasonal variations in feed water quality, or more specifically, to variations in water chemistry and nutrients during cold conditions. These cold condition water quality changes were shown to be an important potential driver of media biofilm community structure. Therefore future BF_{wp} research should use a more sensitive ammonia-N detection method below 0.1 mg/L as well as measure its removal performance. Sequence analysis should be used to taxonomically identify significant changes in community structure. Additionally, protozoan counts should be performed in order to assess the role these organisms play in stabilizing biomass levels during and after the acclimation period, as well as the potential effects they may have during bacterial community differentiation. Finally, future efforts should include investigations into BF_{wp} as a pretreatment for RO membranes, the diversity and structure of biofilter and biofoulant fungal communities, as well as evaluate combination methods for biofouling mitigation, such as biofiltration coupled with membrane chemical cleaning regimens.

References

- Ahimou, F., Semmens, M. J., Haugstad, G., & Novak, P. J. (2007). Effect of protein, polysaccharide, and oxygen concentration profiles on biofilm cohesiveness. *Applied and Environmental Microbiology*, 73(9), 2905–2910.
- Al Ashhab, A., Gillor, O., & Herzberg, M. (2014). Biofouling of reverse-osmosis membranes under different shear rates during tertiary wastewater desalination: Microbial community composition. *Water Research*, 67, 86–95.
- Amirtharajah, A. (1993). Optimum backwashing of filters with air scour: A review. *Water Science and Technology*, 27(10), 195–211.
- Apgar, P. E. D., & Witherspoon, J. (2008). Minimization of Odors and Corrosion in Collection Systems. *Water Intelligence Online*, 7(29), 1-35.
- Azzeh, J., Taylor-Edmonds, L., & Andrews, R. C. (2015). Engineered biofiltration for ultrafiltration fouling mitigation and disinfection by-product precursor control. *Water Science and Technology: Water Supply*, 15(1), 124–133.
- Bai, Y., Liu, R., Liang, J., & Qu, J. (2013). Integrated Metagenomic and Physicochemical Analyses to Evaluate the Potential Role of Microbes in the Sand Filter of a Drinking Water Treatment System. *PLoS ONE*, 8(4).
- Bano, N., Ruffin, S., Ransom, B., Hollibaugh, T., Bano, N., Ruffin, S., Ransom, B., Hollibaugh, J. T. (2004). Phylogenetic Composition of Arctic Ocean Archaeal Assemblages and Comparison with Antarctic Assemblages. *Phylogenetic Composition of Arctic Ocean Archaeal Assemblages and Comparison with Antarctic Assemblages*, 70(2), 781–789.
- Bar-Zeev, E., Belkin, N., Liberman, B., Berman, T., & Berman-Frank, I. (2012). Rapid sand filtration pretreatment for SWRO: Microbial maturation dynamics and filtration efficiency of organic matter. *Desalination*, 286, 120–130.
- Basu, O. D., Dhawan, S., & Black, K. (2016). Applications of biofiltration in drinking water treatment - a review. *Journal of Chemical Technology and Biotechnology*, 91(3), 585–595.
- Beech, I. B., & Sunner, J. (2004). Biocorrosion: towards understanding interactions between biofilms and metals. *Current Opinion in Biotechnology*, 15(3), 181–6.
- Bereschenko, L. A., Prummel, H., Euverink, G. J. W., Stams, A. J. M., & van Loosdrecht, M. C. M. (2011). Effect of conventional chemical treatment on the microbial population in a biofouling layer of reverse osmosis systems. *Water Research*, 45(2), 405–416.
- Bereschenko, L. A., Stams, A. J. M., Euverink, G. J. W., & Van Loosdrecht, M. C. M. (2010). Biofilm formation on reverse osmosis membranes is initiated and dominated by *Sphingomonas* spp. *Applied and Environmental Microbiology*, 76(8), 2623–2632.
- Böhme, A., Risse-Buhl, U., & Küsel, K. (2009). Protists with different feeding modes change biofilm morphology. *FEMS Microbiology Ecology*, 69(2), 158–169.

- Boon, N., Pycke, B. F. G., Marzorati, M., & Hammes, F. (2011). Nutrient gradients in a granular activated carbon biofilter drives bacterial community organization and dynamics. *Water Research*, *45*(19), 6355–6361.
- Borcard, D., Gillet, F., & Legendre, P. (2011). *Numerical Ecology with R*. New York: Springer.
- Brons, J. K., & Van Elsas, J. D. (2008). Analysis of bacterial communities in soil by use of denaturing gradient gel electrophoresis and clone libraries, as influenced by different reverse primers. *Applied and Environmental Microbiology*, *74*(9), 2717–2727.
- Brouwer, H., Meesters, K., & van Groenestijn, J. (2006). Biofouling control in reverse osmosis membranes using rapid biofiltration technology. *Desalination*, *199*(1–3), 15–17.
- Cai, Y., Li, D., Liang, Y., Luo, Y., Zeng, H., & Zhang, J. (2015). Effective start-up biofiltration method for Fe, Mn, and ammonia removal and bacterial community analysis. *Bioresource Technology*, *176*, 149–55.
- Chen, F., Peldszus, S., Elhadidy, A. M., Legge, R. L., Van Dyke, M. I., & Huck, P. M. (2016). Kinetics of natural organic matter (NOM) removal during drinking water biofiltration using different NOM characterization approaches. *Water Research*, *104*, 361–370.
- Chong, T. H., Wong, F. S., & Fane, a. G. (2008). The effect of imposed flux on biofouling in reverse osmosis: Role of concentration polarisation and biofilm enhanced osmotic pressure phenomena. *Journal of Membrane Science*, *325*, 840–850.
- Claessen, D., Rozen, D. E., Kuipers, O. P., Søggaard-Andersen, L., & van Wezel, G. P. (2014). Bacterial solutions to multicellularity: a tale of biofilms, filaments and fruiting bodies. *Nature Reviews. Microbiology*, *12*(2), 115–24.
- Clarke, K. R. (1993). Nonparametric multivariate analyses of changes in community structure. *Australian Journal of Ecology*, *18*(1), 117–143.
- Cornelissen, E. R., Chasseriaud, D., Siegers, W. G., Beerendonk, E. F., & van der Kooij, D. (2010). Effect of anionic fluidized ion exchange (FIX) pre-treatment on nanofiltration (NF) membrane fouling. *Water Research*, *44*(10), 3283–3293.
- Costerton, J. (1995). Microbial biofilms. *Annual Reviews in Microbiology*, *49*(711), 45. Retrieved from <http://www.annualreviews.org/doi/pdf/10.1146/annurev.mi.49.100195.003431>
- Crump, B. C., & Hobbie, J. E. (2005). Synchrony and seasonality in bacterioplankton communities of two temperate rivers. *Limnology and Oceanography*, *50*(6), 1718–1729.
- Culotti, A., & Packman, A. I. (2015). *Pseudomonas aeruginosa* facilitates *Campylobacter jejuni* growth in biofilms under oxic flow conditions. *FEMS Microbiology Ecology*, *91*(12), 1-9
- Dreszer, C., Vrouwenvelder, J. S., Paulitsch-Fuchs, A. H., Zwijnenburg, A., Kruihof, J. C., & Flemming, H.-C. (2013). Hydraulic resistance of biofilms. *Journal of Membrane Science*, *429*, 436–447.

- Dreszer, C., Wexler, A. D., Drusová, S., Overdijk, T., Zwijnenburg, A., Flemming, H.-C., Kruithof, J.S. Vrouwenvelder, J. S. (2014). In-situ biofilm characterization in membrane systems using Optical Coherence Tomography: Formation, structure, detachment and impact of flux change. *Water Research*, 67(0), 243–254.
- Drury, B., Rosi-Marshall, E., & Kelly, J. J. (2013). Wastewater treatment effluent reduces the abundance and diversity of benthic bacterial communities in urban and suburban rivers. *Applied and Environmental Microbiology*, 79(6), 1897–1905.
- DuBois, M., Gilles, K., Hamilton, J. K., Rebers, P., & Smith, F. (1956). Colorimetric method for determination of sugars and related substances. *Analytical Chemistry*, 28(3), 350–356.
- Elhadidy, A. (2013). *Biofiltration as a Pretreatment for Biofouling control of High Pressure Nanofiltration Membranes*. University of Waterloo.
- Elhadidy, A. M. (2015). *Performance of Biological Filters for Drinking Water Treatment and Their Use for High Pressure Membrane Biofouling Control*. University of Waterloo.
- Elhadidy, A. M., Van Dyke, M. I., Chen, F., Peldszus, S., & Huck, P. M. (2017). Development and application of an improved protocol to characterize biofilms in biologically active drinking water filters. *Environmental Science Water Resource Technology*.
- Emelko, M. B., Huck, P. M., Coffey, B. M., & Smith, E. F. (2006). Effects of Media, Backwash, and Temperature on Full-Scale Biological Filtration. *Journal - American Water Works Association*, 98(12), 61–73.
- Eshed, L., Yaron, S., & Dosoretz, C. G. (2008). Effect of permeate drag force on the development of a biofouling layer in a pressure-driven membrane separation system. *Applied and Environmental Microbiology*, 74(23), 7338–7347.
- Evans, P. J., Smith, J. L., Lechevallier, M. W., Schneider, O. D., Weinrich, L., & Jjemba, P. K. (2013). *Biological Filtration Monitoring and Control Toolbox: Guidance Manual*.
- Farnham, I. M., Singh, A. K., Stetzenbach, K. J., & Johannesson, K. H. (2002). Treatment of nondetects in multivariate analysis of groundwater geochemistry data. *Chemometrics and Intelligent Laboratory Systems*, 60(1–2), 265–281.
- Feng, S., Chen, C., Wang, Q. F., Zhang, X. J., Yang, Z. Y., & Xie, S. G. (2013). Characterization of microbial communities in a granular activated carbon-sand dual media filter for drinking water treatment. *International Journal of Environmental Science and Technology*, 10(5), 917–922.
- Fish, K. E., Collins, R., Green, N. H., Sharpe, R. L., Douterelo, I., Osborn, A. M., & Boxall, J. B. (2015). Characterisation of the Physical Composition and Microbial Community Structure of Biofilms within a Model Full-Scale Drinking Water Distribution System. *Plos One*, 10(2), e0115824.
- Flemming, H.-C., Wingender, J., Szewzyk, U., Steinberg, P., Rice, S. A., & Kjelleberg, S. (2016). Biofilms: an emergent form of bacterial life. *Nature Reviews Microbiology*, 14(9), 563–575.
- Flemming, H. C. (1997). Reverse osmosis membrane biofouling. *Experimental Thermal and Fluid Science*, 14(4), 382–391.

- Flemming, H., & Wingender, J. (2010). The biofilm matrix. *Nature Reviews Microbiology*, 8(9), 623–633.
- Fonseca, A. C., Scott Summers, R., & Hernandez, M. T. (2001). Comparative measurements of microbial activity in drinking water biofilters. *Water Research*, 35(16), 3817–3824.
- Fonseca, A. C., Summers, R. S., & Greenberg, A. R. (2007). Extra-Cellular Polysaccharides, Soluble Microbial Products, and Natural Organic Matter Impact on Nanofiltration Membranes Flux Decline. *Environmental Science & Technology*, 41(7), 2491–2497.
- Fromin, N., Hamelin, J., Tarnawski, S., Roesti, D., Jourdain-Miserez, K., Forestier, N., Teyssier-Cuvette, S., Gillet, F., Aragno, M., Rossi, P. (2002). Statistical analysis of denaturing gel electrophoresis (DGE) fingerprinting patterns. *Environmental Microbiology*, 4(11), 634–643.
- García-Armisen, T., Inceoğlu, Ö., Ouattara, N. K., Anzil, A., Verbanck, M. A., Brion, N., & Servais, P. (2014). Seasonal variations and resilience of bacterial communities in a sewage polluted urban river. *PLoS ONE*, 9(3).
- Gibert, O., Lefèvre, B., Fernández, M., Bernat, X., Paraira, M., Calderer, M., & Martínez-Lladó, X. (2013). Characterising biofilm development on granular activated carbon used for drinking water production. *Water Research*, 47(3), 1101–10.
- Gomes, N. C. M., Heuer, H., Schönfeld, J., Costa, R., & Smalla, K. (2001). Bacterial diversity of the rhizosphere of maize (*Zea mays*) grown in tropical soil studied by temperature gradient gel electrophoresis. *Plant and Soil*, 232(1), 167–180.
- GRCA. (2013). Sources of Nutrients and Sediments in the Grand River Watershed. Grand River Watershed Water Management Plan. Cambridge, ON.
- Griebe, T., & Flemming, H. C. (1998). Biocide-free antifouling strategy to protect RO membranes from biofouling. *Desalination*, 118(1–3), 153–156.
- Gutman, J., Herzberg, M., & Walker, S. L. (2014). Biofouling of reverse osmosis membranes: Positively contributing factors of *Sphingomonas*. *Environmental Science and Technology*, 48(23), 13941–13950.
- Flemming, H.C., Schaule, G., Griebe, T., Schmitt, A. T. (1997). Biofouling - the Achilles heel of membrane processes. *Desalination*, (113), 215–225.
- Hallé, C. (2009). *Biofiltration in Drinking Water Treatment: Reduction of Membrane Fouling and Biodegradation of Organic Trace Contaminants*. University of Waterloo.
- Halle, C., Huck, P. M., Peldszus, S., Haberkamp, J., & Jekel, M. (2009b) Assessing the Performance of Biological Filtration As Pretreatment to Low Pressure Membranes for Drinking Water. *Environmental Science & Technology*, 43(10), 3878–3884.
- Hamilton, R. D., & Holm-Hansen, O. (1967). Adenosine Triphosphate Content of Marine Bacteria. *Limnology and Oceanography*, 12(2), 319–324.

- Hammes, F., & Egli, T. (2005). New Method for Assimilable Organic Carbon Determination Using Flow-Cytometric Enumeration and a Natural Microbial Consortium as Inoculum New Method for Assimilable Organic Carbon Determination Using Flow-Cytometric Enumeration and a Natural Microbial Con, *39*(9), 3289–3294.
- Hammes, F., Berney, M., Wang, Y., Vital, M., Köster, O., & Egli, T. (2008). Flow-cytometric total bacterial cell counts as a descriptive microbiological parameter for drinking water treatment processes. *Water Research*, *42*(1–2), 269–277.
- Hammes, F., & Egli, T. (2010). Cytometric methods for measuring bacteria in water: Advantages, pitfalls and applications. *Analytical and Bioanalytical Chemistry*, *397*(3), 1083–1095.
- Heijs, S. K., Laverman, A. M., Forney, L. J., Hardoim, P. R., & Van Elsas, J. D. (2008). Comparison of deep-sea sediment microbial communities in the Eastern Mediterranean. *FEMS Microbiology Ecology*, *64*(3), 362–377.
- Helsel, D. R. (2005). More Than Obvious: Better Methods for Interpreting Nondetect Data. *Environmental Science & Technology*, *39*(20), 419A–423A.
- Herzberg, M. (2010). Osmotic effects of biofouling in reverse osmosis (RO) processes: Physical and physiological measurements and mechanisms. *Desalination and Water Treatment*, *15*(October 2013), 287–291.
- Herzberg, M., & Elimelech, M. (2008). Physiology and genetic traits of reverse osmosis membrane biofilms: a case study with *Pseudomonas aeruginosa*. *The ISME Journal*, *2*(2), 180–194.
- Heuer, H., Krsek, M., Baker, P., Smalla, K., & Wellington, E. M. H. (1997). Analysis of actinomycete communities by specific amplification of genes encoding 16S rRNA and gel-electrophoretic separation in denaturing gradients. *Applied and Environmental Microbiology*, *63*(8), 3233–3241.
- Hilal, N., Al-Zoubi, H., Darwish, N. a., Mohammad, a. W., & Abu Arabi, M. (2004). A comprehensive review of nanofiltration membranes: Treatment, pretreatment, modelling, and atomic force microscopy. *Desalination*, *170*(3), 281–308.
- Hozalski, R. M. & Bouwer, E. J. (2001a). Non-steady state simulation of BOM removal in drinking water biofilters: model development. *Wat. Res.* *35*(1), 198-210.
- Hozalski, R. M. & Bouwer, E. J. (2001b). Non-steady state simulation of BOM removal in drinking water biofilters: applications and full-scale validation. *Wat. Res.* *35*(1), 211-223.
- Hozalski, R. M., Goel, S., & Bouwer, E. J. (1995). TOC removal in biological filters. *Journal / American Water Works Association*, *87*(12), 40–54.
- Hu, J. Y., Song, L. F., Ong, S. L., Phua, E. T., & Ng, W. J. (2005). Biofiltration pretreatment for reverse osmosis (RO) membrane in a water reclamation system. *Chemosphere*, *59*(1), 127–133.
- Huber, S. a., Balz, A., Abert, M., & Pronk, W. (2011). Characterisation of aquatic humic and non-humic matter with size-exclusion chromatography - organic carbon detection - organic nitrogen detection (LC-OCD-OND). *Water Research*, *45*(2), 879–885.

- Huck, P.M., Peldszus, S., Anderson, W.B., Chen, F., Elhadidy, A.M., Legge, R.L., Siembida-Lösch, B., Van Dyke, M.I., Wilson, B. & Walton, T. (2015). Biofiltration With and Without Pre-treatment - Are There Differences? In IWA Specialized Conference of Biofilms in Drinking Water Systems.
- Huck, P. M., Peldszus, S., Hallé, C., Ruiz, H., Jin, X., Van Dyke, M., Amy, G., Uhl, M., Theodoulou, M., Mosqueda-Jimenez, D. B. (2011). Pilot scale evaluation of biofiltration as an innovative pre-treatment for ultrafiltration membranes for drinking water treatment. *Water Science & Technology: Water Supply*, 11(1), 23.
- Huck, P. M., Siembida-Losch, B. K., & Sozanski, M. M. (2013). Biological filtration for diverse applications: towards the development of a unified conceptual design approach.
- Huck, P. M., & Sozański, M. M. (2008). Biological filtration for membrane pre-treatment and other applications: Towards the development of a practically-oriented performance parameter. *Journal of Water Supply: Research and Technology - AQUA*, 57(4), 203–224.
- Huck, P., & Sozański, M. (2011). 3.16 – Chemical Basis for Water Technology. *Treatise on Water Science*, 429–469.
- Huston, C., & Juarez-Colunga, E. (2009). Guidelines for computing summary statistics for data-sets containing non-detects, 177. Retrieved from http://bvcentre.ca/files/research_reports/08-03GuidanceDocument.pdf
- Ivnitsky, H., Katz, I., Minz, D., Volvovic, G., Shimoni, E., Kesselman, E., Semiat, R., Dosoretz, C. G. (2007). Bacterial community composition and structure of biofilms developing on nanofiltration membranes applied to wastewater treatment. *Water Research*, 41(17), 3924–35.
- Jeong, S., Bae, H., Naidu, G., Jeong, D., Lee, S., & Vigneswaran, S. (2013). Bacterial community structure in a biofilter used as a pretreatment for seawater desalination. *Ecological Engineering*, 60, 370–381.
- Jeong, S., Vollprecht, R., Cho, K., Leiknes, T. O., Vigneswaran, S., Bae, H., & Lee, S. (2016). Advanced organic and biological analysis of dual media filtration used as a pretreatment in a full-scale seawater desalination plant. *Desalination*, 385, 83–92.
- Juhna, T., & Melin, E. (2006). Ozonation and biofiltration In Water Treatment. *Techneau*, 5(1), 80.
- Kaarela, O. E., Härkki, H., Palmroth, M. R. T., & Tuhkanen, T. (2014). Bacterial diversity and active biomass in full-scale granular activated carbon filters operated at low water temperatures. *Environmental Technology*, (August 2014), 1–23.
- Kim, T. G., Yun, J., Hong, S.-H., & Cho, K.-S. (2014). Effects of water temperature and backwashing on bacterial population and community in a biological activated carbon process at a water treatment plant. *Applied Microbiology and Biotechnology*, 98, 1417–27.
- Kohler, E., Villiger, J., Posch, T., Derlon, N., Shabarova, T., Morgenroth, E., Pernthaler, J., Blom, J. F. (2014). Biodegradation of microcystins during gravity-driven membrane (GDM) ultrafiltration. *PLoS ONE*, 9(11).

- LaPara, T. M., Wilkinson, K. H., Strait, J. M., Hozalski, R. M., Sadowksy, M. J., & Hamilton, M. J. (2015). The bacterial communities of full-scale biologically active, granular activated carbon filters are stable and diverse and potentially contain novel ammonia-oxidizing microorganisms. *Applied and Environmental Microbiology*, *81*(19), 6864–6872.
- Lauderdale, C., Chadik, P., Kirisits, M. J., & Brown, A. J. (2012). Engineered biofiltration: Enhanced biofilter performance through nutrient and peroxide addition. *Journal - American Water Works Association*, *104*(5), 73–74.
- Laurent, P., Prévost, M., Cigana, J., Niquette, P., & Servais, P. (1999). Biodegradable organic matter removal in biological filters: Evaluation of the CHABROL model. *Water Research*, *33*(6), 1387–1398.
- Lautenschlager, K., Hwang, C., Ling, F., Liu, W.-T., Boon, N., Köster, O., Egli, T., Hammes, F. (2014). Abundance and composition of indigenous bacterial communities in a multi-step biofiltration-based drinking water treatment plant. *Water Research*, *62*, 40–52.
- Lawrence, J. R., Chenier, M. R., Roy, R., Beaumier, D., Fortin, N., Swerhone, G. D. W., Neu, T.R., Greer, C. (2004). Microscale and Molecular Assessment of Impacts of Nickel, Nutrients, and Oxygen Level on Structure and Function of River Biofilm Communities. *Applied and Environmental Microbiology*, *70*(7), 4326–4339.
- LeChevallier, M. W., Schulz, W., & Lee, R. G. (1991). Bacterial nutrients in drinking water. *Applied and Environmental Microbiology*, *57*(3), 857–862.
- Legendre, P., & Legendre, L. (1988). Numerical Ecology, Volume 24. (*Developments in Environmental Modelling*), *24*, 870.
- Li, Y., Jiao, J., Wang, Y., Yang, W., Meng, C., Li, B., ... Wu, J. (2015). Characteristics of nitrogen loading and its influencing factors in several typical agricultural watersheds of subtropical China. *Environmental Science and Pollution Research*, *22*(3), 1831–1840.
- Liao, X., Chen, C., Wang, Z., Wan, R., Chang, C.-H., Zhang, X., & Xie, S. (2013a). Changes of biomass and bacterial communities in biological activated carbon filters for drinking water treatment. *Process Biochemistry*, *48*(2), 312–316.
- Liao, X., Chen, C., Wang, Z., Wan, R., Chang, C.-H., Zhang, X., & Xie, S. (2013b). Pyrosequencing analysis of bacterial communities in drinking water biofilters receiving influents of different types. *Process Biochemistry*, *48*(4), 703–707.
- Liao, X., Chen, C., Zhang, J., Dai, Y., Zhang, X., & Xie, S. (2015). Operational performance, biomass and microbial community structure: impacts of backwashing on drinking water biofilter. *Environmental Science and Pollution Research International*, *22*(1), 546–554.
- Lim, S., Kim, S., Yeon, K. M., Sang, B. I., Chun, J., & Lee, C. H. (2012). Correlation between microbial community structure and biofouling in a laboratory scale membrane bioreactor with synthetic wastewater. *Desalination*, *287*, 209–215.
- Liu, Y., Ngo, H. H., Guo, W., Peng, L., Pan, Y., Guo, J., Chen, X., Ni, B. J. (2016). Autotrophic nitrogen removal in membrane-aerated biofilms: Archaeal ammonia oxidation versus bacterial ammonia oxidation. *Chemical Engineering Journal*, *302*, 535–544.

- Lorenz, T. C. (2012). Polymerase Chain Reaction: Basic Protocol Plus Troubleshooting and Optimization Strategies. *Journal of Visualized Experiments*, (63), 1–15.
- Madoni, P., Davoli, D., Cavagnoli, G., Cucchi, A., Pedroni, M., & Rossi, F. (2000). Microfauna and filamentous microflora in biological filters for tap water production. *Water Research*, 34(14), 3561–3572.
- Magic-Knezev, A., & van der Kooij, D. (2004). Optimisation and significance of ATP analysis for measuring active biomass in granular activated carbon filters used in water treatment. *Water Research*, 38(18), 3971–3979.
- Mauclair, L., Schürmann, A., Thullner, M., Gammeter, S., & Zeyer, J. (2004). Sand filtration in a water treatment plant: Biological parameters responsible for clogging. *Journal of Water Supply: Research and Technology - AQUA*, 53(2), 93–108.
- McCann, K. S. (2000). The diversity-stability debate. *Nature*, 405(May), 228–233.
- Metsämuuronen, S., Sillanpää, M., Bhatnagar, A., & Mänttari, M. (2014). Natural Organic Matter Removal from Drinking Water by Membrane Technology. *Separation & Purification Reviews*, 43(1), 1–61.
- Mittelman, M. W., & Jones, A. D. G. (2016). A Pure Life: The Microbial Ecology of High Purity Industrial Waters. *Microbial Ecology*, 1–10.
- Moll, D. M., & Summers, R. S. (1999). Assessment of Drinking Water Filter Microbial Communities Using Taxonomic and Metabolic Profiles. *Water Science & Technology*, 39(7), 83–89.
- Moll, D. M., Summers, R. S., & Breen, A. (1998). Microbial Characterization of Biological Filters Used for Drinking Water Treatment. *Applied and Environmental Microbiology*, 64(7), 2755–2759.
- Morris, E. K., Caruso, T., Buscot, F., Fischer, M., Hancock, C., Maier, T. S., Meiners, T., Müller, C., Obermaier, E., Prati, D., Socher, S. A., Sonnemann, I., Waschke, N., Wubet, T., Wurst, S., Rillig, M. C. (2014). Choosing and using diversity indices: Insights for ecological applications from the German Biodiversity Exploratories. *Ecology and Evolution*, 4(18), 3514–3524.
- Mosqueda-Jimenez, D. B., & Huck, P. M. (2009). Effect of biofiltration as pretreatment on the fouling of nanofiltration membranes. *Desalination*, 245(1–3), 60–72.
- Muyzer, G., & Smalla, K. (1998). Application of denaturing gradient gel electrophoresis (DGGE) and temperature gradient gel electrophoresis (TGGE) in microbial ecology. *Antonie van Leeuwenhoek, International Journal of General and Molecular Microbiology*, 73, 127–141.
- Neilson, J. W., Jordan, F. L., & Maier, R. M. (2014). NIH Public Access. *Journal of Microbiological Methods*, 92(3), 256–263.
- Newton, R. J., Jones, S. E., Eiler, A., McMahon, K. D., & Bertilsson, S. (2011). *A guide to the natural history of freshwater lake bacteria. Microbiology and molecular biology reviews : MMBR* (Vol. 75).
- Nguyen, T., Roddick, F. A., & Fan, L. (2012). Biofouling of water treatment membranes: A review of the underlying causes, monitoring techniques and control measures. *Membranes*, 2(4), 804–840.

- Niquette, P., Prevost, M., Maclean, R., Thibault, D., Coallier, J., Desjardins, R., Lafrance, P. (1998). Backwashing first-stage sand-BAC filters. *Journal - American Water Works Association*, 90(1), 86–97.
- Orgiazzi, A., Lumini, E., Nilsson, R. H., Girlanda, M., Vizzini, A., Bonfante, P., & Bianciotto, V. (2012). Unravelling Soil Fungal Communities from Different Mediterranean Land-Use Backgrounds. *PLoS ONE*, 7(4): e34847.
- Ortiz-alvarez, R., & Casamayor, E. O. (2016). High occurrence of Pacearchaeota and Woesearchaeota (Archaea superphylum DPANN) in the surface waters of oligotrophic high-altitude lakes. *Environmental Microbiology Reports*, 8(2), 210–217.
- Palmer, R. J., & White, D. C. (1997). Developmental biology of biofilms: implications for treatment and control. *Trends in Microbiology*, 5(11), 435–440.
- Pasmore, M., Todd, P., Smith, S., Baker, D., Silverstein, J. A., Coons, D., & Bowman, C. N. (2001). Effects of ultrafiltration membrane surface properties on *Pseudomonas aeruginosa* biofilm initiation for the purpose of reducing biofouling. *Journal of Membrane Science*, 194(1), 15–32.
- Paul, A., Dziallas, C., Zwirnmann, E., Gjessing, E. T., & Grossart, H. P. (2012). UV irradiation of natural organic matter (NOM): Impact on organic carbon and bacteria. *Aquatic Sciences*, 74(3), 443–454.
- Peldszus, S., Benecke, J., Jekel, M., & Huck, P. M. (2012). Direct biofiltration pretreatment for fouling control of ultrafiltration membranes. *Journal - American Water Works Association*, 104(7), 45–46.
- Pereira e Silva, M. C., Dias, A. C. F., van Elsas, J. D., & Salles, J. F. (2012). Spatial and Temporal Variation of Archaeal, Bacterial and Fungal Communities in Agricultural Soils. *PLoS ONE*, 7(12), e51554.
- Persson, F., Heinicke, G., Uhl, W., Hedberg, T., & Hermansson, M. (2006). Performance of direct biofiltration of surface water for reduction of biodegradable organic matter and biofilm formation potential. *Environmental Technology*, 27(9), 1037–45.
- Pharand, L., Van Dyke, M. I., Anderson, W. B., Yohannes, Y., & Huck, P. M. (2015). Full-scale ozone – biofiltration: Seasonally related effects on NOM removal. *Journal - American Water Works Association*, 107(8), 425–435.
- Pharand, L., Van Dyke, M. I., Anderson, W. B., & Huck, P. M. (2014). Assessment of biomass in drinking water Biofilters by Adenosine triphosphate. *Journal - American Water Works Association*, 106(10), 433–444.
- Pinto, A. J., Xi, C., & Raskin, L. (2012). Bacterial community structure in the drinking water microbiome is governed by filtration processes. *Environmental Science and Technology*, 46(16), 8851–8859.
- Rahman, I. (2013). *Direct Biofiltration and Nutrient (Phosphorous) Enhancement for Polymeric Ultrafiltration Membrane Fouling Control*. University of Waterloo.
- Rahman, I., Ndiongue, S., Jin, X., Van Dyke, M. I., Anderson, W. B., & Huck, P. M. (2014). Fouling of low-pressure membranes during drinking water treatment: effect of NOM components and biofiltration pretreatment. *Water Science & Technology: Water Supply*, 14(3), 453–460.

- Read, S., Marzorati, M., Guimarães, B. C. M., & Boon, N. (2011). Microbial Resource Management revisited: Successful parameters and new concepts. *Applied Microbiology and Biotechnology*, *90*(3), 861–871.
- Reisner, A., Haagen, J. a. J., Schembri, M. a., Zechner, E. L., & Molin, S. (2003). Development and maturation of *Escherichia coli* K-12 biofilms. *Molecular Microbiology*, *48*(4), 933–946.
- Samarajeewa, A. D., Hammad, A., Masson, L., Khan, I. U. H., Scroggins, R., & Beaudette, L. A. (2015). Comparative assessment of next-generation sequencing, denaturing gradient gel electrophoresis, clonal restriction fragment length polymorphism and cloning-sequencing as methods for characterizing commercial microbial consortia. *Journal of Microbiological Methods*, *108*, 103–111.
- Sekiguchi, H., Watanabe, M., Nakahara, T., & Xu, B. (2002). Succession of Bacterial Community Structure along the Changjiang River Determined by Denaturing Gradient Gel Electrophoresis and Clone Library Analysis Succession of Bacterial Community Structure along the Changjiang River Determined by Denaturing Gradient. *Applied and Environmental Microbiology*, *68*(10), 5142–5150.
- Servais, P., Billen, G., Bablon, G. P., & Ven, C. (1991). Microbial Activity in GAC Filters at the Choisy-le-Roi Treatment Plant. *Journal - American Water Works Association*, *83*(2), 62–68.
- Shim, Y., Lee, H.-J., Lee, S., Moon, S.-H., & Cho, J. (2002). Effects of Natural Organic Matter and Ionic Species on Membrane Surface Charge. *Environmental Science and Technology*, *36*(17), 3864–3871.
- Shon, H. K., Phunsho, S., Chaudhary, D. S., Vigneswaran, S., & Cho, J. (2013). Nanofiltration for water and wastewater treatment – a mini review. *Drinking Water Engineering and Science*, (6), 47–53.
- Siembida-Lösch, B., Anderson, W. B., Wang, Y. (Michael), Bonsteel, J., & Huck, P. M. (2015). Effect of ozone on biopolymers in biofiltration and ultrafiltration processes. *Water Research*, *70*, 224–234.
- Simões, M., Simões, L. C., & Vieira, M. J. (2010). A review of current and emergent biofilm control strategies. *LWT - Food Science and Technology*, *43*(4), 573–583.
- Smith, M. W., Allen, L. Z., Allen, A. E., Herfort, L., & Simon, H. M. (2013). Contrasting genomic properties of free-living and particle-attached microbial assemblages within a coastal ecosystem. *Frontiers in Microbiology*, *4*(MAY), 1–20.
- Sonthiphand, P., Cejudo, E., Schiff, S. L., & Neufeld, J. D. (2013). Wastewater effluent impacts ammonia-oxidizing prokaryotes of the Grand River, Canada. *Applied and Environmental Microbiology*, *79*(23), 7454–7465.
- Stewart, P. S. (2003). Diffusion in Biofilms. *Journal of Bacteriology*, *185*(5), 1485–1491.
- Su, X., Sun, F., Wang, Y., Hashmi, M. Z., Guo, L., Ding, L., & Shen, C. (2016). Identification, characterization and molecular analysis of the viable but nonculturable *Rhodococcus biphenylivorans*. *Scientific Reports*, *5*(1), 1–12.
- Tariq, M., Bruijs, C., Kok, J., & Krom, B. P. (2012). Link between culture zeta potential homogeneity and Ebp in *Enterococcus faecalis*. *Applied and Environmental Microbiology*, *78*(7), 2282–2288.

- Tatari, K., Smets, B. F., & Albrechtsen, H. J. (2016). Depth investigation of rapid sand filters for drinking water production reveals strong stratification in nitrification biokinetic behavior. *Water Research*, *101*, 402–410.
- Thorsen, T., & Flogstad, H. (2006). Nanofiltration in drinking water treatment Literature Review Nanofiltration in drinking water treatment Literature Review. *Techneau*, *11*.
- Toole, G. O., Kaplan, H. B., & Kolter, R. (2000). Biofilm Formation Microbial Development. *Annual Review of Microbiology*, *54*, 49–79.
- Uhl, W. (2008). Biofiltration processes for organic matter removal. *Biotechnology Set*, 458–475.
- Urfer, D., & Huck, P. M. (2001). Measurement of biomass activity in drinking water biofilters using a respirometric method. *Water Research*, *35*(6), 1469–1477.
- Urfer, D., Huck, P. M., Booth, S. D. J., & Coffey, B. M. (1997). Biological filtration for BOM and particle removal: a critical review. *Journal - American Water Works Association*, *89*(12), 83–98.
- USEPA. (2000). *Guidance for Data Quality Assessment - Practical Methods for Data Analysis. Report QA/G-9/QA00 Update*.
- Van Dyke, M. I., & McCarthy, J. (2002). Molecular biological detection and characterization of Clostridium populations in municipal landfill sites. *Applied and Environmental Microbiology*, *68*(4), 2049–2053.
- Vanysacker, L., Boerjan, B., Declerck, P., & Vankelecom, I. F. J. (2014). Biofouling ecology as a means to better understand membrane biofouling. *Applied Microbiology and Biotechnology*, *98*(19), 8047–72.
- Vaz-Moreira, I., Egas, C., Nunes, O. C., & Manaia, C. M. (2013). Bacterial diversity from the source to the tap: A comparative study based on 16S rRNA gene-DGGE and culture-dependent methods. *FEMS Microbiology Ecology*, *83*(2), 361–374.
- Velten, S., Boller, M., Köster, O., Helbing, J., Weilenmann, H.-U., & Hammes, F. (2011). Development of biomass in a drinking water granular active carbon (GAC) filter. *Water Research*, *45*(19), 6347–54.
- von Gunten, U. (2003). Ozonation of drinking water: part I. Oxidation kinetics and product formation. *Water Research*, *37*(7), 1443–67.
- Vrouwenvelder, J. S., Bakker, S. M., Cauchard, M., Le Grand, R., Apacandie, M., Idrissi, M., Lagrave, S., Wessels, L. P., van Paassen, J. A. M., Kruithof, J. C., van Loosdrecht, M. C. M. (2007). The membrane fouling simulator: A suitable tool for prediction and characterisation of membrane fouling. *Water Science and Technology*, *55*(8–9), 197–205.
- Vrouwenvelder, J. S., Graf von der Schulenburg, D. A., Kruithof, J. C., Johns, M. L., & van Loosdrecht, M. C. M. (2009). Biofouling of spiral-wound nanofiltration and reverse osmosis membranes: A feed spacer problem. *Water Research*, *43*(3), 583–594.

- Wakelin, S., Page, D., Dillon, P., Pavelic, P., Abell, G. C. J., Gregg, A. L., Brodie, E., DeSantis, T. Z., Goldfarb, K. C., Anderson, G. (2011). Microbial community structure of a slow sand filter schmutzdecke: A phylogenetic snapshot based on rRNA sequence analysis. *Water Science and Technology: Water Supply*, 11(4), 426–436.
- Wang, Y., Liu, L., Chen, H., & Yang, J. (2015). Spatiotemporal dynamics and determinants of planktonic bacterial and microeukaryotic communities in a Chinese subtropical river. *Applied Microbiology and Biotechnology*, 99(21), 9255–9266.
- Weng, S., Miller, S., & Suthaker, S. (2015). Biological Pretreatment Extends Membrane Service Life. *Opflow - American Water Works Association*, 41(6), 24–26.
- White, C. P., DeBry, R. W., & Lytle, D. a. (2012). Microbial survey of a full-scale, biologically active filter for treatment of drinking water. *Applied and Environmental Microbiology*, 78(17), 6390–6394.
- Wilson, B. (2015). *Impact of Biofilter Backwashing on the Biofiltration / Ultrafiltration Process* by. University of Waterloo.
- Wittebolle, L., Marzorati, M., Clement, L., Balloi, A., Daffonchio, D., Heylen, K., ... Boon, N. (2009). Initial community evenness favours functionality under selective stress. *Nature*, 458(2), 623–626.
- Wood, T. L., Guha, R., Tang, L., Geitner, M., Kumar, M., & Wood, T. K. (2016). Living biofouling-resistant membranes as a model for the beneficial use of engineered biofilms. *Proceedings of the National Academy of Sciences*, 201521731.
- Wu, T., Fu, G. Y., Sabula, M., & Brown, T. (2014). Bacterial community in the biofilm of granular activated carbon (GAC) PreBiofilter in bench-scale pilot plants for surface water pretreatment. *World Journal of Microbiology and Biotechnology*, 30(12), 3251–3262.
- Xia, N., Xia, X., Liu, T., Hu, L., Zhu, B., Zhang, X., & Dong, J. (2014). Characteristics of bacterial community in the water and surface sediment of the Yellow River, China, the largest turbid river in the world. *Journal of Soils and Sediments*, 14(11), 1894–1904.
- Xiang, H., Lu, X., Yin, L., Yang, F., Zhu, G., & Liu, W. (2013). Microbial community characterization, activity analysis and purifying efficiency in a biofilter process. *Journal of Environmental Sciences (China)*, 25(4), 677–687.
- Yang, B. M., Liu, J. K., Chien, C. C., Surampalli, R. Y., & Kao, C. M. (2011). Variations in AOC and microbial diversity in an advanced water treatment plant. *Journal of Hydrology*, 409(1–2), 225–235.
- Yu, X., Shi, X., Wei, B., Ye, L., & Zhang, S. (2009). PLFA profiles of drinking water biofilters with different acetate and glucose loadings. *Ecotoxicology*, 18(6), 700–706.
- Yu, Zhang, & Wang. (2003). Improving Removal Efficiency of Organic Matters by Adding Phosphorus in Drinking Water Biofiltration Treatment. *Biomedical and Environmental Science*, 39, 29–39.
- Zearley, T. L., & Summers, R. S. (2012). Removal of trace organic micropollutants by drinking water biological filters. *Environmental Science & Technology*, 46(17), 9412–9.

- Zeng, D.-N., Fan, Z.-Y., Chi, L., Wang, X., Qu, W.-D., & Quan, Z.-X. (2013). Analysis of the bacterial communities associated with different drinking water treatment processes. *World Journal of Microbiology and Biotechnology*, *29*, 1573–1584.
- Zhang, K., Choi, H., Dionysiou, D. D., Sorial, G. a, & Oerther, D. B. (2006). Identifying pioneer bacterial species responsible for biofouling membrane bioreactors. *Environmental Microbiology*, *8*(3), 433–40.
- Zhao, F., Wang, Y., An, H., Hao, Y., Hu, X., & Liao, X. (2016). New Insights into the Formation of Viable but Nonculturable Escherichia coli O157 : H7 Induced by High-Pressure CO₂. *mBio*, *7*(4), 1–11.
- Zularisam, a. W., Ismail, a. F., & Salim, R. (2006). Behaviours of natural organic matter in membrane filtration for surface water treatment - a review. *Desalination*, *194*(1–3), 211–231.

Appendix A

Supplementary Information for Chapter 3

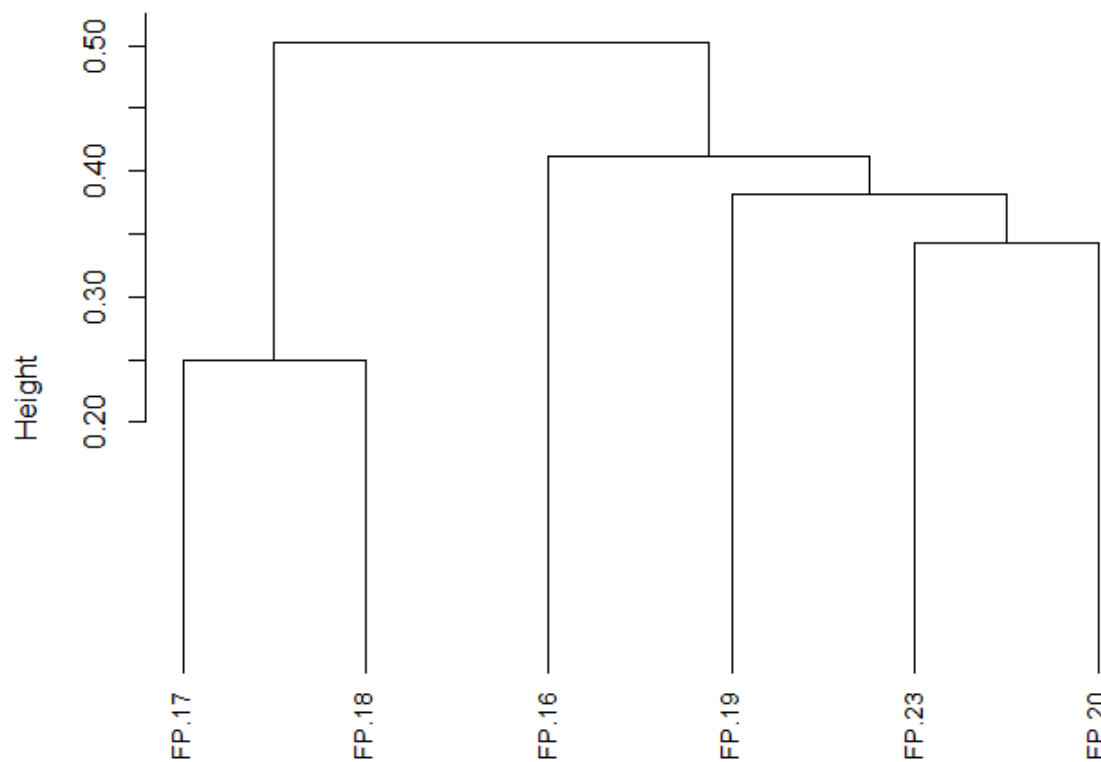


Figure S1: Dendrogram comparing DGGE banding patterns for inter-gel marker controls. Gel FP.17 contained media samples from Sep, Oct and Nov 2015, FP.18 contained Jan and Feb 2015, FP.16 contained Dec 2014, FP.19 contained Jul and May 2015, FP.20 contained feed water samples, FP.22 contained media samples from June and Aug 2015, FP.23 contained feed water samples, and FP.24 contained media and feed water samples from Oct 2014.

Table S1: Averages for several biofilm and performance parameters according to DGGE profile Groups.

Sample Type	DGGE Group	Group Means												
		ng ATP/cm ³	Cells/cm ³	fg ATP/cell	µg D-gluc/cm ³	µg BSA/cm ³	CH:PN	BF	DOC % R	BP % R	HS % R	BB % R	LMW-Acids % R	LMW-Neutrals % R
Water	A	-	-		-	-								
Water	B	-	-		-	-								
Sand	C	3065	1.02E+09	3.5	113.3	191.4	0.59	BF(B)	6.76	32.77	1.4	-1.0	-2.5	13.7
Anth	C	1710	6.7E+08	3.2	69.8	116.6	0.61	BF(A)	5.96	25.05	-0.2	8.3	-2.5	9.3
Sand	D	1562	1.38E+08	27.1	49.3	97.3	0.55	BF(B)	15.30	56.70	9.2	7.1	25.7	24.8
Anth	D	580	9.26E+07	6.3	31.2	72.7	0.43	BF(A)	10.20	38.20	5.6	7.3	22.6	15.8
Sand	E	1770	3.97E+08	5.6	42.7	88.5	0.46	BF(B)	16.01	71.95	10.6	17.0	7.8	22.7
Anth	E	734	2.42E+08	3.7	22.8	50.8	0.44	BF(A)	10.96	53.71	6.8	4.7	13.3	22.0
Sand	D/E	1782	3.68E+08	8.0	43.5	89.4	0.47	BF(B)	15.93	70.25	10.42	15.87	9.79	22.90
Anth	D/E	709	2.26E+08	4.0	23.7	50.8	0.42	BF(A)	10.88	51.98	6.65	5.00	14.34	21.28

Table S2: Pearson correlation analysis comparing BF(A) sand biofilm and BF(A) performance parameters examined in the study. Media samples were taken from 20 cm bed depth. Ammonia data below detection limit was treated as DL/2. Blue, yellow, orange and red cell shading indicate correlation strengths of positive or negative 0.6, 0.7, 0.8 and 0.9 respectively.

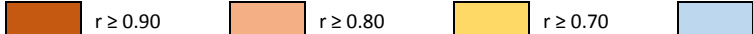
	HMW.OC	IMW.OC	LMW.OC	Diversity	Richness	Cell Count	ATP	ATP/Cell	Carbohydrates	Proteins	CH:PN	% R DOC	% R BP	DOC	NO3	NH3	Ortho-P	pH	Total Iron	Conductivity	Hardness	Temperature	Turbidity	
HMW.OC	1																							
IMW.OC	0.74	1																						
LMW.OC	0.82	0.94	1																					
Diversity	0.47	0.14	0.25	1																				
Richness	0.34	0.01	0.14	0.98	1																			
Cell Count	0.56	0.88	0.70	-0.08	-0.20	1																		
ATP	0.42	0.85	0.69	0.01	-0.07	0.91	1																	
ATP/Cell	-0.81	-0.65	-0.64	-0.71	-0.55	-0.50	-0.41	1																
Carbohydrates	0.42	0.87	0.78	-0.07	-0.13	0.78	0.83	-0.32	1															
Proteins	0.56	0.94	0.86	0.00	-0.09	0.84	0.84	-0.47	0.96	1														
CH:PN	-0.06	0.40	0.34	-0.42	-0.37	0.41	0.56	0.27	0.75	0.55	1													
% R DOC	-0.19	-0.75	-0.65	0.25	0.30	-0.68	-0.67	0.11	-0.88	-0.84	-0.69	1												
% R BP	-0.19	-0.67	-0.55	0.01	0.03	-0.72	-0.86	0.23	-0.88	-0.82	-0.73	0.74	1											
DOC	0.01	-0.44	-0.20	0.36	0.43	-0.69	-0.70	0.15	-0.56	-0.53	-0.47	0.41	0.62	1										
NO3	0.57	0.73	0.78	0.09	0.03	0.55	0.64	-0.41	0.68	0.79	0.32	-0.44	-0.61	-0.32	1									
NH3	0.29	0.80	0.65	-0.23	-0.30	0.75	0.78	-0.25	0.85	0.84	0.58	-0.75	-0.65	-0.70	0.60	1								
Ortho-P	-0.07	0.02	0.17	-0.28	-0.18	-0.06	0.02	0.45	0.22	0.19	0.41	-0.33	-0.28	0.31	0.35	-0.08	1							
pH	-0.63	-0.43	-0.36	-0.41	-0.29	-0.26	-0.07	0.66	-0.11	-0.30	0.51	-0.01	-0.09	-0.05	-0.29	-0.20	0.36	1						
Total Iron	-0.03	0.15	0.26	0.00	0.11	-0.03	0.08	0.24	0.48	0.30	0.69	-0.51	-0.45	0.18	0.11	0.12	0.62	0.38	1					
Conductivity	0.20	0.69	0.50	-0.47	-0.57	0.83	0.79	-0.15	0.74	0.72	0.60	-0.69	-0.63	-0.87	0.45	0.86	-0.12	0.04	-0.05	1				
Hardness	0.13	0.59	0.48	-0.59	-0.63	0.65	0.68	0.09	0.79	0.73	0.81	-0.71	-0.71	-0.68	0.59	0.73	0.32	0.19	0.28	0.84	1			
Temperature	-0.18	-0.70	-0.54	0.25	0.30	-0.71	-0.81	0.14	-0.92	-0.81	-0.84	0.78	0.85	0.70	-0.53	-0.85	-0.08	-0.05	-0.39	-0.81	-0.86	1		
Turbidity	0.29	-0.07	0.09	0.60	0.65	-0.32	-0.19	-0.20	-0.04	-0.12	0.01	0.22	0.04	0.60	0.00	-0.37	0.15	-0.07	0.45	-0.57	-0.30	0.09	1	

Legend: r ≥ 0.90 r ≥ 0.80 r ≥ 0.70 r < 0.70

HMW.OC = high molecular weight organic carbon | IMW.OC = intermediate molecular weight organic carbon | LMW.OC = low molecular weight organic carbon
 % R DOC = Biofilter percent removal of dissolved organic carbon | % R BP = Biofilter percent removal of biopolymers

Table S3: Multiple Pearson correlation for BF(A) Anthracite biofilm and BF(A) performance parameters examined in the study. Media data were taken from 20 cm bed depth. October 2015 data was excluded due to flawed EPS extraction. Ammonia data below detection limit was treated as DL/2. Each of the four multiple correlation tables (S4 to S7) correspond to single media type (sand vs anthracite) and a single biofilter (BF-A vs BF-B).

	HMW.OC	IMW.OC	LMW.OC	Diversity	Richness	Cell Count	ATP	ATP/Cell	Carbohydrates	Proteins	CH:PN	% R DOC	% R BP	DOC	NO3	NH3	Ortho-P	pH	Total Iron	Conductivity	Hardness	Temperature	Turbidity	
HMW.OC	1																							
IMW.OC	0.49	1																						
LMW.OC	0.44	0.86	1																					
Diversity	0.42	0.13	0.09	1																				
Richness	0.37	0.09	0.04	0.97	1																			
Cell Count	0.30	0.77	0.82	0.03	-0.07	1																		
ATP	0.08	0.72	0.85	0.18	0.10	0.87	1																	
ATP/Cell	-0.81	-0.74	-0.59	-0.23	-0.12	-0.69	-0.41	1																
Carbohydrates	0.24	0.84	0.92	0.10	0.10	0.78	0.88	-0.42	1															
Proteins	0.23	0.86	0.96	0.01	-0.01	0.81	0.89	-0.46	0.96	1														
CH:PN	0.13	0.58	0.68	0.04	0.11	0.57	0.66	-0.20	0.87	0.74	1													
% R DOC	-0.26	-0.80	-0.87	-0.02	0.00	-0.65	-0.72	0.40	-0.91	-0.90	-0.71	1												
% R BP	-0.09	-0.66	-0.74	-0.30	-0.32	-0.72	-0.85	0.36	-0.88	-0.84	-0.79	0.74	1											
DOC	0.19	-0.59	-0.54	0.18	0.24	-0.75	-0.80	0.34	-0.62	-0.64	-0.50	0.41	0.62	1										
NO3	0.30	0.52	0.73	0.42	0.42	0.50	0.71	-0.23	0.63	0.67	0.42	-0.44	-0.61	-0.32	1									
NH3	0.02	0.74	0.82	0.01	-0.05	0.73	0.88	-0.23	0.87	0.84	0.67	-0.75	-0.65	-0.70	0.60	1								
Ortho-P	0.11	0.07	0.28	-0.08	0.07	-0.08	-0.01	0.14	0.25	0.32	0.27	-0.33	-0.28	0.31	0.35	-0.08	1							
pH	-0.33	-0.27	-0.07	-0.36	-0.28	-0.16	-0.10	0.27	-0.01	-0.01	0.24	-0.01	-0.09	-0.05	-0.29	-0.20	0.36	1						
Total Iron	0.23	0.29	0.29	0.20	0.35	-0.03	0.06	0.02	0.47	0.34	0.66	-0.51	-0.45	0.18	0.11	0.12	0.62	0.38	1					
Conductivity	0.06	0.73	0.82	-0.23	-0.32	0.87	0.88	-0.45	0.80	0.84	0.61	-0.69	-0.63	-0.87	0.45	0.86	-0.12	0.04	-0.05	1				
Hardness	0.15	0.66	0.85	-0.24	-0.22	0.72	0.78	-0.34	0.86	0.87	0.81	-0.71	-0.71	-0.68	0.59	0.73	0.32	0.19	0.28	0.84	1			
Temperature	-0.10	-0.69	-0.79	-0.05	-0.05	-0.76	-0.87	0.32	-0.94	-0.85	-0.93	0.78	0.85	0.70	-0.53	-0.85	-0.08	-0.05	-0.39	-0.81	-0.86	1		
Turbidity	0.37	-0.33	-0.27	0.59	0.66	-0.31	-0.33	0.07	-0.16	-0.35	0.13	0.22	0.04	0.60	0.00	-0.37	0.15	-0.07	0.45	-0.57	-0.30	0.09	1	

Legend:  $r \geq 0.90$ $r \geq 0.80$ $r \geq 0.70$ $r < 0.70$

HMW.OC = high molecular weight organic carbon | IMW.OC = intermediate molecular weight organic carbon | LMW.OC = low molecular weight organic carbon

% R DOC = Biofilter percent removal of dissolved organic carbon | % R BP = Biofilter percent removal of biopolymers

Table S4: Multiple Pearson correlation for BF(B) sand biofilm and BF(B) performance parameters examined in the study. Media data were taken from 20 cm bed depth. October 2015 data was excluded due to flawed EPS extraction. Ammonia data below detection limit was treated as DL/2. Each of the four multiple correlation tables (S4 to S7) correspond to single media type (sand vs anthracite) and a single biofilter (BF-A vs BF-B).

	HMW.OC	IMW.OC	LMW.OC	Diversity	Richness	Cell Count	ATP	ATP/Cell	Carbohydrates	Proteins	CH:PN	% R DOC	% R BP	DOC	NO3	NH3	Ortho-P	pH	Total Iron	Conductivity	Hardness	Temperature	Turbidity	
HMW.OC	1																							
IMW.OC	0.37	1																						
LMW.OC	0.29	0.87	1																					
Diversity	0.33	0.21	0.15	1																				
Richness	0.34	0.15	0.11	1.00	1																			
Cell Count	0.31	0.86	0.59	0.19	0.15	1																		
ATP	0.09	0.84	0.74	0.00	-0.05	0.86	1																	
ATP/Cell	-0.60	-0.81	-0.63	-0.27	-0.24	-0.77	-0.64	1																
Carbohydrates	-0.02	0.85	0.85	0.01	-0.04	0.69	0.82	-0.58	1															
Proteins	-0.01	0.83	0.89	-0.05	-0.09	0.67	0.82	-0.46	0.96	1														
CH:PN	-0.01	0.60	0.49	0.17	0.11	0.50	0.60	-0.71	0.68	0.47	1													
% R DOC	-0.25	-0.88	-0.79	0.05	0.09	-0.63	-0.68	0.52	-0.82	-0.80	-0.40	1												
% R BP	0.17	-0.70	-0.61	-0.04	0.01	-0.70	-0.82	0.47	-0.91	-0.83	-0.72	0.72	1											
DOC	0.07	-0.60	-0.42	0.25	0.31	-0.71	-0.87	0.52	-0.59	-0.54	-0.58	0.42	0.63	1										
NO3	0.07	0.52	0.49	0.26	0.24	0.42	0.55	-0.14	0.48	0.54	0.04	-0.66	-0.44	-0.32	1									
NH3	-0.09	0.81	0.58	0.02	-0.05	0.78	0.83	-0.49	0.79	0.73	0.54	-0.71	-0.77	-0.78	0.57	1								
Ortho-P	0.05	0.15	0.49	0.24	0.26	-0.06	0.11	0.14	0.35	0.47	-0.07	-0.30	-0.31	0.31	0.35	-0.10	1							
pH	-0.25	-0.06	0.26	-0.31	-0.31	-0.26	0.08	0.12	0.13	0.11	0.24	0.01	-0.18	-0.05	-0.29	-0.14	0.36	1						
Total Iron	0.00	0.25	0.41	0.21	0.20	-0.05	0.08	-0.17	0.53	0.41	0.51	-0.44	-0.50	0.18	0.11	0.09	0.62	0.38	1					
Conductivity	0.11	0.88	0.69	-0.12	-0.18	0.86	0.92	-0.64	0.76	0.74	0.53	-0.70	-0.70	-0.87	0.45	0.90	-0.12	0.04	-0.05	1				
Hardness	0.13	0.84	0.84	-0.22	-0.26	0.69	0.88	-0.51	0.88	0.91	0.45	-0.89	-0.79	-0.68	0.59	0.75	0.32	0.19	0.28	0.84	1			
Temperature	0.09	-0.79	-0.63	0.13	0.19	-0.70	-0.82	0.53	-0.90	-0.81	-0.67	0.87	0.91	0.70	-0.53	-0.87	-0.08	-0.05	-0.39	-0.81	-0.86	1		
Turbidity	0.02	-0.36	-0.38	0.09	0.12	-0.43	-0.50	0.22	-0.25	-0.34	-0.10	-0.06	0.13	0.60	0.00	-0.43	0.15	-0.07	0.45	-0.57	-0.30	0.09	1	

Legend: r ≥ 0.90 r ≥ 0.80 r ≥ 0.70 r < 0.70

HMW.OC = high molecular weight organic carbon | IMW.OC = intermediate molecular weight organic carbon | LMW.OC = low molecular weight organic carbon
 % R DOC = Biofilter percent removal of dissolved organic carbon | % R BP = Biofilter percent removal of biopolymers

Table S5: Multiple Pearson correlation for BF(B) Anthracite biofilm and BF(B) performance parameters examined in the study. Media data were taken from 20 cm bed depth. October 2015 data was excluded due to flawed EPS extraction. Ammonia data below detection limit was treated as DL/2. Each of the four multiple correlation tables (S4 to S7) correspond to single media type (sand vs anthracite) and a single biofilter (BF-A vs BF-B).

	HMW.OC	IMW.OC	LMW.OC	Diversity	Richness	Cell Count	ATP	ATP/Cell	Carbohydrates	Proteins	CH:PN	% R DOC †	% R BP ‡	DOC	NO3	NH3	Ortho-P	pH	Total Iron	Conductivity	Hardness	Temperature	Turbidity	
HMW.OC	1																							
IMW.OC	0.72	1																						
LMW.OC	0.68	0.95	1																					
Diversity	0.09	-0.10	-0.11	1																				
Richness	0.00	-0.20	-0.17	0.98	1																			
Cell Count	0.61	0.84	0.74	0.25	0.18	1																		
ATP	0.37	0.80	0.77	0.17	0.11	0.75	1																	
ATP/Cell	-0.56	-0.43	-0.45	-0.52	-0.49	-0.66	-0.21	1																
Carbohydrates	0.50	0.87	0.83	0.01	-0.06	0.66	0.89	-0.12	1															
Proteins	0.64	0.93	0.90	-0.16	-0.24	0.68	0.74	-0.19	0.92	1														
CH:PN	0.15	0.50	0.44	0.20	0.17	0.41	0.80	0.11	0.81	0.54	1													
% R DOC †	-0.64	-0.89	-0.83	0.02	0.12	-0.57	-0.80	0.05	-0.90	-0.84	-0.68	1												
% R BP ‡	-0.36	-0.77	-0.71	-0.11	-0.09	-0.73	-0.82	0.26	-0.84	-0.70	-0.80	0.72	1											
DOC	-0.21	-0.52	-0.45	-0.12	-0.12	-0.69	-0.79	0.19	-0.51	-0.35	-0.59	0.42	0.63	1										
NO3	0.52	0.58	0.68	0.37	0.33	0.51	0.67	-0.26	0.64	0.66	0.43	-0.66	-0.44	-0.32	1									
NH3	0.19	0.68	0.60	0.21	0.16	0.70	0.95	-0.13	0.83	0.66	0.79	-0.71	-0.74	-0.76	0.57	1								
Ortho-P	0.31	0.39	0.55	-0.36	-0.34	0.03	0.08	-0.03	0.38	0.55	0.08	-0.30	-0.31	0.31	0.35	-0.10	1							
pH	-0.23	0.05	0.09	-0.57	-0.55	-0.22	0.03	0.43	0.09	0.04	0.29	0.01	-0.18	-0.05	-0.29	-0.09	0.36	1						
Total Iron	0.18	0.31	0.34	-0.10	-0.10	-0.04	0.23	0.12	0.55	0.45	0.56	-0.44	-0.50	0.18	0.11	0.15	0.62	0.38	1					
Conductivity	0.41	0.81	0.71	-0.02	-0.10	0.83	0.90	-0.23	0.74	0.66	0.60	-0.70	-0.70	-0.87	0.45	0.87	-0.12	0.04	-0.05	1				
Hardness	0.54	0.88	0.86	-0.21	-0.26	0.65	0.87	-0.05	0.85	0.81	0.65	-0.89	-0.79	-0.68	0.59	0.73	0.32	0.19	0.28	0.84	1			
Temperature	-0.38	-0.77	-0.68	-0.15	-0.09	-0.68	-0.91	0.10	-0.88	-0.70	-0.87	0.87	0.91	0.70	-0.53	-0.87	-0.08	-0.05	-0.39	-0.81	-0.86	1		
Turbidity	0.06	-0.31	-0.31	0.32	0.29	-0.45	-0.35	0.19	-0.14	-0.21	0.04	-0.06	0.13	0.60	0.00	-0.39	0.15	-0.07	0.45	-0.57	-0.30	0.09	1	

Legend: r ≥ 0.90 r ≥ 0.80 r ≥ 0.70 r < 0.70

HMW.OC = high molecular weight organic carbon | IMW.OC = intermediate molecular weight organic carbon | LMW.OC = low molecular weight organic carbon

% R DOC = Biofilter percent removal of dissolved organic carbon | % R BP = Biofilter percent removal of biopolymers

Table S6: Biofilter media biofilm data for diversity, liquid chromatography, biomass and EPS parameters obtained from the 54 media samples used in this study.

Sample Date	Biofilter	Sample Depth (cm)	Media Type	Shannon Diversity	Richness	Cells/cm ³	ATP ng/cm ³	ATP/Cell	Carbohydrates µg D-glucose/cm ³	Proteins µg BSA/cm ³	CH:PN	HMW EPS Organic C µg C/cm ³	IMW EPS Organic C µg C/cm ³	LMW EPS Organic C µg C/cm ³
10/02/2014	BF(A)	20	S	3.24	39	2.29E+07	1052	4.60E-14	24	38	0.61	39	35	96
10/02/2014	BF(A)	20	A	3.33	40	7.29E+07	452	6.20E-15	25	61	0.4	21	18	37
10/02/2014	BF(B)	20	S	3.41	40	2.53E+08	2072	8.19E-15	75	156	0.48	31	36	93
10/02/2014	BF(B)	20	A	3.11	32	1.12E+08	708	6.31E-15	38	84	0.45	23	22	47
12/04/2014	BF(A)	20	S	4.19	81	7.40E+08	2657	3.59E-15	125	180	0.69	41	53	120
12/04/2014	BF(A)	20	A	4.19	80	4.90E+08	1109	2.26E-15	65	97	0.67	21	31	66
12/04/2014	BF(B)	20	S	4.25	82	7.10E+08	2307	3.25E-15	107	161	0.66	38	30	44
12/04/2014	BF(B)	20	A	4.26	81	4.30E+08	1191	2.77E-15	66	99	0.67	23	32	66
12/04/2014	BF(B)	60	S	4.16	76	2.80E+08	829	2.96E-15	43	69	0.62	10	19	42
01/29/2015	BF(A)	20	S	3.89	63	6.00E+08	2604	4.34E-15	117	182	0.64	30	53	123
01/29/2015	BF(A)	20	A	4.02	69	4.10E+08	1560	3.80E-15	65	109	0.59	16	33	76
01/29/2015	BF(B)	20	S	3.73	53	5.70E+08	2772	4.86E-15	109	175	0.62	47	61	52
01/29/2015	BF(B)	20	A	4.04	72	3.40E+08	1840	5.41E-15	73	97	0.75	15	30	66
01/29/2015	BF(B)	60	S	4.05	77	1.60E+08	679	4.24E-15	34	65	0.52	17	17	40
02/16/2015	BF(A)	20	S	3.6	47	1.40E+09	3519	2.51E-15	121	213	0.57	45	65	127
02/16/2015	BF(A)	20	A	3.68	49	9.30E+08	1756	1.89E-15	70	129	0.54	16	36	76
02/16/2015	BF(B)	20	S	4.01	68	1.50E+09	3367	2.24E-15	106	196	0.54	104	122	117

02/16/2015	BF(B)	20	A	4.02	68	1.00E+09	1685	1.68E-15	72	131	0.55	26	42	79
02/16/2015	BF(B)	60	S	4.07	72	3.30E+08	815	2.47E-15	38	74	0.52	15	21	40
05/21/2015	BF(A)	20	S	4.1	75	6.91E+08	2516	3.64E-15	39	84	0.47	#N/A	#N/A	#N/A
05/21/2015	BF(A)	20	A	3.99	64	4.75E+08	997	2.10E-15	24	63	0.38	#N/A	#N/A	#N/A
05/21/2015	BF(B)	20	S	4.28	84	5.75E+08	2373	4.13E-15	41	67	0.61	#N/A	#N/A	#N/A
05/21/2015	BF(B)	20	A	4.12	75	4.27E+08	901	2.11E-15	23	47	0.5	#N/A	#N/A	#N/A
06/18/2015	BF(A)	20	S	4.14	78	3.77E+08	2022	8.39E-15	45	122	0.37	38	36	98
06/18/2015	BF(A)	20	A	4.14	77	2.04E+08	925	2.46E-15	23	65	0.35	28	36	89
06/18/2015	BF(B)	20	S	4.17	81	2.69E+08	2034	9.98E-15	40	110	0.36	34	30	87
06/18/2015	BF(A)	20	A	4.19	82	2.41E+08	812	3.02E-15	28	73	0.38	35	40	107
07/20/2016	BF(A)	20	S	4.14	78	1.93E+08	1231	6.37E-15	33	81	0.41	49	39	117
07/20/2016	BF(A)	20	A	4	68	8.90E+07	416	4.67E-15	15	41	0.37	35	38	82
07/20/2016	BF(B)	10	S	4.19	79	1.29E+08	652	5.06E-15	27	66	0.41	33	26	73
07/20/2016	BF(B)	10	S	4.01	71	1.59E+08	344	2.16E-15	15	39	0.38	36	36	83
07/20/2016	BF(B)	20	S	4.25	83	1.58E+08	1225	7.78E-15	16	42	0.39	36	39	76
07/20/2016	BF(B)	20	S	3.88	61	9.11E+07	482	5.29E-15	35	83	0.42	49	36	81
07/20/2016	BF(B)	60	S	4.08	71	1.46E+08	594	4.06E-15	20	58	0.35	30	22	73
08/24/2016	BF(A)	20	S	4	66	1.85E+08	1236	6.67E-15	21	79	0.27	31	36	79
08/24/2016	BF(A)	20	A	3.83	56	1.76E+08	481	2.73E-15	12	44	0.27	33	39	80
08/24/2016	BF(B)	10	S	3.92	62	4.33E+08	1738	4.02E-15	23	87	0.26	36	38	96
08/24/2016	BF(B)	10	A	3.96	64	2.62E+08	805	3.07E-15	16	53	0.3	33	48	102
08/24/2016	BF(B)	20	S	4.11	76	4.44E+08	1502	5.75E-15	38	88	0.43	37	38	89
08/24/2016	BF(B)	20	A	3.93	65	1.86E+08	497	2.67E-15	10	41	0.24	25	38	84
08/24/2016	BF(B)	60	S	4.14	82	1.53E+08	699	4.58E-15	13	58	0.22	23	22	54
09/30/2015	BF(A)	20	S	4.09	75	2.96E+08	1039	3.51E-15	24	73	0.32	31	24	54
09/30/2015	BF(A)	20	A	3.94	67	1.58E+08	490	3.11E-15	14	41	0.34	28	28	55

09/30/2015	BF(B)	20	S	4.09	75	3.86E+08	1813	4.69E-15	33	60	0.55	43	31	70
09/30/2015	BF(B)	20	A	4.16	83	1.83E+08	544	2.97E-15	13	34	0.39	31	32	64
10/30/2015	BF(A)	20	S	4.18	82	1.37E+08	1799	1.31E-14	15	37	0.39	20	20	36
10/30/2015	BF(A)	20	A	3.93	64	9.47E+07	691	7.29E-15	7	19	0.39	12	20	35
10/30/2015	BF(B)	20	S	3.47	42	1.23E+08	1427	1.16E-14	16	35	0.44	0	0	3
10/30/2015	BF(B)	20	A	4.19	81	8.94E+07	536	5.99E-15	9	18	0.48	14	19	34
11/30/2015	BF(A)	20	S	3.84	59	4.39E+08	1668	3.80E-15	34	73	0.46	40	32	73
11/30/2015	BF(A)	20	S	3.83	59	4.05E+08	764	1.89E-15	20	43	0.46	36	38	80
11/30/2015	BF(B)	20	A	3.87	62	1.48E+08	773	5.21E-15	19	44	0.43	39	41	83
11/30/2015	BF(B)	20	S	3.3	60	4.91E+08	2109	4.29E-15	38	81	0.46	47	38	84

Appendix B

Supplementary Information for Chapter 4

Table S1: Post-hoc Dunn test p values derived from Kruskal-Wallis test on Shannon Diversity results in Chapter 4. Kruskal-Wallis $p=0.0001$, $df=4$, $chi\text{-squared}=23.15$. Dunn test p values adjusted for Bonferroni correction. Asterisk () denotes significant differences.*

Dunn Test with Bonferroni: Shannon

Comparison	Z	P.adj
Media Fall - Media Winter	-0.339	1.000
Media Fall - NF Fall	2.657	0.079
Media Winter - NF Fall	2.960	0.031*
Media Fall - NF Spring	0.108	1.000
Media Winter - NF Winter	0.446	1.000
NF Fall - NF Winter	-2.560	0.105
Media Fall - Water	3.176	0.015*
Media Winter - Water	3.555	0.004*
NF Fall - Water	-0.126	1.000
NF Winter - Water	3.056	0.022*

Appendix C

Backwash Procedures

Backwash procedure for the Mannheim pilot biofilters required the columns to be drained to 30 cm above the media surface by closing the ball valves of both the feed and effluent lines. A backwash pump was used at 450 L/h flow rate to inject effluent into the bottom of the column and sub-fluidize the media while air scour was initiated using 10 psi at 30 mm flow rate. This resulted in collapse pulse conditions and was maintained for 3 minutes. Following air scour, a bed expansion step was used to remove backwash liquor from the column. Depending on water viscosity due to seasonal temperature variation, 10 minutes of 50% bed expansion was maintained at 1500 to 1100 L/h.

Appendix D

Glassware Cleaning Procedures for DOC, LCOCD and EPS Quantification

Sample Bottles and caps – DOC, LCOCD

1. Wash at 50°C with Jet-clean detergent (Fisher Scientific), and rinse thoroughly with deionized water
2. Rinse twice with Milli-Q water
3. Incubate at 105 °C for at least 6 h

Vials – DOC, LC-OCD

1. Wash at 50°C with Jet-clean detergent, and rinse thoroughly with deionized water
2. Rinse twice with Milli-Q water
3. Incubate at 400°C for 1 h

Vials – EPS Quantification Assays

1. Wash at 50°C with Jet-clean detergent, and rinse thoroughly with deionized water
2. Incubate in HCl for 6 h
3. Rinse twice with deionized water and twice with Milli-Q water
4. Incubate at 400°C for 1 h